2018

ONCOGENE INDUCED DNA REPLICATION IN LUNG INJURY REPAIR AND CARCINOGENESIS

Shilpa singh
Virginia Commonwealth University

ONCOGENE INDUCED DNA REPLICATION IN LUNG INJURY REPAIR AND CARCINOGENESIS

A Dissertation submitted in partial fulfillment of the requirements for the degree of Doctor of Philosophy at Virginia Commonwealth University.

by

SHILPA SINGH
M.S. Virginia Commonwealth University, 2012
B.S. Mumbai University, India, 2008

Director: SWATI PALIT DEB
ASSOCIATE PROFESSOR, BIOCHEMISTRY

Virginia Commonwealth University
Richmond, Virginia
May 2018

Acknowledgement

I would like to take this opportunity to recognize some of the individuals who have guided and assisted me throughout this process. I would like to start by expressing my gratitude towards my advisor, Dr. Swati Palit Deb, for her mentorship, patience and molding me into the scientist I have become. I would like to thank members of my committee, starting with Dr. Sumitra Deb for his continued support and guidance in experiments. I would like to thank Dr. Brad Windle and Dr. Steven Grossman for their valuable feedbacks during meetings and Dr. Kristoff Valerie for his efforts and dedication towards my training. I would like to thank fellow lab member Catherine Vaughan and all lab technicians for their scientific input and help in completing my experiments.

I would like to thank Integrative Life Sciences department for giving me with an opportunity to pursue this degree and all the Graduate Assistantships provided over the years. I would like to thank Dr. Stephen Jones, Dr. Jeffery Whitsett and Dr. G. Lozano for providing us with valuable transgenic mice and Dr Arnold Levine for 2A10 antibody. This work was supported by a pilot project from VCU Massey Cancer Center (MCC) (to Dr. Swati Palit Deb), and NCI [CA 121144 to Dr. Sumitra Deb]; and NCI [CA107532 to Dr. Steven Grossman].

Special thanks go out to my family, my father Kashmir Singh, my mother Nirmala Singh for their never ending well of patience and love. My little sister Aakriti Singh Sood for her continued love and support throughout my studies. My mother-in-law Elizabeth

Boothello for encouraging words and prayers. All my friends who have contributed in several ways to my journey. And finally, I would like to express my gratitude for my husband Dr. Rio Boothello for being my rock.

Table of Contents

Page

List of Tables

Page

List of Figures

Page

List of Abbreviations

BSA	Bovine serum albumin
CCSP	Clara cell secretory protein
cDNA	Complementary DNA
ChIP	Chromatin Immunoprecipitation
DMEM	Dulbecco's Modified Eagle's Medium
DMSO	Dimethyl Sulfoxide
DNA	Deoxyribonucleic acid
ECL	Electrochemiluminescence
EGFR	Epidermal Growth Factor Receptor
GAPDH	Glyceraldehyde 3- phosphate dehydrogenase
GFP	Green fluorescent protein
GOF	Gain of function
Hes1	Hairy and enhancer of split 1
MDM2	Mouse Double Minute 2
mRNA	Messenger RNA
NFκB2	Nuclear factor of kappa B
PBS	Phosphate Buffered Saline
PI3K	Phosphatidylinositol-3-kinase
QPCR	Quantitative PCR
Rb	Retinoblastoma susceptibility protein

RNA	Ribonucleic acid
SCLC	Squamous cell carcinoma
shRNA	Short hairpin RNA
siRNA	Small interfering RNA
SPC	Surfactant protein C
TAD	Transactivation domain
WT	Wild type

Abstract

ONCOGENE INDUCED DNA REPLICATION IN LUNG INJURY REPAIR AND CARCINOGENESIS

By Shilpa Singh, Ph.D.

A Dissertation submitted in partial fulfillment of the requirements for the degree of Doctor of Philosophy at Virginia Commonwealth University.

Virginia Commonwealth University, 2018

Major Director: Swati Palit Deb, Ph.D.
Associate Professor, Biochemistry

Deregulation of genome duplication is a common theme in cancer cells. Although multitude of pathways has been discovered and implicated in the ability of oncogenes or loss of function tumor suppressors to induce oncogenesis, most of the pathways ultimately converge in deregulated genome duplication or uncoupling of DNA replication and segregation in cancer cells. It is important to determine how known oncogenes deregulate genome duplication, and if prevention of deregulated genome duplication could be a feasible target to thwart uncontrolled proliferation of cancer cells. Conventional paradigm ascribes the cell proliferative function of the human oncoprotein mouse double minute2 (MDM2)

primarily to its ability to degrade p53. Here we demonstrate that in the absence of p53, MDM2 induces replication stress eliciting an early S-phase checkpoint response to inhibit further firing of DNA replication origins. Our data uncovers a novel pathway, defended by the intra-S-phase checkpoint, by which MDM2 induces unscheduled origin firing and accelerates S-phase entry of cells in the absence of p53. To identify cell proliferative events consequent to MDM2 overexpression in noncancerous lung, transgenic mice expressing human MDM2 in either lung Club or alveolar cells after doxycycline (Dox) treatment were generated. Dox-induced MDM2 expression considerably increased the frequency of DNA replicating Club or alveolar cells after naphthalene or radiation-induced lung injury, and clonal expansion of lung progenitor cells accelerating restoration of the lost epithelial layer.

Gain of function (GOF) p53 mutations, observed frequently in most intractable human cancers, establish dependency for tumor maintenance and progression. We show that GOF p53 increases DNA replication origin firing, stabilizes replication forks, and promotes micronuclei formation, thus facilitating the proliferation of cells with genomic abnormalities. Following genome-wide analyses utilizing ChIP-Seq and RNA-Seq, GOF p53-induced origin firing, micronuclei formation and fork protection were traced to the ability of GOF p53 to transactivate Cyclin A and Chk1. Highlighting the therapeutic potential of Chk1's role in GOF p53 dependency, experiments in cell culture and mouse xenografts demonstrated that inhibition of Chk1 selectively blocked proliferation of cells and tumors expressing GOF p53. Our data suggest the exciting possibility that checkpoint inhibitors could efficiently and selectively target cancers expressing GOF p53 alleles.

Introduction

Genomic instability in cancer: Genomic instability is considered one of the hallmarks of cancer cells. It's also known to be a major driver of tumorigenicity, as found in precancerous lesions (1-5). Normal cells respond to DNA lesions by activating DNA damage checkpoints and by using different repair pathways. In the event of persistent DNA damage, cells can either undergo apoptosis or senescence. Another consequence of persistence DNA damage is cancer development with a long term cellular state of global instability (6). Many factors have been hypothesized to underlie genomic instability found in cancer cell. These include telomere attrition (7), defective DNA damage repair (8), and oxidative stress (9). However, these factors mainly contribute to genomic instability apparent in advanced stages of cancer development. Perturbed DNA replication may underlie the early genomic instability found in cancers.

Replication stress and cancer: DNA replication in normal dividing cells is a tightly controlled process that ensures faithful duplication of genome only once per cell cycle. Replication stress, which is characterized by deceleration of replication fork progression and an increase in stalled and collapsed forks, accounts for early DNA damage and could lead to early cancer development (10). DNA damage signaling in precancerous lesions, is constitutively activated, providing a natural obstacle in delaying or preventing tumorigenesis through the induction of apoptosis or senescence. Interestingly, corresponding constitutive DDR activation is observed upon oncogene-induced

replication stress, providing one of the first links between replication stress and tumorigenesis (11).

Activated oncogenes, or mutated tumor suppressors, selected for their ability to promote proliferation, can cause replicative stress inducing genomic instability and promoting tumorigenesis. In turn replication stress generates genomic instability which allows cells with various genetic alteration to escape senescence and apoptosis (12). Dysfunctional DNA damage response aids tumor progression upon oncogene induced replication stress which is reflective in high occurrence of mutations in DNA damage response pathway factors in human cancers.

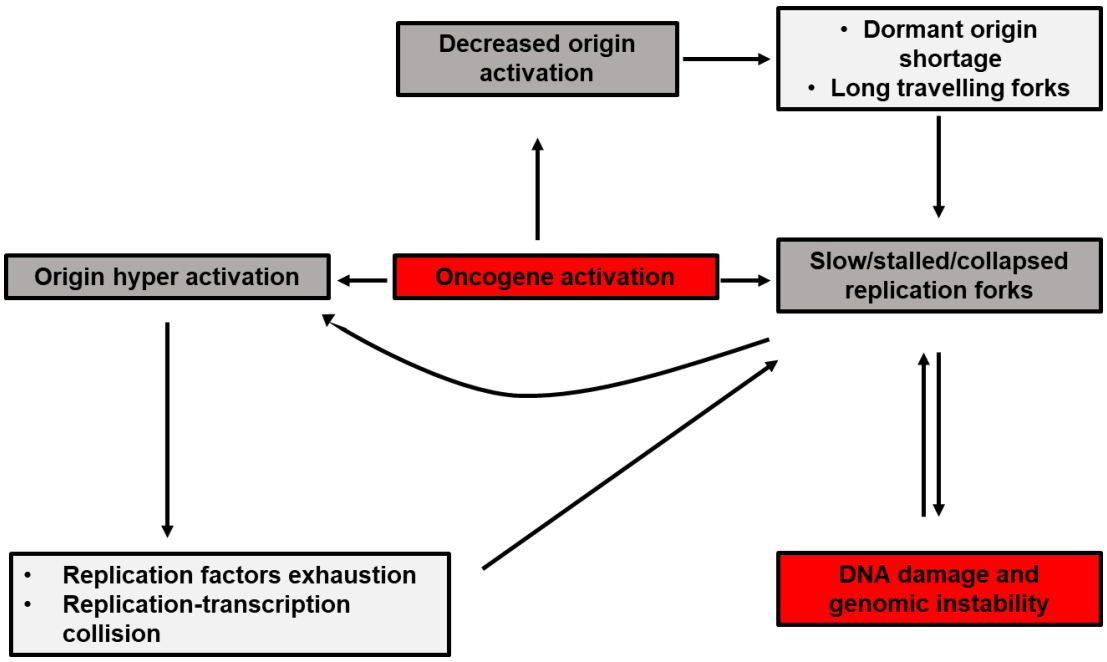

Figure 1. Oncogene-induced replication stress leads to DNA damage and genomic instability. Oncogene activation disrupts replication regulation leading to slow and stalled replication forks, hyper-activation and/or decreased origin activation. Such deregulated

replication causes DNA damage. Dark grey boxes are consequences of deregulated replication, light grey boxes are the potential outcomes of origin deregulation (13).

However, despite its apparent key role in the initial stages of cancer development, little is known about the nature of oncogene-induced replication stress. Recent data suggest that activated oncogenes might have a more direct effect upon the regulation of DNA replication. Several forms of replication perturbation leading to genomic instability have been reported following oncogene activation. These include slowed and arrested replication fork progression, as well as deregulated origin licensing and activation.

DNA replication initiation: The replication of DNA through S phase has been shown to proceed in a controlled temporal order, with specific types of replication events predominating at distinct segments of S phase. This orderly progression of replication through S phase is essential to maintaining the integrity of DNA replication. Eukaryotic cell cycle is driven by periodic fluctuations in the activity of cyclin-dependent kinase (CDK). In response to mitogenic signals, G1 cyclins accumulate and trigger the phosphorylation and inactivation of the retinoblastoma protein (RB), a cell cycle inhibitor. This releases E2F, a transcriptional factor, which then promotes expression of various G1/S and S phase proteins required for progression through S phase (Figure 2).

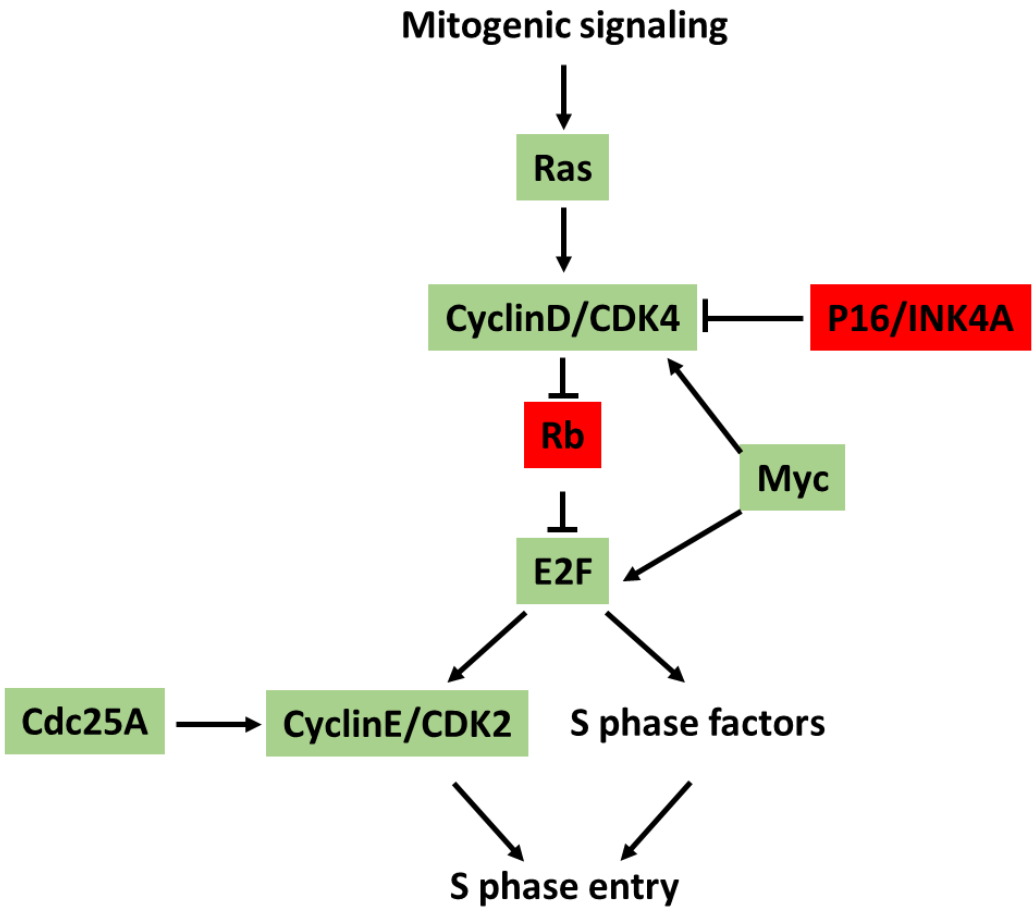

Figure 2. G1/S transition. During G1 phase, mitogenic signals trigger Ras-dependent signaling, which activates cyclin D transcription and cyclin D/CDK4 complex formation. Cyclin D/CDK4 phosphorylates and inactivates RB, which releases E2F from inhibition. E2F then promotes expression of various genes required for S phase entry. Cyclin E is an E2F target, which completes phosphorylation and inactivation of RB, thereby providing positive feedback to drive cells into S phase. The RB–E2F pathway becomes deregulated by various oncogenes (in green) and tumor suppressor genes (in red), to promote S phase entry and cell proliferation.

Activation of DNA replication origins is a tightly regulated mechanism, involving two main steps: (1) "origin licensing," restricted to late mitosis and early G1, when essential replication initiation proteins (ORC1, Cdc6, Cdt1, and Mcm2–7) are sequentially loaded on

origin DNA sequences, forming the "prereplicative complex" (preRC), and (2) "origin firing," occurring throughout S phase, when additional proteins are recruited to the preRC and start unwinding and DNA synthesis (Figure 3). The exact nature of timely activation of origins is largely unknown. However, certain factors such as transcriptional activation, chromatin modifications and, most strikingly, nuclear positioning may all play a role. Thus, deregulation of any of these factors associated with the replication timing program or disruption of any stage in DNA replication may lead to genomic instability.

In this report, the primary goal is to determine how known oncogenes deregulate genome duplication, and if prevention of deregulated genome duplication could be a feasible target to thwart uncontrolled proliferation of cancer cells. Due to frequent occurrence of p53 mutation and MDM2 overexpression in all types of lung cancer, including small cell (SCLC) and non-small cell lung cancer (NSCLC), we plan to determine the consequence of gain of function (GOF) p53 mutation and MDM2 overexpression on regulation of genome duplication in lung. The two known oncoproteins that are widely and frequently overexpressed in cancer cells.

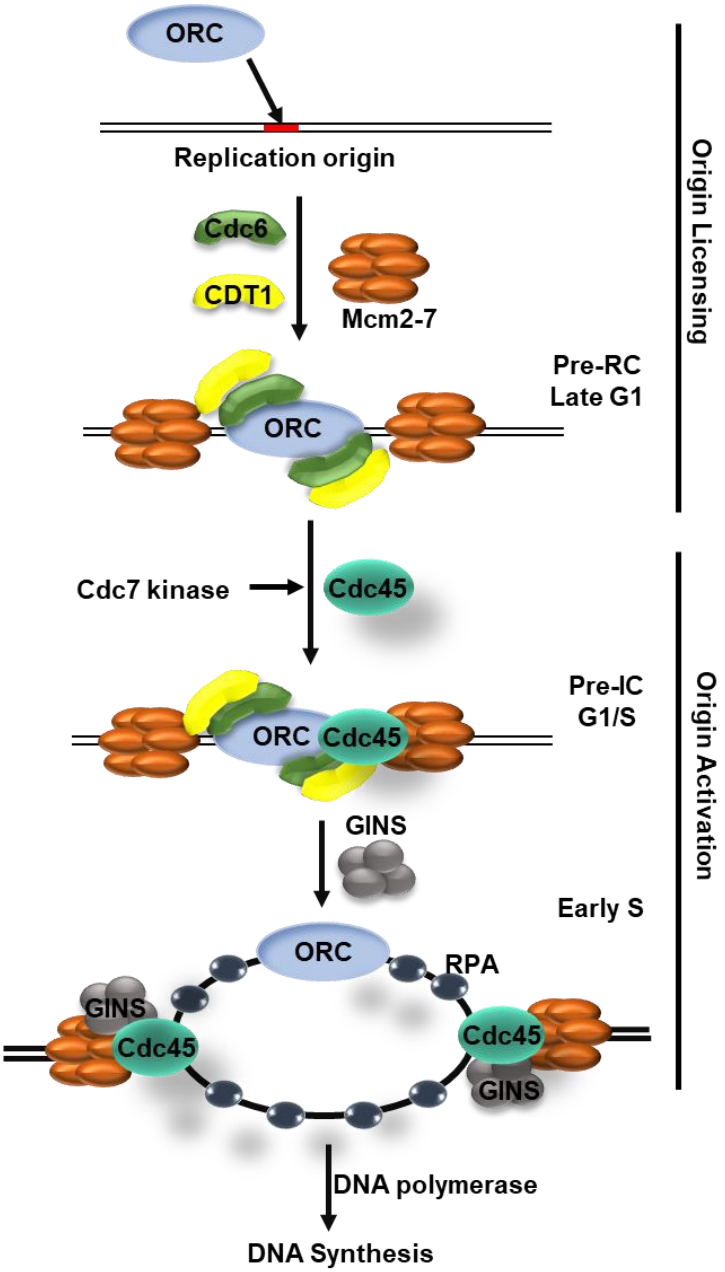

Figure 3. Replication initiation. Replication initiation involves two temporally separated steps, origin licensing and origin activation. Origin licensing occurs between late mitosis and end of G1. ORC, Cdc6 and Cdt1 cooperate to load the MCM2-7 complex onto chromatin. At the G1/S transition, origin firing begins, driven by the action of two kinases, CDK and DDK. Cdc45 and GINS are recruited to form the CMG complex, which stimulates the helicase activity of the MCM2-7 complex. Origins do not fire synchronously during S phase and the time of origin firing is associated with the time of association of firing factors.

MDM2 as an oncogene: MDM2 (Murine Double Minute 2) was originally discovered in a locus amplified on double minute chromosomes in transformed mouse fibroblast (14). Over-expression of MDM2 was found to immortalize rodent primary fibroblasts and induce transformation in cultured cells (15). MDM2 contains several conserved functional domains, which provide the structural basis for MDM2's oncogenic properties. The N-terminal p53-binding domain plays an essential role in binding to tumor suppressor p53 protein and inhibiting the transcriptional activity of p53. The central region contains the nuclear localization sequence (NLS) and the nuclear export signal (NES), which are responsible for the nucleo-cytoplasmic shuttling of MDM2 protein, and the acidic domain and an adjacent zinc finger which mediate the interaction of MDM2 with many ribosomal proteins (RPs). The C-terminus contains the RING finger domain which is responsible for the E3 ubiquitin ligase activity of MDM2. It recruits a ubiquitin-conjugating E2 enzyme to promote the ubiquitination and degradation of the target proteins. Among the many substrates of MDM2, p53 is one of the major ones (16, 17).

MDM2 recognizes the transactivation domain of WTp53 and this interaction physically blocks p53-mediated transcriptional activation. As an E3 ubiquitin ligase, MDM2 binds to p53 and ubiquitinates p53 for proteasomal degradation (18-21). Also, MDM2 blocks p53 translation via two different mechanisms. MDM2 is shown to interact directly with the messenger RNA (mRNA) encoding p53 itself and to suppress its translation (22). It also binds to and ubiquitinates RPL26, marking it for proteasomal degradation. RPL26 increases p53 translation by binding to its 5’-UTR (untranslated) region (23).

In early studies, MDM2 overexpression and p53 mutation was found to be a mutually exclusive event. Since then increased MDM2 levels either by gene amplification or overexpression has been observed in a wide variety of human tumors, including sarcoma, breast carcinoma, melanoma, leukemia, and glioblastoma. MDM2 is also often overexpressed in lung cancers with or without p53 mutation (24-28).Studies involving targeted expression of Mdm2 in specific tissues in the mouse have led to increased cellular proliferation and tumor formation, consistent with a role as an oncogene. In a study performed in mouse, tumor latency was found to be shorter in MDM2/p53 double-knockout mice as compared with p53-null mice that are heterozygous for the MDM2 deletion. In addition, homozygous deletion of MDM2 led to a change in tumor spectrum with an increased incidence of sarcomas (29). These findings support a role for Mdm2 in tumorigenesis that is independent of its effects on p53.

Our published experimental data indicate that MDM2 activates the PI3-kinase/Akt signaling pathway by modulating expression of crucial signaling genes due to its interaction with RE-1 silencing transcription factor (REST) irrespective of p53 status (30), and consequently up-regulates cyclin D2 expression (31). This activity can be found both in cell culture and in transgenic mouse models. Also, we have reported earlier that human oncoprotein MDM2 can induce G1-arrest. While one mechanism of this G1-arrest function involves its ability to enforce timely expression of cyclin A, MDM2 is capable of inhibiting DNA replication irrespective of this function (32). This necessitated a more extensive examination into role of MDM2 in DNA replication.

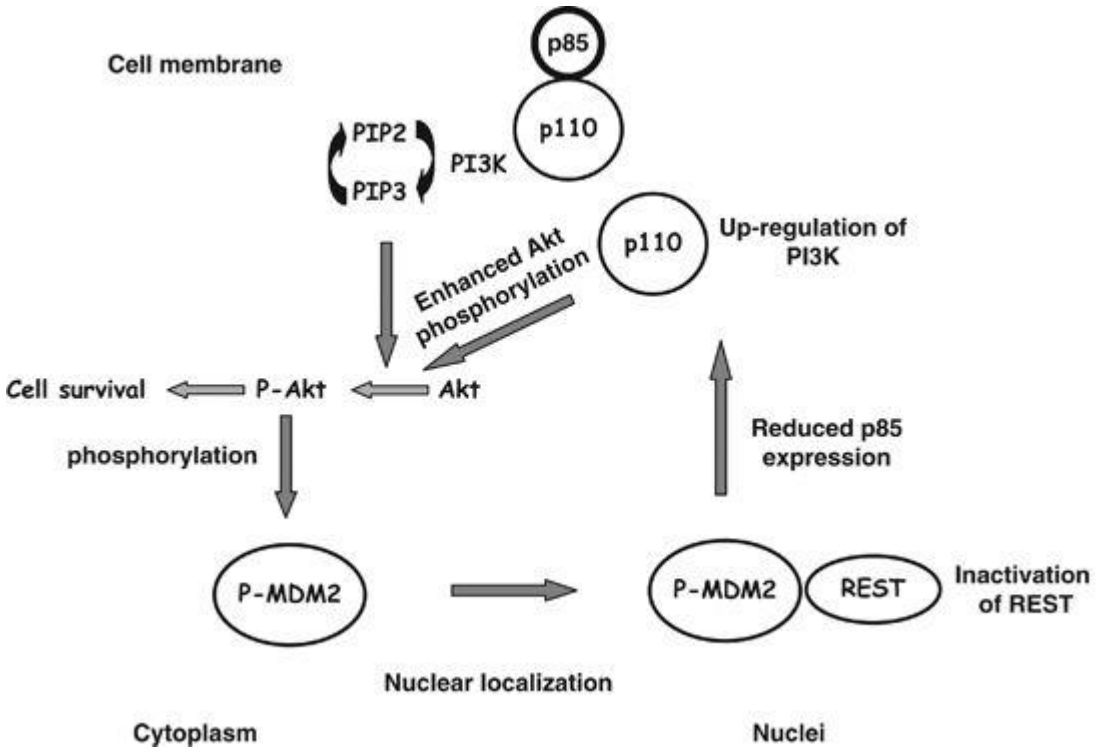

Figure 4. Mechanism of Akt activation by MDM2 overexpression (33).

MDM2 mouse models: Different research groups have generated MDM2 animal models to study its importance in regulating WT p53 (Table 1). Loss of MDM2 leads to embryonic lethality due to excess apoptosis which is completely rescued by concomitant deletion of p53 (34). Role of MDM2 in later stages of mouse lifespan has been studied by generating mouse containing hypomorphic allele. These mice showed decreased lymphoid cells, increased radio sensitivity and increased apoptosis in lymphocytes and epithelial cells (35). Another mouse model used to investigate the function of MDM2 after birth was MDM2 knockout mice with p53 hypomorphic R172P allele background. In this study, MDM2

deletion cause neonatal death due to cell cycle arrest in multiple proliferating tissues, including cerebellum and bone marrow (36). To further examine the role of MDM2 in adult tissues, another lab generated an inducible p53 allele to restore p53 activity in mdm2-/-, p53KI/- mice. These mice died shortly after the restoration of p53 activity and had defects in multiple radiosensitive tissues. This model also indicated that effect of MDM2 inhibition is tissue specific since classically radio insensitive tissues like lungs, kidney, brain, were not affected by the p53 restoration (37).

Mouse models with MDM2 overexpression have shown tumor generation with a significantly higher percentage of sarcoma than the p53 knockout mice, suggesting a p53-independent role of MDM2 in tumorigenesis. Another paper showing massive overexpression of MDM2 in mammary gland, also revealed a p53-independent role of MDM2 in DNA synthesis regulation. MDM2 overexpression caused inhibition of mammary gland development due to uncoupling of S-phase with mitosis in epithelial cells. Multiple rounds of S phase without mitosis lead to multinucleated cells with enlarged nuclei (38).

A single nucleotide polymorphism at the MDM2 promoter leads to MDM2 overexpression(39, 40), with the polymorphic allele found in both cancerous and non-cancerous lung tissues(41-43). These observations suggest that MDM2 overexpression could be one of the early events to exert proliferative effects in the lung increasing vulnerability to lung cancer. Despite presence of MDM2 over-expression in human lung cancers, there is no existing model to determine the consequence of MDM2 over expression targeted in lung. While many mouse models have greatly improved and expanded our

knowledge of inhibitory function of MDM2 on p53, a more defined representation for tissue specific overexpression of MDM2 in required to study its p53-independent functions.

MODEL	PHENOTYPE	REFERENCE
MDM2 KO mice	Embryonic lethal	(34)
MDM2 transgene overexpression in mice mammary gland	S phase uncoupling from M phase, polyploidy, tumors	(38, 44)
MDM2 transgene overexpression in mice	Spontaneous tumor formation, high incidence of sarcomas	(45)
MDM2 transgene overexpression in mice	Skin thickening, desquamation, hyperkeratosis	(46)
MDM2 transgene overexpression in basal cells of mice epidermis	Hyperplasia, pre-malignant lesions	(47)
MDM2 transgene overexpression in Drosophila	Eye and wing phenotypes showing developmental defects	(48)
MDM2 hypomorphic allele expression in mice	Lymphocytopenia, increased radio-sensitivity, increased apoptosis	(35)

Table 1: Genetic animal models of MDM2

Gain-of-function mutant p53: p53 also considered as the “guardian of genome”, gets activated from various stress signals. It is a tumor suppressor that acts mainly through activating transcription of many downstream targets. p53 has a very short protein half-life, and its protein levels are low in normal cells and tissues under non-stressed conditions (49-52). It gets activated through different post translational modifications like phosphorylation, acetylation, and methylation. Upon activation it binds to consensus DNA binding sequence located in the promoter or intron of its target genes to regulate their expression in cell type specific and stress-signal specific manner. It transcriptionally activates various genes involved in processes including apoptosis, cell cycle arrest, DNA repair, senescence, etc., to maintain the integrity of genome and prevent the tumor initiation and progression (53, 54). Recent reports have also demonstrated a proactive role of WT p53 in increasing processivity of DNA replication and preventing DNA damage (55). p53 is the most frequently mutated gene in human cancer with almost 50% of all human cancers carrying a mutation in the p53 gene. Loss of p53 function is often a prerequisite for tumor formation and progression as demonstrated in patients suffering from Li-Fraumeni syndrome (56-59). In addition to p53 mutation, p53 function is also attenuated and the p53 signaling is disrupted in human cancer through multiple mechanisms, including overexpression and/or amplification of p53 regulators such as MDM2, MDM4, Pirh2 and Cop1 (50, 60-63).

While the key role of wild-type (WT) p53 in tumor suppression has been firmly established, increasing evidence has proved that many tumor-associated mutant p53 protein not only loses the tumor suppressive function of wild type p53 but also gain tumor promoting function. This is either through exerting a dominant-negative regulation of remaining WT

p53 or independently of WT p53 (64-66). Majority of these mutations have been identified as missense mutations and are found to be located within its DNA binding domain (67, 68). These mutations are broadly classified as either DNA contact (R248W, R248Q, R273H) or structural (R249S, R245S, R175H) mutant based on the function of the residues altered (64). DNA contact mutant occur in amino acid residue that directly bind p53 target DNA sequences and are critical for binding. Conformational mutants usually result in a dramatic change in p53 protein structure. Different cell based, and animal assays suggest that these mutations also differ in the gain of function phenotype (64, 69).

Gain of function (GOF) ability of mutant p53 has been demonstrated in many cell-based experiments. These include promoting tumor cell proliferation, survival, migration, invasion, enhancing chemoresistance, promoting cancer cell metabolism and increased tumor angiogenesis (70-74). Even though mutant p53 can no longer recognize and bind to p53 DNA-binding elements, many tumor-associated mutant p53 proteins localize in the nucleus mainly and regulate the transcription of some genes through mechanism that are different from WT p53. It can for example, bind to TAp63 and TAp73 and inhibit their transcriptional activity (75-78). TAp63 and TAp73 are p53 family members that have the ability to regulate p53 target genes and compensate for its tumor-suppressive function (79). Mutant p53 can also interact with other transcriptional factors like Ets1, Sp1, NF-Y, NRF2 and VDR to stimulate tumor development (80-83). Mutant p53 can also modify chromatin structure to regulate the expression of some genes (84).

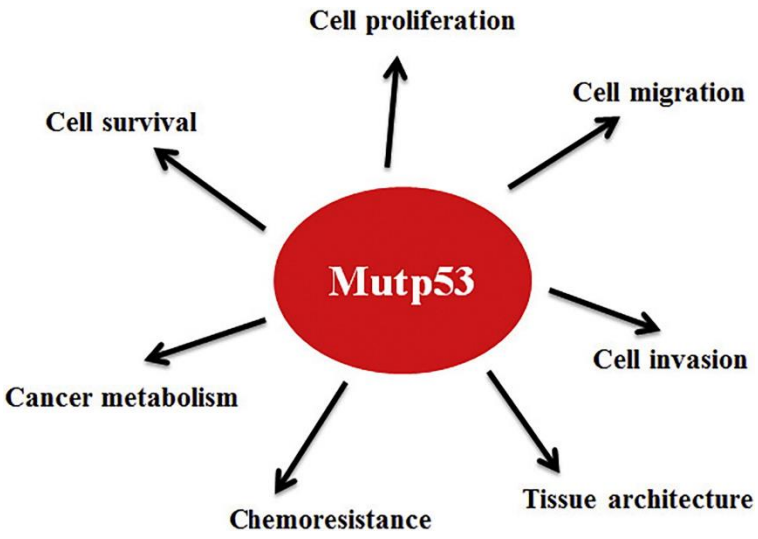

Figure 5. GOF p53 in tumorigenesis (85)**.**

Although many of the pathways involved in mutant p53 gain of functions have been thoroughly examined, many still need to be explored. Surprisingly, very few studies have investigated role of mutant p53 in DNA replication. Published data from our laboratory demonstrate that proliferation of lung cancer cells carrying GOF p53 mutation is dependent on the presence of the oncoprotein. Knockdown of mutant p53 or MDM2 in human lung cancer cells reduces tumor growth, cell proliferation and genetic abnormality (86). Consistently, GOF p53 dependence of tumors carrying the mutations have been reported by other laboratories (87). Since DNA replication is one of the two significant events in proliferating cells, it is important to further examine role of mutant p53 in DNA replication.

Specific Aims

Oncogene activation is an endogenous source of replication stress, disrupting replication regulation and inducing DNA damage. Oncogene-induced replication stress and its role in cancer development have been studied comprehensively, however its molecular basis is still unclear. This dissertation is designed to determine how two known oncogenes- MDM2 and GOF p53, deregulate genome duplication, and if prevention of deregulated genome duplication could be a feasible target to thwart uncontrolled proliferation of cancer cells. Following are the specific aims that constitute the different chapters of my dissertation:

1. **Determine the contribution of MDM2-induced signaling pathways in accelerated DNA replication and oncogenesis.**
2. **Develop a mouse model to investigate cell proliferative events consequent to MDM2 overexpression in noncancerous lung.**
3. **Determine the implication of GOF p53 mediated DNA replication stress on genetic instability and tumorigenesis.**

Contribution of MDM2-induced signaling pathways in deregulating DNA replication

The work presented in this chapter has been published in the Nucleic Acid Research journal (Nucleic acids research. 2014; 42(2):926-40.). Fiber spreading experiments were performed by Rebecca Frum and Catherine Vaughan assisted in generating cell lines from mouse lungs.

Introduction

The human homologue of the mouse double minute2 (*mdm2*) gene is known to code for an oncoprotein. Despite its oncogenic function, elevation of MDM2 expression induces G1-arrest in the presence or absence of WT p53 (88-90). Elimination of the growth inhibitory domains of MDM2 rescues its tumorigenic potential (88). Furthermore, in apparently normal cells such as early passage mouse embryo fibroblasts (MEF) or limited passage human lung fibroblast (such as WI38) MDM2 inhibits expression of cyclin A (32). Genetic defects such as absence of WT p53, the cyclin dependent kinase inhibitor p16 or the transcription factor BRG1, that deregulate the timely expression of cyclin A, also abrogate ability of MDM2 to inhibit expression of cyclin A expression, but not its ability to induce G1 arrest (32, 88) suggesting that MDM2 expression restricts an event downstream of cyclin A expression, and led us to investigate how MDM2 controls initiation of DNA replication.

Initiation of DNA replication takes place at DNA replication origins, recognized by loading of pre-replication complex during late mitosis and G1 phase, a process known as "licensing". During G1/S transition and at different time during the S phase, replication initiation factors are recruited to only a fraction of licensed origins forming pre-initiation complex, activating the MCM2-7 helicases and assembly of other replication factors and inducing local DNA unwinding. Origin firing is activated by cyclin dependent kinases complexed with cyclins E and A and by cdc7/DBf4 (91). In mammalian cells replication origin firing is regulated by checkpoint kinases, ATR and chk1, during normal unperturbed S phase in response to the single stranded DNA exposed at replication forks (92-94).

In this report we present evidence to show that elevated expression of MDM2 in cells lacking p53 elevates endogenous levels of cyclins D2 and A, hastens S phase entry and activation of chk1 phosphorylation. Activation of chk1 phosphorylation is known to stabilize a histone methyl transferase coded by the mixed lineage lymphoma (MLL) gene, which methylates lysine 4 of histone H3 (H3k4) at late replication origins to delay DNA replication (95). Our data show that MDM2 overexpression follows a similar course of events activating chk1 phosphorylation, leading to accumulation of MLL histone methyl transferase and checkpoint-dependent tri-methylation of H3K4 (H3K4Me3) causing inhibition of origin firing. We also show that the MDM2 mediated checkpoint activation is dependent on activation of DNA replication origins by cyclin-dependent kinases. Inhibition of this step using a specific inhibitor of cyclin dependent kinases abrogates activation of chk1 phosphorylation by MDM2 at the onset of S phase. These data signify that in cells

overexpressing MDM2, compromised checkpoint activity would enhance S phase entry and untimely origin firing, which is known to induce genomic instability (94, 96, 97)

Materials and Methods.

Plasmids and lentiviral vectors: The ecdysone inducible plasmid vector system was purchased from Invitrogen, and plasmids expressing MDM2 was constructed by inserting MDM2 cDNA at the multiple cloning site as described earlier (98). Generation of plasmids and lentiviral vectors (pLKO.1) expressing short hairpin (sh) RNA against MDM2 or non-endogenous green fluorescence protein (GFP) from U6 promoter and harboring a puromycin resistance gene has been described earlier (30, 32).

Generation of p53-/-, MDM2 transgenic mice: p53-/-, MDM2 transgenic (p53-/-, MDM2Tr) mice were generated by crossbreeding p53 +/-, MDM2 transgene +/- mice (gift from Stephen Jones, (45) as described earlier (30, 33).

Cells, transfections, and generation of stable transfectants: H1299 cells were purchased from ATCC and were maintained in media as suggested by the suppliers. H1299 cells expressing MDM2 from ecdysone inducible promoter was generated following supplier's (Invitrogen) protocol. The ecdysone inducible H1299 cells expressed 3 to 4-fold higher MDM2 transcripts after 24 hours of induction with ponasterone. Generation of stable transfectants and cultured lung cells from littermate MDM2 transgenic and non-transgenic mice with p53-/- background has been described earlier (33). QPCR analysis of genomic DNA of these cells showed a 10-fold higher copy number of the MDM2 gene than littermate non transgenic mice (30). To generate stable transfectants expressing shRNA against

MDM2 or GFP, appropriate cells were infected with lentiviral vectors expressing respective shRNA and selected with appropriate antibiotics and individual colonies were expanded after analysis.

Chemicals and Drugs: Iododeoxyuridine (IdU), chlorodeoxyuridine (CldU) and caffeine were purchased from (Sigma). Caffeine was used at a concentration of 2mM for 30 minutes (99, 100), Ponasterone A (Invitrogen) was used at 1mM concentration for 24 hours as suggested by the supplier, and PHA767491 (Tocris Bioscience) was used at a concentration of 10 μM for 60 minutes (101, 102).

Western Blot Analysis: Western blot analysis was performed as described previously (33).

Identification of DNA replication origin firing: DNA replication origin firing was determined by DNA fiber spreading analysis as described earlier (100). Briefly, cells were pulse-labeled sequentially with the nucleotide analogues IdU (40 μM) and CldU (100 μM) to track the replication pattern and directionality of fork movement. Cells were collected by trypsinization, and genomic DNA of approximately 600 cells was aligned on slides by fiber spreading as described earlier. Slides were then air dried and fixed in 3:1 methanol /acetic acid and dried overnight. After acid treatment (2.5N HCl, 30 minutes) and blocking (2% BSA in PBS), DNA fibers on slides were immunostained with primary antibodies against IdU and CldU followed by fluorescently labeled secondary antibodies, and finally fluorescently labeled tertiary antibodies, washed dried and mounted in antifade. Images were collected by confocal microscopy (Zeiss, LSM700). Newly initiated single origins were detected as red track flanked on both sides by green track as explained in Figure 1A

and B. Approximately 200 to 500 fibers from each sample were scored and analyzed using Image J software (NIH).

Statistical analysis: Distribution of four types of fibers classified as bi-directional origin, origin clusters, elongating forks and terminating forks generated by sequential labeling of replicating DNA over different samples in each experimental set has been tested for independence with Fisher exact test, or by chi-square test in case the computation of Fisher exact test was not feasible due to computer limitations. The null hypothesis of these tests is that the distribution remains independent of the categories, and a significant p value below 0.05 indicates departure from the hypothesis of independence. All statistical analysis was done using the statistical software R v2.13.0.

Detection of S phase nuclei: For detection of S phase nuclei, density arrested cells were replated on cover slips and labeled with 40 μM IdU for 20mins at desired time. IdU was washed off using PBS. Cells were fixed with 3% paraformaldehyde solution. For antibody staining, the cells were treated for 5 minutes with 0.5% triton X-100, followed by 1-hour treatment with 2.5 N HCl to denature the DNA. The acid was neutralized with three washes of 0.1 M Sodium Borate. Cells were then washed with 0.1% tween in PBS (wash buffer) and blocked in 2% BSA in wash buffer for an hour. Primary antibody against IdU was diluted in 1% BSA in wash buffer, added to cover slips and incubated for an hour. Following three washes with wash buffer, the cells were incubated with Alexafluor 594-conjugated secondary antibody diluted in 1% BSA in wash buffer for an hour. The cover slips were then washed and mounted on slides with Prolong Gold Antifade with DAPI (4', 6'-

diamidino-2-phenylindole hydrochloride, Molecular Probes) and imaged using confocal microscopy (Zeiss LSM700).

Antibodies: Antibodies against MDM2 were chosen depending on the species. N-20 and SMP14 (Santa Cruz) were used following supplier's protocol. 2A10 antibody was a gift from Arnold Levine. Antibodies against Erk2, chk1, cyclin A, cyclin D2 were from Santa Cruz Biotechnology, phospho chk1 (p-chk1) from Cell Signaling Technology, MLL^{C180}, H3K4Me3 and H3 were from Millipore, and were used following manufacturer's protocol.

IdU was detected by mouse anti-bromodeoxyuridine (Becton Dickinson) primary antibody and Alexafluor 594-conjugated rabbit anti-mouse (Molecular Probes) and Alexafluor 594-conjugated goat anti-rabbit (Molecular Probe) secondary and tertiary antibodies. CldU was detected by rat anti-bromodeoxyuridine (Accurate) primary antibody, and Alexafluor 488-conjugated chicken anti-rat (Molecular Probe) and Alexafluor 488-conjugated goat anti-chicken (Molecular Probes) secondary and tertiary antibodies as described earlier (100).

RNA extraction, generation of cDNA and quantitative PCR (QPCR): Total RNA was isolated from exponentially growing cultured cells using TRIzol reagent (Life Technologies, Invitrogen) following a protocol supplied by the manufacturer. cDNA was synthesized using the Thermoscript reverse transcription-PCR system (Invitrogen). QPCR was performed using a LightCycler system (Roche). Primers were designed using OLIGO 5 software (Molecular Biology Insights) and were synthesized by Integrated DNA Technologies. Reactions were performed in triplicate utilizing SYBR green dye, which

exhibits a higher fluorescence upon binding of double-stranded DNA. The methods have been described previously (32). Reactions were performed in triplicate.

Experimental Results.

MDM2 inhibits DNA replication origin firing: We have previously reported that elevated expression of MDM2 induces G1 arrest in cells irrespective of its p53 status (32, 88, 103). In apparently normal cells, MDM2 inhibits expression of cyclin A (32). In cells lacking WT p53, MDM2 does not inhibit cyclin A expression, but induces G1-arrest (32, 103). This observation led us to investigate how MDM2 controls the firing of DNA replication origin, an event downstream of cyclin A expression.

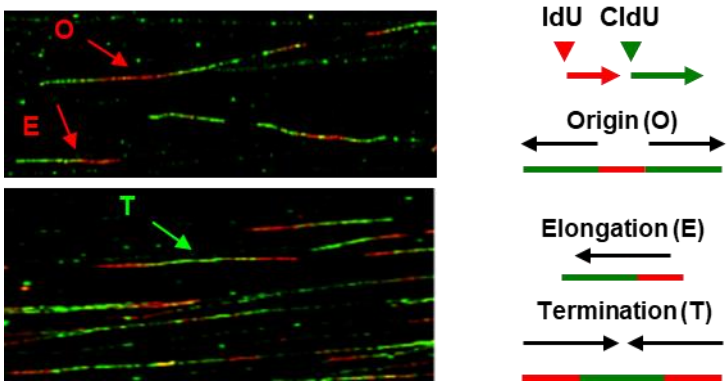

Figure 6. **Representative fiber images**. An example of fiber images generated from sequential labeling of replicating DNA by IdU and CldU in H1299 cells and immunostaining with fluorescently labeled antibodies. The figure shows (A) classification of the labeled fibers as newly initiated bi-directional origin (O), elongation (E) or termination (T) indicated by arrows along with a cartoon (B).

Since the cyclin A inhibitory function of MDM2 is disabled in H1299 cells (32), we constructed H1299 cells that express MDM2 from an ecdysone inducible promoter. After treatment with Ponasterone A for 24 hours, the cells were pulse-labeled sequentially with the nucleotide analogues IdU and CldU to track the replication pattern and directionality of fork movement. Cellular genomic DNA was then aligned on slides by fiber spreading following established techniques (100, 104). Incorporated IdU and CldU in the DNA fibers were detected using red or green fluorescent-tagged antibodies, respectively, and visualized by confocal microscopy (Figures 6A, 7A). Newly initiated origins are indicated by a red track flanked on both sides by green, since these patterns were obtained because of replication origin initiating during the first pulse detected by an antibody tagged with red fluorescence and replication forks moving bidirectionally during the second pulse detected by an antibody tagged with green fluorescence. Similarly, unidirectional red and green tracks indicated elongation, and merging forks were detected by merging green tracks flanked by red tracks as demonstrated in Figure 6. Scoring of 200 to 400 stained untangled DNA fibers from Ponasterone A or ethanol (vehicle) treated cells as shown in the representative images (Figure 7A) revealed that induction of MDM2 expression (Figure 7B) significantly reduced the frequency of origin firing in repeated experiments (Figure 7C, p-value = $4.104X10^{-5}$). This observation indicates that MDM2 controls the frequency of bi-directional single origin firing.

MDM2-mediated inhibition of origin firing can be rescued by caffeine, an inhibitor of checkpoint kinases: To test whether inhibition of origin firing by MDM2 is a result of a

checkpoint response often elicited by oncogenes (105, 106) the ecdysone-inducible H1299 cells were induced to express MDM2 by treatment with Ponasterone A for 24 hours, followed by a brief (30 minutes) treatment with caffeine, an inhibitor of ATM, ATR kinases (107, 108) A. Cells were then processed for fiber spreading analysis of replicating DNA as described above. Scoring of stained untangled DNA fibers (Figure 8A) showed that Ponasterone A and ethanol treated cells had a similar frequency of origin firing after caffeine treatment (Figure 8B). The p value (0.050) indicated no significant difference in origin firing between Ponasterone A and ethanol treated cells. This data show that MDM2-mediated inhibition of origin firing at 24 hours was rescued by caffeine treatment and suggests that inhibition of DNA replication origin firing by MDM2 could be a consequence of a checkpoint response as they can be rescued by caffeine, an inhibitor of ATM or ATR kinases.

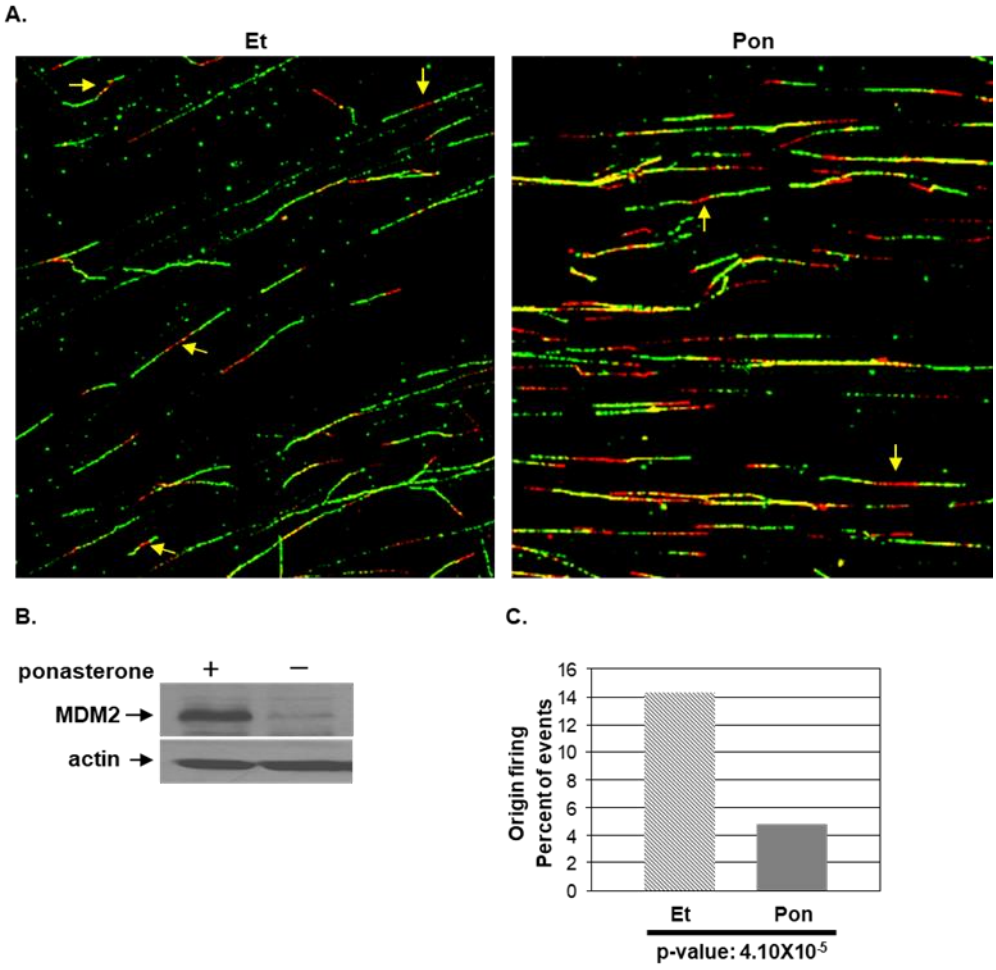

Figure 7. MDM2 inhibits firing of DNA replication origins. The figure shows fiber analysis of replicating DNA from H1299 cells that express MDM2 when induced by Ponasterone A for 24 hours, sequentially pulse labelled for 10 minutes by IdU and 20 minutes by CldU and immunostained with fluorescently labeled antibodies. Representative images of labeled DNA fibers from ethanol (Et) or Ponasterone A (Pon)-treated H1299 cells (A) are shown. Arrows show newly fired single origins. Expression of MDM2 in Ponasterone A or ethanol treated cells was determined by Western blot analysis (B). Actin was used as a loading control. Percentages of bi-directional single origins in Ponasterone A (Pon) or ethanol (Et) treated cells are shown by bar graphs (C). Two hundred to 500 fibers were scored for each sample. p-values are indicated at the bottom of the bar graphs.

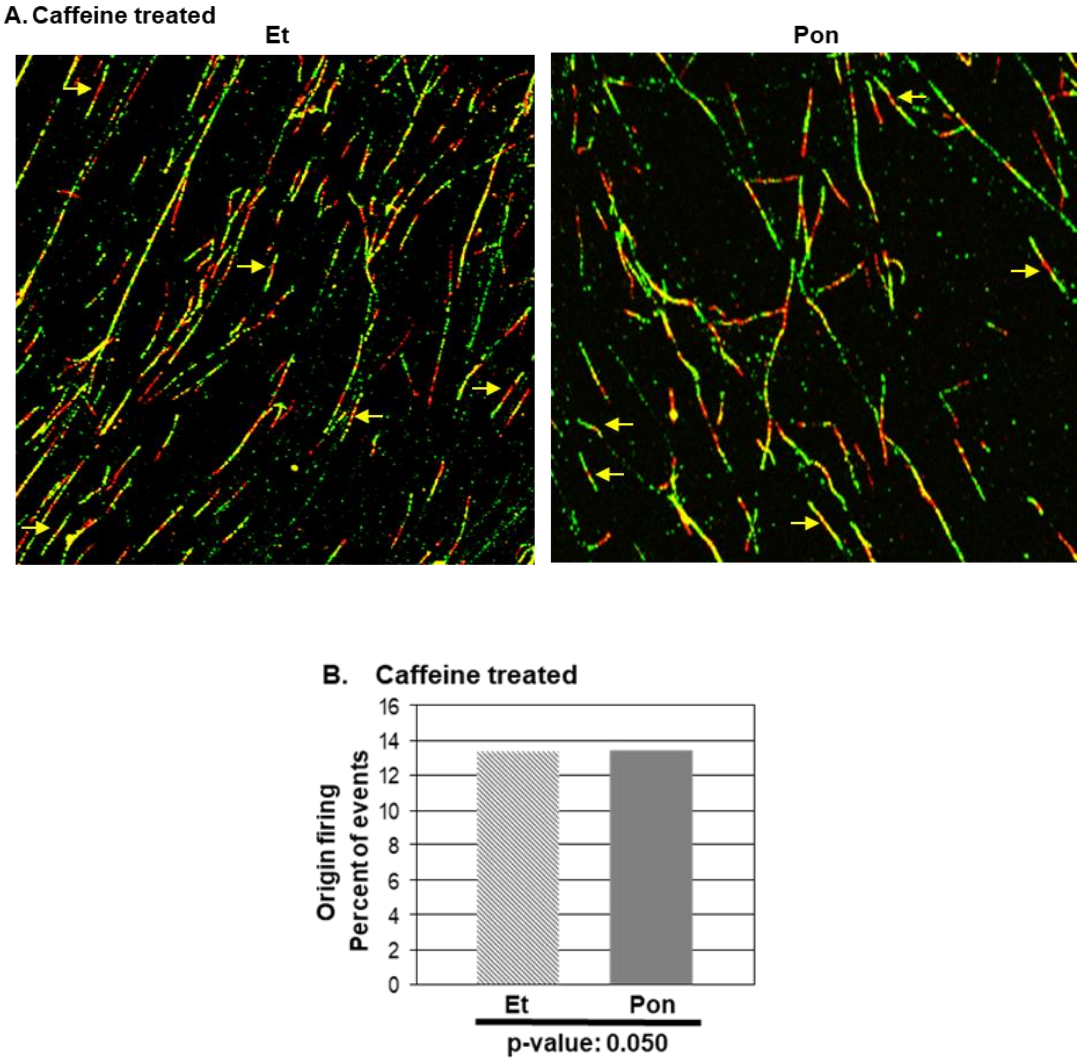

Figure 8. MDM2-mediated inhibition of origin firing can be rescued by caffeine. The figure shows fiber analysis of replicating DNA from H1299 cells induced to express MDM2 with Ponasterone A for 24 hours, followed by treatment with caffeine for 30 minutes and sequentially pulse labeled with IdU and CldU as described above. Representative images of labeled DNA fibers are shown (A). Arrows indicate newly fired single origins. Percentages of bi-directional single origins are shown by bar graphs (B). Three hundred to 600 fibers were scored for each sample. p-values are indicated at the bottom of the bar graphs

MDM2 inhibits firing of DNA replication origins at the onset of S phase, and the inhibition can be rescued by caffeine: Since MDM2 reduced the frequency of origin firing in ecdysone inducible H1299 cells (Figure 7), we determined whether MDM2 inhibits origin firing at the early or late S phase. As reasoned above, we determined the cyclin A-independent replication inhibitory function of MDM2 using lung cells isolated from littermate p53-/- and p53-/-:MDM2Tr mice. Cells were partially synchronized by density arrest and replating. The time of onset of the S phase was determined by pulse labeling with bromodeoxyuridine (BrdU) and identifying labeled nuclei at different time intervals. Fiber analysis of replicating DNA from these cells (Figure 9) was performed at different time intervals after release from contact inhibition, as described above. Scoring of untangled labeled fibers (Figure 9A) revealed that, in comparison to p53-/- lung cells, the frequency of origin firing was drastically reduced in p53-/-:MDM2 transgenic lung cells at 12 hours after release of contact inhibition. This difference in origin firing not only disappeared, but also exceeded the frequency of fired origins in p53-/- cells at 16 hours (Figure 9B, p-value= $3.479X10^{-11}$). Analysis at subsequent time points did not show a significant difference in origin firing between the two cell-types (p-value = 0.195). Expression of MDM2 was confirmed by Western blot analysis (Figure 9C). This data suggests that MDM2 inhibits origin firing at the onset of S phase, and this inhibition disappears at a later time point.

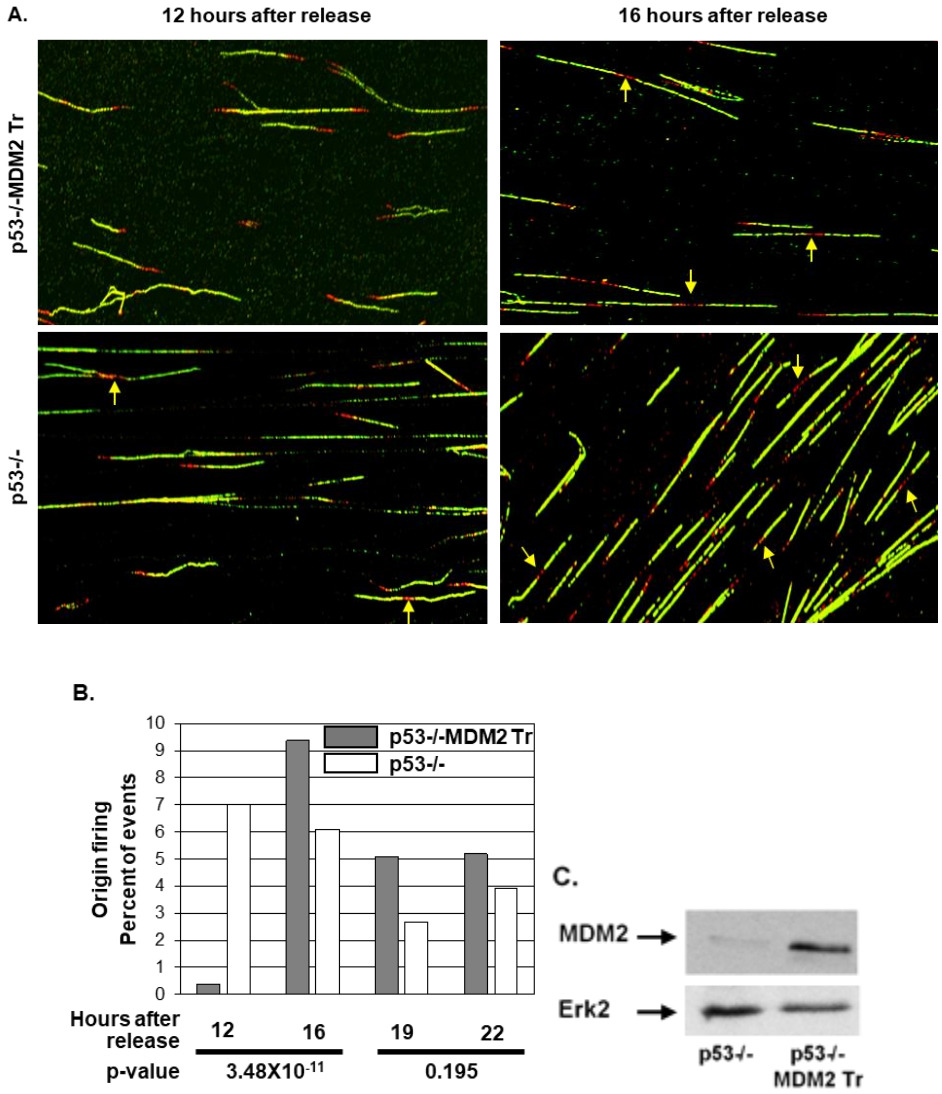

Figure 9. MDM2 inhibits firing of DNA replication origins at the early S phase. The figure shows fiber analysis of replicating DNA from cultured lung cells of p53-/- and p53-/-:MDM2Tr mice sequentially pulse labeled by IdU for 10 minutes and CldU for 20 minutes at different times after replating of density arrested cells. Representative images of labeled DNA fibers at 12 and 16 hours after replating are shown (A). Arrows indicate newly fired single origins. The bar graphs show the percentage of bi-directional single origins at different time intervals after replating. (B). Approximately 150 to 250 labeled fibers were scored for each sample. p-values are indicated at the bottom of the bar graphs. Expression of MDM2 was determined by Western blot analysis (C). Erk-2 was used as a loading control.

The transient nature of inhibition of origin firing at the onset of S phase led us to investigate if MDM2-mediated inhibition of origin firing at the early S phase is a result of an activated checkpoint response. To test this hypothesis, the lung cells from littermate p53-/- and p53-/- and p53-/-:MDM2Tr described above were partially synchronized by density arrest and replating. The cells were treated with caffeine, and fiber analysis of replicating DNA was performed at 12 hours as described above (Figure 10A, B). Our data showed that at 12 hours after replating, inhibition of origin firing was reversed by caffeine treatment in p53-/-:MDM2Tr lung cells drastically increasing the percentage of fired origins (Figure 10C, p-value = $4.567X10^{-5}$). Lung cells from littermate p53-/- mice did not show an increase in origin firing at this time point (Figure 10C, p-value = 0.04). Thus, elevated levels of MDM2 inhibit origin firing at the onset of S phase, which can be reversed by caffeine, an inhibitor of checkpoint kinases, suggesting an involvement of intra-S phase checkpoint control in the process.

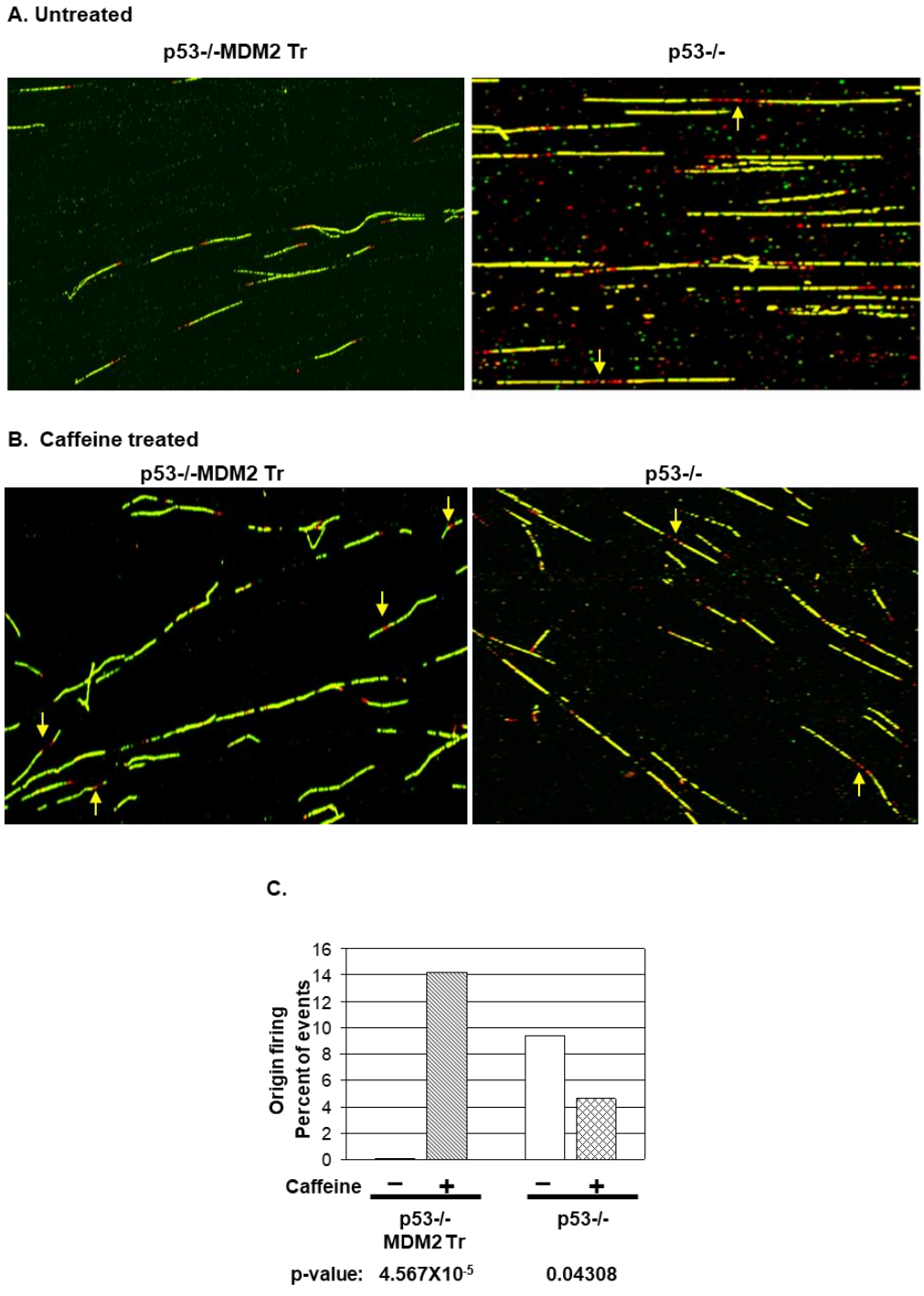

Figure 10. Inhibition of origin firing by MDM2 can be rescued by caffeine. The figure shows fiber analysis of replicating DNA from cultured lung cells of p53-/- and p53-/-:MDM2Tr mice, untreated or treated with caffeine and sequentially pulse labeled by IdU

and CldU at 12 hrs after replating of density arrested cells. Representative images of labeled DNA fibers without (A) or with (B) caffeine treatment at 12 hours after replating are shown. Arrows indicate newly fired single origins. The bar graphs show the percentage of bi-directional single origins determined by fiber analysis (C). p-values are indicated at the bottom of the bar graphs. Approximately 100 to 200 labeled fibers were scored for each sample.

MDM2 induces chk1 phosphorylation at the onset of S phase: As discussed earlier, oncogenes are known to induce a checkpoint response (106, 109, 110). Since MDM2 is a known oncogene, and it inhibits origin firing at the early S phase, which can be overridden by the checkpoint kinase inhibitor, caffeine (Figures 8 and 10), we investigated if MDM2 activates the intra-S phase checkpoint kinase during DNA replication in the absence of WT p53. As described above, matched sets of lung cells isolated from littermate p53-/- and p53-/-:MDM2Tr were partially synchronized by density arrest and replating. Presence of p-chk1 was measured at 12 hrs after replating by Western blot analysis of the cell extracts. Our data indicated that 12 hours after replating, p-chk1 levels in lung cells from p53-/-:MDM2Tr mice increased sharply compared to that in the p53-/- mice (Figure 11A).

To confirm that the increased p-chk1 level is due to the presence of elevated levels of MDM2, MDM2 was knocked down in p53-/-:MDM2Tr lung cells. Lung cells from and p53-/-:MDM2Tr mice were infected with lentiviral vectors expressing shRNA against MDM2 or GFP control. Cells generated from isolated colonies expressing shRNA against MDM2 or a control shRNA against GFP were partially synchronized by contact inhibition and replating. Twelve hours after replating, p-chk1 levels were determined by Western blot analysis. Our data showed that knockdown of MDM2 levels drastically diminished p-chk1 levels (Figure 11B).

We also investigated if elevation of MDM2 expression in H1299 cells leads to activation of chk1 phosphorylation. H1299 cells expressing MDM2 from ecdysone-inducible promoter were induced to express MDM2 with Ponasterone A, and p-chk1 levels in the Ponasterone A and control (ethanol treated) cells were determined by Western blot analysis of the cell extracts. Our data indicated that elevation of MDM2 levels by Ponasterone A leads to elevation of p-chk1 levels (Figure 11C). Thus our results indicate that MDM2 can activate phosphorylation of the intra-S phase checkpoint kinase chk1.

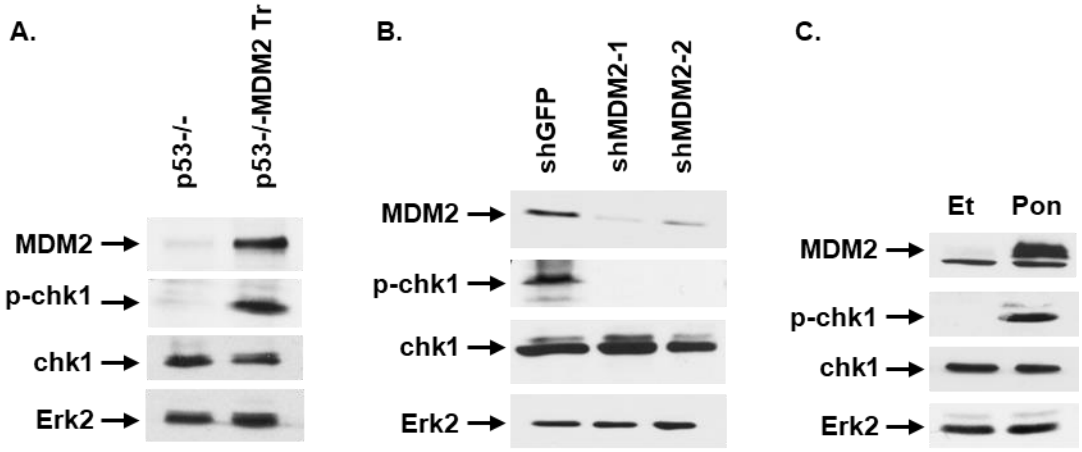

Figure 11. MDM2 induces chk1 phosphorylation at the onset of S phase. The figure shows detection of MDM2, p-chk1 and chk1 by Western blot analysis of extracts prepared from cells expressing either elevated or knocked-down levels of MDM2. Cultured lung cells of p53-/- and p53-/-:MDM2Tr mice (A), and cultured lung cells of p53-/-:MDM2Tr mice stably expressing shRNA against MDM2 (shMDM2-1, shMDM2-2) or GFP (shGFP) (B), at 12 hours after replating following density arrest were used. Western blot analysis of extracts from H1299 cells expressing MDM2 from an ecdysone inducible promoter after treatment with Ponasterone A (Pon) or Ethanol (Et) for 24 hours (C) is also shown. Erk-2 was used as a loading control.

MDM2 hastens the intra-S phase checkpoint response: Checkpoint kinases are known to limit origin firing during normal S phase progress (111, 112). Since p53-/-:MDM2Tr lung cells showed a drastic increase in chk1 phosphorylation and inhibition of origin firing compared to p53-/- lung cells 12 hours after contact inhibition and replating, we determined if p53-/- cells activate a checkpoint response at a later time point. For this purpose p53-/- and p53-/-:MDM2Tr lung cells were contact inhibited and replated. DNA replication origin firing and chk1 phosphorylation were determined at 16 hours after replating of density arrested cells as described above. Scoring of labeled DNA fibers (Figure 12A) revealed that consistent with the experiment shown in Figure 4, a similar percentage of origins were fired in both the cell types (Figure 12A, C). Inhibition of checkpoint dependent origin firing was evidenced by release of this inhibition by treatment with caffeine to a similar extent (approximately 2.4-fold) in the two cell types (Figure 12B, C, p value = 4.849X10-5). Consistent with these observations both the cell types showed chk1 phosphorylation to a similar extent at 16 hours after replating (Figure 12D). These data indicate that the p53-/-:MDM2Tr cells induce S phase checkpoint response earlier than p53-/- cells.

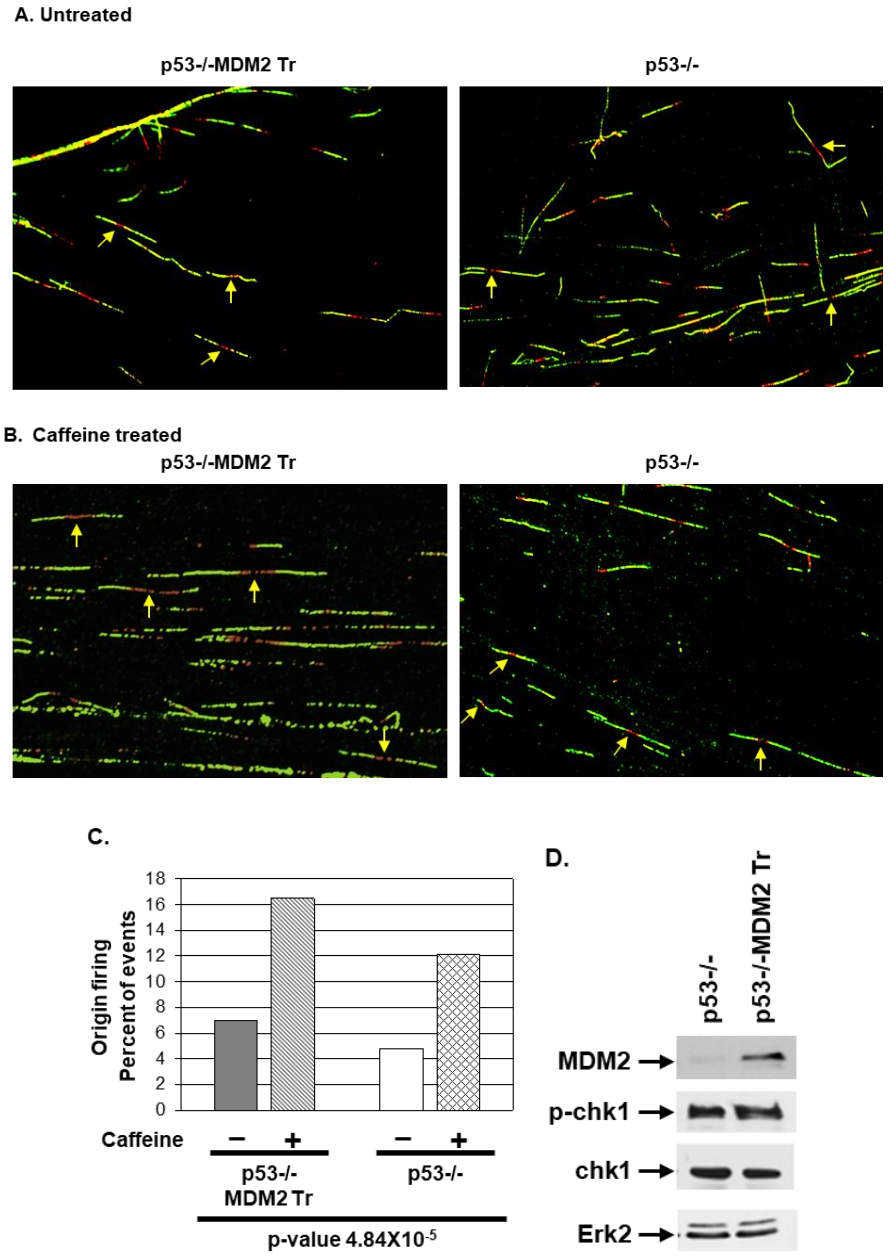

Figure 12. MDM2 hastens intra-S phase checkpoint response. The figure shows that firing of DNA replication origins is increased by caffeine treatment at 16 hours after replating of density arrested cultured lung cells of both p53-/- and p53-/-:MDM2Tr mice. Representative Fiber images of replicating DNA from cultured of p53-/- and p53-/-:MDM2Tr lung cells untreated (A) or treated with (B) caffeine and pulse labeled at 16 hours after replating are shown. Arrows indicate newly fired single origins. The bar graphs show the percentage of bi-directional single origins determined by fiber analysis (C). p-values are

indicated at the bottom of the bar graphs. Approximately 230 to 270 labeled DNA fibers were scored for each sample. Expression of MDM2 and chk1 phosphorylation at 16 hours after replating of the density arrested p53-/- and p53-/-:MDM2Tr lung cells is shown by Western blot analysis of the cell extracts in the right panel (D). Erk-2 was used as loading control. Migration of MDM2, p-chk1, chk1 and Erk2 are shown by arrows.

MDM2 elevates MLL histone methyl transferase levels: Next we wished to determine how early induction of chk1 phosphorylation by MDM2 would lead to inhibition of origin firing. Although the phosphatase CDC25A that control activation of cyclin dependent kinases have been implicated in inhibition of origin firing by chk1 phosphorylation (94, 111), MDM2 did not alter CDC25A levels in our experiments (data not shown). Alternatively, stabilization of MLL histone methyl transferase has been reported to inhibit origin firing (95). Translocation of the MLL gene has been related to childhood and adult leukemia (113). The gene codes for a precursor protein, which is processed to generate a heterodimer, $MLL^{N320/C180}$. MLL deficiency causes S-phase checkpoint dysfunction (114). MLL contributes to crucial cellular functions by methylating H3K4 by its C-terminal SET domain. Intra S phase ATR signaling phosphorylates MLL histone methyl transferase (MLL^{C180}) preventing its degradation (95). Accumulated MLL^{C180} then methylates H3K4 diminishing CDC45 loading to delay DNA replication (95).

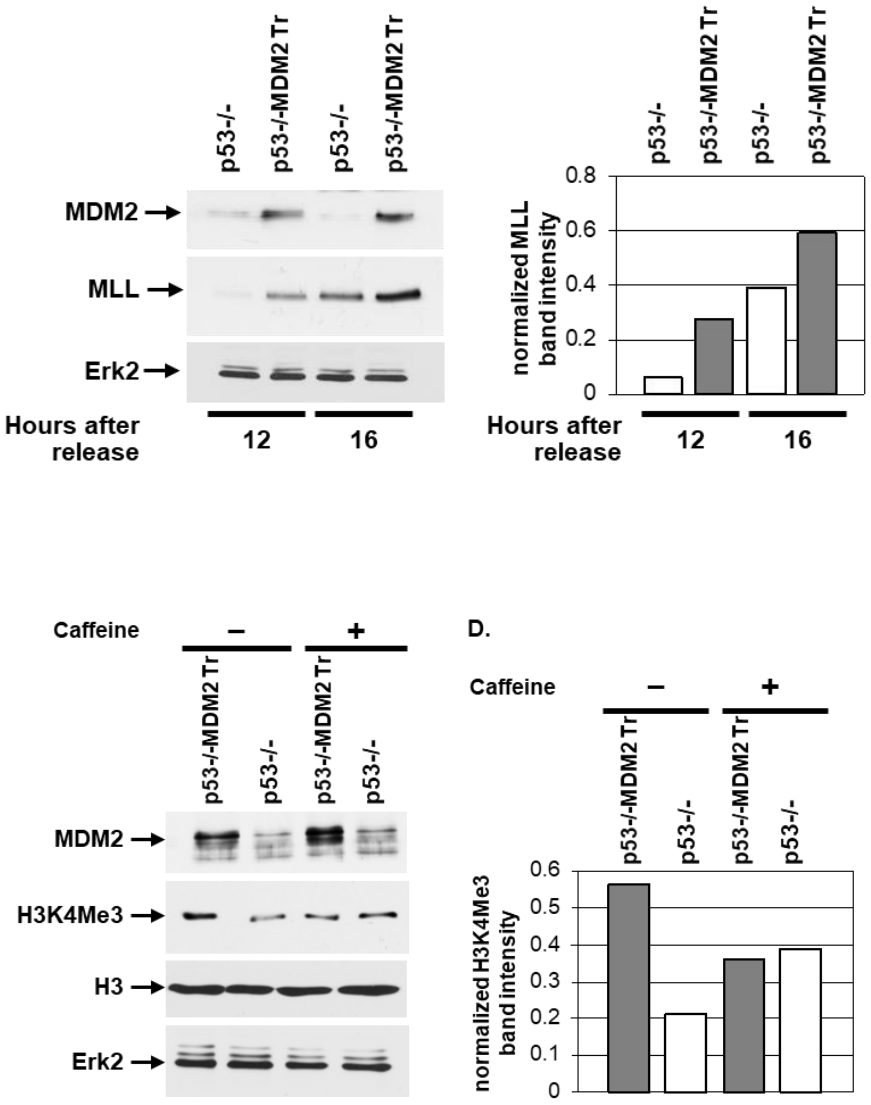

Figure 13. MDM2 elevates MLL histone methyl transferase levels (A, B) and H3K4 tri-methylation in a checkpoint dependent manner (C, D). The figure shows Western blot analysis of extracts prepared from cultured lung cells of p53-/- and p53-/-:MDM2Tr mice at 12 and 16 hours after replating of density arrested cells to determine accumulation of MLL histone methyl transferase levels using a specific antibody (A), and acid extracts prepared from cultured lung cells of p53-/- and p53-/-:MDM2Tr mice at 12 hours after replating of density arrested cells with or without caffeine treatment to determine H3K4Me3 levels using a specific antibody (C). Erk-2 was used as a loading control in both the experiments. Migration of MDM2, MLL histone methyl transferase (MLL), H3K4Me3, H3 and Erk2 are shown by arrows. Differences in the MLL histone methyl transferase (B) and

H3K4Me3 (D) levels were determined by densitometry and are shown by bar graphs at the right panel of each blot.

Since elevation of MDM2 levels caused chk1 phosphorylation and inhibition of origin firing, we investigated if MDM2 elevates MLL^{C180} levels at the onset of S phase. We determined MLL^{C180} levels in extracts prepared from p53-/- and p53-/-:MDM2Tr lung cells at 12 and 16 hours after density arrest and replating by Western blot analysis as described above. Our data (Figure 13A) showed that compared to p53-/- lung cells, MLL^{C180} levels are remarkably elevated in p53-/-:MDM2Tr lung cells at 12 hours. Densitometric analysis (Figure 13B) revealed a 4.5-fold increase in MLL^{C180} levels p53-/-:MDM2Tr lung cells. However, at 16 hours the MLL^{C180} levels also increased in p53-/- lung cells, and the difference in the MLL^{C180} levels in the two cell types was reduced (1.5-fold). This result indicates that presence of MDM2 leads to early accumulation of MLL^{C180}.

MDM2 upregulates H3K4 tri-methylation in a checkpoint dependent manner: Early accumulation of MLL^{C180} in p53-/-:MDM2Tr lung cells led us to investigate if these cells show enhanced tri-methylation of H3K4 (H3K4Me3), and if increase in H3K4Me3 levels is checkpoint dependent. Acid extraction of the genomic DNA of p53-/- and p53-/-:MDM2Tr lung cells harvested 12 hours after density arrest and replating followed by Western blot analysis revealed higher H3K4Me3 levels in p53-/-:MDM2Tr than p53-/- lung cells (Figure 13C). Densitometric analysis (Figure 13D) revealed a more than 2.5-fold increase in the H3K4Me3 levels in p53-/-:MDM2Tr compared to p53-/- lung cells. To determine if the increase in H3K4Me3 levels is due to checkpoint activation by MDM2, p53-

/- and p53-/-:MDM2Tr lung cells were treated with caffeine before harvesting at 12 hours. Cells were then harvested and their genomic DNA was subjected to acid extraction. Western blot analysis of the extracts revealed that caffeine treatment abrogates the increase in H3K4Me3 levels in p53-/-:MDM2Tr lung cells (Figure 13C, D). This data indicate that inhibition of checkpoint activation in cells with elevated levels of MDM2 abrogates the increase in tri-methylation of H3K4.

MDM2 up-regulates cyclin D2 and cyclin A expression in the absence of p53: We next investigated how MDM2 may activate the intra-S phase checkpoint in the absence of p53. Although MDM2 inhibits cyclin A expression in normal cells with WT p53 (32), our unpublished gene expression analysis in p53-/- lung cells suggested that MDM2 up-regulates expression of cyclin D2 in the absence of WT p53. Overexpression of cyclins is known to induce excessive origin firing causing replication stress (101) and slowing of DNA replication. This information led us to investigate if MDM2 up-regulates expression of cyclin D2. We therefore determined expression of cyclin D2 in p53-/- and p53-/-:MDM2Tr lung cells both at the level of protein by Western blot analysis and RNA by QPCR as described earlier (33). Our data showed elevated levels of cyclin D2 protein (Figure 14A) and RNA (Figure 14B) in p53-/-:MDM2Tr lung cells compared to p53-/- lung cells. Densitometric analysis revealed a more than 3-fold increase in the cyclin D2 protein levels, and QPCR data showed approximately 3-fold increase in the RNA levels (middle panels) suggesting that MDM2 upregulates cyclin D2 expression. Induction of MDM2 expression

from an ecdysone inducible promoter using Ponasterone A in H1299 cells showed similar data confirming that MDM2 upregulates cyclin D2 (Figure 15).

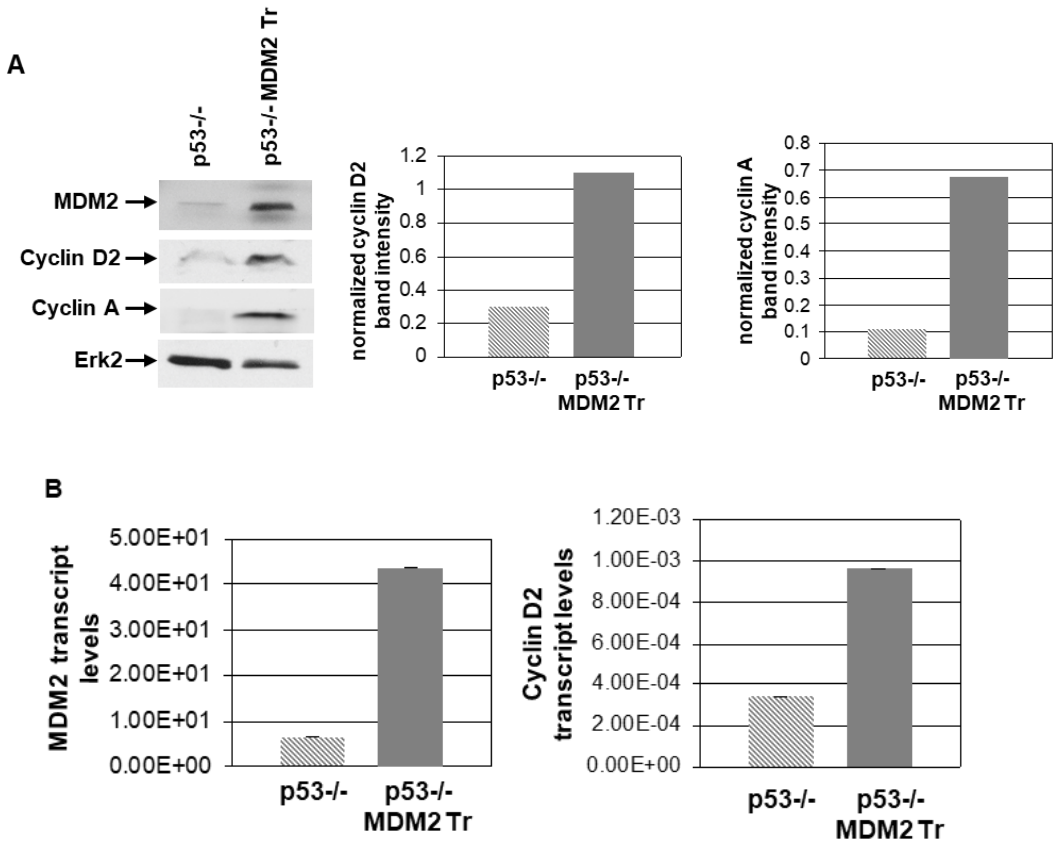

Figure 14. MDM2 increases expression of cyclin D2 and cyclin A in cultured lung cells from p53-/- and p53-/-:MDM2Tr mice. The figure shows MDM2 and endogenous cyclin D2 and cyclin A protein levels (A) and MDM2 and cyclin D2 transcripts (B) in lung cells of p53-/- and p53-/-:MDM2Tr mice determined by Western blot analysis and QPCR respectively. Erk2 was used as a loading control in Western blot analysis. Arrows indicate migration of MDM2, cyclin D2, cyclin A and Erk2. The densitometric analysis of cyclin D2 and cyclin A expression are shown by bar graphs on the right (A), and the transcript levels were normalized by GAPDH expression, and are shown by bar graphs (B).

Since elevated expression of cyclin D2 should allow crossing of the restriction point of cell cycle and thus should lead to an increase in cyclin A expression, we determined cyclin

A protein levels in p53-/- and p53-/-:MDM2Tr lung cells by Western blot analysis. Indeed, compared to p53-/- lung cells, p53-/-:MDM2Tr lung cells showed a sharp elevation of cyclin A levels (Figure 9A, top right panel) suggesting that elevation of cyclin D2 levels boosted cell cycle progress. H1299 cells expressing MDM2 from an ecdysone-inducible promoter when induced to express MDM2 with Ponasterone A also showed elevated levels of cyclin A (Figure 15B) implicating MDM2 in the accelerated progress towards initiation of DNA replication.

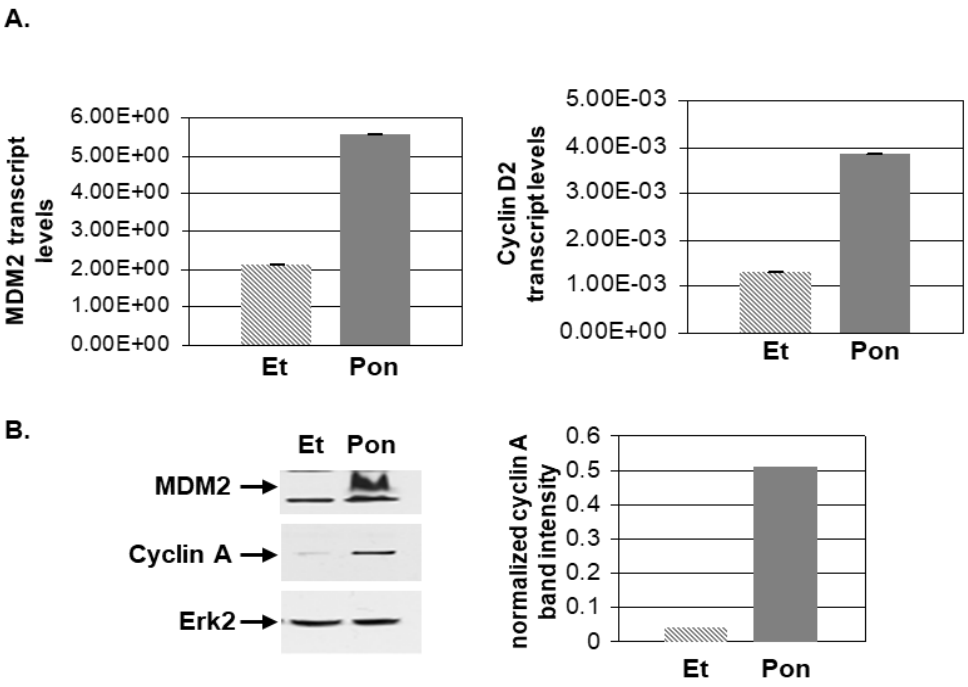

Figure 15. MDM2 increases the expression of cyclin D2 and cyclin A in H1299 lung cancer cells. The figure shows MDM2 and endogenous cyclin D2 transcript (A) and cyclin A protein levels (B) in H1299 cells expressing MDM2 from an ecdysone inducible promoter determined by QPCR and Western blot analysis respectively after treatment with Ponasterone A (Pon) or ethanol (Et) for 24 hours. The transcript levels were normalized by GAPDH expression, and are shown by bar graphs (A), and the densitometric analysis of cyclin A expression are shown by bar graphs on the right (B). Erk2 was used as a loading control. Arrows indicate migration of MDM2, cyclin A and Erk2.

Overexpression of MDM2 in p53-null human osteosarcoma Saos-2 cells, which harbors nonfunctional RB (115, 116), increased cyclin D2 expression., However, increase in cyclin A expression, and checkpoint phosphorylation by MDM2 was less significant compared to that of ponasterone induced H1299 or p53-/- MDM2Tr cells (Figures 11 and 14) suggesting that defects in cyclin D2 downstream pathway desensitizes intra-S phase checkpoint response (Figure 16).

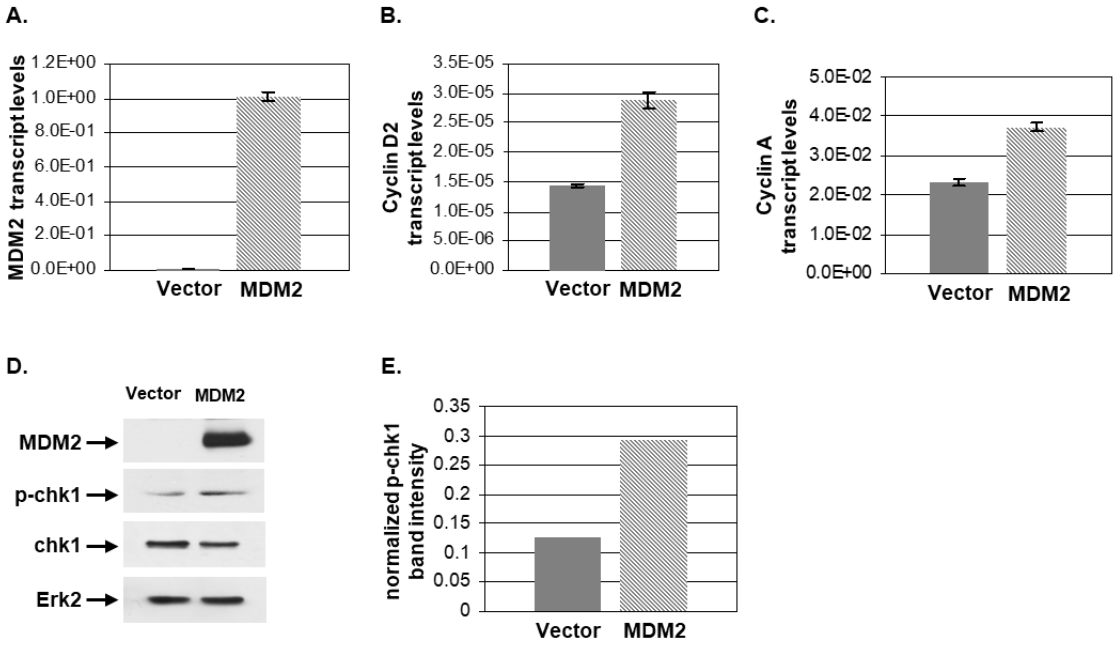

Figure 16. MDM2 overexpression in Saos-2 cells elevates cyclin D2 expression, but not cyclin A or chk1 phosphorylation significantly. MDM2 expression plasmid or an empty vector (5 μg) was introduced in p53-null human osteosarcoma Saos-2 cells ($3X10^6$), which harbor nonfunctional RB, by nucleofection. Cells were harvested after 12 hours and either processed for RNA extraction and cDNA preparation or for Western blot analysis. MDM2 (A), cyclin D2 (B) and cyclin A (C) transcript levels normalized by GAPDH expression are shown by bar graphs. MDM2, p-chk1, chk1 and erk2 levels were determined by Western blot analysis (D). Arrows indicate migration of MDM2, p-chk1, chk1 and Erk2. Erk2 was used as a loading control in Western blot analysis. The densitometric analysis of MDM2, p-chk1, chk1 levels are shown by bar graphs on the right (E). The data show that

MDM2 increased cyclin D2 expression (B). However, increase in cyclin A expression (C), and checkpoint phosphorylation (D, E) by MDM2 was not significant suggesting that defects in cyclin D2 downstream pathway desensitizes intra-S phase checkpoint response.

To confirm that increased levels of cyclin D2 expression in p53-/-:MDM2Tr lung cells is due to elevated levels of MDM2, we determined if knock down of MDM2 in these cells would diminish cyclin D2 expression. Our data showed that knockdown of MDM2 decreased cyclin D2 expression both at the levels of RNA and protein (Figure 17).

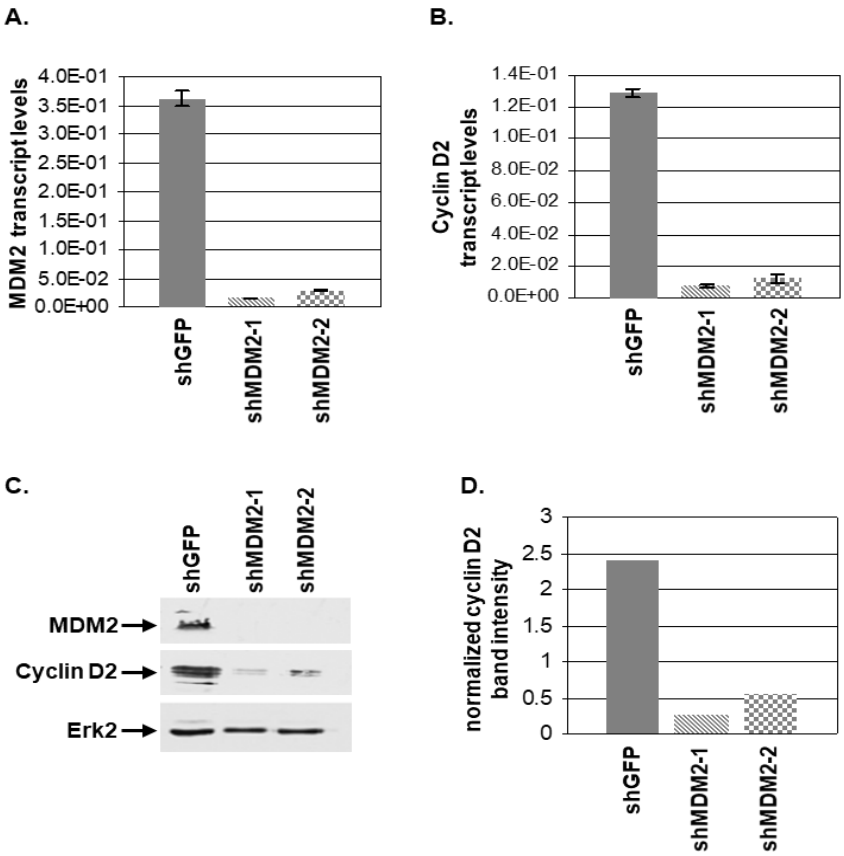

Figure 17. Knockdown of MDM2 decreases cyclin D2 expression drastically. To confirm that increased levels of cyclin D2 expression in lung cells of p53-/-:MDM2Tr mouse is due to elevated levels of MDM2, we determined if knock down of MDM2 in these cells would diminish cyclin D2 expression. Expression of MDM2 (A) and cyclin D2 (B) transcripts in p53-/-:MDM2Tr lung cells expressing shRNA against MDM2 (shMDM2-1,

shMDM2-2) or GFP (shGFP) are shown by bar graphs. Transcript levels were normalized by GAPDH expression. MDM2 cyclin D2 and Erk2 protein expression was determined by Western blot analysis. Arrows indicate migration of MDM2, cyclin D2 and Erk2. Erk2 was used as a loading control in Western blot analysis. The densitometric analysis of MDM2 and cyclin D2 protein levels normalized by Erk2 levels are shown by bar graphs on the right (D). Our data showed that knockdown of MDM2 decreased cyclin D2 expression.

Cyclin D2 is expressed in response to mitogenic signals (117) , and PI3-kinase pathway regulate cyclin D2 expression (118). Since MDM2 up-regulates PI3-kinase activity(30), we determined if MDM2-mediated upregulation of cyclin D2 expression is susceptible to a PI3-kinase inhibitor, Wortmannin (119). Our data show that Wortmannin inhibits increase in cyclin D2 expression by MDM2- Figure 18), implicating MDM2-mediated activation of PI3 kinase activity in cyclin D2 up-regulation by MDM2.

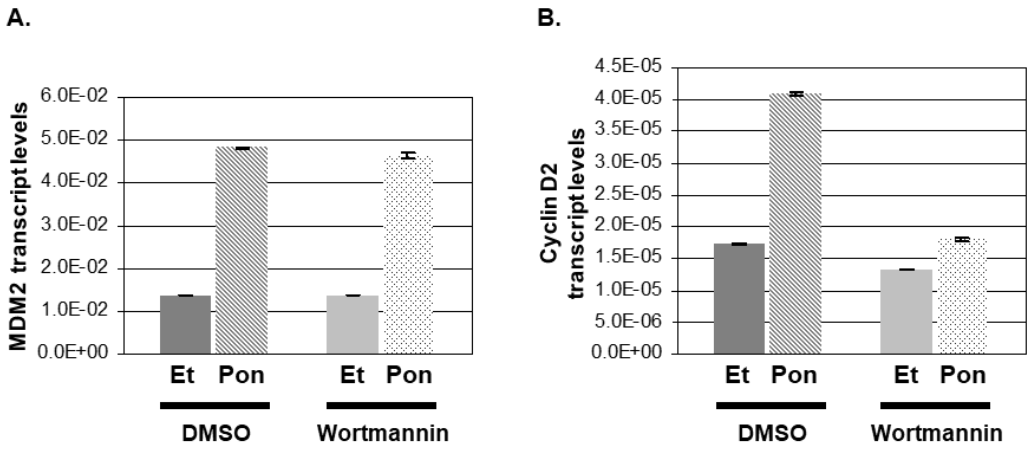

Figure 18. The PI3-kinase inhibitor Wortmannin inhibits MDM2-mediated up-regulation of cyclin D2 expression. Cyclin D2 is expressed in response to mitogenic signals (117), and PI3-kinase pathway has been shown to regulate cyclin D2 expression (118). Since MDM2 up-regulates PI3-kinase activity (30), we determined if MDM2-mediated upregulation of cyclin D2 expression is susceptible to a PI3-kinase inhibitor, Wortmannin (119). To determine whether wortmannin inhibits increase in cyclin D2 expression by MDM2, H1299 cells expressing MDM2 from ecdysone inducible promoter were either induced to express MDM2 by Ponasterone A (Pon) treatment or left uninduced with ethanol

(Et) treatment for 24 hours in the presence of Wortmannin (50nM) or DMSO for last 4 hours. Expression of MDM2 and cyclin D2 transcript levels normalized by GAPDH expression is shown by bar graphs. Our data show that Wortmannin inhibits increase in cyclin D2 expression by MDM2.

MDM2 hastens S phase entry of cells: Since elevated levels of MDM2 increased cyclin D2 expression, we determined if the presence of MDM2 accelerated S phase entry of cells thus activating the intra-S phase checkpoint response sooner in p53-/-:MDM2Tr lung cells compared to p53-/- lung cells to prevent further origin firing. We therefore investigated the number of p53-/- and p53-/-:MDM2Tr lung cells entering S phase at 12 hours after replating of density arrested cells. Cells were pulse labeled with IdU at different time intervals, fixed, acid treated, stained with a specific antibody and mounted in antifade with DAPI as described in materials and methods. Images (Figure 19A) of 150 to 200 nuclei were collected by confocal microscopy from each sample and percentage of IdU labeled nuclei was determined. Our data showed lack of IdU incorporation until 11 hrs after replating (data not shown). At 12 hours the cells showed IdU incorporation (Figure 19A), and an average of 7% p53-/- lung cells incorporated IdU as opposed to 17% of p53-/-:MDM2Tr lung cells (Figure 19B). These data suggest accelerated S phase entry of p53-/-:MDM2Tr lung cells compared to p53-/- lung cells at early S phase.

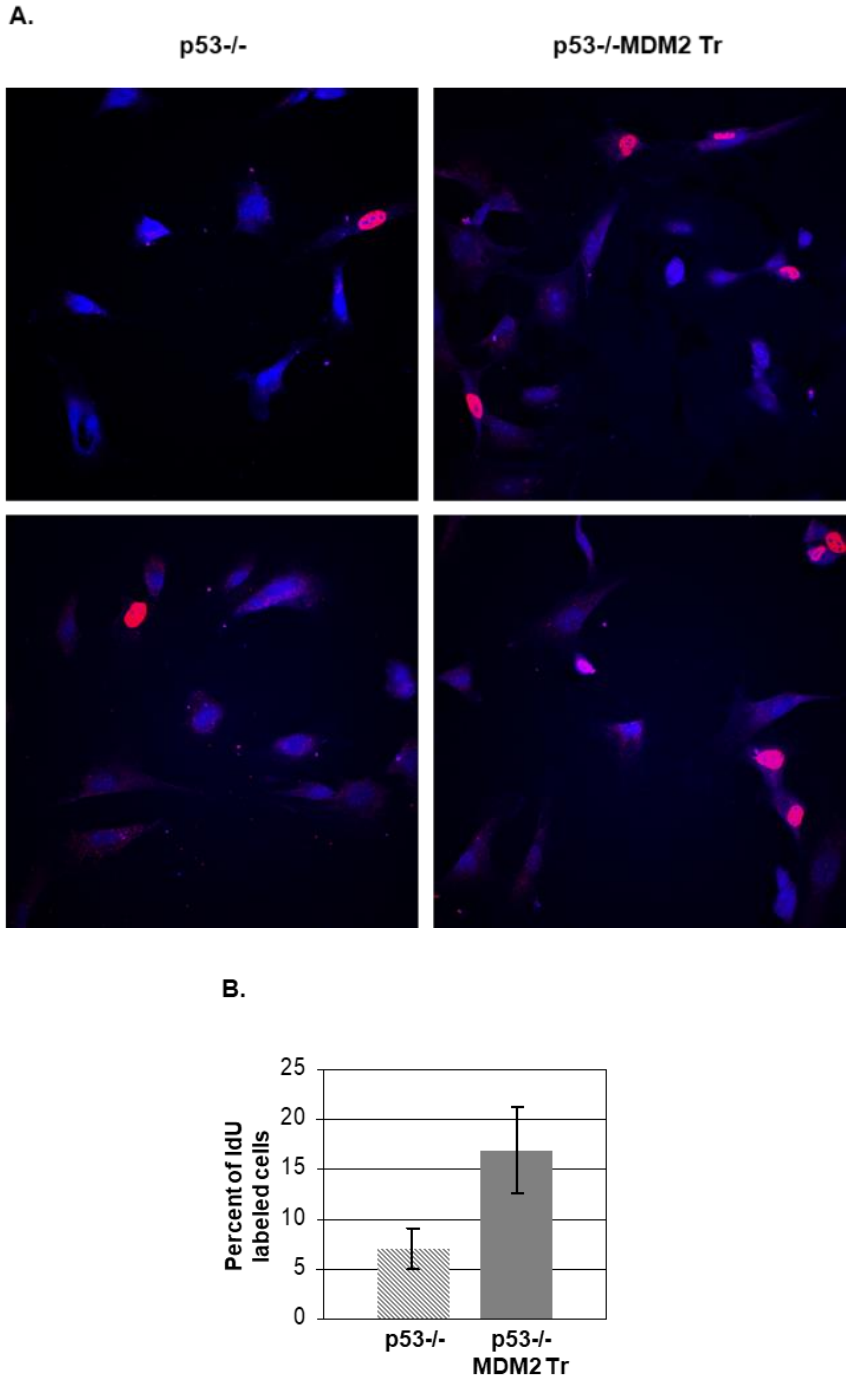

Figure 19. MDM2 hastens S phase entry of cells. Cultured lung cells of p53-/- and p53-/-:MDM2Tr mice were pulse labeled by IdU at 12 hours after replating of density arrested cells and immunostained with fluorescently labeled antibodies. Cells were stained with DAPI for detection of nuclei. One hundred fifty to 200 nuclei were scored in each of

triplicate sets of experiments. Two representative images of each of labeled p53-/- or p53-/-:MDM2Tr lung cells are shown (A). The bar graph (C) shows the percentage of IdU labeled p53-/- or p53-/-:MDM2Tr lung cells at 12 hours after replating of density-arrested cells.

Inhibition of cyclin dependent kinases that activate replication origins abrogates MDM2-mediated chk1 phosphorylation: In metazoan cells, origins are activated by cyclin dependent kinases and cdc7 kinases, which phosphorylate the minichromosome maintenance (MCM) proteins 2-7 activating the MCM helicases and inducing melting of double stranded DNA at the origin of replication (93, 120). Since MDM2 upregulates cyclin D2 and cyclin A expression in cells lacking WT p53, we considered if an increase in expression of cyclins led to enhanced activation of cyclin dependent kinases, and thus activation of origins, generating replication stress and intra-S phase checkpoint signaling. A cdc7 kinase inhibitor PHA767491 has been shown to specifically prevent activation of origins by inhibiting DNA helicases, but not to impede fork progression (101, 102).

To test whether origin activation by MDM2 induces chk1 phosphorylation, p53-/- and p53-/-:MDM2Tr lung cells were partially synchronized by density arrest and replating; cells were then treated with PHA767491 to prevent origin activation before harvesting at 12 hours, and chk1 phosphorylation in the cell extracts was determined by Western blot analysis. Our data (Figure 20) showed that indeed treatment with the cdc7 inhibitor abrogated MDM2 mediated chk1 phosphorylation. These data indicate that an increase in cyclin D2 and consequently cyclin A expression by MDM2 hastens untimely origin activation promoting chk1 phosphorylation at the onset of S phase. Consistently, overexpression of MDM2 in human cancer cell Saos-2 with deleted p53 and inactive RB

although upregulates cyclin D2 does not increase cyclin A expression and chk1 phosphorylation significantly.

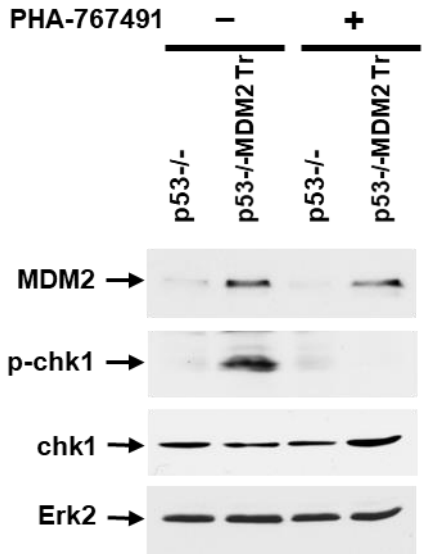

Figure 20. A specific inhibitor, PHA 767491, of cyclin dependent kinases that activate replication origins abrogates MDM2 mediated chk1 phosphorylation. Induction of chk1 phosphorylation was determined by Western blot analysis of extracts prepared from cultured lung cells of p53-/- and p53-/-:MDM2Tr mice at 12 hours after replating of density arrested cells with or without PHA 767491 (10μM) treatment for 1 hour. Erk-2 was used as a loading control. Migration of MDM2, p-chk1, chk1 and Erk2 are shown by arrows.

Discussion.

Oncogene overexpression is widely known to confer growth advantage in cells. On the other hand, several oncogenes that are frequently overexpressed in cancer cells and are used as predictive markers, can also hinder cell proliferation (105, 106, 109, 110, 121). According to the traditional model, the primary cause of oncogenesis mediated by the human

oncoprotein MDM2 has been ascribed to its ability to interact with and degrade WT p53. While this model is well supported, it does not explain amplification or overexpression of MDM2 in cancer cells that lack WT p53. In this chapter, we report a novel pathway by which MDM2 overexpression leads to unscheduled activation of DNA replication origins in the absence of p53, and a mechanism by which non-transformed cells may combat this function. Loss of this defense mechanism would lead to unscheduled initiation of DNA replication, which has been related to genome instability (94, 96, 97) .

We have reported earlier that MDM2 overexpression induces G1-arrest in the presence or absence of p53 (32, 88, 103). In apparently normal non-transformed cells, MDM2 inhibits expression of cyclin A. However, it requires p53 for this function (32). Although MDM2 cannot inhibit cyclin A expression in the absence of p53, it induces G1-arrest (88, 103). In this report, we show evidence that in the absence of p53 elevated levels of MDM2 induces a checkpoint response and thus inhibits firing of DNA replication origins (Figures 12, 14, 16) earlier than p53-/- cells expressing low levels of MDM2. As expected, p53-/- cells which express low levels of f MDM2 exhibit intra-S phase checkpoint arrest and inhibition of origin firing, but at a later time point than p53-/-:MDM2Tr cells (Figure 12).

We also show that an increase in MDM2 expression in the absence of p53 elevates cyclin D2 and cyclin A levels accelerating S phase entry (Figures 14 and 15). D-type cyclins have redundant functions, and are expressed at the early G1 (122). Cyclin D2 is activated by mitogenic signals and thought to convey extracellular signals that lead to DNA replication and cell proliferation (117). PTEN/GSK3 β pathway regulates cyclin D2 expression (118). Recently we have shown that MDM2 upregulates PI-3 kinase and GSK3 β phosphorylation.

In this chapter, we have provided evidence to implicate MDM2-mediated upregulation of PI3-kinase activity in cyclinD2 up-regulation by MDM2 (Figure 17). The exact mechanism of this transcriptional activation by MDM2 is under investigation at present. Also several transcription factors including Shh (sonic hedgehog) and Gli are known to participate in cyclin D2 expression (123). It remains to be determined how MDM2 may integrate in these pathways.

Presence of a higher percentage of IdU labeled p53-/-:MDM2Tr cells compared to p53-/- cells at 12 hours after contact inhibition and replating (Figure 12) indicates that cells expressing MDM2 initiate DNA replication earlier than p53-/- cells, and is consistent with elevation of cyclin D2 and cyclin A expression by MDM2. Elevation of cyclin D2 expression by MDM2 is expected to enable the cells to cross the restriction point of the cell cycle, leading to activation of origins. However, acceleration of origin activation (DNA melting) by MDM2 during S phase entry at 12 hours activates a checkpoint response (Figure 11), which allows activated origins to progress as evidenced by pulse labeled nuclei (Figure 11), but inhibits further origin firing in the cells (Figures 7 and 9). The S phase checkpoint response restricts origin firing at 16 hours in both p53-/- and p53-/-:MDM2Tr cells as evidenced by chk1 phosphorylation and increase in bi-directional single origin firing by caffeine (Figure 12). Consistently, a specific block in origin activation abrogates the MDM2-mediated checkpoint response (Figure 20). Our proposed model (Figure 21) depicts this pathway.

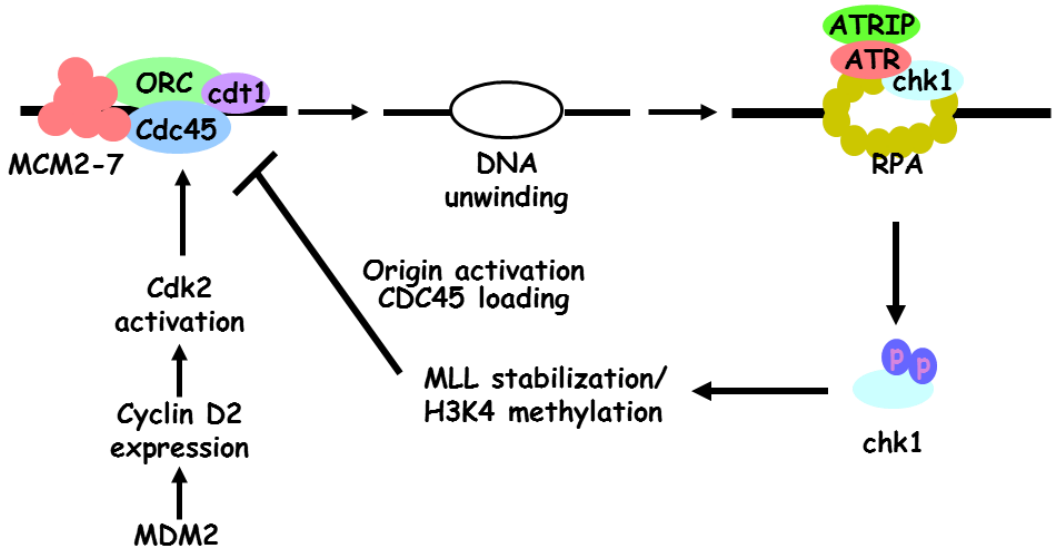

Figure 21. The proposed mechanism of MDM2-mediated checkpoint response.

Accumulation of MLL histone methyl transferase and consistently increase in H3K4 methylation by MDM2 suggest a mechanism by which the MDM2-mediated checkpoint response would lead to inhibition of origin firing. We also show that MDM2-mediated H3K4 methylation is checkpoint dependent, as it can be inhibited by caffeine (Figure 8C).

Conclusion.

Our data signifies that a compromised checkpoint response would allow an increase in untimely origin firing by MDM2. ATR and chk1 kinases are required for cell survival (124), and mutation or inactivation of ATR or chk1 kinases are not a frequent event observed during oncogenesis. However, mutation in the downstream participants, such as translocation of

N-terminal 1400 amino acids of MLL, has been observed frequently in leukemia and other cancers (95, 113). MLL fusion proteins have been demonstrated to function as dominant negative mutants that abrogate ATR mediated stabilization of MLL and compromise the S phase checkpoint (95). Therefore, overexpression or amplification of MDM2, which has also been reported in leukemia and lung cancers (24, 125), in cells with compromised MLL histone methyl transferase function could accelerate untimely DNA replication, which is known to induce gene abnormality (94, 96, 97).

Role of human oncoprotein MDM2 in lung epithelial injury repair

(Manuscript under preparation. Catherine Vaughan contributed towards generating the mouse constructs. Chris Rabender helped in performing radiation experiment.)

Introduction.

The conventional paradigm ascribes the tumorigenic function of MDM2 to its ability to destabilize the tumor suppressor p53. MDM2 interacts with wild-type (WT) p53, ubiquitinates and targets the tumor suppressor for degradation(126, 127). While studies in animal models suggest an essential role of MDM2 in development(34, 128), its function in normal adult animals is not clear. Consequences of MDM2 overexpression in animal models have been context dependent. Transgenic mice overexpressing MDM2 show tumor formation, although at a slower rate than p53-null mice(45). Targeted overexpression of MDM2 in lactating mammary gland of mice, although prevents normal development or morphogenesis of mammary gland, increases frequency of polyploid cells(38). MDM2 expression in the basal layer of epidermis at the embryonic stage generates hyperplasia and premalignant lesion(47), and in wing and eye of drosophila induces apoptosis(48). The role of MDM2 in the maintenance of nephron progenitor cells during organogenesis has been ascribed to its E3 ligase function balancing p53 levels(129, 130). A recent study has reported that MDM2 prevents differentiation of cultured mesenchymal stem cells independent of p53, promotes induced pluripotency (iPSC) in cultured mouse embryonic fibroblasts and induces clonogenic survival of cancer cells(131). These reports suggest that MDM2 may facilitate

cell proliferative events in a context dependent manner. The context-dependent cell proliferative effects of MDM2 overexpression suggest specific requirements for MDM2-mediated cell proliferation. However, the time, place, or steps of the proliferative events in the complex organs remain unknown to date.

Although MDM2 is overexpressed in human lung cancer, there is no existing mouse model to determine the consequence of MDM2 overexpression in adult lung. Given the frequent MDM2 overexpression found in human lung cancer in the presence of WT or mutant p53, the proliferative events induced by targeted MDM2 overexpression in adult mouse lungs in the presence of WT or mutant p53 were investigated in a mouse model capable of expressing human MDM2 in the lungs of adult mice from Club cell secretory protein (CCSP) or surfactant protein C (SPC) promoter after induction with Dox. The results revealed ability of MDM2 to induce proliferation of lung progenitor cells after lung injury, leading to epithelial regeneration. Furthermore, mice with one mdm2 allele displayed compromised ability of epithelial regeneration after lung injury, implicating active participation of MDM2 in lung injury repair in normal adult animals.

Materials and Methods.

Animal Studies: PCMV Tetracycline Response Element-TightMDM2 (pTRE-TightMDM2) mice were generated using C57BL/6 mice with the help of Institutional Transgenics Core. Club Cell Secretory Protein-rtTA (CCSP-rtTA) mice were a gift from Jeffery Whitsett, Cincinnati Children's Hospital, OH (132). Surfactant Protein C-rtTA (SPC-rtTA) and tetO-cre mice were purchased from Jackson Laboratory (Maine) (132, 133). p53

Lox-Stop-Lox R172H (p53 LSL R172H) mice were purchased from NCI Mouse Repository (Maryland)(134). P53+/-MDM2+/- mice were a gift from Guillermina Lozano, M.D. Anderson Cancer Center, TX (34). pTRE-TightMDM2 mice were crossed with CCSP-rtTA or SPC-rtTA mice to generate litter of mixed genetic background and allow inducible expression of human MDM2 in Club or the AT II cells of the mice lung. To direct p53-R172H and MDM2 expression to Club cells, LSL R172H mice were cross bred with pTRE-TightMDM2, tetO-Cre, and CCSP-rtTA to produce the desired strain of mice. MDM2 expression and/or p53-R172H expression in these mice were induced by feeding them 500μg/mL doxycycline in 5% w/v sucrose drinking water. Littermate mice on 5% w/v sucrose drinking water (D and CCSP-rtTA or SPC-rtTA only mice on dox were used as controls. All animals used in this study were maintained and assayed in accordance with federal guidelines and those established by the Institutional Animal Care and Use Committee.

Drug Treatments: For inducing injury in Club cells, naphthalene (Sigma-Aldrich) was dissolved in corn oil at 25 mg/ml concentration and administered intraperitoneally at a dosage of 250mg/kg. Lungs were harvested 72 hours after injury. For proliferation studies, mice were given intraperitoneal injections of 100mg/kg BrdU (Sigma) dissolved in sterile PBS 5 hours before sacrifice. For Akt inhibitor studies, MK-2206 HCl (Selleck Chemicals) was dissolved in 30% Captisol (Fisher) and administered orally at a dose of 120 mg/kg.

Irradiation protocol: CT-based treatment planning and execution used the Small Animal Radiation Research Platform (SARRP) from Xstrahl (Suwanee, Georgia). Animals were anesthetized with 2% isofluorane during CT-scanning and radiotherapy. Three beams

were generated post CT, delivering a total dose of 14Gy to the left lobe of the lung(135). The mice were euthanized, and lungs harvested 3 months after the irradiation.

Immunohistochemistry and fluorescence: All staining was performed on paraffin embedded sections. Samples were fixed in 4% para-formaldehyde for at least 24 hours. Tissue embedding, and sectioning was performed by Institutional Macromolecule Core Laboratory. Immunohistochemistry was performed with the Vectastain ABC Kit (Vector Labs) according to manufacturer's instructions and mounted using Permount solution (Fisher). BrDU incorporated sections were stained using BrdU staining kit (Life Technologies) following company's protocol. All counterstaining was performed using Hematoxylin solution (Vector Labs). Immunohistochemistry images were created using Labophot-2 microscope, captured using a 1080p HD 6MP microscope camera and processed using ISCapture software. Fluorescent stained sections were mounted using ProLong Gold Anitfade with DAPI and imaged by confocal microscopy (Zeiss LSM700) at 40x magnification. Average corrected fluorescence was measured using Image J software(136).

Antibodies: Antibodies used included MDM2-N20, CCSP, SP-C, p-GSK3β, p53-FL393 (Santa-Cruz Biotechnology), p-H3, Vimentin, p-β-Catenin Ser552 (Cell Signaling Technology), Ki-67 (Millipore), N-Cadherin (Thermo Scientific) and NICD (Abcam) were used according to manufacturer's protocol. For fluorescent immunostaining, BrDU was detected by mouse anti-bromodeoxyuridine (Becton Dickinson) primary antibody. All fluorescent staining was performed using Alexafluor 488-conjugted chicken anti-goat, Alexafluor 594-conjugated donkey anti-rabbit IgG and, Alexafluor 594-conjugated rabbit

anti-mouse secondary antibodies (Life Technologies) and mounted using ProLong Gold anti-fade reagent (Molecular Probes). Counter staining was performed using DAPI (Sigma).

***qPCR*:** RNA was isolated from lung accessory lobes and cDNA was synthesized using the Thermoscript Reverse Transcription-PCR system (Life Technologies). QPCR was carried out using a LightCycler system (Roche). Primers were designed using OLIGO 5 software (Molecular Biology Insights) and were synthesized by Integrated DNA Technologies. Reactions were performed in triplicate utilizing SYBR green dye, which exhibits a higher fluorescence upon binding of double-stranded DNA. The methods have been described previously (137). Reactions were performed in triplicate.

Immunoblot analysis and quantification: Immunoblot analysis was performed following standard techniques. Antibodies are described above. Quantitative comparisons were performed using Quantity One 4.6.2 software (Bio-Rad).

Statistics: For BrdU labeling, and BASC quantification, 16 different bronchioles were counted with the samples obtained from at least 3 different lungs preparations. All results are expressed as mean ± SEM. The significance of differences between sample means was determined by a Student's *t* test. *P* values less than 0.05 were considered statistically significant. Average corrected fluorescence and re-epithelialization data was collected from blind images of five bronchioles in three different sets of mice. Results were plotted using a Box-and-Whisker plot and significance of differences between sample measurements was determined by Mann-Whitney-Wilcoxon test. *P* values less than 0.05 were considered statistically significant. At least three mice of each genotype were used for each experiment. The experiments were done in triplicates.

Results.

Mouse model characterization: Transgenic mouse lines carrying a plasmid (pTREtightMDM2) that expresses human MDM2 from a promoter with Dox-inducible response element (TRE) (Figure 22A) were generated and crossbred with CCSPrtTA transgenic mice (rtTA) that express the Dox-responsive reverse transactivator, rtTA, from CCSP promoter, and activates TRE (132). Dox-induced MDM2 expression in lungs of these pTREtightMDM2 rtTA transgenic mice (tightMDM2) at RNA (Figure 22B) and protein levels (Figure 22C) was confirmed by quantitative PCR (QPCR) and immunoblot analysis respectively. Cultured lung cells of these mice showed MDM2 expression after Dox-treatment (Figure 22D). Immunohistochemical (IHC) analysis of formalin fixed paraffin embedded (FFPE) lung tissue sections from Dox-treated tightMDM2 mice confirmed Dox-induced MDM2 expression in the respiratory bronchioles with Club cells. Sucrose-treated (Dox-untreated) mice or Dox-treated rtTA mice did not show significant MDM2 expression (Figure 22B, E). These data indicate that tightMDM2 transgenic mice express MDM2 in lung bronchiole after Dox-treatment.

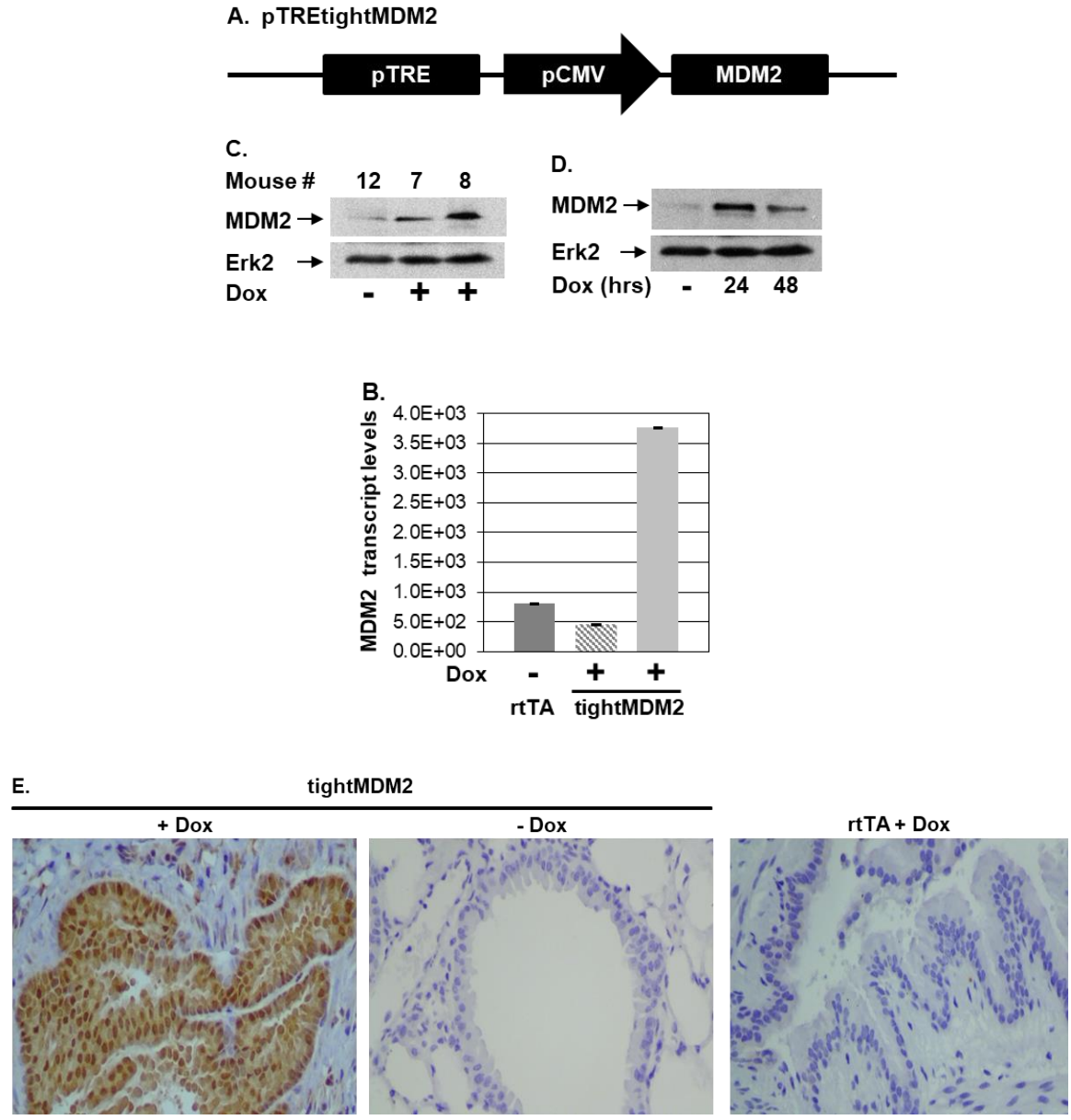

Figure 22. Generation of transgenic mice expressing human MDM2 in response to Doxycycline (Dox) in lung Club cells. (a) pTREtightMDM2 construct designed to express MDM2 from a tetracycline response element (TRE)-controlled CMV promoter. (b) MDM2 RNA and (c) protein expression in lung tissue from pTREtightMDM2 CCSP-rtTA (tightMDM2) transgenic mice after Dox or sucrose(-Dox) treatment, and (d) MDM2 expression in 0, 24 or 48 hours Dox-treated cultured lung cells from tightMDM2 mice. MDM2 transcript levels were determined by QRTPCR. The bar graph (b) shows transcript levels normalized by GAPDH expression. MDM2 protein expression was determined by

immunoblot analysis using an antibody against human MDM2. Erk2 was used as loading control. (e) Representative photographs showing immunostained lung tissue sections from tightMDM2 mice with and without Dox treatment and CCSP-rtTA transgenic mice (rtTA) after Dox treatment using antibody against human MDM2. MDM2 protein expression (brown) can be detected in Club cells around the respiratory bronchiole (RB) after Dox-treatment.

Lung-specific induction of MDM2 expression in mice leads to expression of interphase markers but not DNA replication. Since elevated MDM2 levels may induce proliferation of Club or alveolar cells in lung tissue, expression of interphase markers by Dox-induced MDM2 in lung bronchiole was investigated by IHC staining of serial FFPE lung tissue sections from Dox-treated or untreated tightMDM2 and Dox-treated rtTA mice. MDM2-expressing lung cells (Figure 23A) around respiratory bronchioles showed more frequent and stronger expression of the interphase markers Ki67 (Figure 23B) and phospho (Ser10)-histone H3 (p-H3) (Figure 23C) compared to that of Dox-untreated tightMDM2 or Dox-treated rtTA mice, suggesting progression of cells to interphase by Dox-induced MDM2. Consistently, lung tissue of Dox-treated tightMDM2 mice expressed higher levels of Cyclin D2 transcript compared to that of Dox-untreated tightMDM2 or Dox-treated rtTA mice (Figure 23D). These data indicate that Dox-induced MDM2 expression from CCSP promoter overrides the restriction point of the cell cycle(138). Although p-H3 has been implicated in chromosome condensation in mitotic cells, p-H3 is also found in interphase cells and is needed for phorbol ester (TPA)-induced transcriptional activation (139). Therefore, the ability of Dox-induced MDM2 to accelerate DNA replication in CCSP expressing cells was investigated.

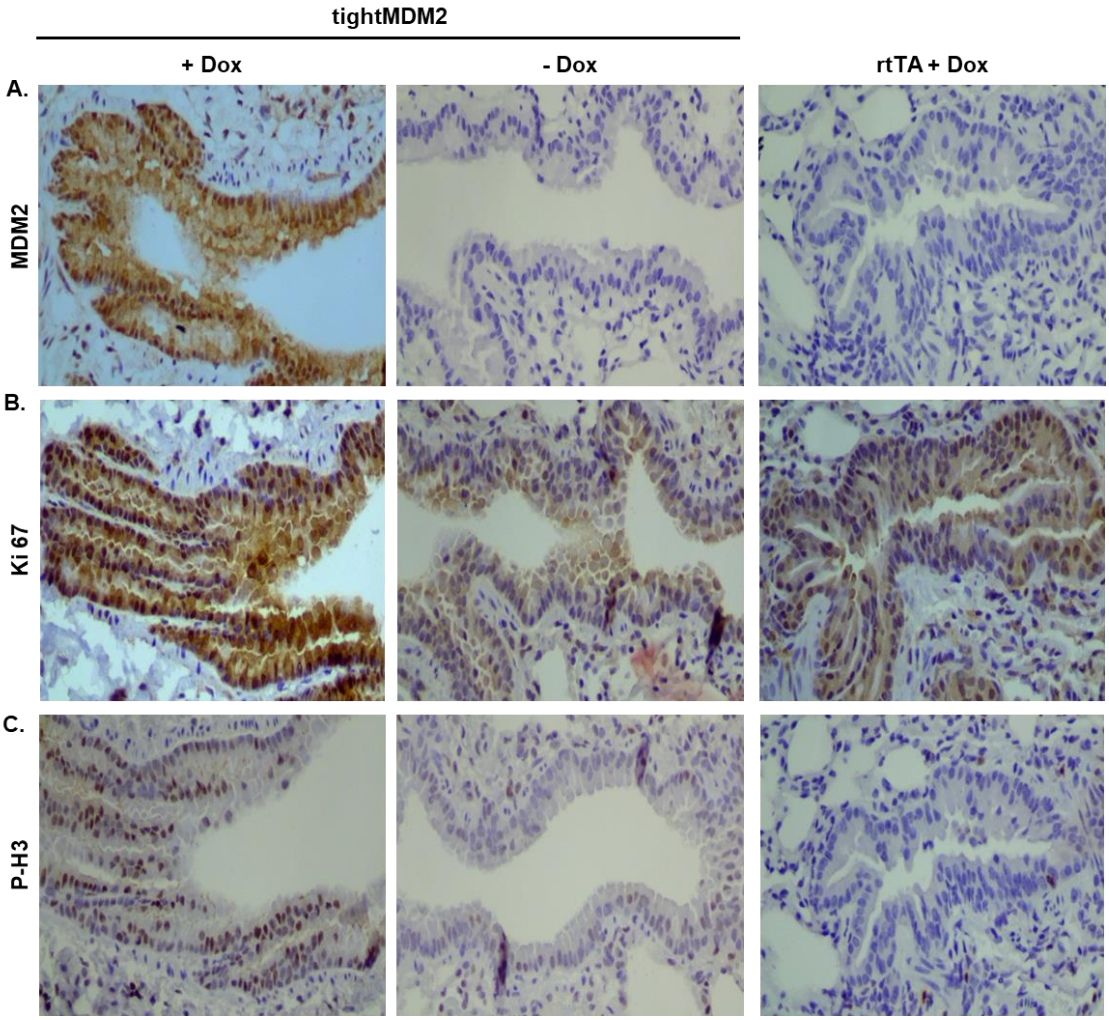
tightMDM2
+ Dox
- Dox
rtTA + Dox
A.
MDM2
B.
Ki 67
C.
P-H3

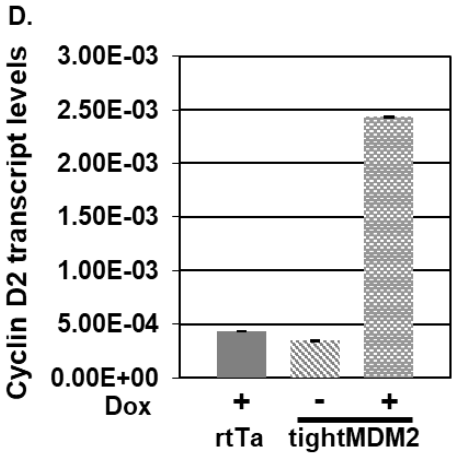
D.
Cyclin D2 transcript levels
3.00E-03
2.50E-03
2.00E-03
1.50E-03
1.00E-03
5.00E-04
0.00E+00
Dox
+
-
+
rtTa
tightMDM2

Figure 23. Induction of MDM2 expression in lung Club cells increases expression of proliferation markers. (A-C) Immunostaining of serial FFPE lung tissue sections from Dox-treated (Dox+) or sucrose-treated (Dox-) tightMDM2 mice and Dox-treated rtTA mice show (A) MDM2 (brown), (B) Ki67 (brown), and (C) p-H3 (brown) expression in lung Club cells around respiratory bronchiole. Representative photographs are shown. (D) Cyclin D2 transcript levels from lung tissues of Dox-treated control rtTA and Dox-treated or -untreated pTREtight rtTA MDM2 mice determined by QRTPCR. Transcript levels were normalized by GAPDH expression and are shown by bar graphs.

Introduction of a nucleotide analogue BrdU (bromo-deoxy uridine) in Dox-induced tightMDM2 mice, however, did not show any BrdU incorporation in the respiratory bronchiole region of lung, despite efficient MDM2 expression (Figure 24). Dox-untreated tightMDM2 and Dox-treated rtTA mice showed similar data. These data indicate that Dox-induced MDM2 expression from the CCSP promoter drives lung Club cells to interphase, but not to S phase and DNA replication.

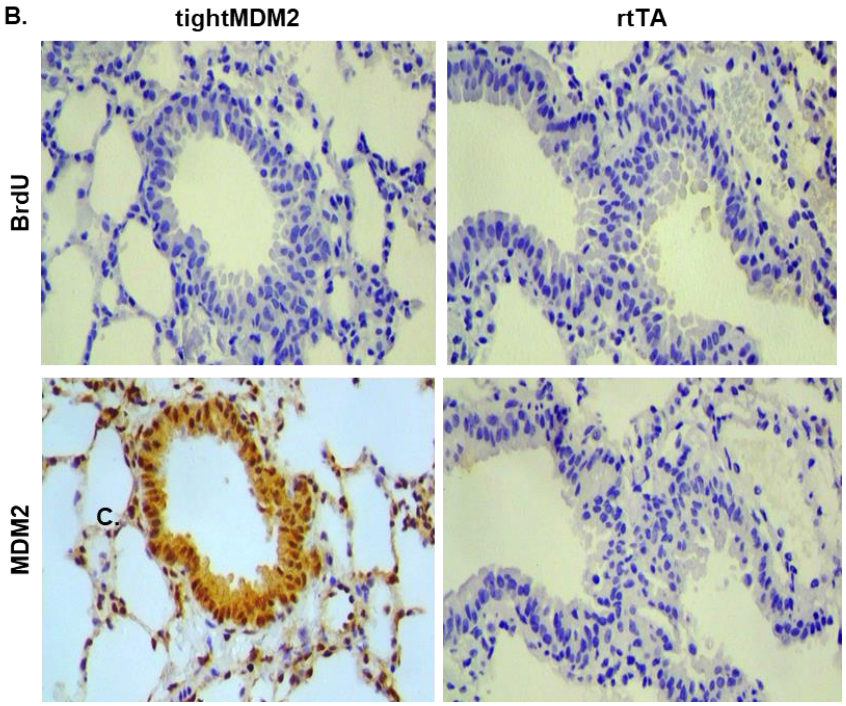

Figure 24. Induction of MDM2 expression in lung Club cells do not induce BrdU incorporation. Immunostaining of BrdU and MDM2 (brown) in serial lung tissue sections from Dox-treated tightMDM2 and rtTA mice. Representative photographs are shown.

Elevated levels of MDM2 induces DNA replication consequent to depletion of club cells after naphthalene injury. Lung is a highly quiescent organ with regenerative potential. Depletion of Club cells reactivates the CCSP-expressing lung progenitor cells(140-142). Since Dox induces MDM2 expression from the CCSP promoter in Club and CCSP-expressing progenitor cells, cell proliferating ability of MDM2 in tightMDM2 mice was tested during regeneration of lung progenitor cells. In mouse Club cells, an enzyme cytochrome P-450 2F2 efficiently generates cytotoxic metabolite, which depletes Club cells sparing naphthalene-resistant CCSP-expressing variant Club (vClub) or bronchioalveolar stem cells (BASC), which lack the enzyme(141, 142). Depletion of Club cells is known to reactivate the regenerative potential of vClub and BASC cells (140-142).

Accordingly, Dox-treated tightMDM2 or rtTA and Dox-untreated tightMDM2 mice were injected with naphthalene followed by BrdU, and were harvested at 72 hours after naphthalene treatment and 5 hours BrdU delivery. Consistent with the literature, IHC analysis of serial FFPE lung tissue sections showed appearance of BrdU incorporating cells in tightMDM2 or control groups after naphthalene treatment (Figure 25A-C). However, Dox-treated tightMDM2 mice displayed doubled frequency of BrdU incorporating cells with MDM2 and CCSP co-expression in comparison to the control groups (Figure 25A-C). These data indicate that Dox-induced MDM2 expression activates

DNA replication in naphthalene resistant CCSP expressing cells of lung bronchiole after naphthalene treatment.

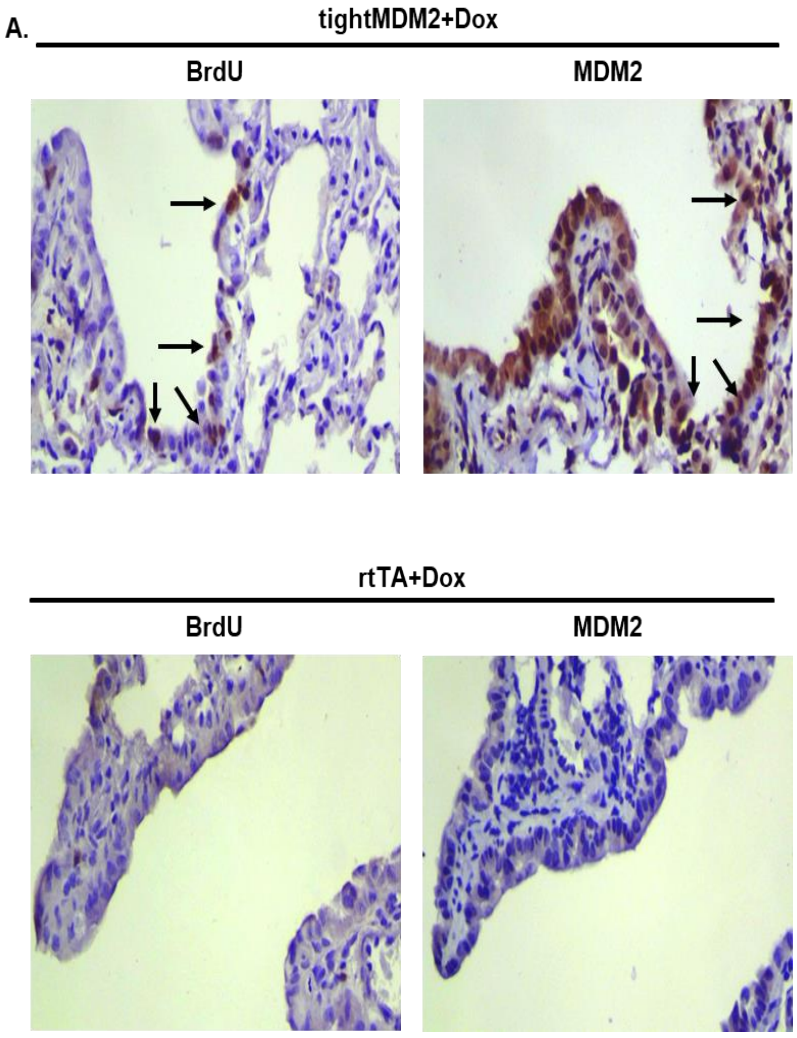

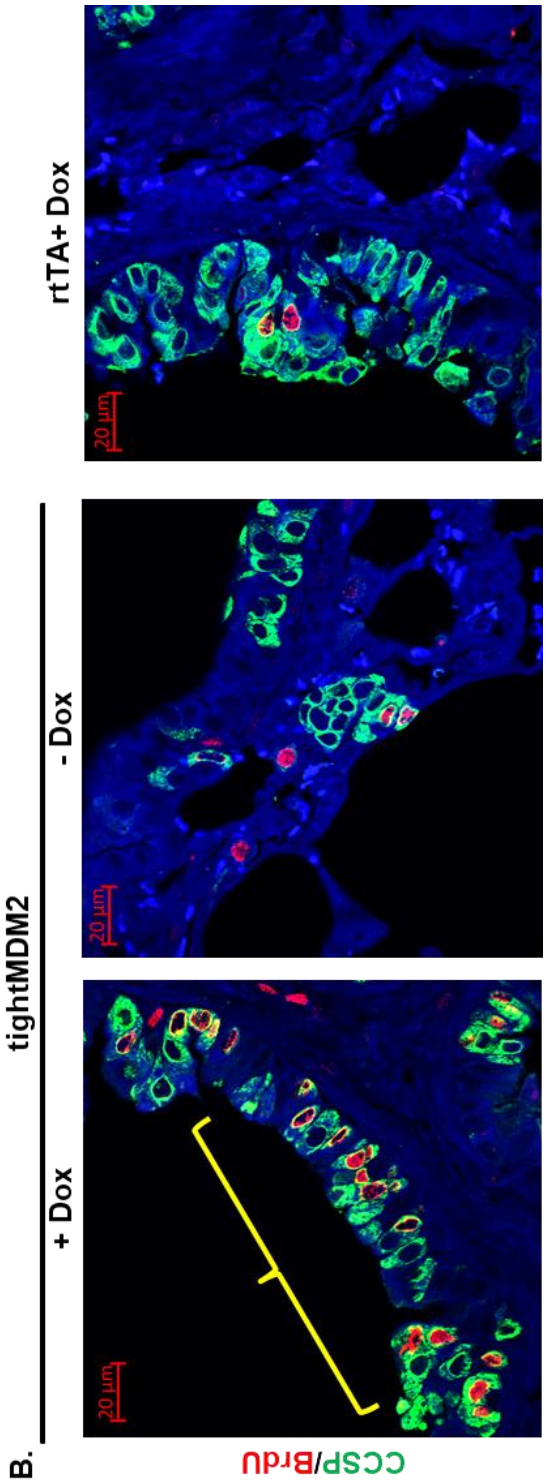
B.
tightMDM2
rtTA+ Dox
- Dox
+ Dox
20 µm
CCSP/BrdU

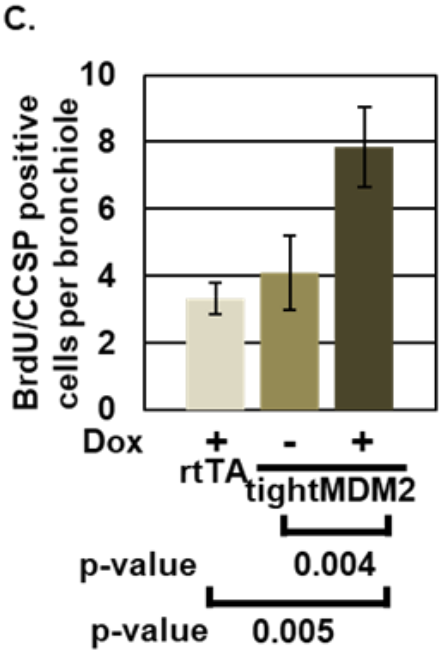
C.
BrdU/CCSP positive cells per bronchiole
10
8
6
4
2
0
Dox
+
-
+
rtTA
tightMDM2
p-value
0.004
p-value
0.005

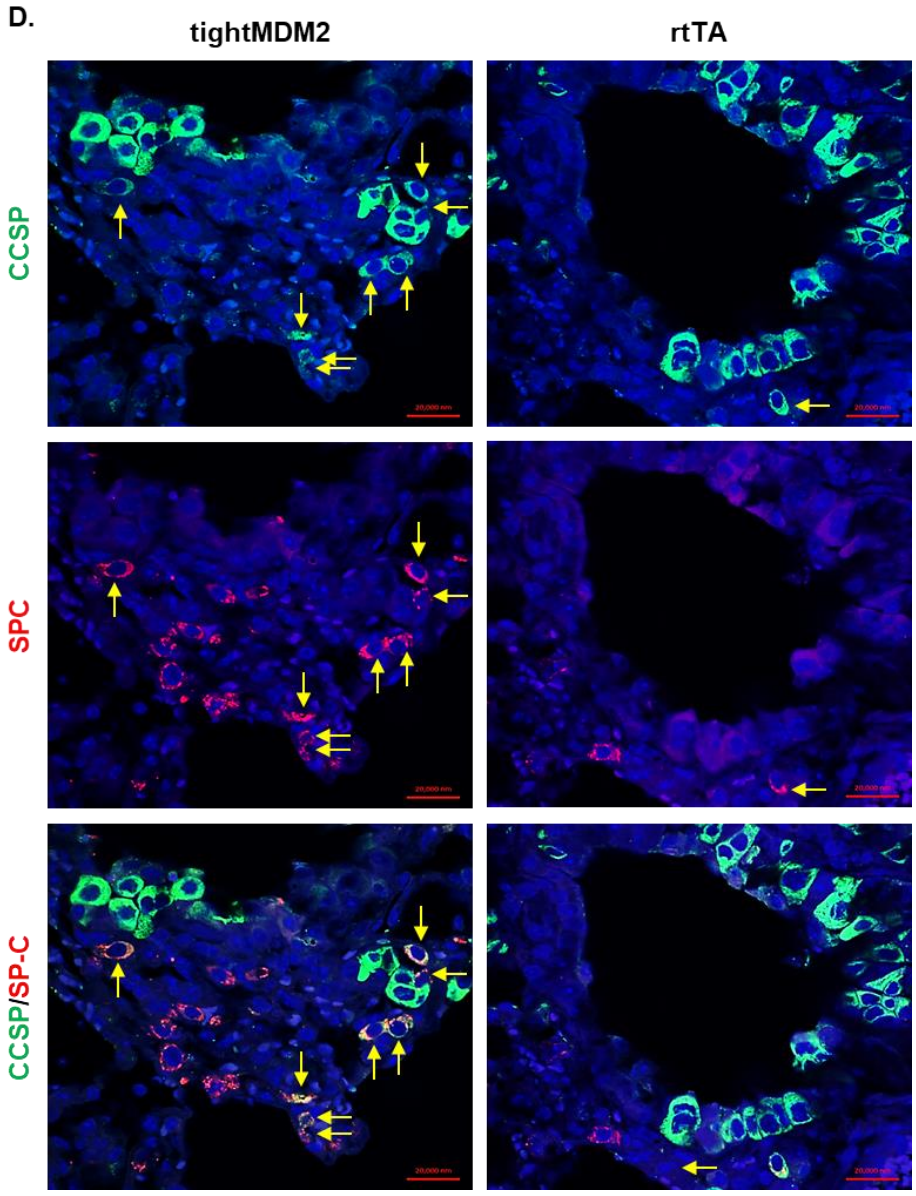
D.
tightMDM2
rtTA
CCSP
SPC
CCSP/SP-C

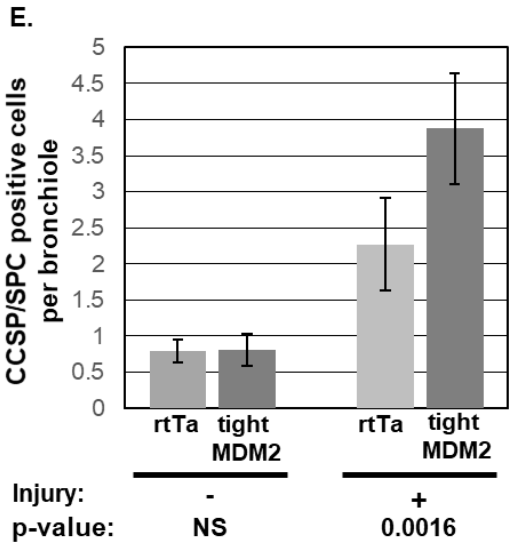
E.
CCSP/SPC positive cells per bronchiole
5
4.5
4
3.5
3
2.5
2
1.5
1
0.5
0
rtTa
tight MDM2
rtTa
tight MDM2
Injury:
-
+
p-value:
NS
0.0016

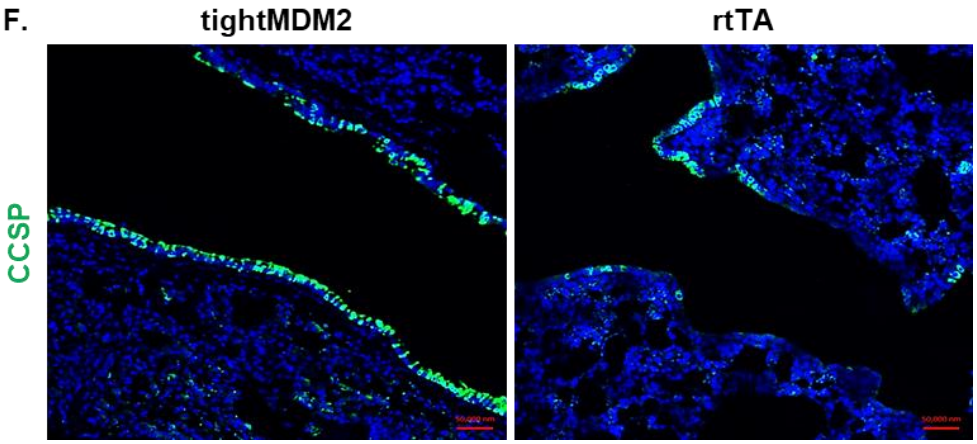
F.
tightMDM2
rtTA
CCSP

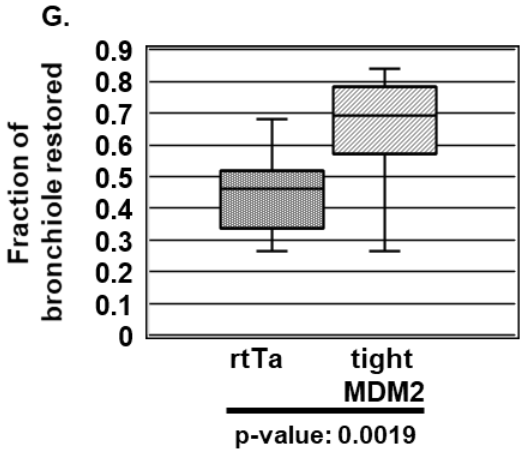
G.
Fraction of bronchiole restored
0.9
0.8
0.7
0.6
0.5
0.4
0.3
0.2
0.1
0
rtTa
tight MDM2
p-value: 0.0019

Figure 25. Dox-induced MDM2 expression in Club cells of mouse lung increases frequency of DNA replicating lung progenitor cells after naphthalene injury leading to faster restoration of CCSP expressing epithelial layer. (A) Representative photographs showing Immunostained sequential FFPE lung tissue sections from Dox-treated tightMDM2 or rtTA mice after naphthalene-treatment and BrdU delivery using antibodies against human MDM2 and BrdU. Arrows indicate BrdU incorporation (brown) and MDM2 expression (brown) in similar region of lung bronchiole. (B) Representative photographs showing immunostained tissue sections to detect BrdU incorporating (red nuclear fluorescence) CCSP expressing (extranuclear green fluorescence) cells. (C) Frequency of BrdU incorporating CCSP positive cells in lung bronchioles of Dox+ rtTA and Dox- or Dox+ tightMDM2 mice are shown by a bar graph. (D) Representative photographs showing CCSP (green) and SPC (red) co-expressing progenitor cells (arrows) in the lung bronchioles of Dox-treated tightMDM2 and rtTA mice detected by immunostaining. (E) Frequency of CCSP and SPC co-expressing cells in the lung bronchioles are shown by a bar graph. (F) Representative photographs showing restoration of epithelial layers with CCSP expressing cells in bronchioles of Dox-treated tightMDM2 and rtTA mice. (G) Box and Whisker plots comparing fraction of bronchioles restored in Dox-treated rtTA and tightMDM2 mice. In all graphs, p-values are indicated. NS: not significant.

Elevated levels of MDM2 induces expansion of CCSP and SPC labeled progenitor cells in lung bronchiole and bronchioalveolar duct junction (BADJ) inducing rapid re-epithelialization of lung bronchioles. Induction of DNA synthesis consequent to depletion of Club cells suggests proliferation of lung progenitor cells for injury repair(140, 143). Therefore, consequence of Dox-induced MDM2 expression on expansion of lung progenitor cells (such as vClub and BASC cells), which restore bronchoalveolar epithelium, was examined. Dox-treated tightMDM2 or rtTA mice were injected with naphthalene. Since vClub and BASC cells express both Club cell marker CCSP and alveolar cell marker SPC, the presence of CCSP and SPC co-expressing cells in the bronchiole and bronchoalveolar duct junctions (BADJ) was investigated by immunostaining naphthalene-treated lung tissue sections with fluorescent dye-tagged antibodies. Consistent with the increase in DNA replicating cells, a robust expansion of CCSP and SPC co-expressing cells in lung

bronchioles and BADJ of Dox-treated tightMDM2 mice was observed compared to that of rtTA mice (Figure 25D, E). Furthermore, the ability of Dox-induced MDM2 to accelerate restoration of the bronchiolar epithelium after naphthalene injury was examined by immunostaining and quantifying the fraction of bronchioles that restored CCSP-expressing Club cells. The results indicated that 66% of the bronchiole of Dox-treated tightMDM2 mice was consistently repopulated compared to that of rtTA mice, which showed 45% repopulation at 72 hours after naphthalene treatment (Figure 25F, G) indicating accelerated restoration of bronchiolar epithelium by MDM2.

MDM2 activates the signaling pathway for re-epithelialization and injury repair: Naphthalene injury activates cell signaling pathways for re-epithelialization(144). Accelerated epithelial regeneration by Dox-induced MDM2 expression suggest that MDM2 may accelerate injury-induced signaling pathway. Since human and mouse MDM2 activates Akt phosphorylation and thus phosphorylation of GSK3β, and Cyclin D2 expression in cultured lung cells (30, 31), ability of MDM2 to activate Akt signaling during epithelial regeneration consequent to naphthalene injury was determined. After naphthalene treatment, a robust increase in Akt phosphorylation at Ser 473 (Figure 26A, B) and phosphorylation of Akt-substrates, phospho (Ser 9)-GSK3β (Figure 26C, D) and phospho (Ser 552)-β catenin (Figure 26E, F) was observed in CCSP expressing cells of lung bronchioles from Dox-treated tightMDM2 mice compared to that from rtTA mice. These observations indicate that Dox-induced MDM2 expression accelerates Akt signaling initiated by naphthalene injury in CCSP expressing cells of lung bronchioles. Since Notch-

1 is required for regeneration of Club cells during airway injury repair (145), and GSK3β regulates Notch-1 function(146), ability of MDM2 to induce Notch-1expression, and nuclear translocation of Notch intracellular domain (NICD) in Club cells during injury repair was investigated. As expected, Dox-induced MDM2 expression promoted expression of Notch-1and nuclear translocation of NICD in CCSP expressing cells activating expression of HES-1, a downstream transcriptional target of NICD (Figure 26G-J). These data indicate MDM2-induced activation of repair signaling pathway after naphthalene injury in lung.

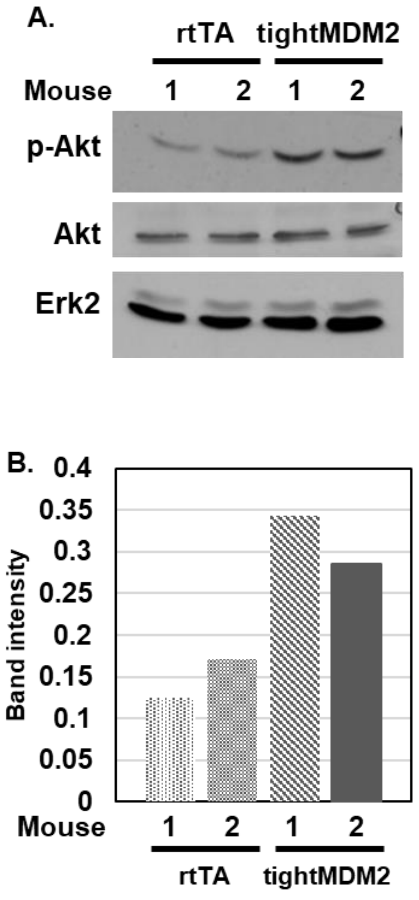

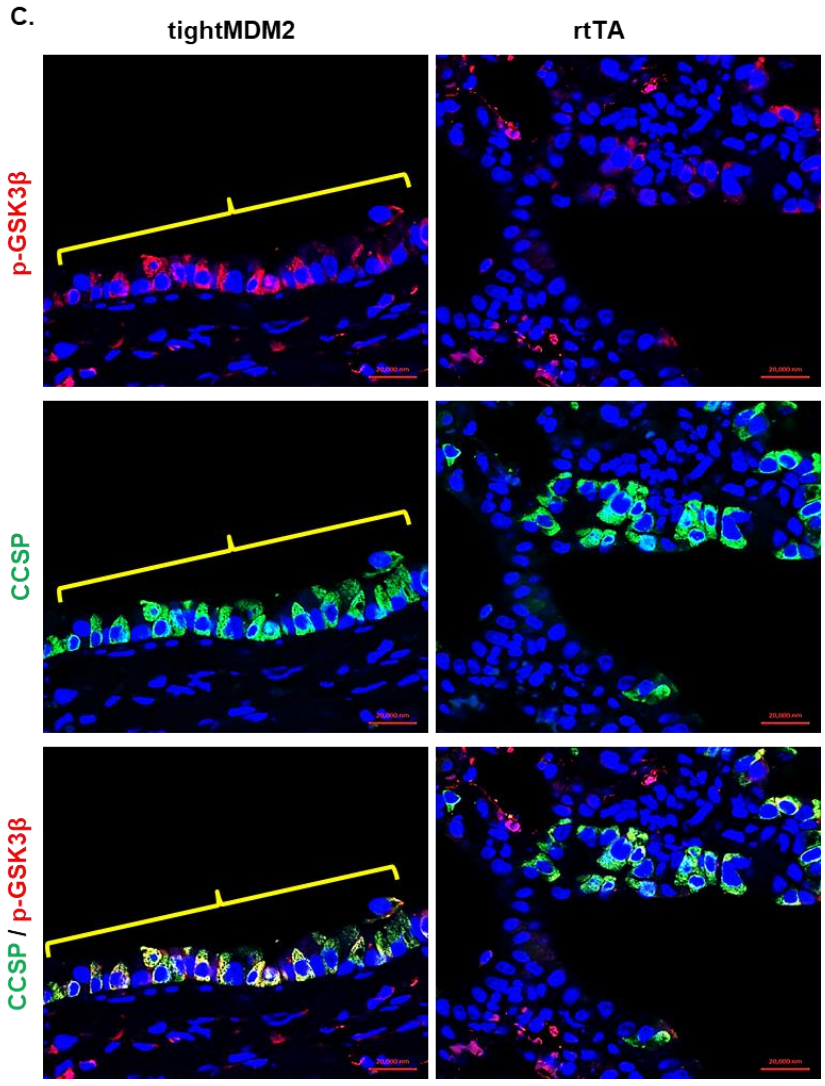
C.
tightMDM2
rtTA
p-GSK3β
CCSP
CCSP / p-GSK3β

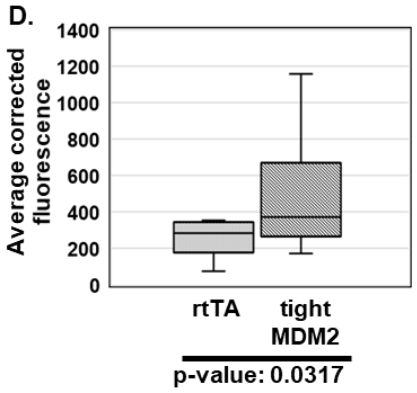
D.
Average corrected fluorescence
1400
1200
1000
800
600
400
200
0
rtTA
tight MDM2
p-value: 0.0317

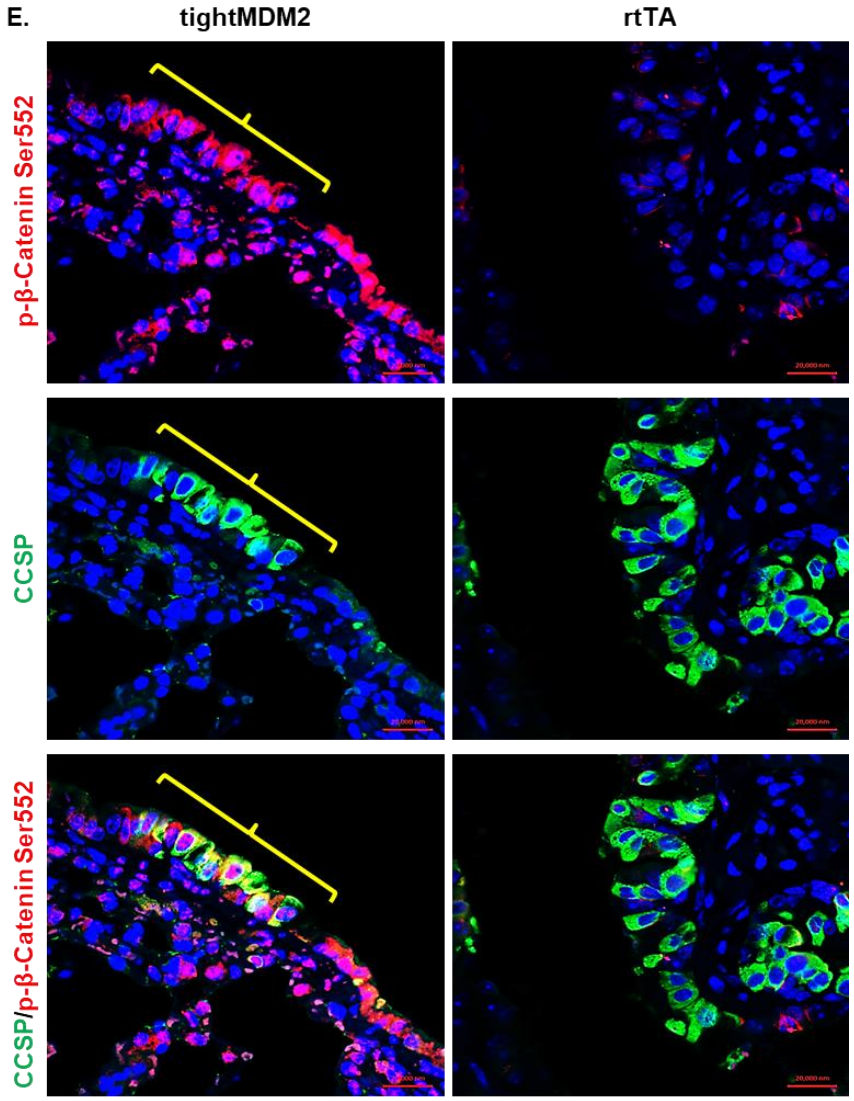
E.
tightMDM2
rtTA
p-β-Catenin Ser552
CCSP
CCSP/p-β-Catenin Ser552

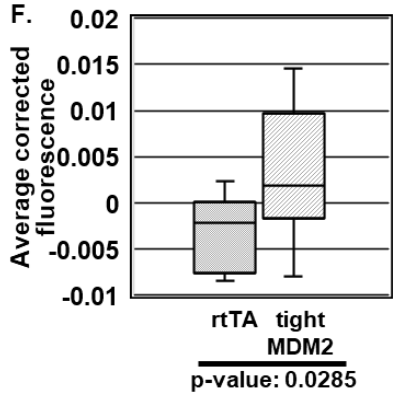
F.
Average corrected fluorescence
0.02
0.015
0.01
0.005
0
-0.005
-0.01
rtTA
tight MDM2
p-value: 0.0285

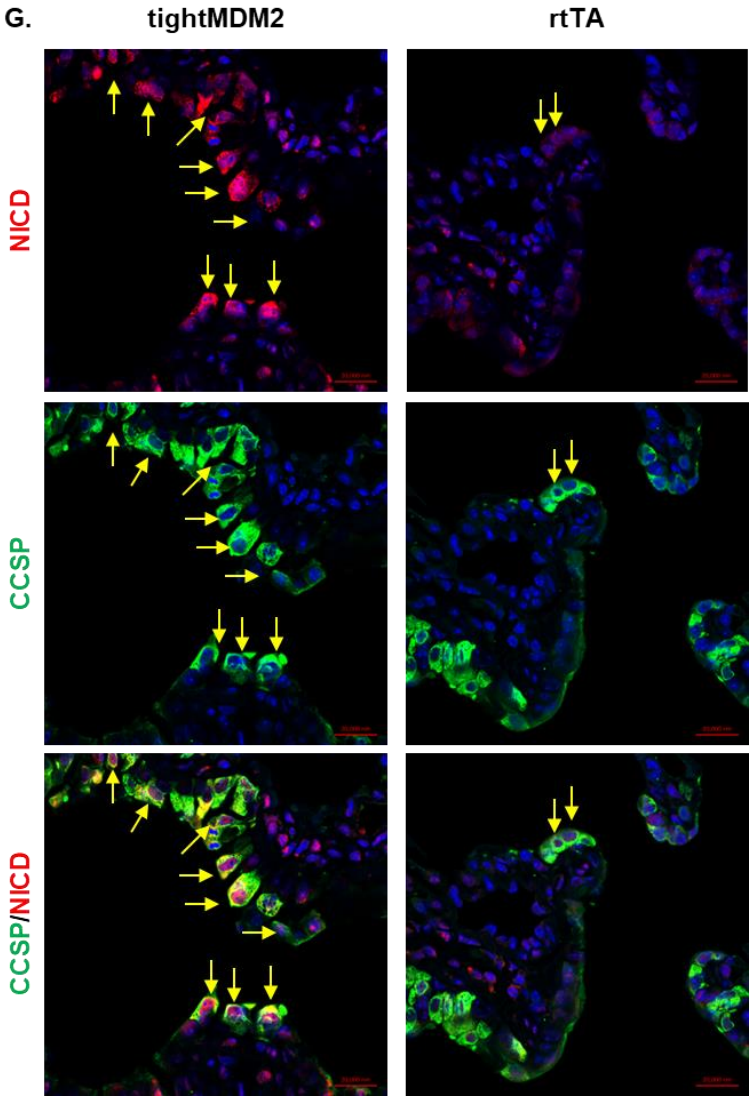
G.
tightMDM2
rtTA
NICD
CCSP
CCSP/NICD

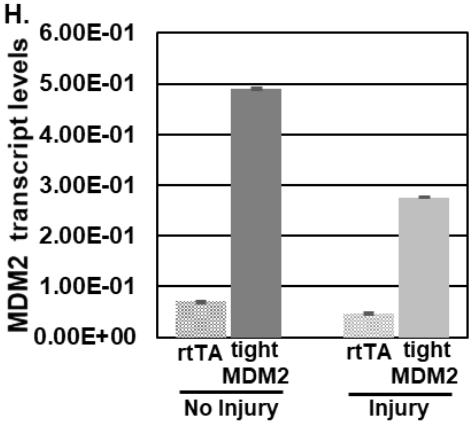
H.
MDM2 transcript levels
6.00E-01
5.00E-01
4.00E-01
3.00E-01
2.00E-01
1.00E-01
0.00E+00
rtTA
tight MDM2
rtTA
tight MDM2
No Injury
Injury

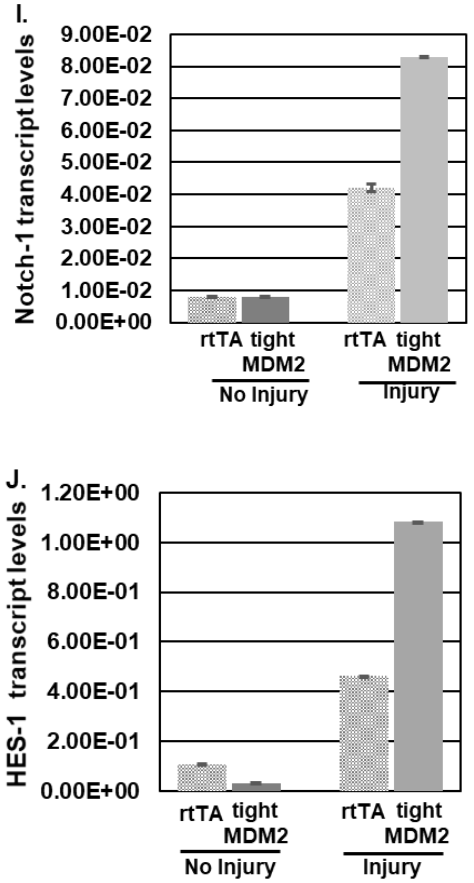

Figure 26. MDM2 activates the signaling pathway for re-epithelialization consequent to naphthalene injury. Lung tissue extracts or FFPE tissue sections from Dox-treated rtTA and tightMDM2 mice were analyzed for Akt signaling pathway 72 hours after naphthalene treatment. (A, B) immunoblot analysis of Akt phosphorylation at Ser 473 (a) and a bar graph comparing band intensities (B), (C,D) immunostaining of GSK3β phosphorylation at Ser 9 (brackets) in CCSP expressing cells (C) and Box and Whisker plot comparing average fluorescence of each bronchioles (D), (E, F) immunostaining of phospho (Ser 552) β-Catenin (yellow brackets) in CCSP expressing cells (E) and Box and Whisker plots comparing average fluorescence of each bronchiole (F); (G) Immunostaining of activated Notch-1, NICD, (arrows) in CCSP expressing cells; (H-J) MDM2 (H), Notch-1 (I) and Hes-1 (J) transcript levels in lung tissue determined by QRTPCR.

Inhibition of Akt abrogates MDM2-induced lung cell proliferation: To further explore the significance of MDM2-induced Akt phosphorylation on replication of

bronchiolar progenitor cells, Dox-induced tightMDM2 mice were treated with an Akt inhibitor (MK2206) after naphthalene injury, and phosphorylation (Ser9) of GSK3β and BrdU incorporation in CCSP expressing cells in lung bronchiole were examined. As expected, treatment with MK2206 reduced downstream GSK3β phosphorylation (Figure 27A) indicating the effectiveness of the Akt inhibitor. Furthermore, MK2206 also reduced number of BrdU-labeled CCSP expressing cells in bronchioles of Dox-treated tightMDM2 mice (Figure 27B, C), indicating that the Akt signaling is needed for MDM2-induced proliferation of CCSP expressing cells.

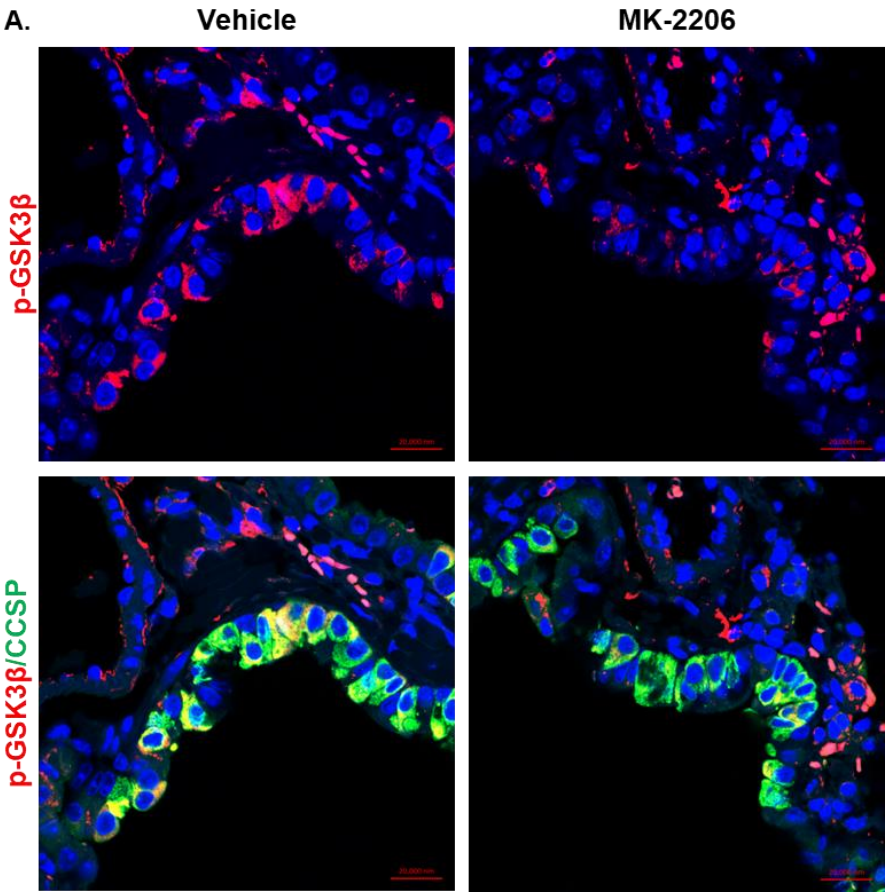

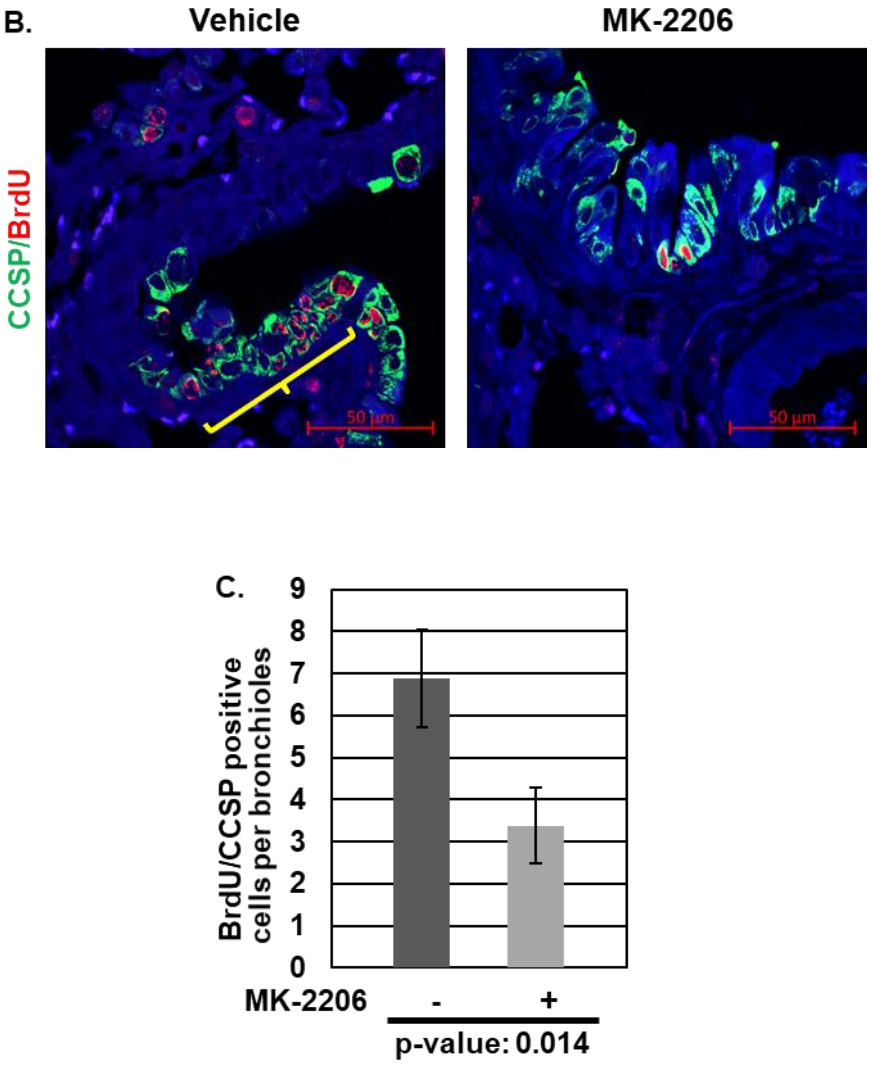

Figure 27. Inhibition of Akt abrogates MDM2-induced lung cell proliferation. (A-C) An Akt inhibitor (MK-2206) inhibits MDM2 activated GSK3β phosphorylation at Ser 9 (A) and BrdU incorporation in CCSP expressing cells (B). Frequency of BrdU incorporating CCSP positive cells in the absence or presence of MK-2206 were quantified and shown by a bar graph (C). Representative photographs are shown for all immunostained sections. p-values are indicated.

MDM2 enhances expression of EMT markers consequent to naphthalene-induced lung injury: Since epithelial regeneration after naphthalene induced lung injury should involve EMT, expression of EMT markers, such as Vimentin and N-Cadherin expression in CCSP expressing lung progenitor cells were investigated. The results (Figure 28A-D) indicated a remarkable increase in N-Cadherin and Vimentin in CCSP expressing cells in the bronchiole of Dox-treated tightMDM2 mice compared to rtTA control. These data indicate that induction of MDM2 expression in CCSP expressing lung cells accelerates Akt signaling pathway after naphthalene injury leading to EMT.

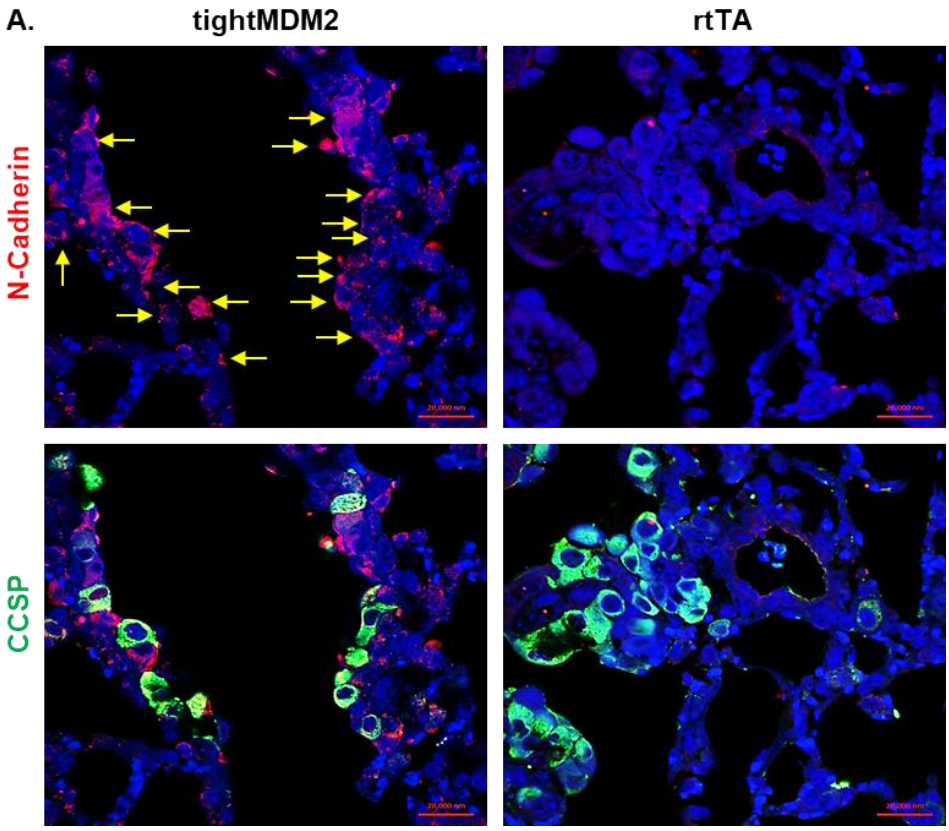

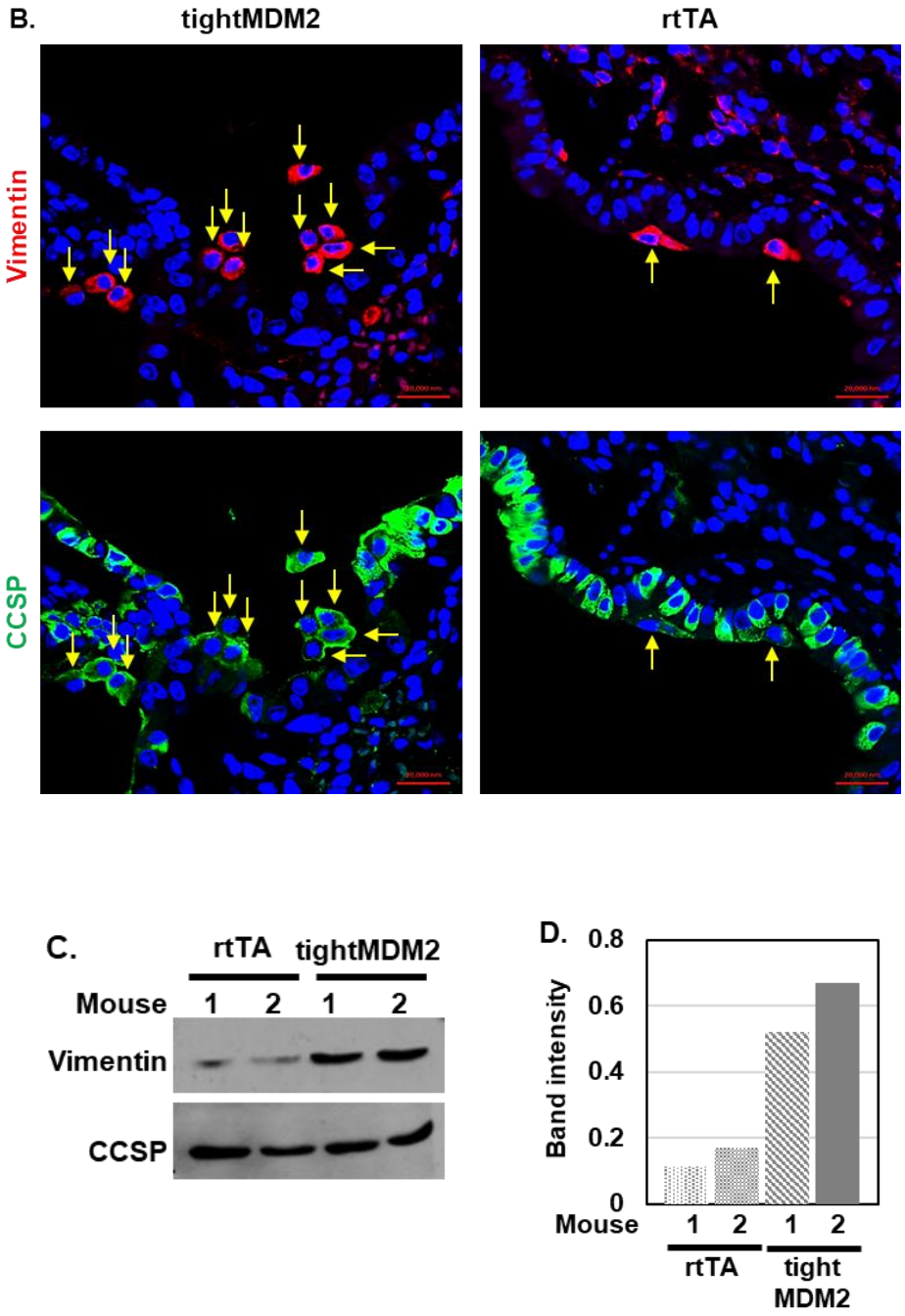

Figure 28. MDM2 enhances expression of EMT markers consequent to naphthalene-induced lung injury. (A-D) immunostaining of N-Cadherin (A, arrows) and Vimentin (B, arrows) in CCSP expressing cells, and (C, D) immunoblot analysis of Vimentin (C) in lung tissue extracts along with a bar graph comparing band intensity (D).

Targeted induction of MDM2 expression in lung alveoli activates DNA replication after treatment with ionizing radiation: To determine whether induction of MDM2 expression in lung alveolar type II (ATII) cells activates DNA replication after injury, transgenic pTREtightMDM2 SPC-rtTA (SPC-tightMDM2) mice were generated by crossbreeding of pTREtightMDM2 with transgenic SPC (surfactant protein C)-rtTA mice. SPC-tightMDM2 mice express rtTA in lung alveolar type II cells, and thus induce MDM2 expression after treatment with Dox (Figure 29). Consistent with the results found in lung bronchiole, FFPE lung sections from SPC-tightMDM2 mice showed increased Ki67 expression in alveolar epithelial cells upon Dox-treatment compared to Dox-untreated SPC-tightMDM2 or Dox-treated SPC-rtTA mice (Figure 29). Also, no BrdU incorporation was observed in any of the constructs after delivery of the nucleotide analogue (Figure 29).

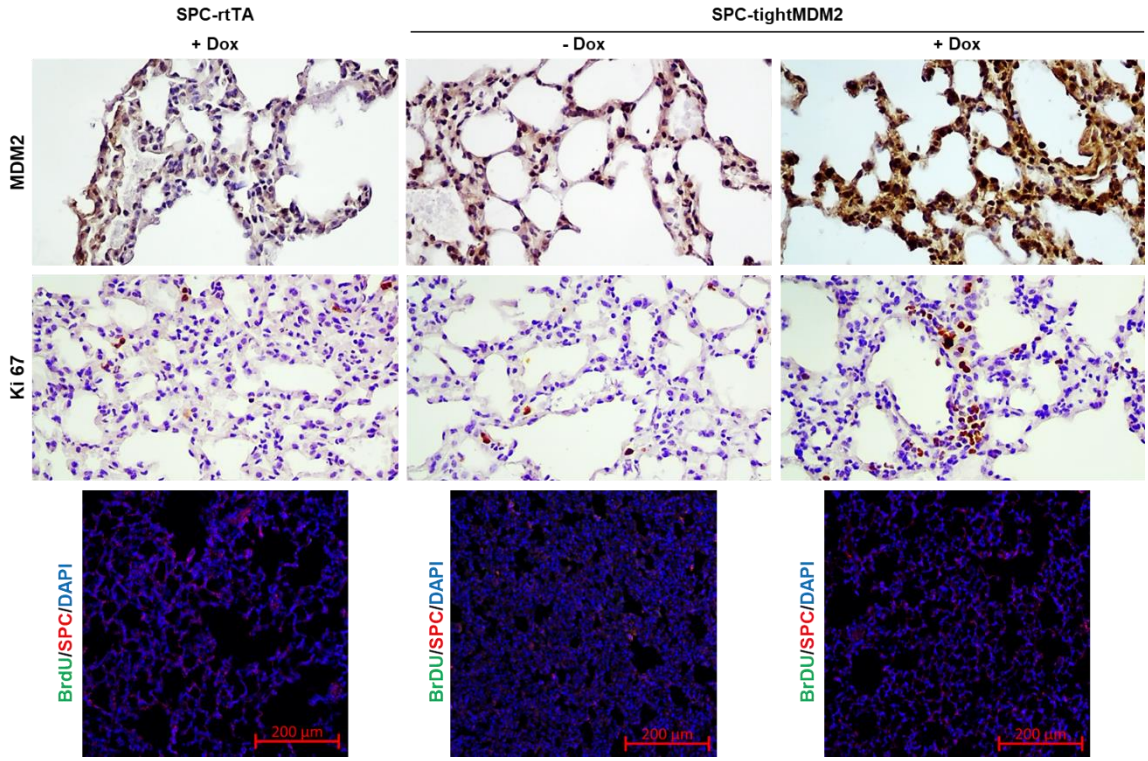

Figure 29. Induction of MDM2 expression in lung alveolar cells increases expression of proliferation markers but does not induce BrdU incorporation in cells. Immunostaining of serial lung tissue sections from Dox-treated SPC-rtTA or Dox-treated or untreated SPC-tightMDM2 mice show MDM2 (brown) and Ki67 (brown) expression, but not BrdU incorporating cells after BrdU delivery. Representative photographs are shown.

To determine the contribution of MDM2 in ATII cell proliferation in response to lung injury, SPC-tightMDM2 and control SPC-rtTA mice were exposed to ionizing radiation (14Gy). Since DNA labeling in ATII cells of mouse lung can be observed at 3 months post irradiation (147), contribution of MDM2 in ATII cell proliferation was determined using BrdU incorporation at 3 months after irradiation. Consistent with the results observed in naphthalene induced Club cell depletion, appearance of BrdU positive SPC expressing cells were observed three months after radiation exposure in lung alveolar region of all irradiated mice. However, Dox-treated SPC-tightMDM2 lung FFPE sections showed an increase in the frequency of BrdU labelled SPC expressing alveolar cells compared to that from Dox-treated SPC-rtTA or Dox-untreated SPC-tightMDM2 mice (Figure 30A, B). Furthermore, Dox-treated SPC-tightMDM2 lung sections also showed an increase in Vimentin expressing ATII cells compared to ATII cells of irradiated control groups (Figure 30C-E). These results indicate that MDM2 accelerates proliferation and EMT of ATII cells after radiation injury.

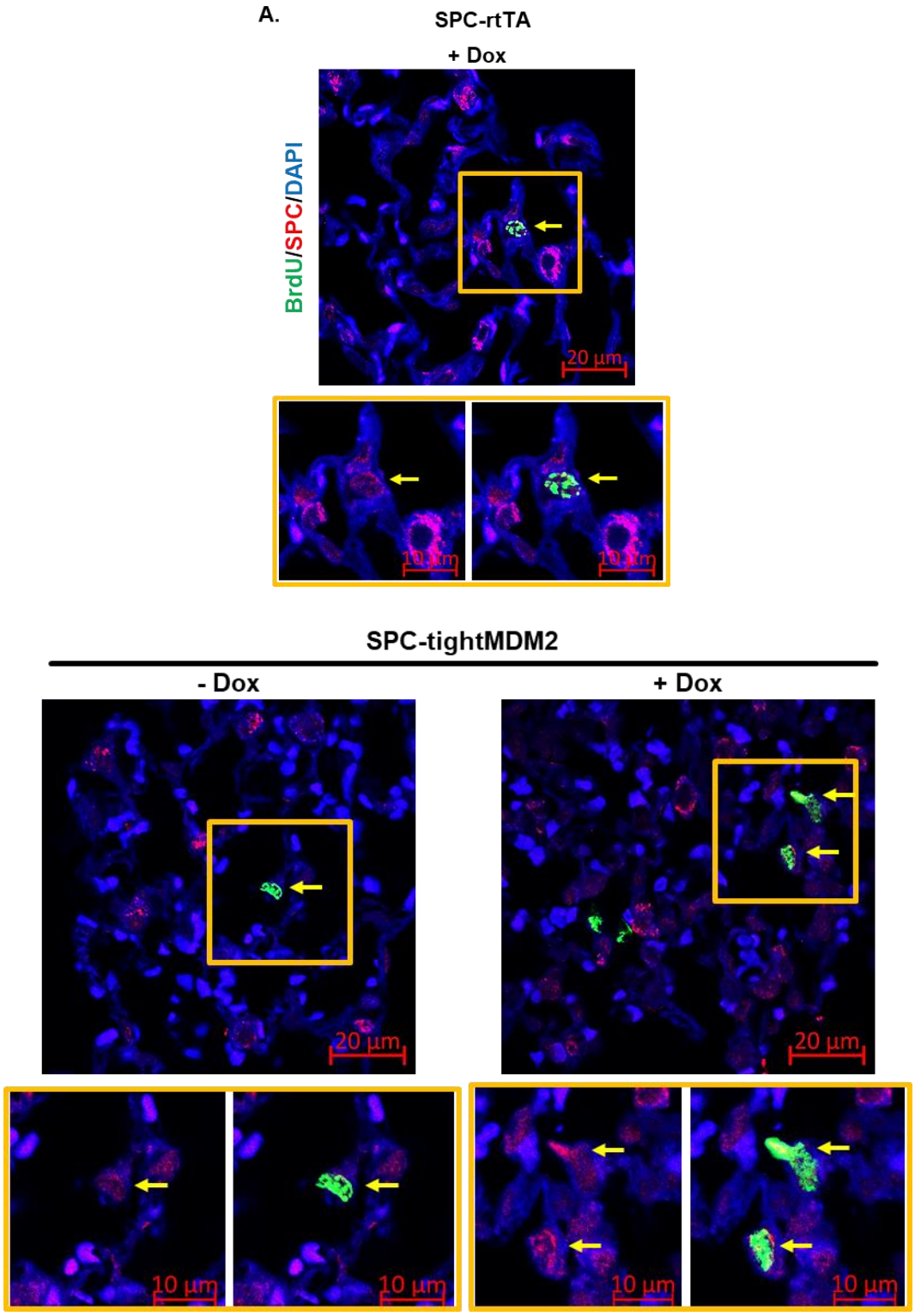
A.
SPC-rtTA
+ Dox
BrdU/SPC/DAPI
20 µm
10 µm
10 µm
SPC-tightMDM2
- Dox
+ Dox
20 µm
20 µm
10 µm
10 µm
10 µm
10 µm

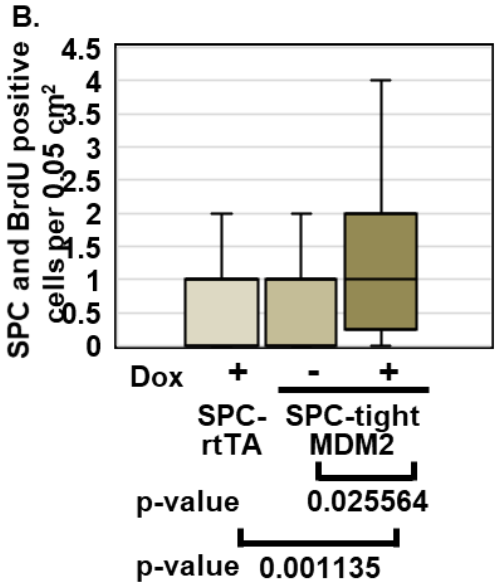
B.
SPC and BrdU positive cells per 0.05 cm²
4.5
4
3.5
3
2.5
2
1.5
1
0.5
0
Dox
+
-
+
SPC-rtTA
SPC-tight MDM2
p-value
0.025564
p-value
0.001135

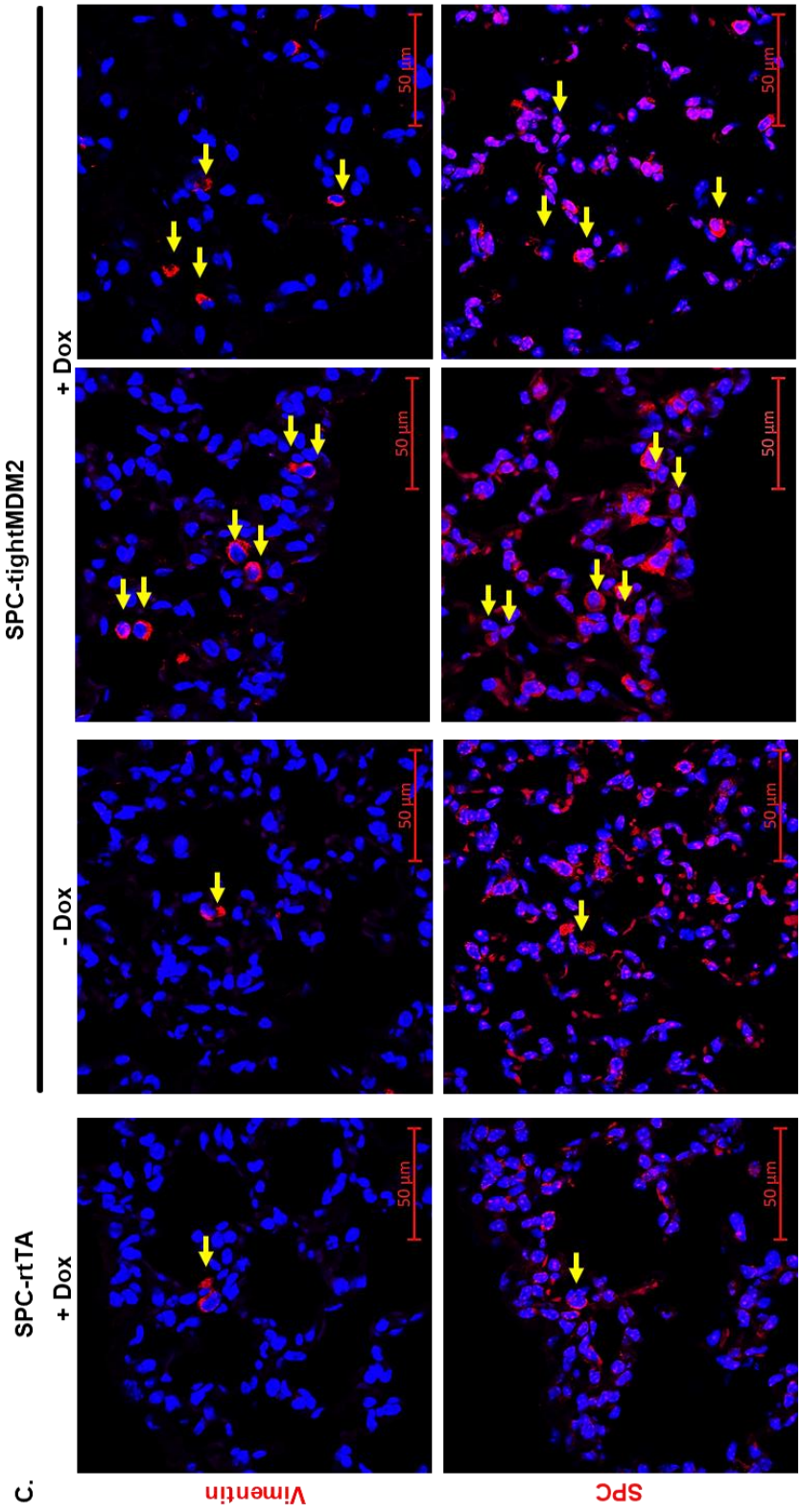
C.
SPC-rtTA
+ Dox
SPC-tightMDM2
- Dox
+ Dox
SPC
Vimentin
50 µm

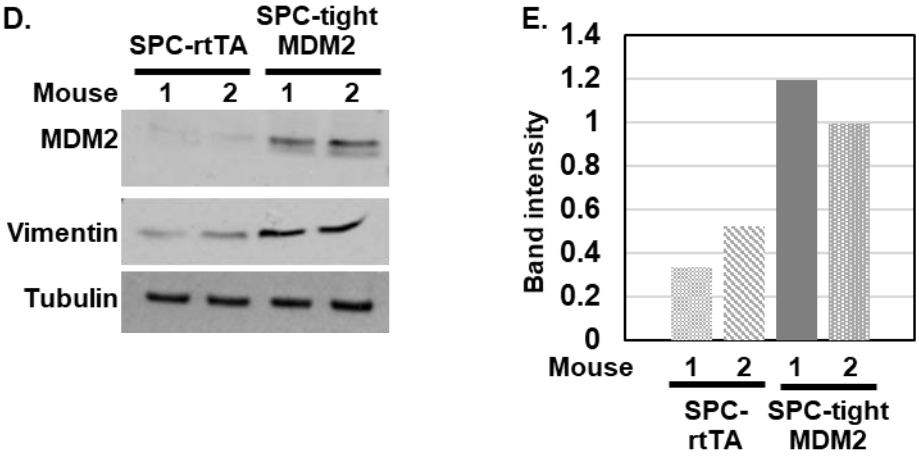

Figure 30. Induction of MDM2 expression in lung alveolar cells from a Dox-inducible SPC promoter increases frequency of DNA replicating lung progenitor cells in SPC-tightMDM2 mice after exposure to ionizing radiation. (A) Representative photographs of immunostained lung tissue sections from Dox-treated SPC-rtTA and Dox-treated or untreated SPC-tightMDM2 mice harvested three months after exposure to ionizing radiation after BrdU delivery using antibodies against SPC and BrdU. BrdU incorporating (green) SPC expressing (red) cells are shown by arrows in a box. Lower panel shows enlarged picture. (B) Frequency of BrdU and SPC co-expressing cells (box) are shown by a Box and Whisker plot. Both Dox+ and Dox-p-values are indicated. (C-E) Representative photographs of immunostained serial lung tissue sections to detect Vimentin expression in SPC expressing cells (C). Arrows indicate similar areas in the serial sections. Immunoblot analysis (D) along with densitometry (E) of tissue extracts from Dox-treated SPC-rtTA and Dox-treated or untreated SPC-tightMDM2 mice, harvested three months after exposure to ionizing radiation.

MDM2-induced re-epithelialization of lung bronchioles after naphthalene injury is independent of WT p53. Increased frequency of proliferating lung progenitor cells by MDM2 could be a result of its ability to inactivate WT p53(126). Since lung cancers with p53 mutation often show MDM2 overexpression(28, 148, 149), ability of MDM2 to accelerate DNA replication, expansion of CCSP and SPC co-expressing progenitor cells and re-epithelialization was determined in the absence of WT p53. TightMDM2, LSL (lox-stop lox) R172H (knock-in) mice were generated that can co-express a p53 mutant p53-R172H

and MDM2 in CCSP-expressing cells after Dox-induction. As in the case of tightMDM2, immunostaining of FFPE lung sections from these mice showed Dox-induced MDM2 expression in the bronchioles of LSL R172H tightMDM2 mice increased the number of interphase cells expressing Ki67 and p-H3 markers (Figure 31A). As expected, BrdU delivery did not show BrdU incorporating cells (Figure 31B).

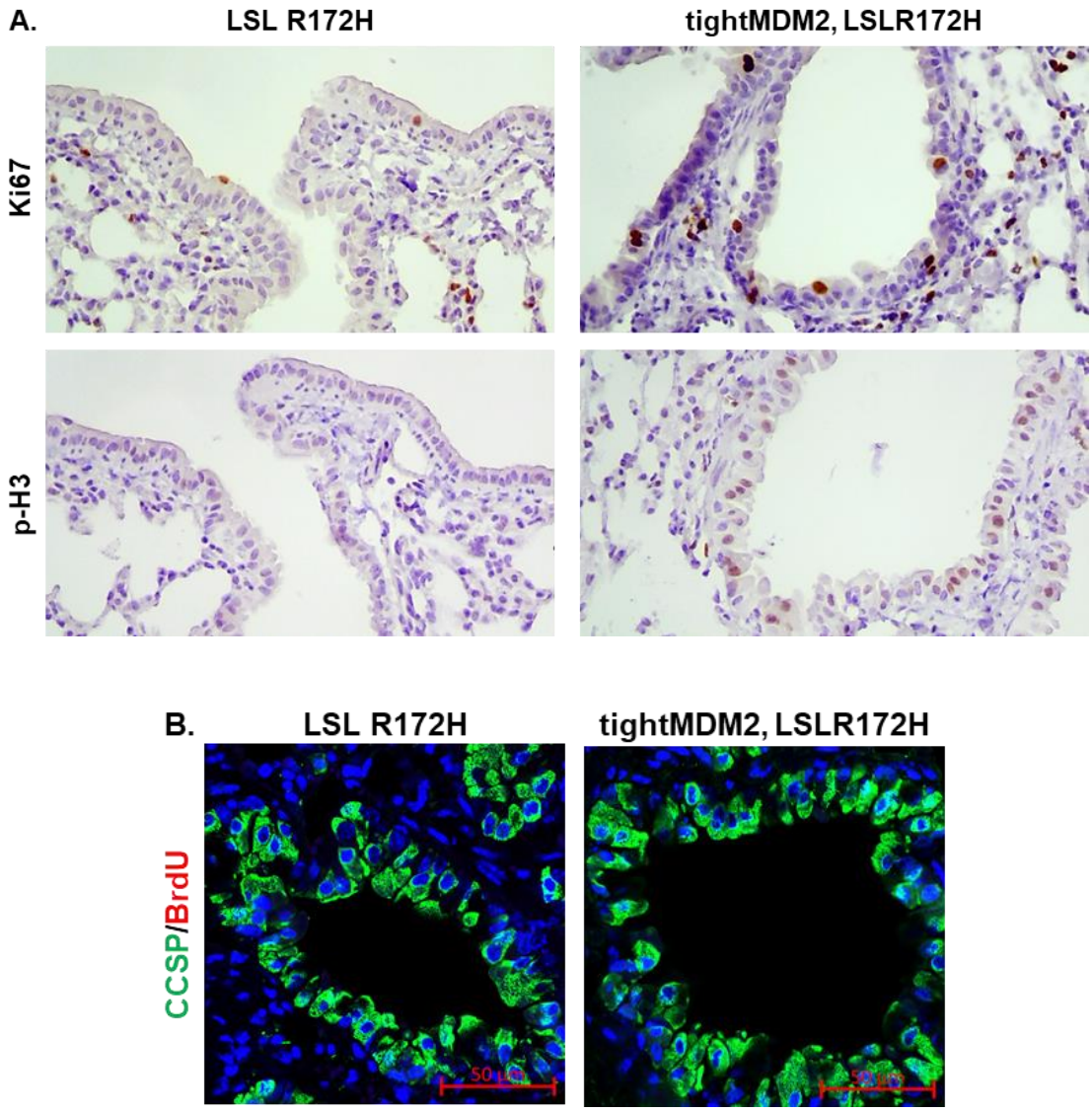

Figure 31. Induction of MDM2 and p53-R172H co-expression in lung Club cells MDM2 overexpression increases expression of proliferation markers but does not induce BrdU incorporation. (A) Immunostaining of serial lung tissue sections from Dox-treated LSL R172H and LSL R172H, tightMDM2 mice show (A) Ki67 (brown), and p-H3 (brown) expression in lung Club cells around respiratory bronchiole, (B) but not BrdU incorporating cells after BrdU delivery. Representative photographs are shown.

Naphthalene treatment activated BrdU incorporation in CCSP expressing cells, while bronchioles from MDM2 and p53 co-expressing mice consistently displayed a higher frequency of BrdU-labeled CCSP expressing cells compared to bronchioles from mice expressing p53-R172H alone (Figure 32B, C). Consistently, MDM2 and p53-R172H co-expressing bronchioles showed accelerated expansion of CCSP and SPC co-expressing cells compared to bronchioles with p53-R172H alone after naphthalene treatment (Figure 32D, E). Furthermore, CCSP staining of injured lung bronchioles showed a robust increase in the efficiency of re-epithelialization of Dox-induced tightMDM2, LSL R172H bronchioles compared to LSL R172H bronchioles (Figure 32F, G). These data indicate a WT p53-independent contribution of MDM2 in naphthalene-induced injury repair in lung.

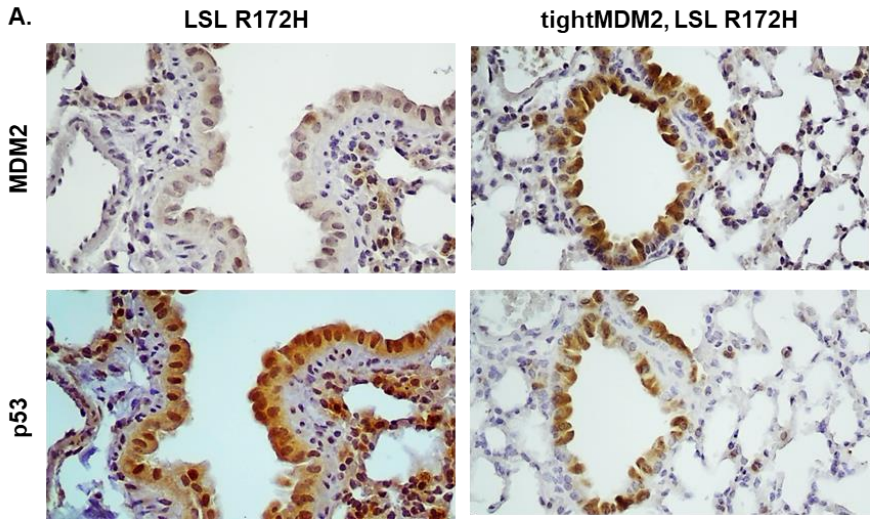
A.
LSL R172H
tightMDM2, LSL R172H
MDM2
p53

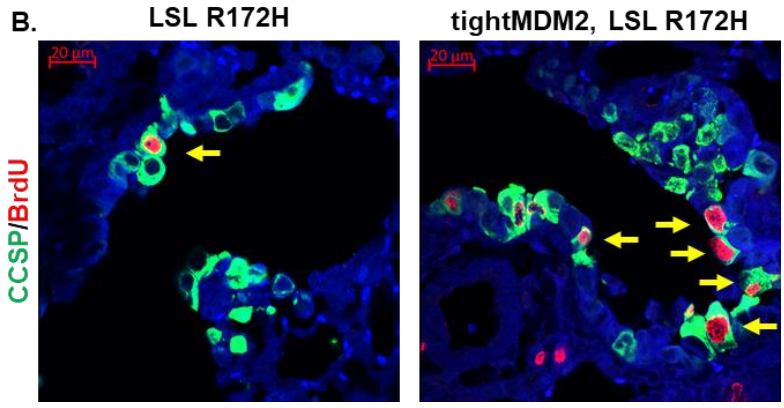
B.
LSL R172H
tightMDM2, LSL R172H
20 µm
20 µm
CCSP/BrdU

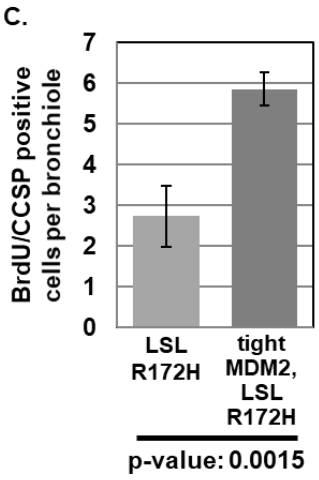
C.
BrdU/CCSP positive cells per bronchiole
7
6
5
4
3
2
1
0
LSL R172H
tight MDM2, LSL R172H
p-value: 0.0015

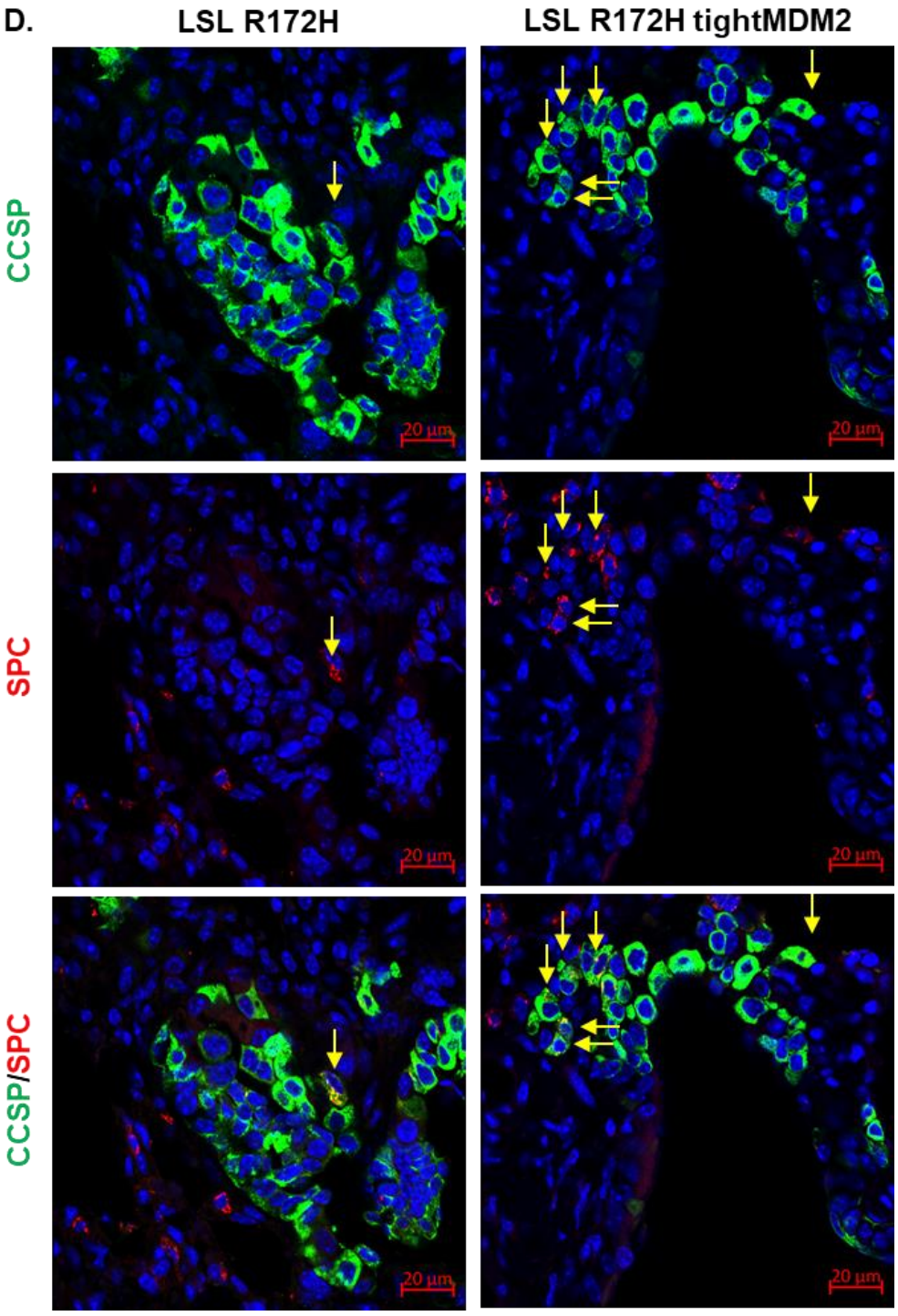
D.
LSL R172H
LSL R172H tightMDM2
CCSP
SPC
CCSP/SPC
20 µm

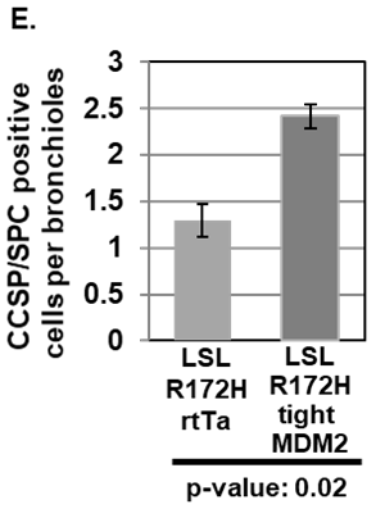
E.
CCSP/SPC positive cells per bronchioles
3
2.5
2
1.5
1
0.5
0
LSL R172H rtTa
LSL R172H tight MDM2
p-value: 0.02

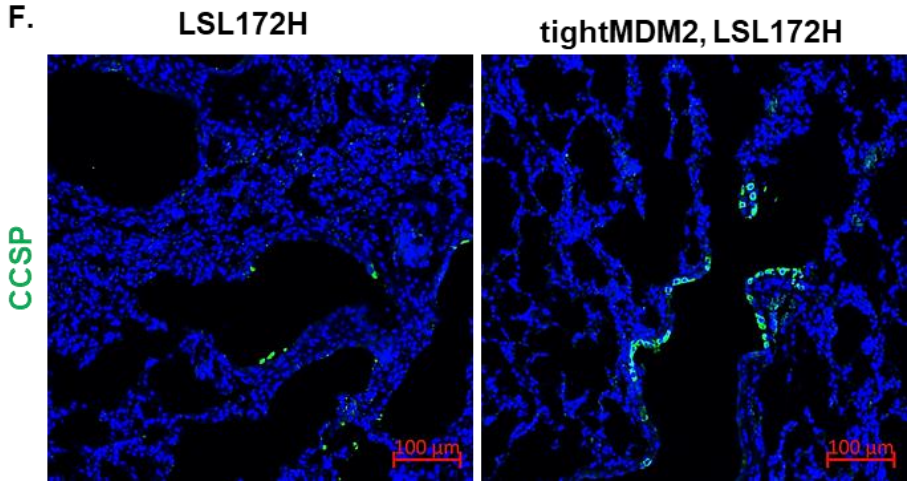
F.
LSL172H
tightMDM2, LSL172H
CCSP
100 µm
100 µm

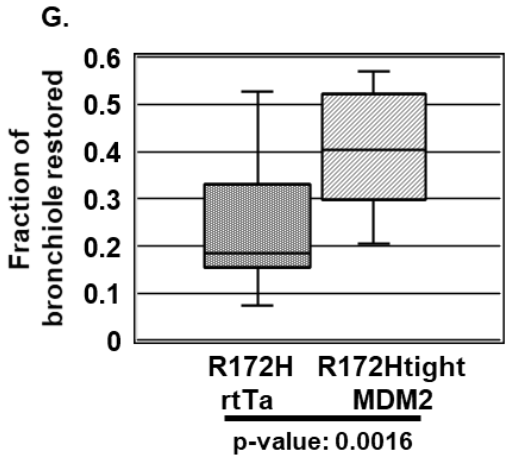
G.
Fraction of bronchiole restored
0.6
0.5
0.4
0.3
0.2
0.1
0
R172H rtTa
R172Htight MDM2
p-value: 0.0016

Figure 32. MDM2-induced DNA replication and re-epithelialization of lung bronchioles after naphthalene injury is independent of WT p53. Representative photographs showing (A) Dox-induced CCSP-driven co-expression (brown) of MDM2 and mutant p53-R172H in lung bronchiole detected by immunostaining of serial lung tissue sections, (B) BrdU incorporation (red) in CCSP (green) expressing cells in lung bronchiole detected by immunostaining. (C) Frequency of BrdU incorporating CCSP positive cells are shown by a bar graph. (D) Representative photographs showing CCSP (green) and SPC (red) co-expressing progenitor cells (arrows) in lung bronchioles of Dox-treated LSL R172H or LSL R172H, tightMDM2 mice consequent to naphthalene injury were detected by immunostaining. (E) Frequency of CCSP and SPC co-expressing cells in lung bronchiole are shown by a bar graph. (F) Representative photographs showing restoration of epithelial layer with CCSP expressing cells in lung bronchioles of Dox-treated LSL R172H and LSL R172H, tightMDM2 mice 72 hours after naphthalene injury. (G) Fraction of bronchioles restored have been compared using Box and Whisker plots. In all graphs, p-values are indicated.

MDM2 is needed for repair of lung injury: Ability of Dox-induced MDM2 to facilitate repair of naphthalene-induced lung injury, raised the possibility that MDM2 is needed for repair of lung injury. Since loss of both alleles of mdm2 is embryonically lethal in the presence of WTp53, p53-/-:mdm2-/- mice, obtained infrequently, were tested. However, mice with loss of one or both alleles of mdm2 with p53-/- background proved to be vulnerable to naphthalene injury and did not survive more than 24 hours. Since 24 hours could be inadequate to determine repair of naphthalene-induced lung injury, efficiency of repair were investigated in p53+/-:mdm2+/- mouse lungs compared to p53+/-:mdm2+/+ controls. Accordingly, p53+/-:mdm2+/- and p53+/-:mdm2+/+ mice were injected with naphthalene followed by BrdU, and were harvested at 72 hours after treatment.

IHC analysis of serial FFPE lung tissue sections from p53+/-:mdm2+/- mice showed a robust reduction of BrdU labeled CCSP positive cells (Figure 33A, B) and a consistent decrease in CCSP and SPC co-expressing cells in the bronchiole and BADJ compared

sections from p53+/-:mdm2+/+ mice (Figure 33C, D). In addition, bronchioles of p53+/-:mdm2+/- showed reduced efficiency of re-epithelialization (Figure 33E, F). These data indicate that loss of one endogenous mdm2 allele impedes repopulation of bronchiolar epithelium after naphthalene injury, signifying that MDM2 is needed for injury repair.

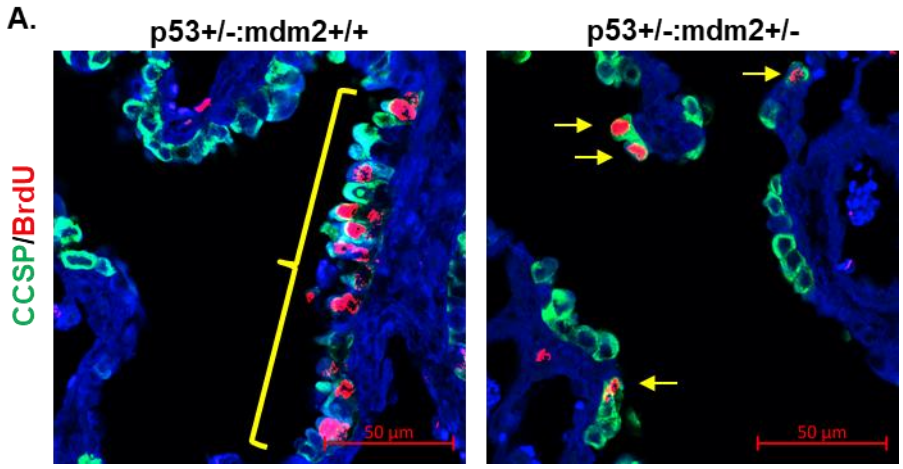

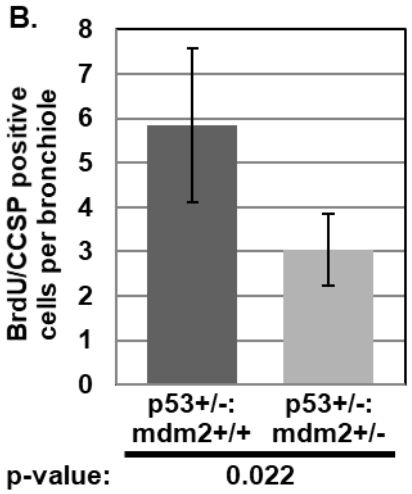

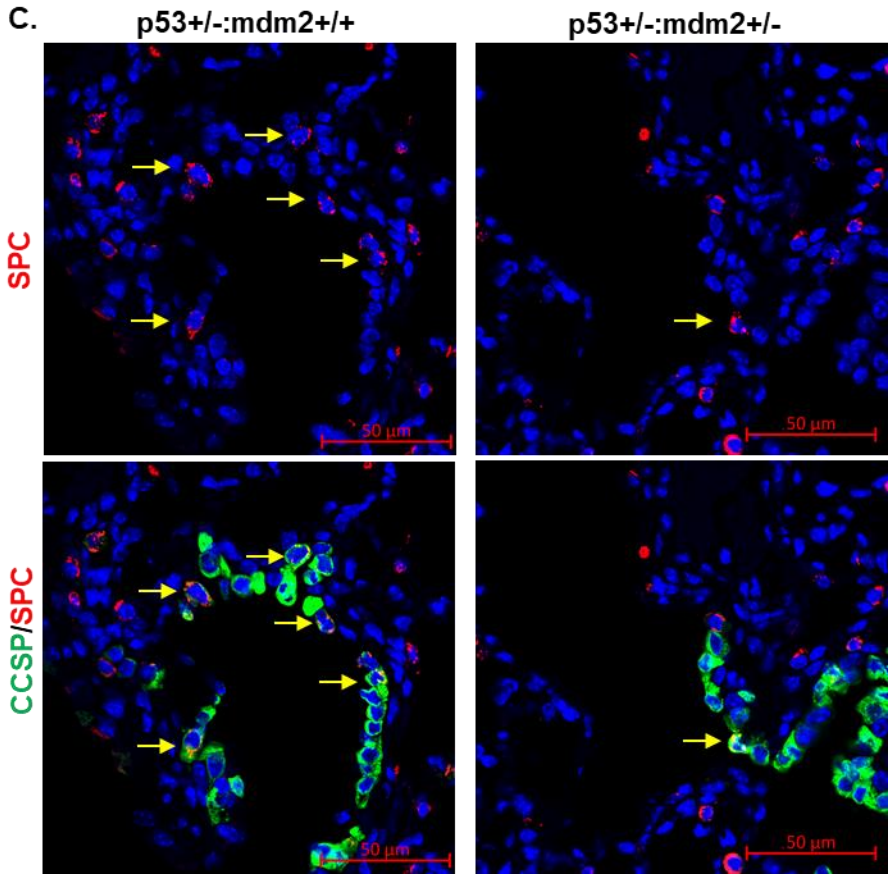
C.
p53+/-:mdm2+/+
p53+/-:mdm2+/-
SPC
CCSP/SPC
50 µm
50 µm
50 µm
50 µm

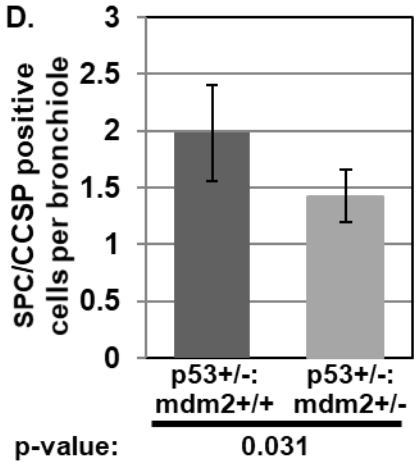
D.
SPC/CCSP positive cells per bronchiole
3
2.5
2
1.5
1
0.5
0
p53+/-: mdm2+/+
p53+/-: mdm2+/-
p-value:
0.031

Figure 33. Loss of one mdm2 allele reduces efficiency of re-epithelialization after naphthalene injury. p53+/-:mdm2+/+ and p53+/-:mdm2+/- mice were harvested 72 hours after naphthalene injury and 5 hours after BrdU delivery, and FFPE sections of lungs were analyzed by immunostaining. Representative photographs showing (A) BrdU incorporation (red) in CCSP (green) expressing cells in lung bronchioles, (B) a bar graph showing frequency of BrdU incorporating CCSP positive cells, (C) representative photographs showing CCSP (green) and SPC (red) co-expressing progenitor cells (arrows) in lung bronchioles, (D) a bar graph showing frequency of CCSP and SPC co-expressing cells in lung bronchioles, (E) representative photographs showing restoration of epithelial layer with CCSP expressing cells in lung bronchioles, (F) Box and Whisker plots to demonstrate fraction of bronchioles restored. In all graphs, p-values are indicated.

Discussion.

This chapter demonstrates that increased expression of human oncoprotein MDM2 accelerates proliferation and expansion of lung progenitor cells in response to naphthalene and radiation injury along with rapid repopulation of lost epithelial layers (Figure 23, 29, 30). Consistently, the presented data also show that loss of one endogenous allele of MDM2 impedes proliferative activities of lung progenitor cells and restoration of bronchiolar epithelium implicating MDM2 in epithelial restoration after lung injury (Figure 33). Presented data also show that lung injury in the context of MDM2 overexpression leads to accelerated proliferation and EMT of lung progenitor cells. While these data reveal a novel role of MDM2 in repair of lung injury (Figure 34), it also suggests a mechanism by which deregulated progenitor cell proliferation after lung injury may induce tumor formation or may facilitate lung fibrosis. Since lung injury has been reported to generate growth factors (144, 150), increased or sustained exposure to growth factors could also cooperate with cell proliferative activities of MDM2. Arguing for this hypothesis, co-occurrence of MDM2 and growth factor overexpression in human cancers (151-153) has often been reported signifying

their cooperation during tumorigenesis. These observations are consistent with earlier reports suggesting resistance of cancer cells with MDM2 overexpression to radiation therapy (126, 154).

Although p53-independent oncogenic functions of MDM2 have gained attention recently (155, 156), biological functions of MDM2 including its tumorigenic ability have been primarily ascribed to its E3-ubiquitin ligase functions, particularly to its ability to inactivate and degrade tumor suppressor p53 (126, 157). While MDM2 overexpression is common in human lung cancer (126), how MDM2 overexpression establishes cell proliferation in normal adult lungs, and whether inactivation of WT p53 is responsible for this function is not known. The presented data indicate that although MDM2 overexpression drives Club or alveolar epithelial cells to interphase, it requires injury-induced signaling to motivate the cells to replicate DNA. Proliferative activity in adult lungs are mostly detected as a response to injury (141), which is known to induce secretion of growth factors, eliciting the injury signaling pathway, and causing progenitor cell proliferation and re-epithelialization (144, 150).

MDM2 is capable of Akt phosphorylation(30), and the presented data indicate that this activity of MDM2 is needed for inducing DNA replication in lung progenitor cells and re-epithelialization of bronchiolar epithelium. Transient up-regulation of MDM2 facilitates repair of lung injury, while inhibition of MDM2-induced Akt signaling prevents proliferation of lung progenitor cells that endogenously overexpresses MDM2 (Figure 26, 27). However, the Akt inhibitor did not ablate basal proliferative activity induced by lung injury (Figure 26B, C), suggesting the presence of an alternative Akt-independent pathway

operative in lung. These observations signify that inhibition of Akt signaling in the context of MDM2 overexpression may restrict deregulated progenitor cell proliferation and therefore fibrosis or tumor formation after lung injury. This observation could be clinically important, because if cell proliferative activity of MDM2 consequent to lung injury is due to its Akt phosphorylation function, an Akt inhibitor rather than the inhibitors of MDM2-p53 interaction would be needed to combat expansion of MDM2-overexpressing lung progenitor cells.

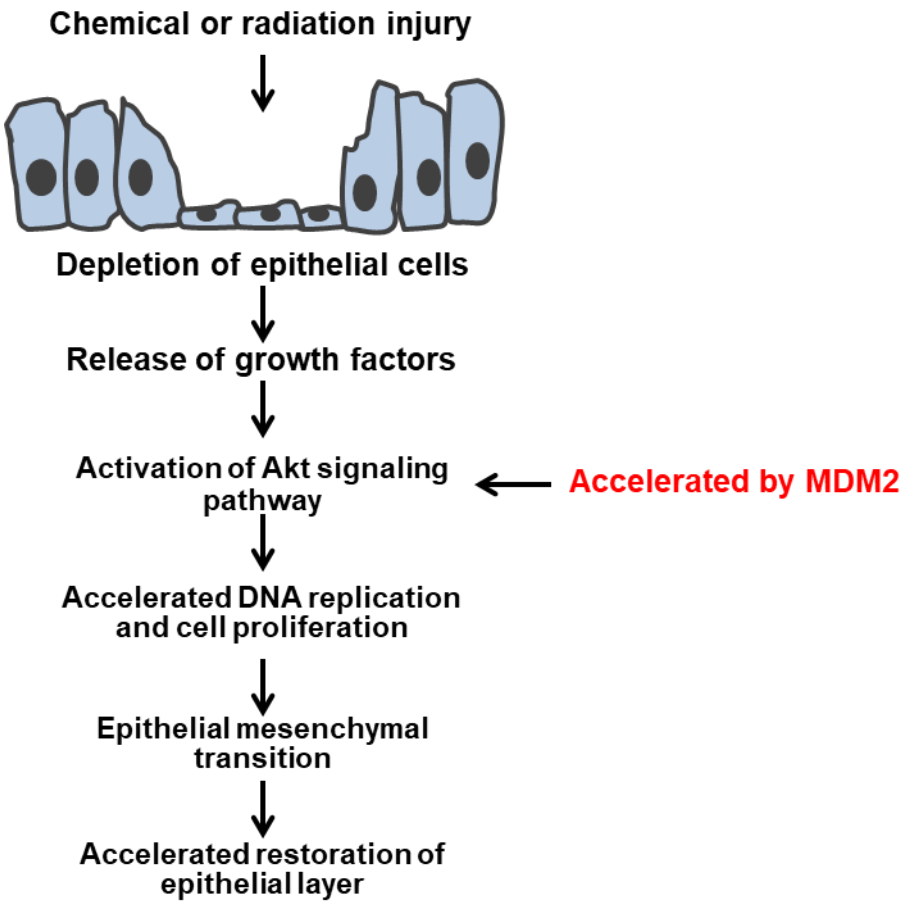

Figure 34. Consequence of lung injury in the context of MDM2 overexpression. MDM2-induced Akt phosphorylation accelerates proliferation of lung progenitor cells restoring epithelial layer depleted by injury.

Conclusion.

The presented data is consistent with earlier reports that MDM2 contributes to wound repair (130, 158) or renal development (129), and maintenance of hematopoietic stem cells (159). However, these studies were essentially designed to determine the consequence of WTp53 degradation by MDM2, and therefore is distinct from the observed WTp53-independent regenerative properties that accelerate DNA replication, expansion of lung progenitor cells, and re-epithelialization even in the context of p53 mutation.

While the presented data reveals a novel role of MDM2 in accelerated repair of lung injury, it also suggests a mechanism by which deregulated progenitor cell proliferation after lung injury may induce tumor formation or may facilitate lung fibrosis. Since lung injury has been reported to generate growth factors (144, 150), increased or sustained exposure to growth factors could also cooperate with cell proliferative activities of MDM2. Arguing for this hypothesis, co-occurrence of MDM2 and growth factor overexpression in human cancers (151-153) has often been reported signifying their cooperation during tumorigenesis.

Implication of GOF p53 mediated DNA replication stress on genetic instability and tumorigenesis.

The work presented in this chapter has been published in the Journal of Clinical Investigation (J Clin Invest. 2017 May 1;127(5):1839-1855.) ChIP analysis and sequencing assays were performed by Catherine Vaughan.

Introduction.

Loss of WT p53 or expression of GOF p53 are both known to deregulate the cell cycle and to induce untimely S phase entry (160), yet GOF p53 also specifically confers a selective proliferation advantage. To determine the mechanism of GOF p53-dependent growth of cancer cells, we investigated the architecture of genome duplication in the presence and absence of GOF p53. Since GOF p53 mutation is prevalent in lung cancer, human lung cancer or primary mouse lung cells were used for these experiments. Our data indicate that in comparison to p53-null, p53-depleted or loss of function (non-GOF) p53-expressing cells, lung cells with GOF p53 show a higher frequency of origin firing at early S phase, promoting rapid genome duplication with errors, as demonstrated by early entry into mitosis and increase in micronuclei formation. Consistent with its increased origin firing activity, GOF p53 increased expression of the intra-S phase checkpoint kinase, Chk1, known to prevent collapse of replication forks. Thus, in comparison to p53-/- cells, cells with GOF p53 show higher levels of Chk1 and phosphorylated Chk1 and reduced frequency of replication fork

collapse. In contrast, p53-/- or p53-depleted cells show decreased origin firing, higher frequency of replication fork collapse and increased levels of chromatin associated γH2AX. Compromise of GOF p53-mediated transcriptional activation abrogated its ability to increase origin firing, form micronuclei and activate the intra-S phase checkpoint, re-establishing replication fork collapse and reduced cell proliferation. Genome-wide analyses revealed that GOF p53 recognizes the promoters of Cyclin A, needed for origin firing (161-163), and Chk1, needed for preventing collapse of replication forks (164-166), and activates their expression in a cell cycle dependent manner at the level of transcription.

Collapse of replication forks is known to induce either cell death or gross chromosomal rearrangement due to incomplete DNA replication (167, 168). Consistently, experiments utilizing a mouse xenograft model revealed that inhibition of Chk1 reduced the size of tumors generated from a human lung cancer cell line with GOF p53 mutation more efficiently than GOF p53 knockdown cells, and selectively reduced proliferation of cultured lung cancer cells with GOF p53 mutation. These data provide compelling evidence that GOF p53 establishes oncogene addiction in cancer cells by generating and fostering DNA replication forks, and inactivation of these functions of GOF p53 may represent a promising therapeutic avenue in cancer.

Materials and methods.

Plasmids, lentiviral vectors and cell lines: Generation of plasmids, lentiviruses and stable transfectants expressing GOF p53 or shRNA against GFP or p53 has been carried out using pLKO.1 expression vector purchased from Open Biosystem (Lafayette, Co) following

supplier's protocols. Lung cells from mice were generated and cultured following standard protocols (30, 31). CCNA2 promoter is a gift from Dr. Toshio Nikaido (169). CHEK1 promoter was constructed by isolating upstream promoter region. H1299 and H1048 cell lines were obtained from American Type Culture Collection (ATCC). VMRC cell line was obtained from JCRB Cell Bank (Japan).

Animals: p53-null and p53 R172H knock-in (KI) mice were generated by crossbreeding corresponding heterozygous (p53+/- and p53R172H/WTp53 respectively) mice [gifts from Guillermina Lozano (34, 170)]. Nude mice were obtained from Jackson Laboratory.

Chemicals and Drugs: Iododeoxyuridine (IdU) and chlorodeoxyuridine (CldU) were purchased from Sigma. PHA767491 (Tocris Bioscience) was used at a concentration of 10 μM for indicated times (101, 102). Chk1 inhibitor PF-00477736 was purchased from (Sigma) and used at a concentration of 50 nM for 24 hours for treatment of cultured cells and 10 mg per kg for treatment of tumors (171).

Antibodies: Antibodies used included anti-p53 (sc-6243), Chk1 (sc-56288), Cyclin A (sc-751) , ERK-2 (sc-154), Actin (sc-47778) from Santa-Cruz Biotechnology, phospho Chk1 (2348s) from Cell Signaling Technology, γ-H2AX (05-636) and H3 (1953330) from Millipore, were used per manufacturer's protocol. Mitotic cells were identified by staining with α-Tubulin antibody (T9026) from Sigma. Anti-human p53 monoclonal antibody was a gift from David Lane. IDU was detected by mouse anti-bromodeoxyuridine (347580) from Becton Dickinson primary antibody and Alexafluor 594-conjugated rabbit anti-mouse and Alexafluor 594-conjugated goat anti-rabbit (Life Technologies) secondary and tertiary antibodies respectively. Cldu was detected by rat anti-bromodeoxyuridine (OBT0030G)

primary antibody from Accurate, and Alexafluor 488-conjugated chicken anti-rat and Alexafluor 488-conjugated goat anti-chicken (Life Technologies) secondary antibodies.

Detection of replicating nuclei: Replicating nuclei were detected following methods described earlier (31). Briefly, density arrested cells were replated on cover slips and labeled with 40 μM Iodo deoxy uridine(IdU) for 20 minutes at desired time after replating. IdU was washed off using PBS. Cells were fixed with 3% paraformaldehyde solution. Fixed cells were treated for 5 minutes with 0.5% triton X-100, followed by 1 hour treatment with 2.5 N HCl to denature the DNA, and neutralized with three washes of 0.1M sodium borate. Cells were then washed with 0.1% tween in PBS (wash buffer) and blocked in 2% BSA in wash buffer for an hour. The cells were then sequentially incubated with primary and Alexafluor 594-conjugated secondary antibodies each for an hour in 1% BSA in wash buffer. The cover slips were washed and mounted on slides with Prolong Gold Antifade with DAPI (4', 6'- diamino-2-phenylindole hydrochloride, Life Technologies) and imaged using confocal microscopy (Zeiss LSM700).

Detection of replicating cells by flow cytometry: Flow cytometric analysis of replicating cells was performed using methods described earlier (88, 172). Cells were labeled with nucleotide analogue bromodeoxy uridine (BrdU) as described above. For flow cytometry, cells were fixed with 70% ethanol at 4°C overnight. Acid base treatment and immunostaining were conducted using protocol described above using an Alexafluor 488 conjugated anti-BrdU antibody (BD Biosciences). DNA was stained with propidium Iodide (PI). The samples were analyzed using a BD FACScanto II flow cytometer using BD FACS Diva software.

Identification of DNA replication origin firing: DNA replication origin firing was determined by DNA fiber spreading analysis following published protocols (31, 99, 100, 173). Briefly, cells were pulse-labeled sequentially with nucleotide analogues IdU (40 μM) and CIdU (100 μM) to track the replication pattern and directionality of fork movement. Cells were collected by trypsinization, and genomic DNA of approximately 600 cells was aligned on slides by fiber spreading as described earlier. Slides were then air dried and fixed 3:1 methanol/acetic acid and dried overnight. After acid treatment (2.5N HCl 30 minutes) and blocking (2% BSA in PBS), DNA fibers on slides were immunostained with primary antibodies against IdU and CIdU followed by fluorescently-labeled secondary and tertiary antibodies, washed dried and mounted in Prolong Gold Antifade (Life Technologies). Images were collected by confocal microscopy (Zeiss LSM700). Newly initiated single origins were detected as red track flanked on both sides by green track as explained in Figure 4A. Approximately 150 to 200 fibers from each sample were scored and analyzed using Image J software (NIH).

Cell cycle analysis and detection of mitotic nuclei: Cell cycle analysis was performed by ethanol fixation and propidium iodide staining at different time intervals after replating density arrested cells and flow cytometry (BD FACSCanto II). Cell cycle analysis was performed using BD FACSDiva software. For identification of mitotic nuclei, density arrested cells were replated on coverslips and fixed using 3% paraformaldehyde. The cells were then treated with 0.1% triton X-100 for 10 minutes, followed by PBS washes and 1 hour blocking in 5% BSA. The primary antibody incubation was performed in the blocking buffer for 1 hour followed by PBS wash and 1-hour incubation with Alexa 488-conjugated

secondary antibody. Cells were briefly stained with DAPI solution, washed and mounted on slides using Prolong Gold Anitfade and imaged by confocal microscopy (Zeiss LSM700) at 40x magnification.

Detection of micronuclei: Cultured cells were plated on coverslips and fixed using 3% paraformaldehyde, mounted on slides with Prolong Gold Antifade with DAPI and imaged using confocal microscopy (Zeiss LSM700). Presence of micronuclei was examined for 500 randomly selected cells.

Detection of γH2AX: Cultured cells were washed with PBS and harvested. The cell pellet was digested in lysis buffer (10mM HEPES pH 7.9, 1.5mM $MgCl_2$, 10mM KCl, 0.5mM DTT, 1.5mM PMSF) containing 0.2N HCl for 30mins. The supernatant was neutralized with phosphate buffer. Chromatin bound γH2AX was detected by immunoblot analysis. For detection of γH2AX foci, cultured cells were plated on coverslips and fixed using 3% paraformaldehyde. The cells were then treated with 0.1% triton X-100 for 10 minutes, followed by PBS washes and 1 hour blocking in 5% BSA. The primary antibody incubation was performed in the blocking buffer for 1 hour followed by PBS wash and 1 hour incubation with Alexa 488-conjugated secondary antibody. Coverslips were mounted on slides using Prolong Gold Anitfade with DAPI and imaged by confocal microscopy (Zeiss LSM700) at 40x magnification. 250 cells were randomly examined for presence of γH2AX.

Immunoblot analysis and quantification: Immunoblot analysis was performed following standard techniques. Antibodies have been described above. Quantitave comparisons were performed using Quantity One 4.6.2 software (Biorad).

RNA extraction and sequencing: Total RNA was isolated from exponentially growing cultured cells lines using TRIZOL reagent (Life Technologies) following supplier's protocols. For RNA sequencing, 4ug of total RNA was processed and sequenced at Donnelly Sequencing Center at the University of Toronto. RNA samples were run on the Illumina HiSeq 2500 System and individual fastq files were used for analysis. Sequences were aligned to the human genome (HG19) and analyzed using the DNASTAR ArrayStar (version 12) software. All RNA-Seq experiments were normalized by assigned Reads Per Kilobase of template per Million (RPKM) mapped reads.

Chromatin Immunoprecipitation (ChIP) analysis and sequencing: ChIP and ChIP-seq was performed using standard methods (174). Briefly, exponentially growing H1299 cells expressing either empty vector or the p53 mutant p53R273H were fixed with formaldehyde, extracted and immunoprecipitated with antibodies against p53 (DO1 and FL-393, Santa Cruz Biotechnology). DNA fragments were eluted from immunoprecipitates, reverse crosslinked and purified. Purified DNA (150ng) was sequenced at the Donnelly Sequencing Center at the University of Toronto. ChIP samples were run on the Illumina HiSeq 2500 System and individual fastq files were used for analysis. Sequences were aligned to the human genome (HG19) and analyzed using the DNASTAR ArrayStar (version 12) software. Peaks were visualized using a SeqMan Pro software (DNASTAR). ChIP-Seq experiments were normalized by Reads assigned Per Million mapped reads (RPM). Regions on the genome that showed binding of p53 in the p53-R273H expressing cells but no binding in the vector cells or where there was greater than 1.5-fold higher binding in the p53-R273H cells were considered significant. Gene lists for the RNA-seq and ChIP-seq were compared

to determine which were up-regulated by mutant p53 and which also have p53 binding to the promoter. For ChIP analysis, DNA samples were suspended in water and the presence of cyclin A and chk1 promoter fragments were analyzed by three contiguous sets of primers.

Generation of cDNA and quantitative PCR (QPCR): RNA extraction, cDNA preparation and QPCR were performed following standard protocols (175). cDNA was synthesized using the Thermoscript Reverse Transcription-PCR system (Life Technologies). QPCR was carried out using a LightCycler system (Roche). Primers were designed using OLIGO 5 software (Molecular Biology Insights) and were synthesized by Integrated DNA Technologies. Reactions were performed in duplicates utilizing SYBR green dye, which exhibits a higher fluorescence upon binding of double-stranded DNA.

Analysis of Cyclin A and Chk1 Promoter activity: H1299 cells were transfected with 200 ng of luciferase reporter plasmid (pGL3), with luciferase reporter under the control of CCNA2 (169) or CHEK1 promoter sequences or empty pGL3 basic vector (Promega, Madison, WI) and 1 ug of the indicated p53 expression plasmid using Lipofectamine 2000 (Invitrogen) following the manufacturer's instructions. Cell lysates were prepared 48 hours after transfection, and luciferase activity was determined. Luciferase analysis was carried out using the luciferase assay system (E1500) and instructions from Promega. Experiments were performed in triplicate as described before (86).

Xenograft studies: Nu/nu mice were used for the tumorigenicity studies. Eight-week-old mice were injected with 1×10^7 cells subcutaneously in both flanks and measured periodically following published protocols (176). H1048 cell line expressing shRNA against p53 or GFP was used. Tumor size was assessed at day 10 and mice were equally distributed

into two groups to receive daily 10mg/kg of PF-0047773 dissolved in 2% DMSO, 40% PEG or vehicle by intraperitoneal injection.

Statistical analysis: Unless otherwise specified, all experiments were performed in triplicates and representative data is shown. Presence of bi-directional origins as well as collapsed forks detected by sequential labeling of replicating DNA in different samples in each experiment set was compared using student's *t* test. Percent mitotic cells between different samples were compared using Student's *t* test. Micronuclei per cell for different samples were evaluated using chi-square test. QPCR reactions were performed in duplicates and repeated in three independent experiments. All the immunoblots have been repeated three times and representative data is shown. Unless otherwise specified for all the experiments a p-value of less than 0.05 was considered significant.

Study Approval: All animals used in this study were maintained and assayed in accordance with federal guidelines and those established by the Institutional Animal Care and Use Committee at the Virginia Commonwealth University, Richmond, Virginia.

Results.

GOF p53 mutation and loss of WT p53 hasten time of S phase entry to a similar extent. While loss of p53 deregulates the cell cycle to enter S phase (160), several laboratories have demonstrated that GOF p53 accelerates cell proliferation and tumor growth in comparison to p53-null or knockdown cells (86, 177) and up-regulates expression of cell proliferating genes (175). Therefore, experiments were carried out to determine whether GOF p53 hastens the time of S phase entry compared to p53-null cells. Short-term cultures

of lung cells from p53R172H (human R175H) knock-in (KI) and p53-null mice were partially synchronized by density arrest, and their ability to incorporate the nucleotide analogue IdU (iododeoxyuridine) was determined at various times after replating by immunostaining IdU, and scoring IdU labeled cells using confocal microscopy. The data showed that lung cells from p53-null and p53R172H-KI mice entered S phase at similar times with 20 to 23% cells incorporating IdU at 12 hours after replating density arrested cells, while lung cells from normal (WTp53) mice show 5 to 7% IdU labeled cells under similar conditions (Figure 35). These data suggest that the absence of p53 or presence of p53R172H hastens S phase entry to a similar extent.

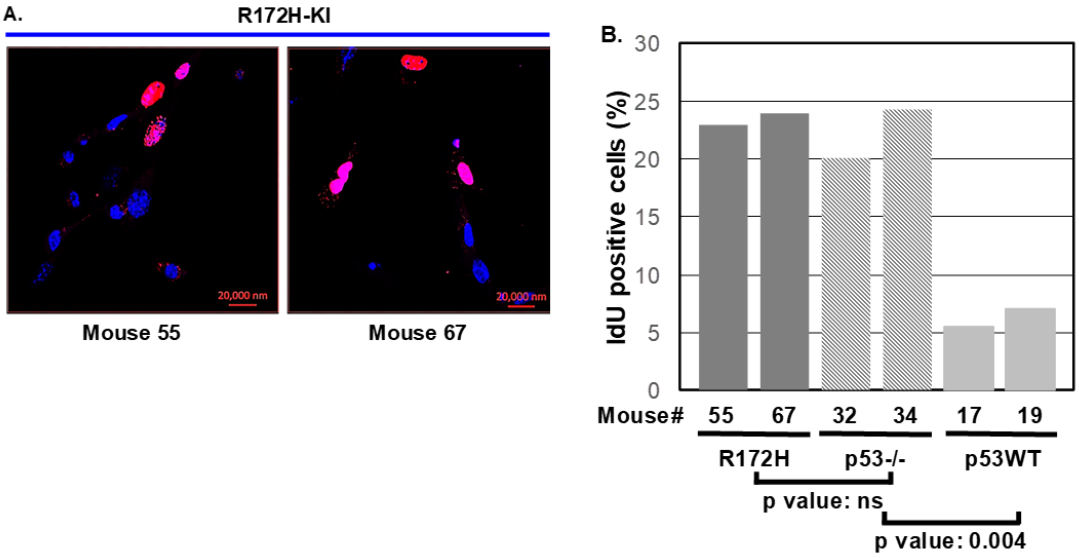

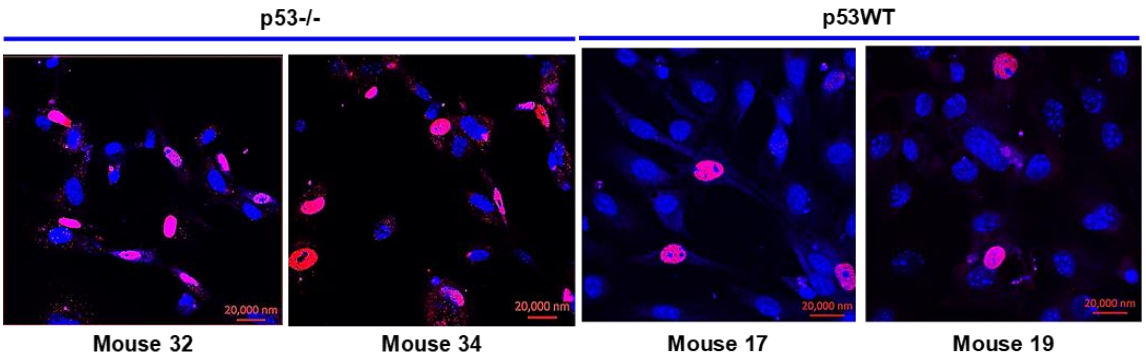

Figure 35. GOF p53 mutants do not hasten the S phase entry of cells. The figure shows representative images of lung cells from (A) p53R172H-KI (R172H), p53-/- and WT (p53 WT) mice pulse-labeled with IdU at 12 hours after confluence-arrest and replating. Cells were immunostained by Alexa 594 tagged IdU antibody, stained with DAPI and analyzed by confocal microscopy (20X). Lung cells from two different mice for each construct were analyzed. Two hundred nuclei were scored in each experiment. Percent of nuclei incorporating IdU in lung cells from p53R172H-KI, p53-/- or p53 WT mice are shown by bar graphs. The p-values calculated using Student's *t* test is shown at the bottom of the bar graph. ns: Not significant

Compared to p53-null cells, the frequency of DNA replication origin firing is higher in cells expressing GOF p53 mutants. Since GOF p53 mutants activate expression of genes required for DNA replication (175), the ability of these mutants to increase firing of DNA replication origins during S phase entry was determined. To determine if GOF p53 mutants alter frequency of DNA replication origin firing in otherwise normal cells, lung cells from p53-/- and p53R172H-KI mice were cultured and the frequency of origin firing during early S phase was determined using fiber analysis of replicating DNA using methods published earlier (31, 100, 173). Cells were partially synchronized by density-arrest and replating, and sequentially labeled with IdU and CldU at early S phase. Cellular genomic DNA was then spread on slides and replicating DNA fibers were detected by

immunostaining of incorporated IdU and CldU using red and green fluorescence tagged antibodies respectively followed by confocal microscopy. Scoring of bidirectional origins in untangled immunostained DNA fibers revealed that the frequency of origin firing in lung cells from p53R172H-KI mice was at least double of that in lung cells from p53-null mice (Figure 36A-C), whereas frequency of origin firing in replicating lung cells isolated from normal mice (WT p53) was approximately 3-fold lower than that in p53-null mice (Figure 36B) as expected. These results suggest that the presence of the GOF p53 mutant R172H in non-transformed lung cells accelerates the frequency of origin firing at early S phase.

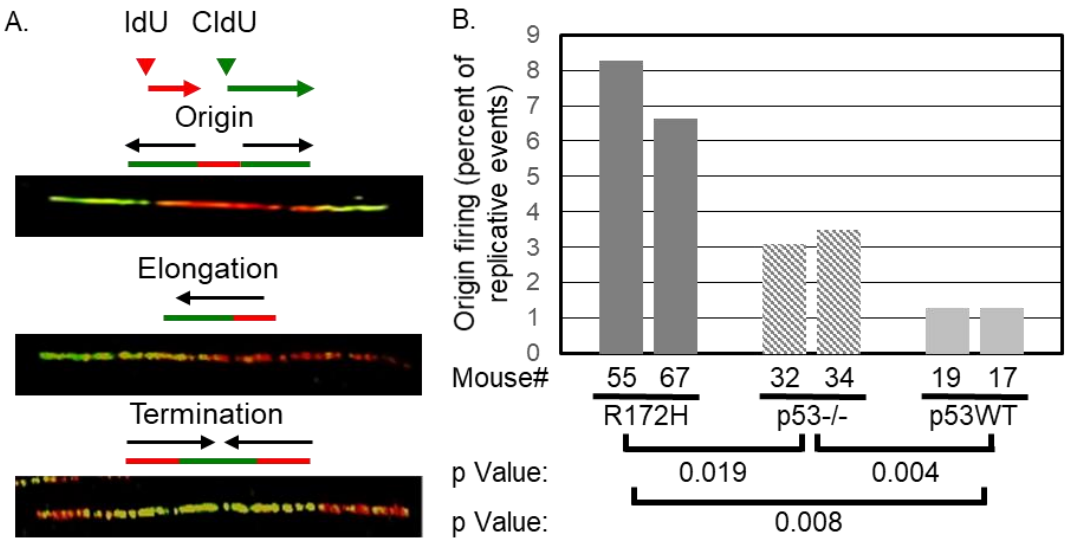

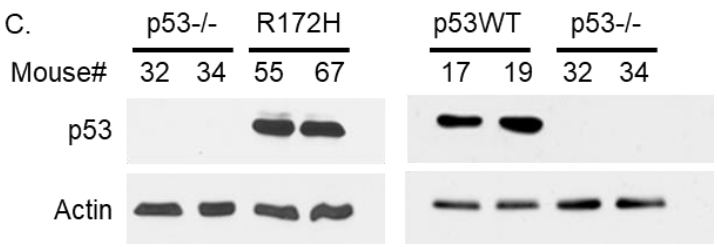

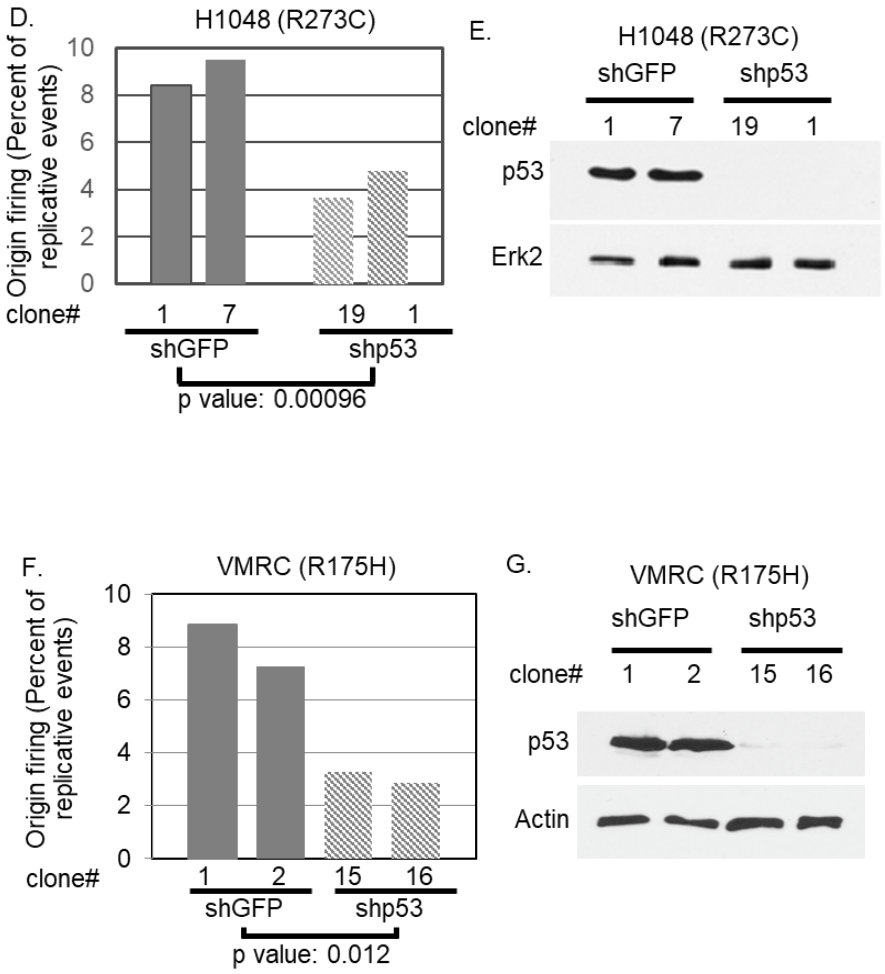

Figure 36. Compared to p53-null or -depleted cells, transformed or non-transformed lung cells harboring GOF p53 fire more DNA replication origins at early S phase. Fiber images (A) display bi-directional origin, elongating or terminating forks. Percent of origins in replicating fibers from lung cells of p53-/-, p53R172H-KI (R172H) and WT (p53WT) mice (B), and mock-depleted (shGFP) or p53-depleted (shp53) lung cancer cell lines H1048 (D), which harbors R273C, and VMRC, which harbors R175H, (F) are shown by bar graphs. Expression of p53 was determined by immunoblot analysis in each experiment (C, E, G). WT p53 expression (C) was visualized by analyzing higher protein (6-fold over p53R172HKI lung cell extract) and longer exposure. Actin is a loading control. Lung cells from two mice of each construct or two clones stably expressing shGFP or shp53 were analyzed. The p-values calculated using Student's *t* test are shown at the bottom of the bar graphs.

Knockdown of GOFp53 mutant in human lung cancer cells reduces the frequency of origin firing. The ability of GOF p53 mutants to increase origin firing in a human lung cancer cell line that naturally expresses GOF p53 was also determined. For this purpose endogenous p53R273C expression in the human SCLC lung cancer cell line H1048 or R175H expression in human NSCLC VMRC cell line was stably knocked down by expressing shRNA against p53 (shp53) or a control shRNA against GFP (shGFP) from a lentiviral expression vector (86). H1048 and VMRC cells stably expressing shGFP or shp53 were synchronized by density arrest and replating. Fiber analysis of replicating DNA from these cells was performed as described above. Scoring of bi-directional origins in untangled immunostained DNA fibers showed that knockdown of endogenous p53 significantly reduced frequency of origin firing in both the cell lines (Figure 36D-G). These results indicate that GOF p53 mutants accelerate firing of DNA replication origins at early S phase in cells harboring p53 mutation.

GOF p53 upregulates expression of intra-S phase checkpoint kinase Chk1 preventing collapse of replication forks. Hyper-replicative activities of oncogenes induce cellular checkpoint responses (106, 109) to prevent collapse of progressing replication forks, and thus cell death (164, 166, 178, 179). Intra-S phase Chk1 is known to protect replication forks, while inactivation of Chk1 leads to fork collapse, which could be evidenced by phosphorylation of histone H2AX (γH2AX) (164, 166, 178). Since GOF p53 accelerates origin firing at early S phase, its ability to activate intra-S phase checkpoint for preventing collapse of replication forks in cells harboring the mutation was investigated. For this

purpose, lung cells from p53-null and p53R172H-KI mice were partially synchronized by density arrest and replating, and the cell extracts were analyzed for Chk1 expression and phosphorylation at S345 by immunoblot analysis. Results (Figure 37A) of these experiments revealed that in comparison to lung cells from p53-/- mice, lung cells from p53R172H-KI mice show a significantly higher level of p-Chk1 (9- to 10-folds) and Chk1 (2- to 3-folds) at early S phase in repeated experiments, suggesting that GOF p53 may increase Chk1 phosphorylation during increased origin firing by up-regulating Chk1 expression.

Since GOF p53 increases Chk1 and p-Chk1 levels, the oncoprotein may reduce replication fork collapse, and therefore γH2AX foci formation. The presence of chromatin associated γH2AX in lung cells from p53-null and p53R172H-KI mice was determined by acid extraction of γH2AX from the chromatin fractions and immunoblot analysis. The result of this experiment showed that compared to lung cells from p53-null mice, chromatin associated γH2AX levels in lung cells from p53R172H-KI mice were drastically reduced (Figure 37A, B). Similar analysis using mock-depleted or p53 depleted H1048 human lung cancer cells stably expressing non-targeting shGFP or shp53 showed reductions in p-Chk1 and Chk1 levels and increases (approximately 2- to 6-fold) in γH2AX levels in shp53 expressing H1048 cells compared to H1048 cells expressing shGFP (Figure 37C, D). These results indicate that expression of GOF p53 increases p-Chk1 and Chk1 levels and reduces chromatin bound γH2AX levels, signifying that checkpoint activation by GOF p53 prevents collapse of replication forks and thus γH2AX foci formation.

Next, the ability of GOF p53 to reduce frequency of replication fork collapse was tested. For this purpose, partially synchronized lung cells from p53-null and p53R172H-KI mice were sequentially labeled for 20 minutes with IdU and 20 minutes with CldU at early S phase. Replicating fibers and direction of fork progression were detected in these cells by immunostaining IdU and CldU with red and green fluorescence tagged antibodies, respectively. It was reasoned that if the progressing forks collapse during the incorporation of IdU, these forks should not incorporate CldU, and therefore the red-only tracks should indicate collapse of progressing replication forks (Figure 37E). Untangled replicating DNA fibers were scored for the presence of red-only tracks. Result of this experiment revealed that in comparison to lung cells from p53-null mice, the frequency of red-only tracks was drastically reduced in lung cells from p53R172H-KI mice (Figure 37E, F) indicating a reduction in fork collapse in lung cells expressing p53R172H.

Reduction of replication fork collapse due to activation of Chk1 expression by GOF p53 should reduce chromatin association of γH2AX. To complete the analysis of GOF p53 mediated modulation of fork collapse, this possibility was examined. For this experiment, cultured lung cells from p53R172H-KI mice were treated with a Chk1 inhibitor, PF00477736. Chromatin associated γH2AX was extracted and analyzed by immunoblot analysis. Results of this experiment indicated that the Chk1 inhibitor PF00477736 elevates the levels of chromatin-associated γH2AX more than 6-fold (Figure 37G, H), as opposed to 1.6-fold increase in p53-null lung cells. Consistent with earlier studies (12, 171), inhibition of Chk1 upregulated RPA phosphorylation (at Ser 4 and 8) due to generation of replication stress (Figure 37G). These data indicate that the GOF p53-mediated reduction in γH2AX

can be overridden by inhibition of Chk1. These observations signify that cell proliferation induced by GOF p53 is at least partly due to its ability to increase expression of Chk1, activity of which prevents collapse of increased number of replication forks generated by the mutant protein, allowing rapid completion of genome duplication and cell proliferation sooner than p53-null cells. Thus, the ability of GOF p53 to upregulate Chk1 expression, and therefore its activity, may contribute to its ability to confer an addictive influence to the cells expressing the mutant protein.

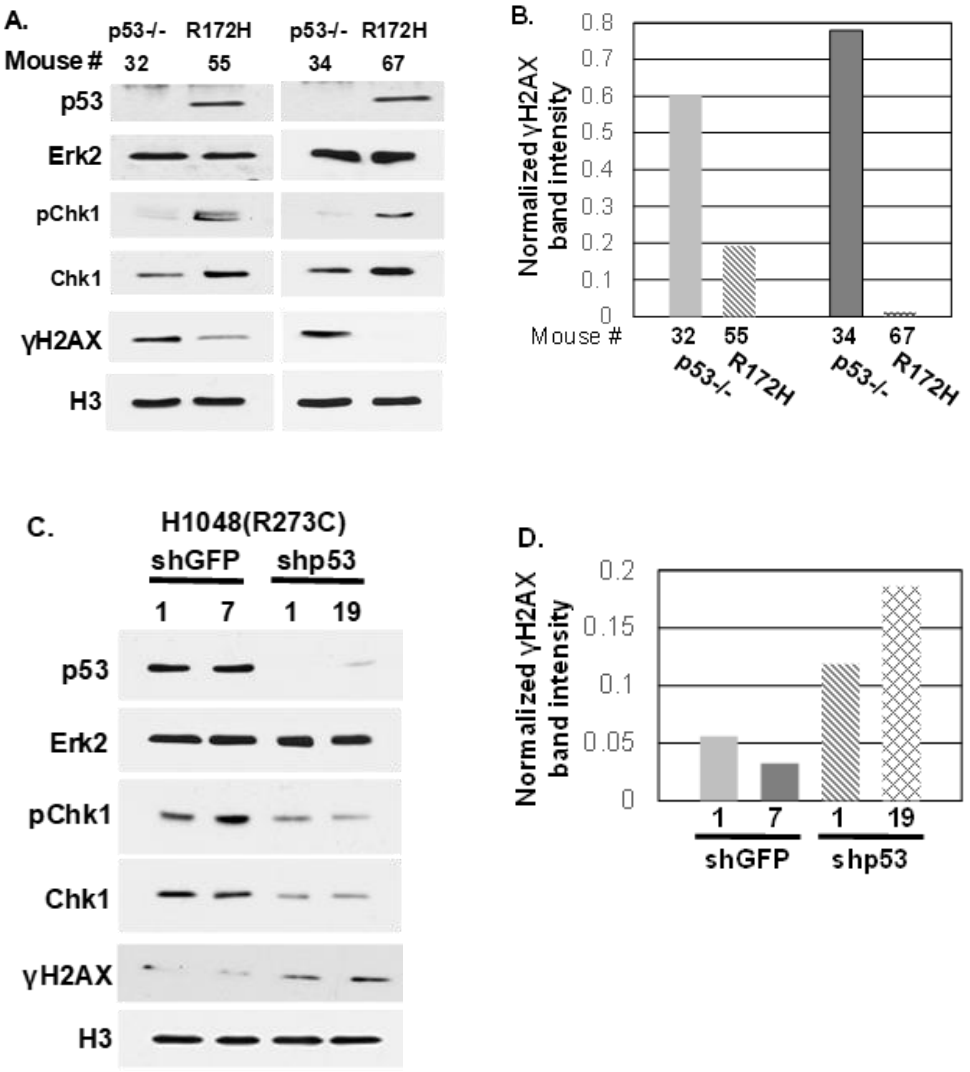

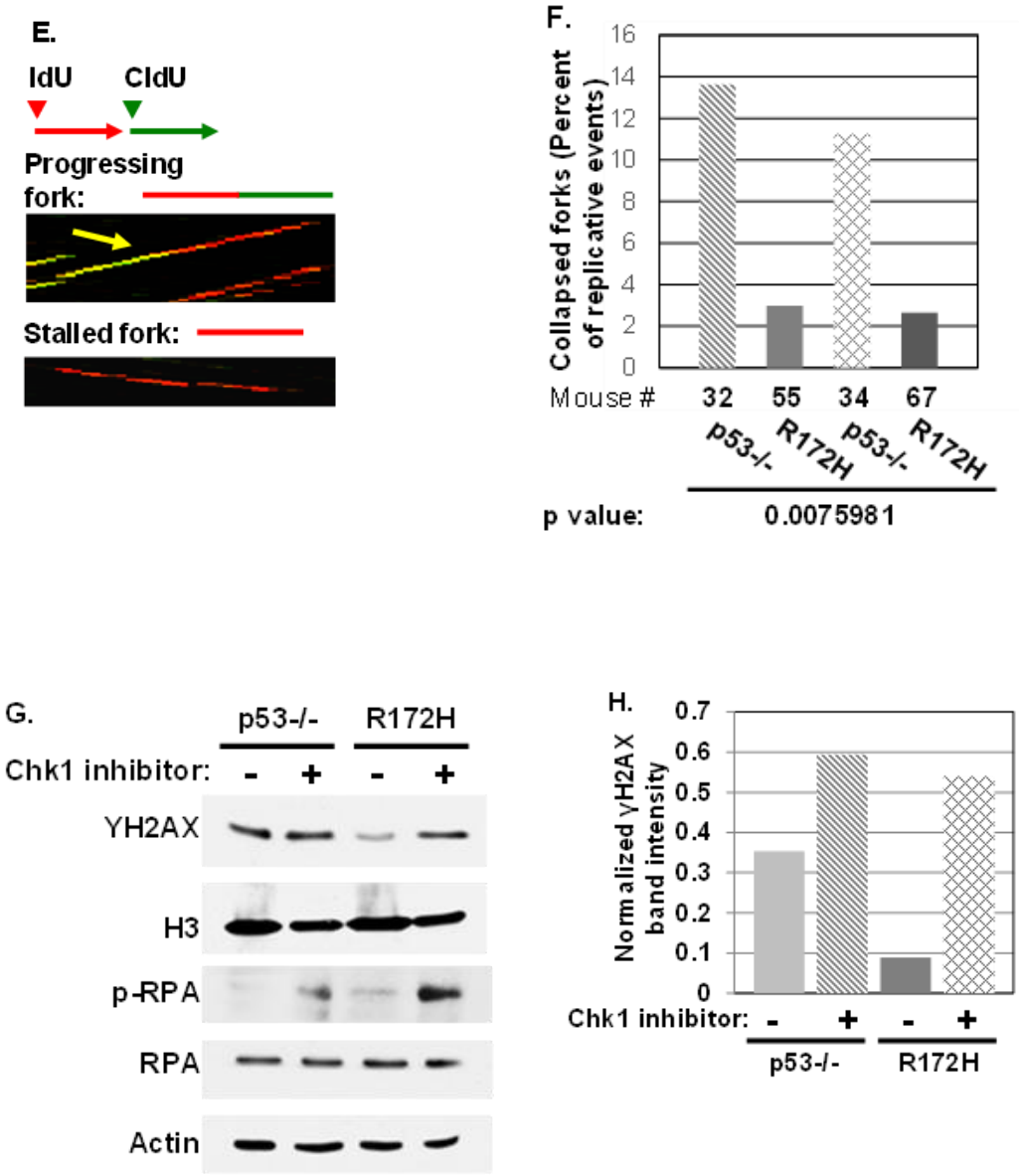

Figure 37. GOF-p53 activates intra-S phase checkpoint preventing collapse of replication forks. Detection of p-Chk1, Chk1 and chromatin associated γH2AX by immunoblot analysis using (A) lung cells of p53-/- and p53R172H-KI (R172H) mice, and (C) mock-depleted (shGFP) or p53-depleted (shp53) H1048 lung cancer cells. For detection of chromatin associated γH2AX, insoluble chromatin fraction was acid-extracted and analyzed by immunoblotting. Band intensities of γH2AX normalized by H3 levels are shown by bar graphs (B, D). Lung cells from two mice of each construct or two clones stably expressing shGFP or shp53 were analyzed. The experimental strategy for detection of replication fork collapse by fiber analysis is shown by a cartoon (E). Collapse of progressing

replication forks was assayed by fiber analysis of replicating DNA. The bar graph (F) compares the percent of red-only tracks (indicated by arrows in the fiber images) in replicating fibers. Approximately 200 untangled fibers from each sample were scored. The p-value calculated using Student's *t* test is indicated at the bottom of the bar graph (F). Lung cells from two mice of each construct were analyzed. Chromatin associated γH2AX levels in lung cells from p53-/- and R172H mice after treatment with a Chk1 inhibitor, PF477736, were determined by immunoblot analysis (G). γH2AX band intensities normalized by H3 levels are shown by bar graphs (H). Phosphorylated (Ser4/8) RPA (p-RPA) was detected by immunoblot analysis (G) to ensure activity of PF477736.

GOF p53 promotes rapid genome duplication and mitotic entry. Increased number of origin firing, and successful progression of generated replication forks should lead to rapid genome duplication. Therefore, we determined whether GOF p53 promotes quicker genome duplication in comparison to p53-null cells, by analyzing S phase progression and mitotic entry of partially synchronized lung cells from p53-null and p53R172H-KI mice generated as described above. Flow cytometric analysis of propidium iodide (PI) stained cells at 12 and 16 hours after release from density arrest showed that lung cells from both p53R172H-KI and p53-null mice entered S phase at a similar time and frequency with approximately 29% of p53R172H-KI and 21% p53-null cells in the S phase at 12 hours after release. However, with progress through S phase, at 16 hours lung cells from p53-null mice accumulated in S phase (43.5%), whereas lung cells from p53R172H-KI mice progressed to G2/M showing 29.6% S phase cells (Figure 38A). Accordingly, at 16 hours 23.7% p53R172H-KI cells completed genome duplication and entered G2/M phase as opposed to 15.3% lung cells from p53-null mice (Figure 39A-D). This data was further confirmed by identifying replicating cells at 12 and 16 hours after release from density arrest by pulse labeling with BrdU followed by PI staining. Flow cytometric analysis (Figure 39E, F)

showed that consistent with the data shown in Figure 38A, similar percentages lung cells from p53R172H-KI or p53-null mice incorporated BrdU (18.8 and 16% respectively) at 12 hours. However, at 16 hours 28.5% of p53-null cells incorporated BrdU, most (90%) of which remained in early or mid S phase. In contrast, only 10.8% lung cells from p53R172H-KI mice were found in early and mid-S phase (Figure 38B). Next, mitotic entry of the lung cells at 16 hours after release of density arrested cells was determined. Mitotic cells (Figure 40) were identified by immunostaining microtubule with α-tubulin antibody and staining nuclei with DAPI (4', 6'- diamino-2-phenylindole hydrochloride). Percent of cells in mitosis were determined by scoring 500 cells for mitotic nuclei under fluorescent microscope. The results revealed that lung cells from p53R172H-KI mice entered mitosis at a 2.5 to 2.8-fold higher frequency than that of p53-null lung cells (Figure 38C). These results show that p53-null lung cells take longer time to complete genome duplication to enter mitosis compared to p53R172H-KI lung cells, which complete genome duplication and enter mitosis sooner than p53-null lung cells.

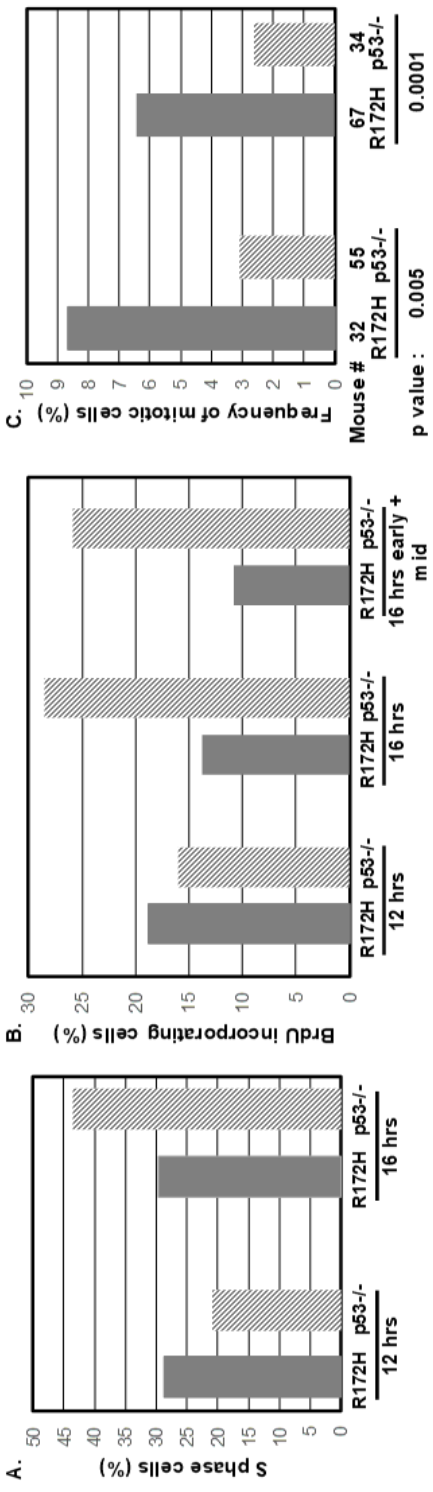
A.
S phase cells (%)
50
45
40
35
30
25
20
15
10
5
0
R172H p53-/-
12 hrs
R172H p53-/-
16 hrs
B.
BrdU incorporating cells (%)
30
25
20
15
10
5
0
R172H p53-/-
12 hrs
R172H p53-/-
16 hrs
R172H p53-/-
16 hrs early + mid
C.
Frequency of mitotic cells (%)
10
9
8
7
6
5
4
3
2
1
0
Mouse # 32 55 67 34
R172H p53-/- R172H p53-/-
p value : 0.005 0.0001

Figure 38. GOF-p53 promotes rapid genome duplication and mitotic entry. Percentages of S phase (A) and actively DNA replicating (B) lung cells generated from p53-null and p53R172H-KI mice and their frequency of mitotic entry (C) at 12 and 16 hours after density arrest and replating are shown by bar graphs. S phase and DNA replicating cells were identified by PI staining or BrdU pulse labeling and PI staining followed by flow cytometry. Approximately 500 cells were counted in each sample. The p-value calculated using Student's *t* test is shown at the bottom of the bar graph.

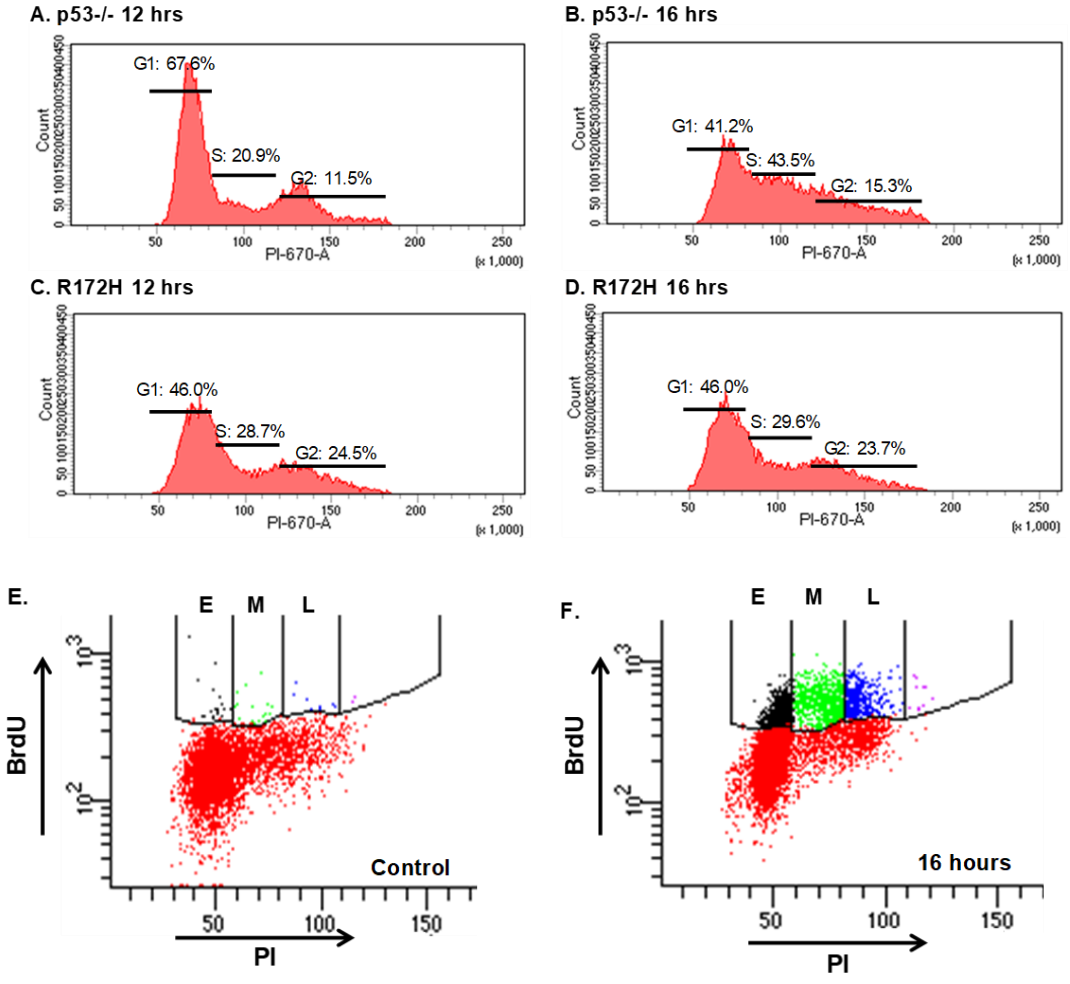

Figure 39. Flow cytometric gating of lung cells from p53-/- and p53R172H-KI (R172H) mice. DNA histogram (A-D) show percentages of cells in G1, S, G2/M phases at 12 (A, C) and 16 hours (B, D) after density arrest and replating. Representative bivariate dot plot generated by flow cytometry of lung cells after BrDU incorporation, immunostaining and PI staining at 16 hours after releasing cell cycle arrest (E, F). As a background control, antibody immunostaining and PI staining were performed without

BrDU incorporation (E). Gating to identify BrDU positive cells in early (E), mid (M), and late (L) S phase of the cell cycle is indicated.

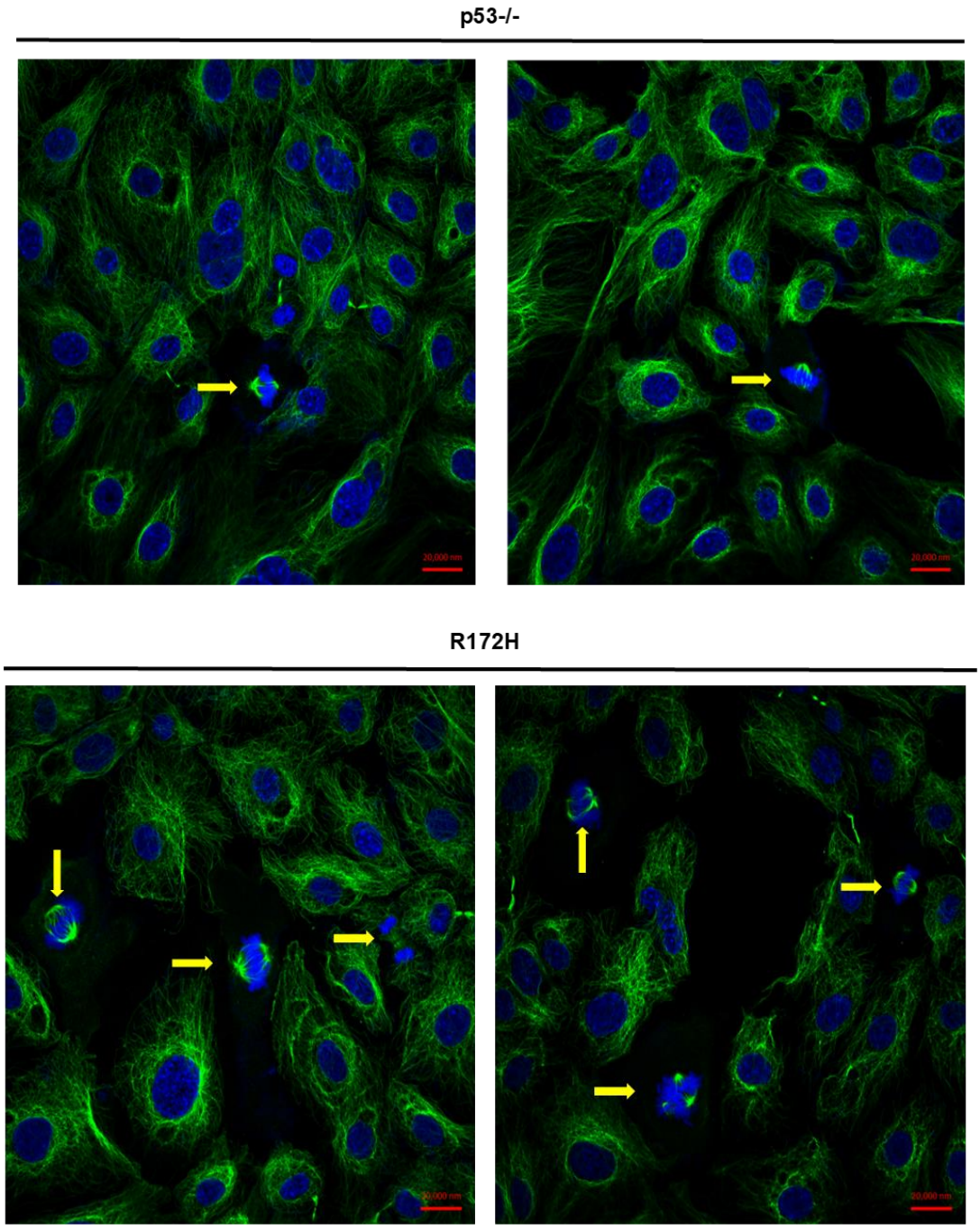

Figure 40. Representative images to show mitotic lung cells from p53-/- and p53R172H-KI (R172H) mice. Cells undergoing mitosis are indicated by arrows.

GOF p53 induces micronuclei formation, which can be prevented by blocking origin firing. Increased frequency of origin firing have been implicated in genomic abnormality (4, 164, 166, 180-182), and one of the indicators of genomic abnormality is micronuclei formation (183-185). Although an increase in Chk1 level would protect collapse of replication forks stalled due to increased origin firing, it has been reported that the topological stress during progress of increased number of forks may lead to genome abnormality by mechanisms such as fork reversal, which could be evidenced by micronuclei formation (181, 182). Since GOF p53 increases origin firing, the frequency of micronuclei formation in the presence or absence of GOF p53 was determined. For this purpose, cultured lung cells generated from p53-null or p53R172H-KI mice were plated on coverslips, fixed and stained with DAPI, and cells with micronuclei were scored by confocal microscopy. Scoring of cell nuclei associated with micronuclei revealed that lung cells from p53R172H-KI mice formed micronuclei at a significantly higher frequency than lung cell from p53-null mice (Figure 41A, B). Furthermore, it was determined whether knockdown of p53 reduces micronuclei formation in human lung cancer cells. H1048 cells (p53R273C), expressing shGFP or shp53, were cultured on coverslips, fixed and stained with DAPI, and scored for cells with micronuclei. Results of this experiment revealed a significant reduction in the frequency of cells generating micronuclei in H1048 cells stably expressing shp53 compared to those expressing shGFP (Figure 41C, D). These data indicate that GOF p53 increases micronuclei formation, an index of genetic abnormality.

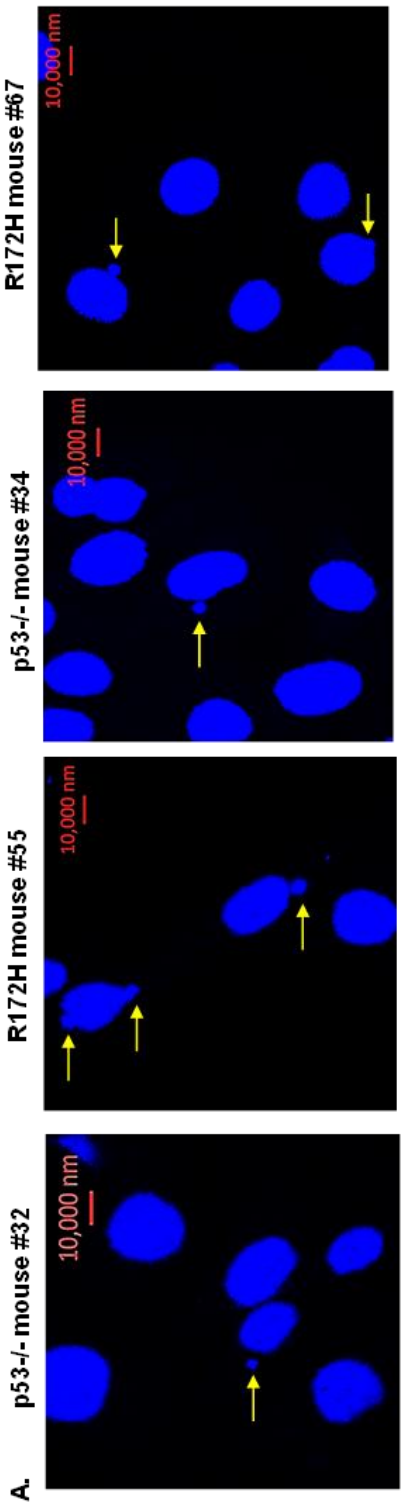
A.
p53-/- mouse #32
R172H mouse #55
p53-/- mouse #34
R172H mouse #67
10,000 nm

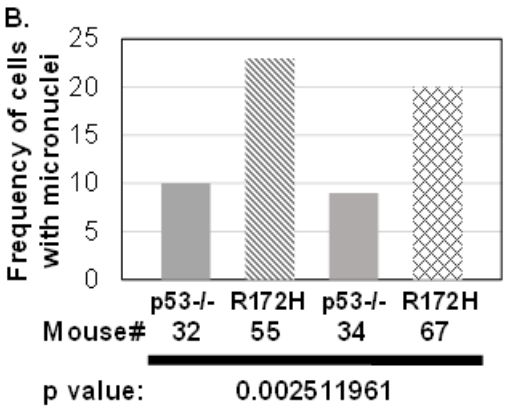
B.
Frequency of cells with micronuclei
25
20
15
10
5
0
p53-/- R172H p53-/- R172H
Mouse# 32 55 34 67
p value: 0.002511961

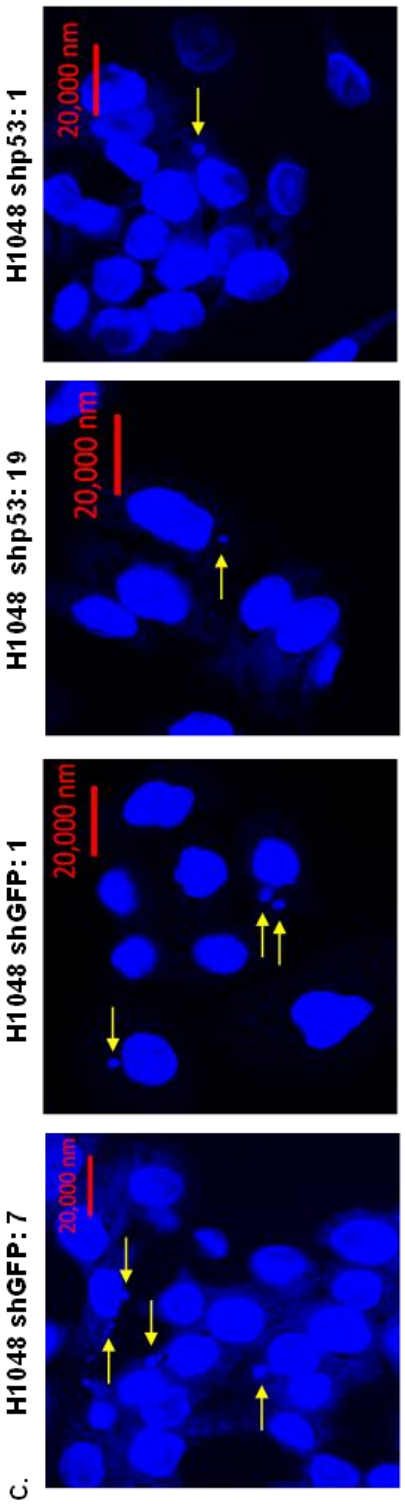
C.
H1048 shGFP: 7
H1048 shGFP: 1
H1048 shp53: 19
H1048 shp53: 1
20,000 nm

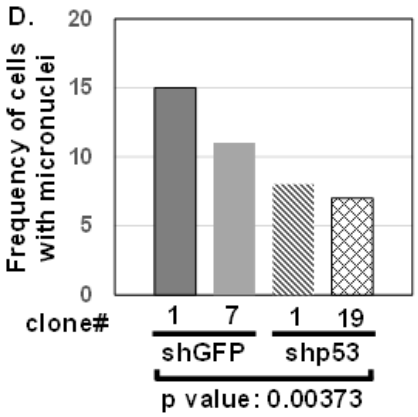
D.
Frequency of cells with micronuclei
20
15
10
5
0
clone#
1
7
1
19
shGFP
shp53
p value: 0.00373

Figure 41. Lung cells with GOF-p53 form micronuclei at a higher frequency than lung cells from p53-null mice: Representative images of micronuclei (indicated by arrows) from lung cells of p53-/-, and p53 R 172H-KI (R172H) mice (A), and mock-depleted (shGFP) or p53-depleted (shp53) H1048 lung cancer cells (C), detected by confocal microscopy (magnification 40X) after DAPI staining. The bar graphs (B, D) compare the percent of cells with micronuclei in each sample. Lung cells from two mice of each construct or two clones stably expressing shGFP or shp53 were analyzed. The p-values calculated using Chi square test are shown at the bottom of the bar graphs.

Next, experiments were designed to determine whether increase in the frequency of origin firing elevates micronuclei formation by GOF p53. It is known that in mammalian cells, DNA replication origins are activated by cyclin dependent kinases (cdk) and cdc7 kinase, which induces melting of double stranded DNA at the origin of replication (93, 120). Since GOF p53 induces origin firing, a cdc7 kinase inhibitor PHA767491, which specifically prevents activation of origins, but does not prevent fork progression (101, 102), was used to determine whether inhibition of origin firing in lung cells harboring GOF p53 mutation would reduce frequency of micronuclei formation. Lung cells from p53R172H-KI mice were treated with PHA76749 or vehicle (DMSO) for three replication cycles (approximately 72 hours), and the frequency of micronuclei formation was determined as described above. The results (Table 2) of this experiment showed a highly significant reduction in percentage of nuclei associated with micronuclei in lung cells from p53R172H-KI mice. These data indicate that inhibition of origin firing in lung cells from p53R172H-KI mice reduces their ability to generate micronuclei.

Mouse number	Treatment	Nuclei with Micronuclei (500 scored)	p value
55	DMSO	36	0.0014249
	PHA76749 (6μM)	25	
67	DMSO	39	
	PHA76749 (6μM)	27	

Table 2. An inhibitor of origin firing reduces micronuclei formation in lung cells of p53R172HKI mice

The transactivation function of GOF p53 mutants is required for its ability to accelerate cell growth, increase firing of DNA replication origins, form micronuclei and protect replication forks. GOF p53 mutants activate transcription of growth promoting genes using its transactivation domains [Figure 42A, (65, 186-188)]. The transactivation function of GOF p53 mutants has been related to its ability to induce tumorigenesis and cell proliferation (189, 190). Therefore, experiments were designed to investigate whether the transactivation function of GOF p53 is also required for its ability to increase cell growth, origin firing, micronuclei formation, Chk1 expression and to reduce γH2AX foci formation. For this purpose, plasmids expressing p53R273H or p53R273H with compromising mutations (Figure 5A) of transactivation domain I (TADI, L22Q, W23S), or transactivation domains I and II (TADI & II, L22Q, W23S, L53Q, F54S) were stably introduced into p53-null H1299 human lung cancer cells, and the ability of the stable transfectants to perform the above biological activities was determined. Examination of the rate of cell proliferation revealed that H1299 cells expressing p53R273H proliferated more rapidly than cells

expressing either empty vectors or TADI mutants of p53R273H (Figure 42B, C). Fiber analysis of replicating DNA from H1299 cells expressing p53R273H, p53R273HTADI or p53R273HTADI/TADII at early S phase showed that H1299 cells expressing p53R273H fired almost 3-fold more origins than either of the TAD mutants (Figure 42D). This observation indicates that to induce origin firing, p53R273H requires its transactivation function.

The ability of the transactivation-deficient p53R273HTADI or TADI/TADII mutants to induce micronuclei formation was determined by staining of fixed cells on coverslips with DAPI and scoring cells with micronuclei by confocal microscopy. The results revealed that H1299 cells expressing the transactivation deficient p53R273HTADI or TADI/TADII formed micronuclei less frequently than H1299 cells expressing transactivation competent p53R273H (Figure 42E). Consistently, transactivation deficient p53R273HTADI did not activate expression and phosphorylation of Chk1 (Figure 42F). Immunostaining of γH2AX foci showed a drastic increase in foci formation in H1299 cells expressing transactivation deficient p53R273H TADI mutants compared to H1299 cells expressing p53R273H (Figure 42G, H). These results indicate that the ability of GOF p53 mutants to accelerate cell proliferation, increase origin firing and micronuclei formation, up-regulate expression and phosphorylation of Chk1and protect fork collapse requires its transactivation function.

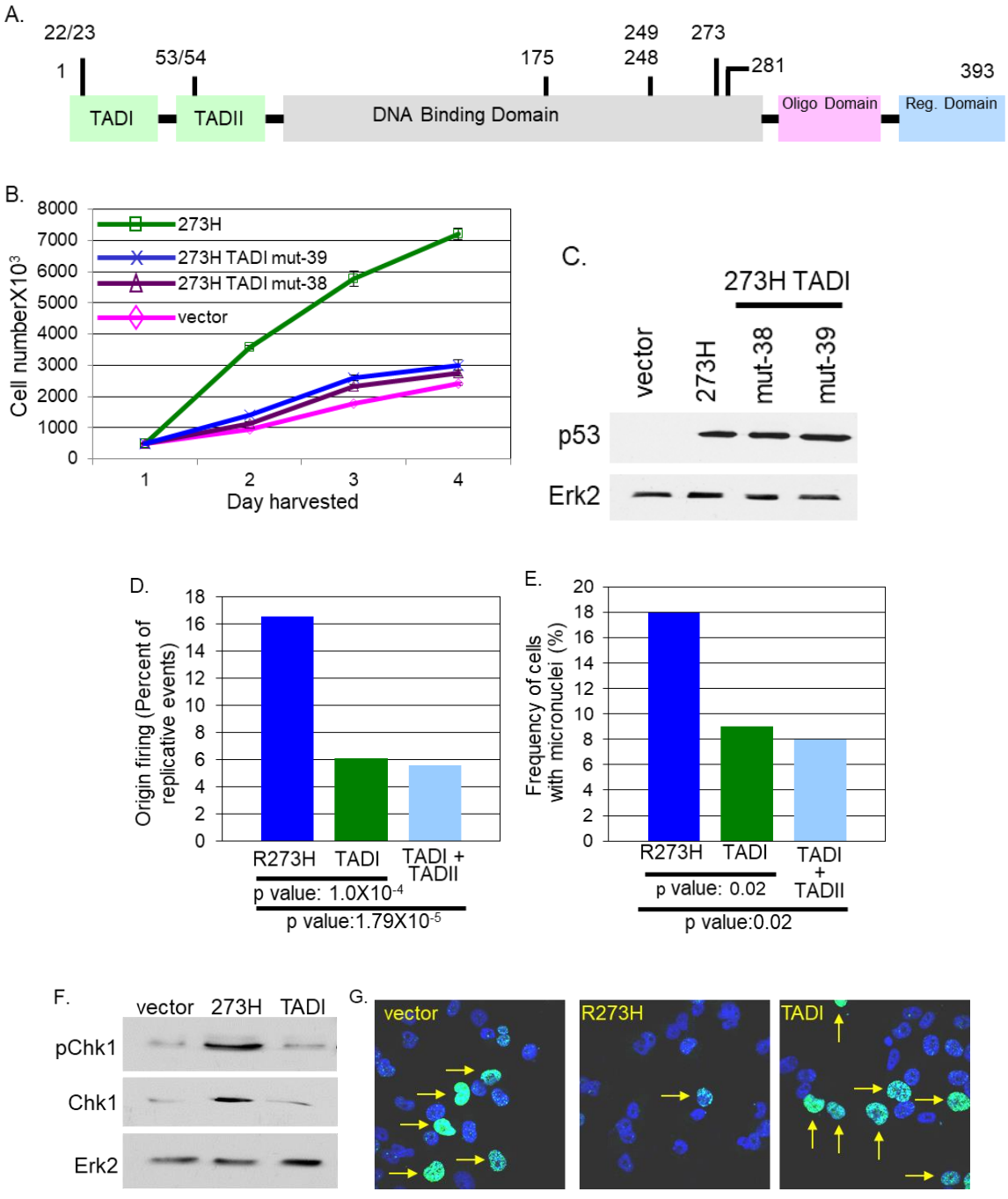
A.
22/23
1
53/54
175
249
248
273
281
393
TADI
TADII
DNA Binding Domain
Oligo Domain
Reg. Domain
B.
Cell numberX10³
273H
273H TADI mut-39
273H TADI mut-38
vector
Day harvested
C.
273H TADI
vector
273H
mut-38
mut-39
p53
Erk2
D.
Origin firing (Percent of replicative events)
R273H
TADI
TADI + TADII
p value: 1.0X10⁻⁴
p value:1.79X10⁻⁵
E.
Frequency of cells with micronuclei (%)
R273H
TADI
TADI + TADII
p value: 0.02
p value:0.02
F.
vector
273H
TADI
pChk1
Chk1
Erk2
G.
vector
R273H
TADI

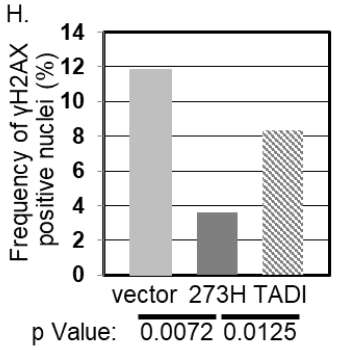

Figure 42. The transactivation function of GOF p53 is required for cell proliferation, increased frequency of replication origin firing, micronuclei formation, Chk1 expression and phosphorylation and replication fork protection. Functional domains of p53, including its transactivation domains I and II (TADI, TADII), sites of hot spot mutations and created mutations on TADI (L22Q and W23S)) and TADII (L53Q and F54S) are shown by a cartoon (A). Rate of proliferation of H1299 cells stably expressing p53R273H or its TADI mutant was determined (B). Data is presented as mean ± SD of triplicate experiments. Two clones of TADI mutants were used. p53 expression was confirmed by immunoblot analysis (C). Origin firing was determined by fiber analysis of replicating DNA. Data obtained by scoring 200 untangled fibers are shown by a bar graph. The p value calculated using Student's *t* test is shown at the bottom of the graph (D). Micronuclei formation was determined by DAPI staining. Data obtained by scoring 500 cells are shown by bar graphs (E). The p value calculated using Chi square test is shown at the bottom of the bar graphs. Expression of Chk1 and phospho-Chk1 (p-Chk1 at S345) in H1299 cells expressing p53R273H or its TADI mutant was determined by immunoblot analysis (F). γH2AX foci formation in H1299 cells expressing p53R273H or TADI mutant was determined by immunostaining with Alexa 488 coupled γH2AX antibody followed by confocal microscopy (G). Arrows indicate nuclei with green foci. Frequency of nuclei with γH2AX foci in each construct is shown by bar a graph (H). Two hundred fifty cells were scored and p value was calculated using Student's *t* test.

GOF p53 mutants up-regulate expression of genes involved in cell cycle regulation and DNA replication. Several laboratories have demonstrated that GOF p53 accelerates cell proliferation and tumor growth in comparison to p53-null or GOF p53-knockdown cells (86, 177, 187). Since the data presented above indicate that GOF p53 requires its transactivation domains to increase origin firing and to prevent replication fork collapse, the

profile of genes activated by GOF p53 mutant R273H were determined by RNA-seq analysis. RNA was extracted from H1299 cells stably expressing p53R273H or stably transfected with empty vector and the expression profiles were compared. To determine the mechanism by which GOF p53 mutants increase origin firing and prevent collapse of replication forks, profile of genes involved in the regulation of DNA replication was analyzed. The analysis revealed that indeed GOF p53 mutants up-regulate an array of genes that regulate cell cycle and DNA replication (Figure 43A).

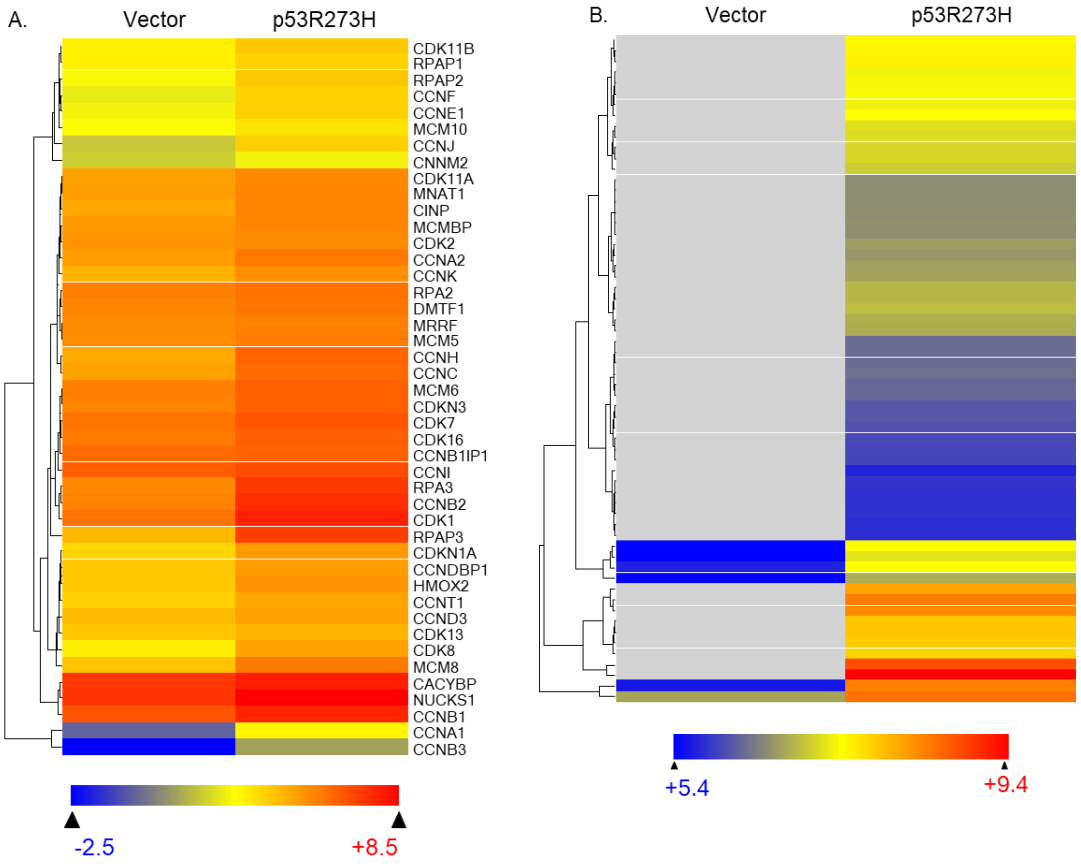

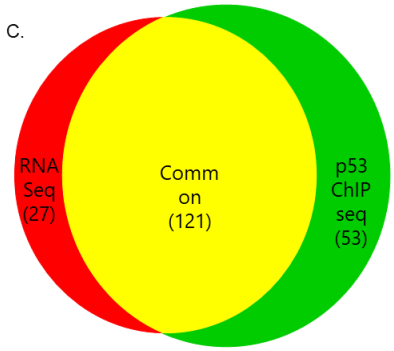

Figure 43. GOF p53 up-regulates expression of an array of genes involved in regulation of cell cycle and DNA replication and localizes on their upstream regulatory sequences. Heat maps of transcripts generated from RNA-seq analysis (A) and DNA fragments generated from ChIP-seq analysis (B) of H1299 cells stably transfected with vector (Vector) and stably expressing p53R273H (R273H). Number of sequences identified in (B) was too numerous to be listed in the figure. Gray areas indicate no p53 binding. A Venn diagram (C) show 121 genes common between the RNA-seq and ChIP-seq gene list, representing 81.75% of the RNA-seq genes and 69.54% of the p53 ChIP-seq genes that are involved in cell cycle and DNA replication. Genes that showed greater than two-fold up-regulation by expression of the p53R273H mutant and whose p-value was less than 0.01 were considered significant.

GOF p53 mutants recognize regulatory elements upstream of cell cycle and DNA replication genes. To determine whether GOF p53 mutants localize on the regulatory elements of the DNA replication genes, chromatin immunoprecipitation (ChIP) using H1299 cells stably expressing p53R273H was performed. Chromatin fragments bound to p53R273H were pulled down using two p53 antibodies, DO1 and FL393. Pulled down fragments were analyzed by ChIP-seq. H1299 cells stably transfected with vector, and IgG isotypes of the antibodies were used as controls. Four to ten million reads obtained from Illumina HiSeq were analyzed using the ArrayStar 11 (DNASTAR) program. The analysis revealed that p53R273H localizes on the upstream regulatory sequences of an array of genes involved in cell cycle regulation and DNA replication (Figure 43B). A Venn diagram

(Figure 43C) show that there are 121 genes in common between RNA-seq and p53 ChIP-seq data, representing 81.75% of the genes detected by RNA-seq and 69.54% of the genes detected by p53 ChIP-seq that are involved in cell cycle and DNA replication, two of which are Cyclin A and Chk1. These results strongly support the hypothesis that p53R273H activates expression of DNA replication genes by targeting their regulatory sequences.

Gain of function p53 mutants recognize upstream regulatory sequences of *CCNA2* and *CHEK1* transcription start sites. The ChIP-seq analysis described above detected localization of p53R273H on the upstream sequences of the *CCNA2* and *CHEK1* genes, expression of which are needed for firing of DNA replication origins (161-163) and stability of initiated replication forks (164-166), respectively. Therefore, experiments were performed to confirm localization of p53R273H on the upstream regulatory sequences of these genes. ChIP analysis (Figure 44) showed that an anti-p53 antibody immunoprecipitated DNA fragments spanning a 335 base pair (bp) region 106 bp upstream of the *CCNA2* transcription start site (Figure 44A-C) and a 1000 bp region 200 bp upstream of the *CHEK1* transcription start site (Figure 44D-F). These data show that p53R273H localizes on the upstream sequences of the *CCNA2* and *CHEK1* transcription start sites.

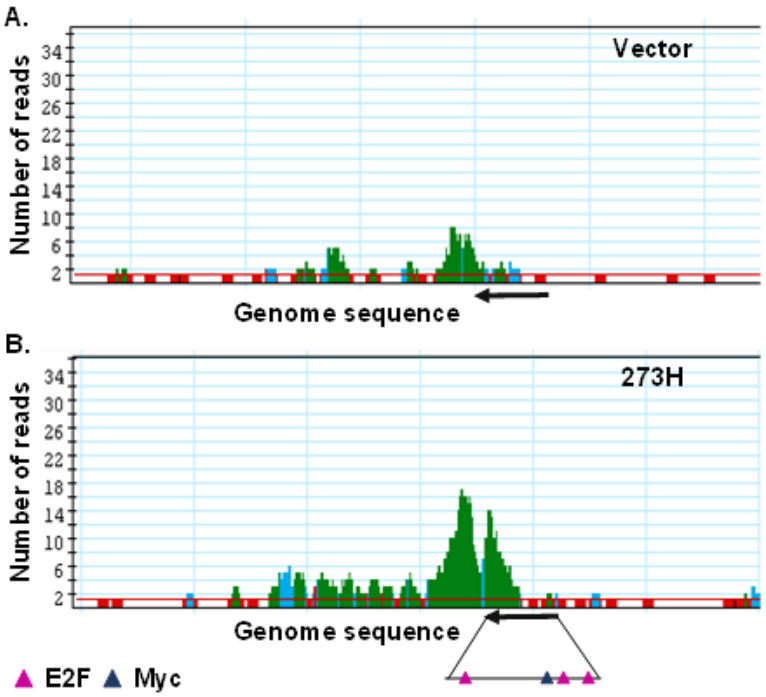
A.
Vector
Number of reads
34
30
26
22
18
14
10
6
2
Genome sequence
B.
273H
Number of reads
Genome sequence
E2F
Myc

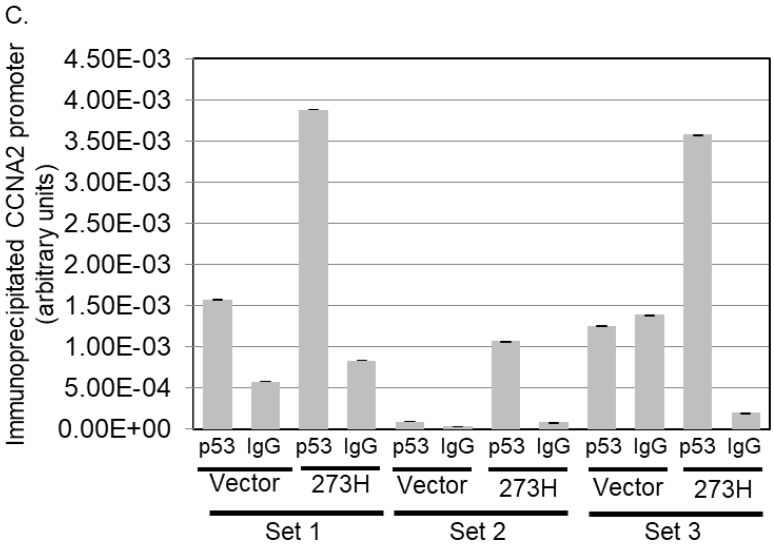
C.
Immunoprecipitated CCNA2 promoter (arbitrary units)
4.50E-03
4.00E-03
3.50E-03
3.00E-03
2.50E-03
2.00E-03
1.50E-03
1.00E-03
5.00E-04
0.00E+00
p53 IgG p53 IgG p53 IgG p53 IgG p53 IgG p53 IgG
Vector
273H
Vector
273H
Vector
273H
Set 1
Set 2
Set 3

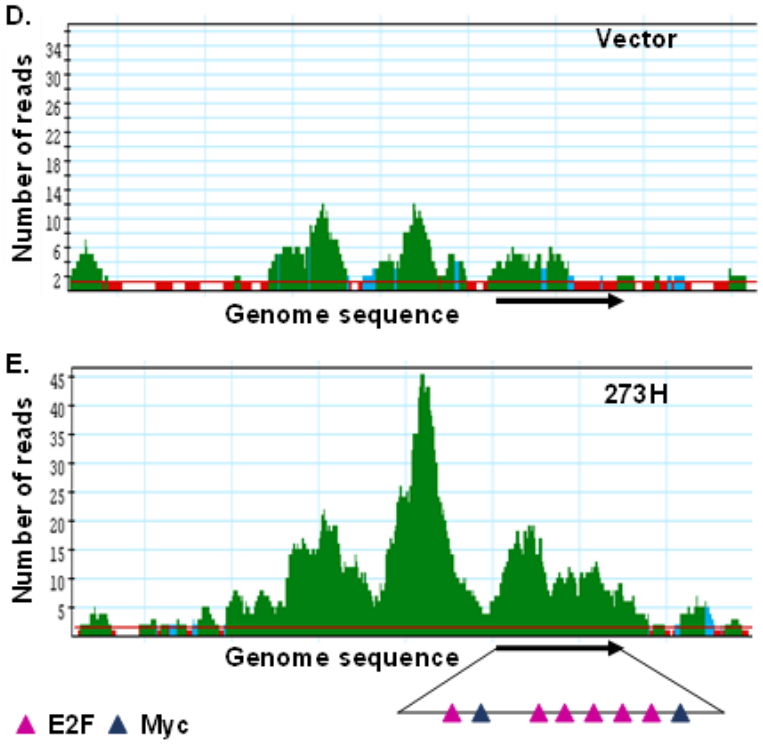
D.
Vector
Number of reads
34
30
26
22
18
14
10
6
2
Genome sequence
E.
273H
Number of reads
45
40
35
30
25
20
15
10
5
Genome sequence
E2F
Myc

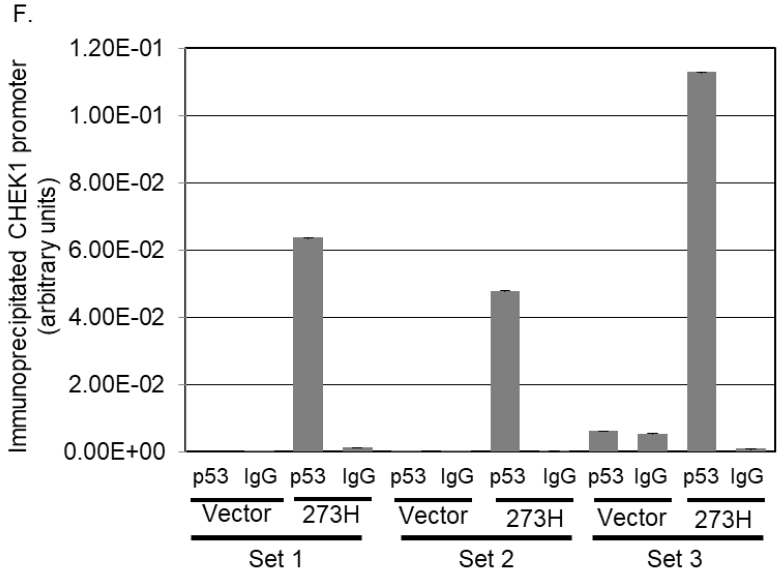
F.
Immunoprecipitated CHEK1 promoter (arbitrary units)
1.20E-01
1.00E-01
8.00E-02
6.00E-02
4.00E-02
2.00E-02
0.00E+00
p53 IgG p53 IgG p53 IgG p53 IgG p53 IgG p53 IgG
Vector
273H
Vector
273H
Vector
273H
Set 1
Set 2
Set 3

Figure 44. **GOF p53 localizes on the upstream sequences of *CCNA2* and *CHEK1* genes.** The peaks represent areas under which maximal p53R273H binding occurs as apparent by next generation sequence analysis of ChIP fragments. Peaks of ChIP fragments on CCNA2 promoter from H1299 cells stably transfected with control vector (A) or stably expressing p53R273H (B). ChIP analysis (C) to confirm localization of p53R273H on *CCNA2* promoter. Peaks of ChIP fragments on *CHEK1* promoter from H1299 cells stably transfected with control vector (D) or stably expressing p53R273H (E). ChIP analysis (F) to confirm localization of p53R273H on *CHEK1* promoter. Results from triplicate sets of extracts of H1299 cells expressing p53R273H (273H) or empty vector (Vector) are shown by bar graphs as mean ± SEM. ChIP using IgG control (IgG) has been included in each case. The region of genome showing p53R273H-specific binding as determined by ChIP and the direction of coding sequences are indicated by arrows. Blue and purple arrow heads indicate Myc and E2F binding sites respectively on the identified promoter sequences.

Gain of function p53 mutants activate expression of Cyclin A and Chk1 at early S phase. Since RNA-seq data (Figure 43A) presented above suggest that GOF p53 increases Cyclin A and Chk1 expression and recognizes their upstream regulatory sequences (Figure 44), experiments were performed to confirm whether GOF p53 up-regulates Cyclin A and Chk1 expression at early S phase in the absence of other known gene mutation. Cell cycle dependent expression of Cyclin A and Chk1 in partially synchronized lung cells from p53-null and p53R172H-KI mice at early S phase were compared. RT-QPCR of transcripts and immunoblot analysis of extracts prepared from these cells showed a significant increase in Cyclin A and Chk1 expression at the RNA (Figure 45A and B, respectively) and protein levels (Figure 45C-E) in lung cells from p53R172H-KI mice in comparison to lung cells from p53-null mice. These data are consistent with the immunoblot analysis (Figure 37A), which showed that lung cells from p53R172H-KI mice express higher levels of Chk1 in comparison to lung cells from p53-null mice, suggesting that an increase in Chk1 expression leads to an increase in p-Chk1.

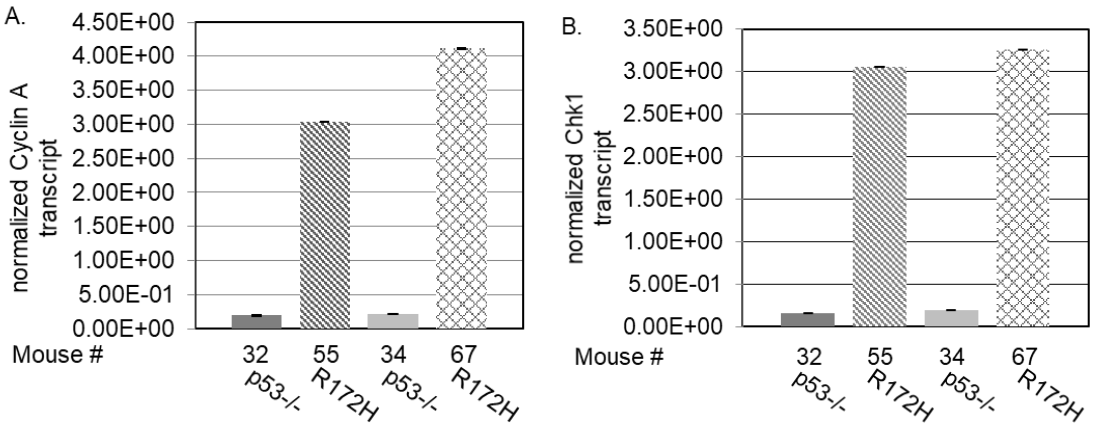
A.
normalized Cyclin A transcript
4.50E+00
4.00E+00
3.50E+00
3.00E+00
2.50E+00
2.00E+00
1.50E+00
1.00E+00
5.00E-01
0.00E+00
Mouse #
32 p53-/-
55 R172H
34 p53-/-
67 R172H
B.
normalized Chk1 transcript
3.50E+00
3.00E+00
2.50E+00
2.00E+00
1.50E+00
1.00E+00
5.00E-01
0.00E+00
Mouse #
32 p53-/-
55 R172H
34 p53-/-
67 R172H

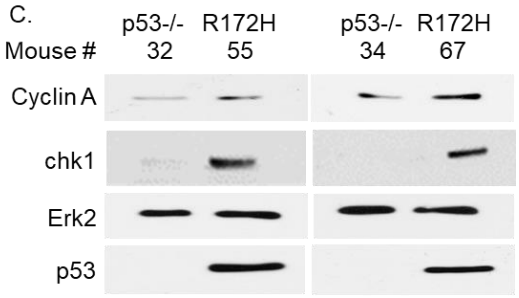
C.
p53-/- R172H p53-/- R172H
Mouse # 32 55 34 67
Cyclin A
chk1
Erk2
p53

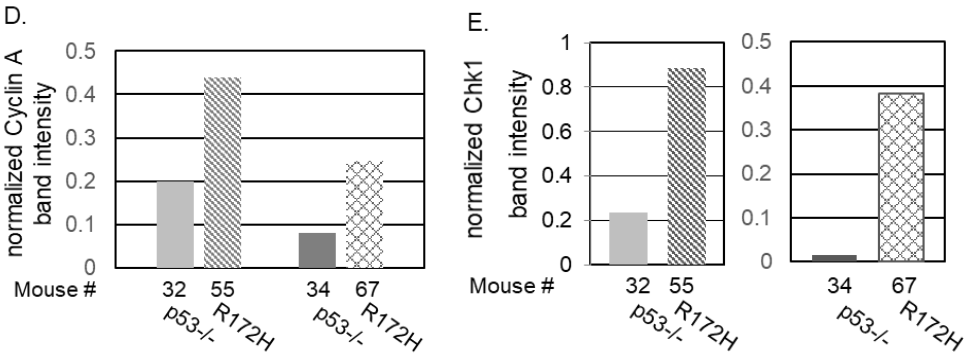
D.
normalized Cyclin A band intensity
0.5
0.4
0.3
0.2
0.1
0
Mouse #
32 p53-/-
55 R172H
34 p53-/-
67 R172H
E.
normalized Chk1 band intensity
1
0.8
0.6
0.4
0.2
0
0.5
0.4
0.3
0.2
0.1
0
Mouse #
32 p53-/-
55 R172H
34 p53-/-
67 R172H

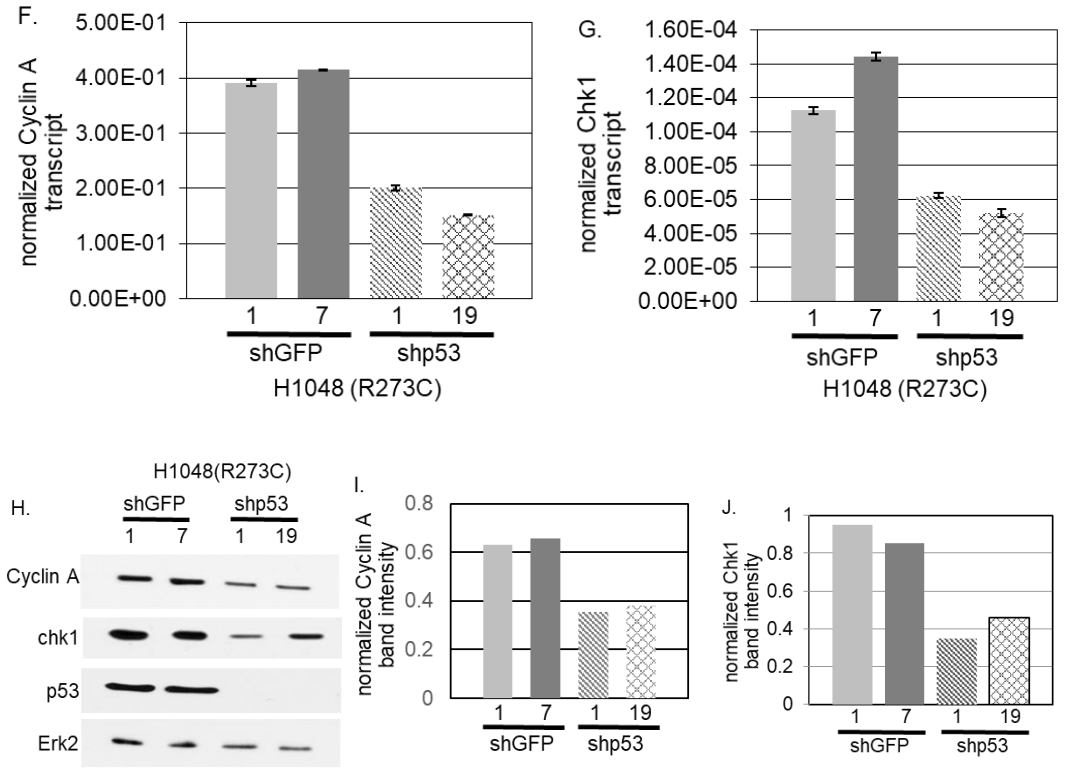

Figure 45. GOF p53 induces Cyclin A and Chk1 expression. Transcript levels of Cyclin A and Chk1 in lung cells from p53-null or R172H-KI (R172H) mice (A, B) and H1048 human lung cancer cells stably expressing shRNA against GFP or p53 (F, G), determined by RT-QPCR. Data is plotted as mean ± SEM. Cyclin A and Chk1 protein levels (C-E and H-J) were determined by immunoblot analysis. Bar graphs show band intensities of Cyclin A (D, I) and Chk1 (E, J) determined by densitometry and normalized by Erk2 loading control. Lung cells from two mice of each construct or two clones stably expressing shGFP or shp53 were analyzed.

Knockdown of GOF p53 diminishes Cyclin A and Chk1 expression at early S phase in a human lung cancer cell line. To further confirm whether GOF p53 increases Cyclin A and Chk1 expression at early S phase, GOF p53 was knocked down in H1048 lung cancer cell lines. H1048 cells stably expressing control shGFP or shp53 RNA were partially synchronized by confluence arrest and replating. Expression of Cyclin A and Chk1 was

analyzed at early S phase. RT-QPCR of transcripts and immunoblot analysis of cell extracts prepared from these cells showed that knockdown of GOF p53 significantly reduces Cyclin A and Chk1 expression at the RNA (Figure 45F, G) and protein levels (Figure 45H-J). Consistently in a similar experiment, knockdown of p53R175H in VMRC human lung cancer cells also reduced localization of GOF p53 on *CCNA2* and *CHEK1* promoters and expression of Cyclin A and Chk1 transcript and protein levels (Figure 46). Taken together, these results show that GOF p53 mutants increase Cyclin A and Chk1 expression at early S phase, and inactivation of this function abrogates cell proliferation, increase in origin firing, micronuclei formation, Chk1 activation and chromatin association of γH2AX.

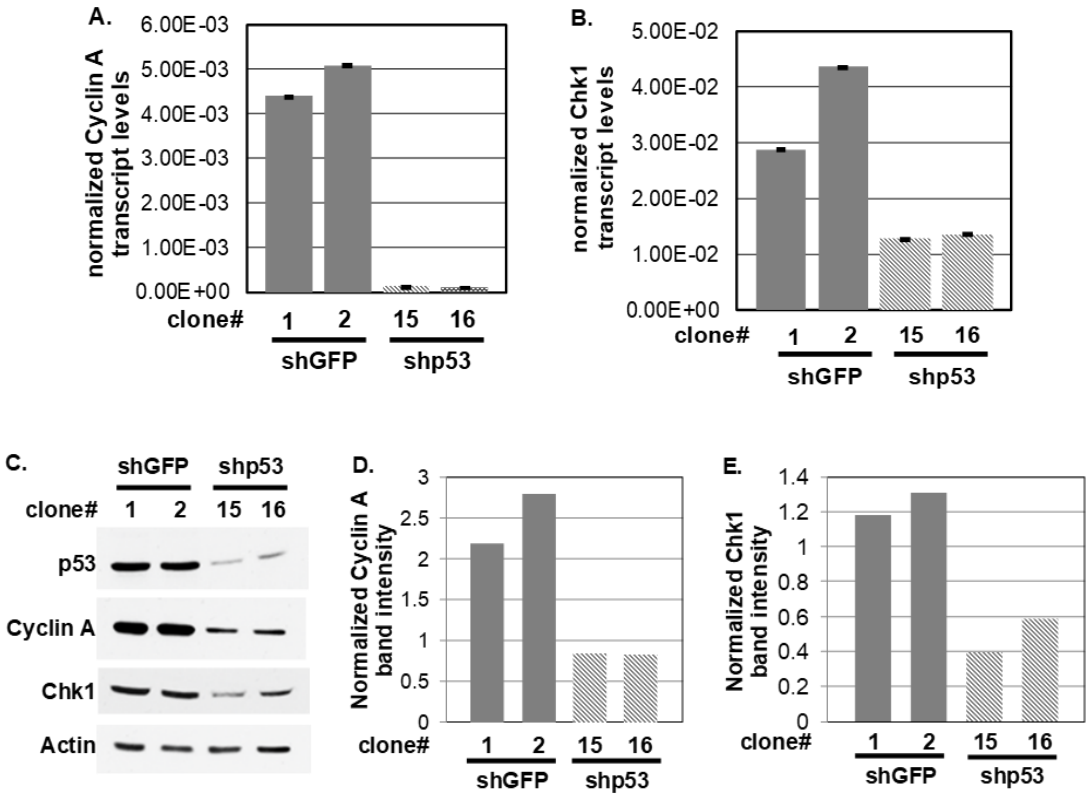

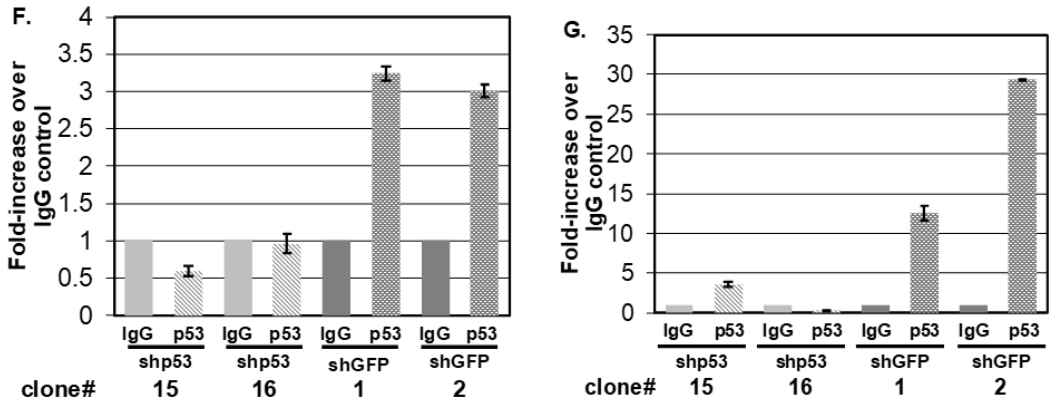

Figure 46. Knockdown of p53 (R175H) in human lung cancer VMRC cells reduces Cyclin A and Chk1 expression and localization on *CCNA2* and *CHEK1* promoter. Transcript levels of Cyclin A (A) and Chk1(B) in VMRC cells stably expressing shGFP or shp53 from a lentiviral vector were determined by RT-QPCR. Data represents QPCR values normalized to GAPDH levels and plotted as mean ± SEM. Cyclin A and Chk1 protein levels were determined by immunoblot analysis (C). Band intensities of Cyclin A (D) and Chk1 (E) were determined by densitometry and normalized by Actin loading control. p53 ChIP analyses of *CCNA2* (F) and *CHEK1* (G) promoters in p53-depleted (shp53) and mock-depleted (shGFP) VMRC cells. Fold increase over IgG control are plotted as mean ± SEM.

p53 mutants with compromised tumor formation ability do not show localization on CCNA2 or CHEK1 promoter, do not upregulate Cyclin A and Chk1 promoter to increase expression of respective transcripts, and fire fewer origins than GOF p53 mutants. GOF p53 mutation often show allele specificity. To determine whether the ability of GOF p53 mutants to localize on the CCNA2 or CHEK1 promoter, upregulate expression of Cyclin A and Chk1 and increase origin firing relates to its tumor formation ability, we chose a naturally occurring p53 mutant, R267P, in human lung cancer cell line H1437. Tumor formation ability of H1437 cell line is not dependent on R267P (177). In addition, we tested a deletion mutant of GOF p53, D281G Δ100-300, that removes its central binding

domain (residues 100-300), and thus removes the site of hot spot mutation. ChIP analysis using p53-null H1299 lung cancer cells stably expressing empty vector, p53 D281G Δ100-300, R267P, R175H, R248W or D281G as described above showed that as in the case of H1299 cells stably expressing R273H (Figure 44), anti-p53 antibodies immunoprecipitated upstream promoter fragments of CCNA2 and CHEK1 from cells expressing p53 mutants R175H, R248W or D281G, but not from cells expressing empty vector, p53 D281G Δ100-300, R267P (Figure 47).

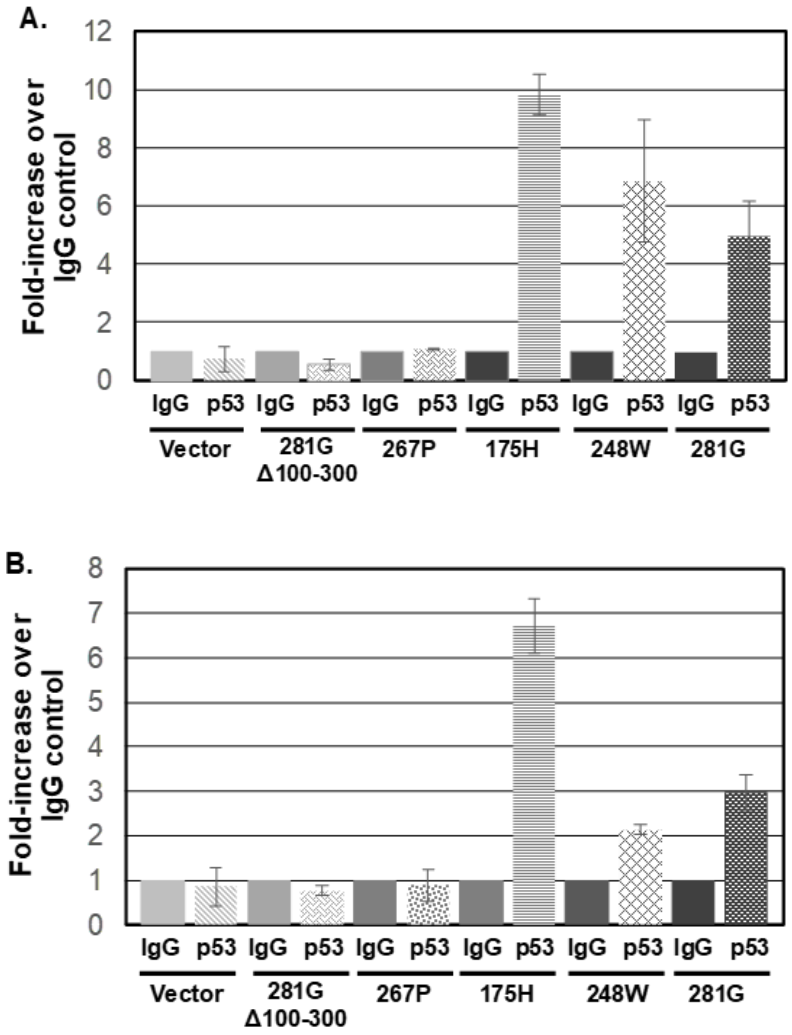

Figure 47. p53 mutants with compromised tumor formation ability do not show localization on *CCNA2* (A) and *CHEK1* (B) promoters. p53 ChIP analysis *CCNA2* and *CHEK1* promoters from H1299 cells stably expressing p53 mutants with (175H, 248W, 281G) and without (267P, 281GΔ100-300) GOF activity. Increase in immunoprecipitated promoter fragments by anti-p53 antibody over control IgG are shown by bar graphs. H1299 cell line stably expressing empty vector was used as control. Data is shown in bar graphs and plotted as mean ± SEM.

Next, we analyzed the abilities of the p53 mutants to upregulate Cyclin A and Chk1 promoter activities. Cyclin A and Chk1 promoters containing the GOF p53-interaction sites

as determined from our ChIP analysis (Figure 48) were inserted upstream of luciferase gene in a reporter plasmid. The plasmids were introduced in p53-null H1299 cells along with the individual p53 mutants or vector plasmid, and luciferase activity was determined as reported earlier (86). Our data (Figure 48A-C) show that expression of GOF p53 mutants R175H, R248W, R273H or D281G significantly upregulated luciferase activity compared to empty vector, or compared to the mutants p53 D281G Δ100-300, R267P. RT-QPCR of transcripts and immunoblot analysis of extracts prepared from partially synchronized H1299 cells stably expressing the p53 mutants showed that consistent with the promoter activity, R175H, R248W, R273H or D281G significantly increased Cyclin A and Chk1 transcript and protein levels compared to empty vector, or compared to the mutants p53 D281G Δ100-300, R267P (Figure 48D-H). Fiber analysis of replicating DNA from H1299 stable transfectants expressing the p53 mutants D281G Δ100-300, R267P, R175H and 281G at early S phase showed that H1299 cells expressing R175H and 281G fire almost 3 to 4-fold more origins than cells expressing either D281G Δ100-300 or R267P (Figure 48I). These results show that GOF p53 mutants localize on the CCNA2 and CHEK1 promoter sequences, increase Cyclin A and Chk1 promoter activities and their expression and increase origin firing at early S phase, whereas p53 mutants deficient in GOF properties are inactive in these functions.

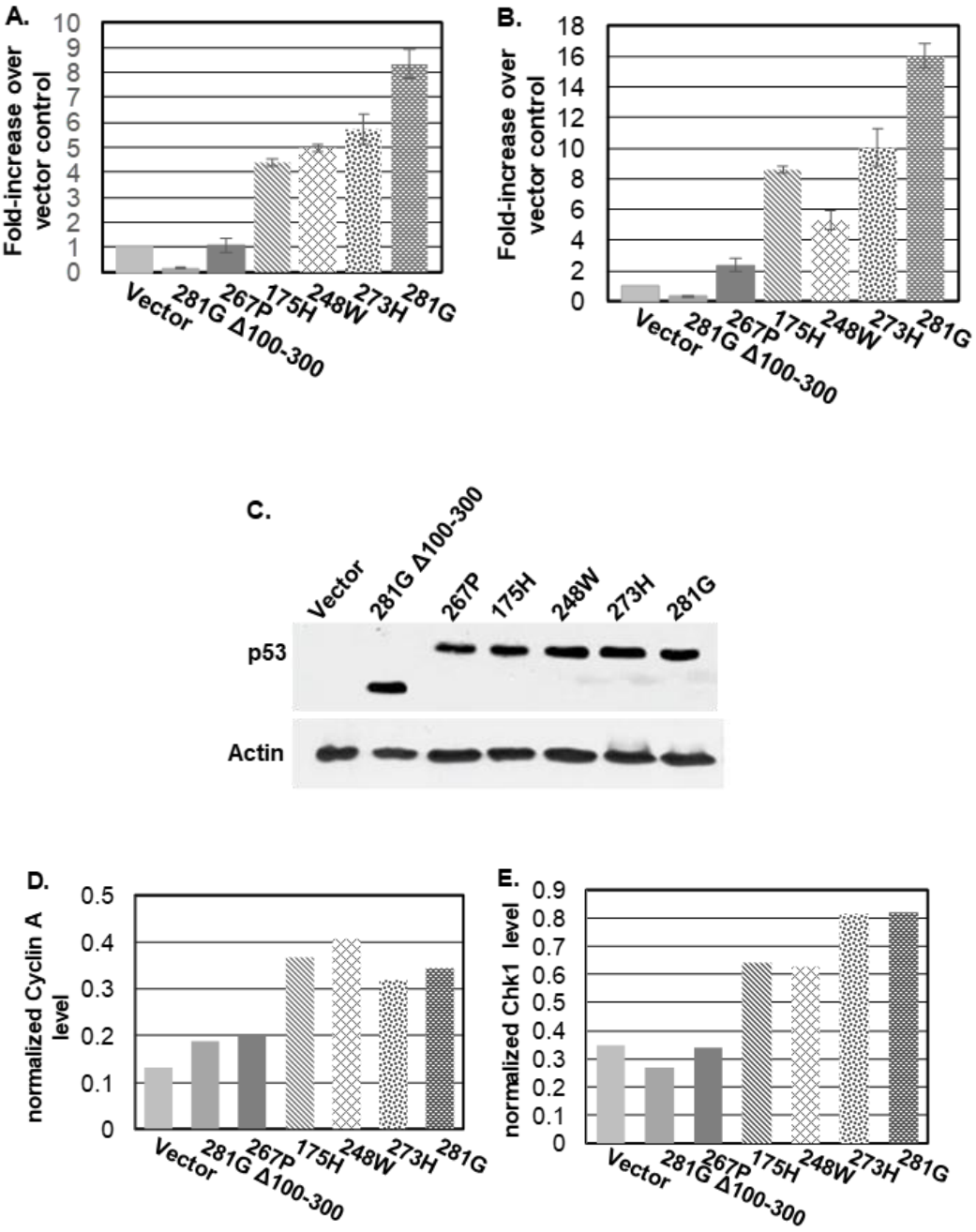
A.
Fold-increase over vector control
0
1
2
3
4
5
6
7
8
9
10
Vector
281G Δ100-300
267P
175H
248W
273H
281G
B.
Fold-increase over vector control
0
2
4
6
8
10
12
14
16
18
Vector
281G Δ100-300
267P
175H
248W
273H
281G
C.
Vector
281G Δ100-300
267P
175H
248W
273H
281G
p53
Actin
D.
normalized Cyclin A level
0
0.1
0.2
0.3
0.4
0.5
Vector
281G Δ100-300
267P
175H
248W
273H
281G
E.
normalized Chk1 level
0
0.1
0.2
0.3
0.4
0.5
0.6
0.7
0.8
0.9
Vector
281G Δ100-300
267P
175H
248W
273H
281G

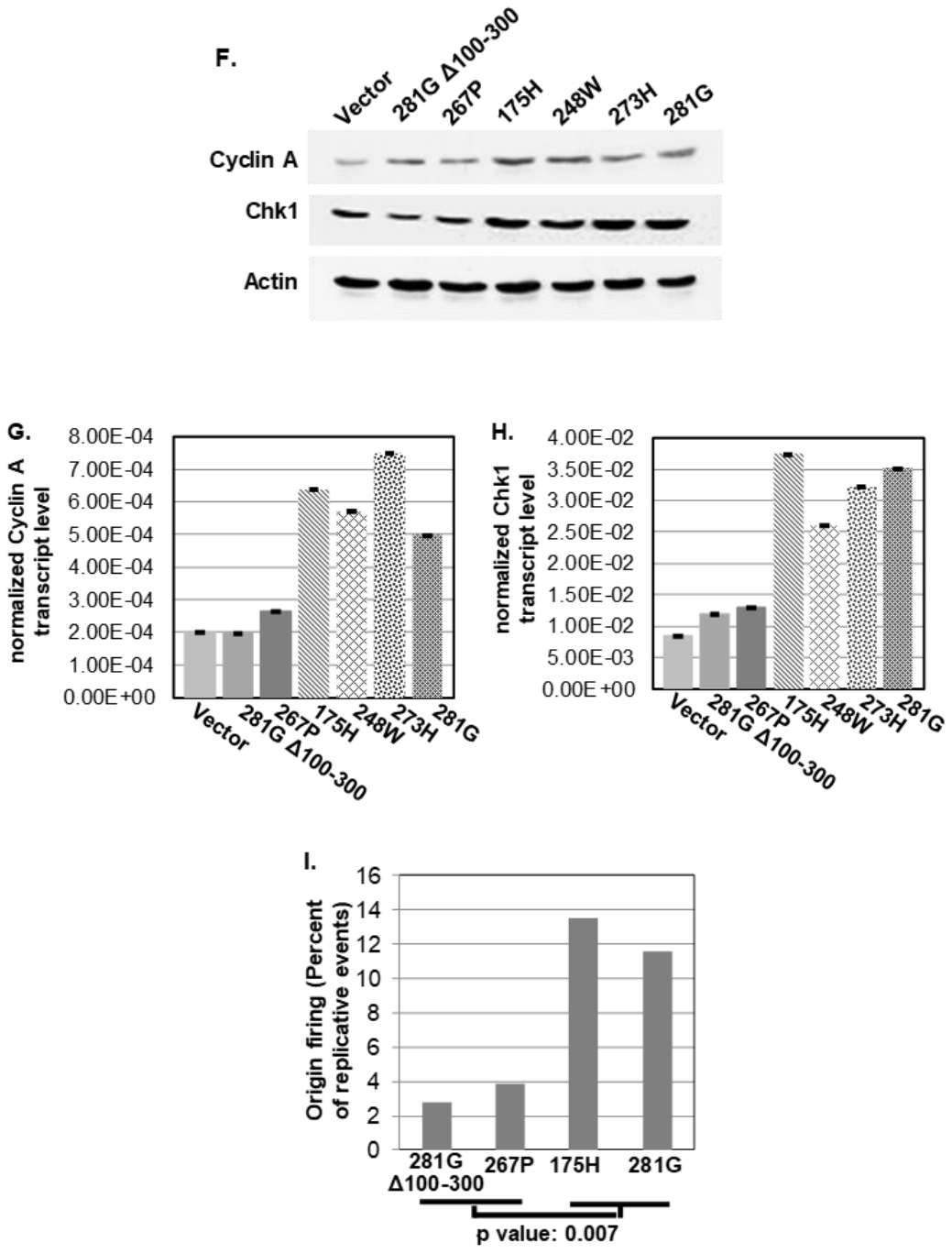

Figure 48. p53 mutants with compromised tumor formation ability do not upregulate of Cyclin A and Chk1 promoter activity (A-C) or expression of Cyclin A and Chk1 protein (D-F) and transcripts (G, H), and do not induce firing of DNA replication origins (F) in H1299 lung cancer cells. CCNA2 (A) and CHEK1 (B) promoter

activities in the presence of p53 mutants with and without GOF activity were determined by transient transfection analysis using luciferase reporter. Increase in luciferase activities over vector control are shown by bar graphs as mean ± SEM of triplicate experiments. p53 expression was determined by immunoblot analysis (C). Actin is a loading control. Expression of Cyclin A and Chk1 protein were determined by immunoblot analysis and quantified by densitometry (D-F). The bar graphs (D, E) show densitometric values normalized to loading control (actin) of a representative experiment. Cyclin A and Chk1 transcripts (G, H) were determined by RT-QPCR. Data shown in bar graphs (G, H) are values normalized to GAPDH levels plotted as mean ± SEM of a representative experiment. Origin firing in early S phase by p53 mutants in H1299 cells were determined by fiber analysis of replicating DNA as described in the text and are shown by bar graphs as percent of origins in replicating fibers in each sample (I). Two non-GOFp53 mutants (281G Δ100-300, 267P) and two GOFp53 mutants (175H, 281G) were analyzed. The p-values are shown at the bottom of the bar graph calculated using Student's *t* test.

A small molecule inhibitor of Chk1 selectively reduces tumor size and growth of lung cancer cells with p53 mutation. If increased expression of Chk1 by GOF p53 protects replication fork progression (Figure 37) and thus accelerates genome duplication (Figure 38) and cell proliferation (Figure 42B), GOF p53-mediated cell proliferation should be selectively prevented by inhibition of Chk1 activity. To test this possibility, H1299 lung cancer cells stably expressing p53R273H or its transactivation deficient mutant p53R273H TADI (Figure 42A) and H1299 cells stably transfected with vector control were treated with a Chk1 inhibitor PF00477736, and the rate of cell proliferation was determined. The results of these experiments show that PF00477736 preferentially inhibited growth of cells expressing GOF p53R273H compared to p53R273H TADI or cells expressing vector control (Figure 49A). In a similar experiment, H1299 cells expressing p53 mutants D281G Δ100-300, R267P, R175H and 281G were treated with PF00477736 and cell number at 5 days were determined. Consistent with the previous finding, results (Figure 49B) of this experiment show that PF00477736 inhibited growth of H1299 cells expressing p53R175H

or p53D281G more efficiently than cells expressing D281G Δ100-300, R267P. Similarly, H1048 lung cancer cells (which naturally express p53R273C) stably expressing shRNA against p53 or control GFP were also treated with the Chk1 inhibitor, and rate of cell proliferation was determined by counting cell number in each case. Our data show that knockdown of GOF p53 remarkably reduced (2.5 to-3-fold) the sensitivity of the human lung cancer cell line H1048 to the chk1 inhibitor (Figure 49C, 52A). These observations indicate that the growth of H1299 cells expressing GOF p53 mutants are dependent on Chk1 induction by GOF p53 and signify potential therapeutic efficiency of the Chk1 inhibitor in lung cancer cells expressing GOF p53 alleles.

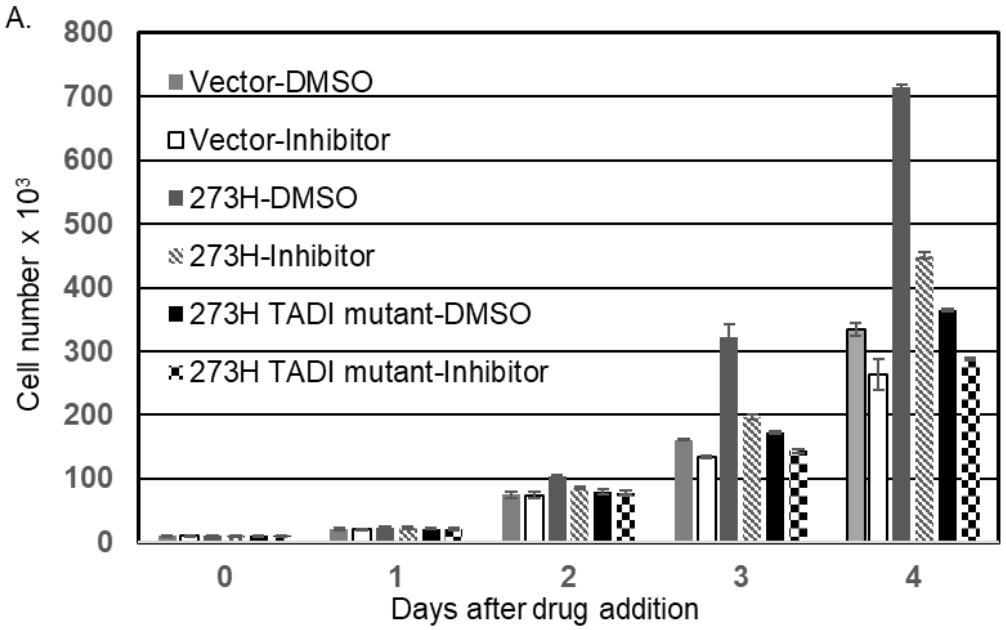

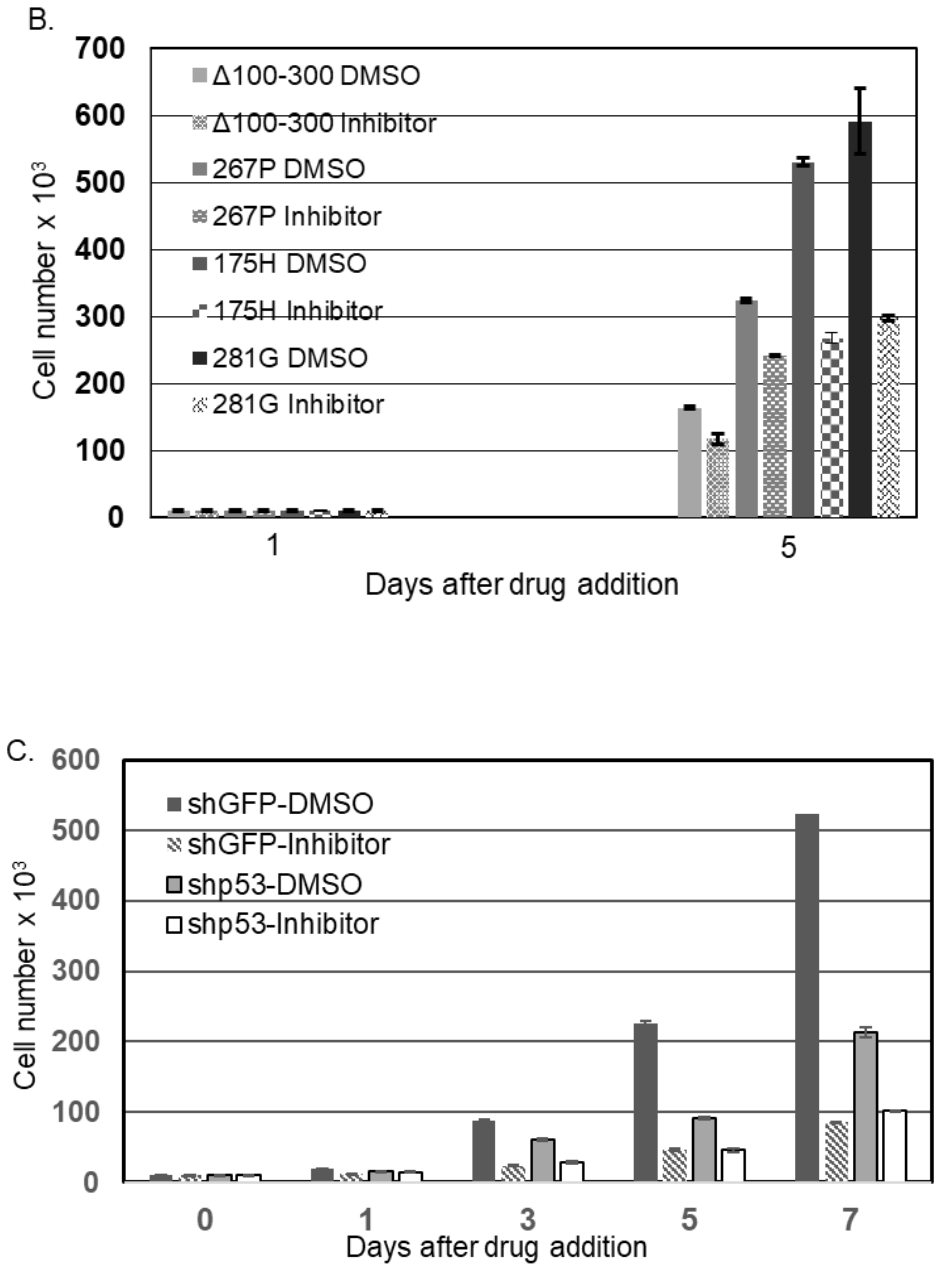

Figure 49. A small molecule inhibitor of Chk1 selectively inhibits growth and reduces tumor size of lung cancer cells with p53 mutation. Rate of proliferation of (A) H1299 cells stably expressing p53R273H, or its TADI mutant or a vector control, (B) proliferation of H1299 cells stably expressing p53 mutants 281GΔ100-300, 267P, 175H and 281G and (C) H1048 lung cancer cells stably expressing shp53 or shGFP in the presence of

a Chk1 inhibitor PF00477736 (100nM) (Inhibitor), or only solvent (DMSO). Data is shown as mean± SD from triplicate experiments.

To determine whether the Chk1 inhibitor preferentially target cells that proliferate faster independent of GOF p53, we boosted cell proliferation by enriching growth media using 20% fetal bovine serum and compared the efficiency of growth inhibition of mock-depleted and shp53-depleted H1048 lung cancer cells or of vector-transfected H1299 cells with GOF p53 R273H expressing H1299 cells in normal media by the Chk1 inhibitor, PF00477736. Our data (Figure 50) show that the enriched media increased cell growth in the presence or absence of Chk1 inhibitor. Although growth acceleration of p53-depleted H1048 cells was higher in the absence of Chk1 inhibitor compared to its presence, mock-depleted H1048 cells showed more sensitivity to Chk1 inhibitor in normal or enriched media (Figure 50A). Enhanced proliferation of H1299 lung cancer cells (vector control) in enriched media did not increase efficiency of growth inhibition by Chk1 inhibitor (Figure 50). These data suggest that the efficiency of inhibition of cell growth by Chk1 inhibitor is not dependent on rate of proliferation alone.

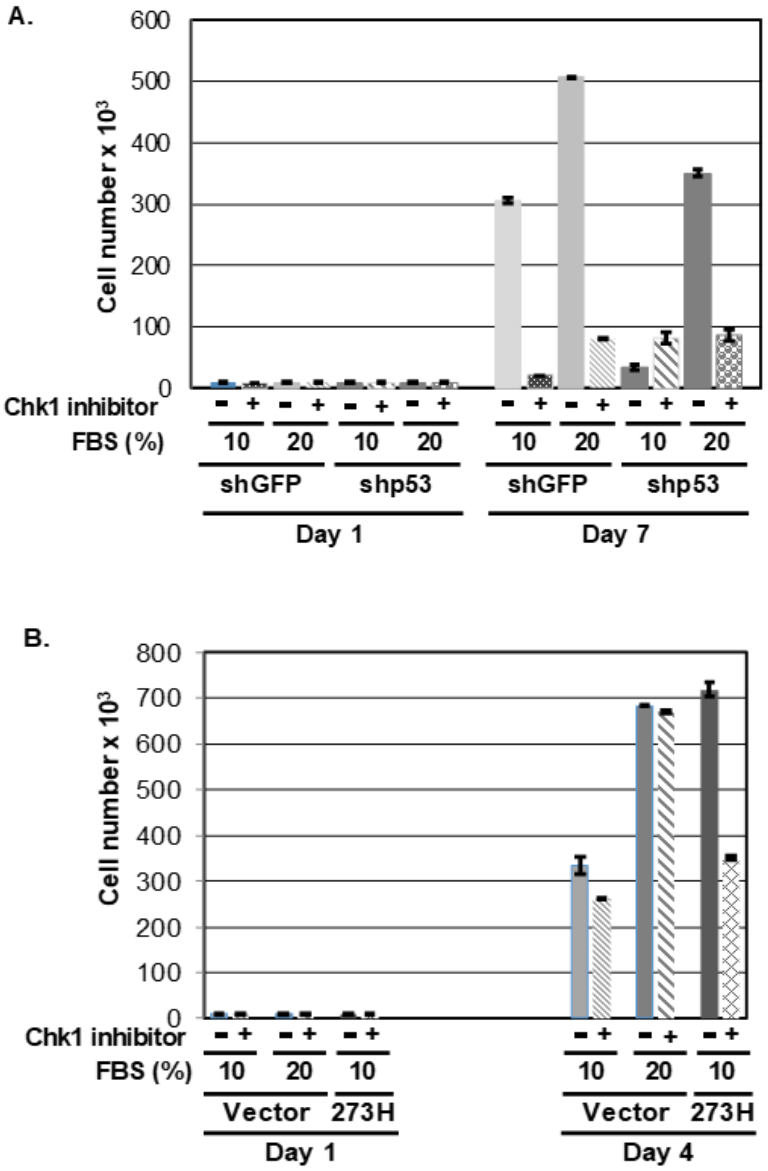

Figure 50. Artificial growth acceleration does not sensitize p53-null or GOF p53 expressing lung cancer cells to Chk1 inhibitor PF0047736. Proliferation of mock-depleted or p53-depleted H1048 lung cancer cells (A) or H1299 cells stably expressing p53R273H (273H) or a vector control (B) in the presence of Chk1 inhibitor PF00477736 (100nM), or only solvent (DMSO) and growth medium with 10% or 20% FBS. Data is shown as mean ± SD from triplicate experiments.

If an increase in Chk1 expression, and therefore replication fork protection, renders cancer cells addicted to p53, inhibition of Chk1 should also reduce tumor growth. This possibility was examined using a mouse xenograft model. Subcutaneous tumors were allowed to form in *Nu/Nu* mice by introducing H1048 cells stably expressing shGFP or shp53, and the effect of Chk1 inhibitor PF00477736 on tumor growth was examined. H1048 cells expressing shGFP efficiently formed tumors, while PF 00477736 treatment significantly reduced the size of the tumors (Figure 51). Knockdown of p53R273C with shp53 also efficiently reduced tumor size, however PF 00477736 treatment did not reduce the size of the H1048shp53 tumors appreciably. Comparing the effect on H1048 shGFP and shp53 cells, PF 00477736 reduced size of tumors generated from H1048shGFP cells at 3.6 to 4-fold higher efficiency than that from H1048 shp53 cells (Figure 52). These data indicate that tumors expressing GOF p53 are targeted efficiently and selectively by PF 00477736 in comparison to tumors not expressing GOF p53.

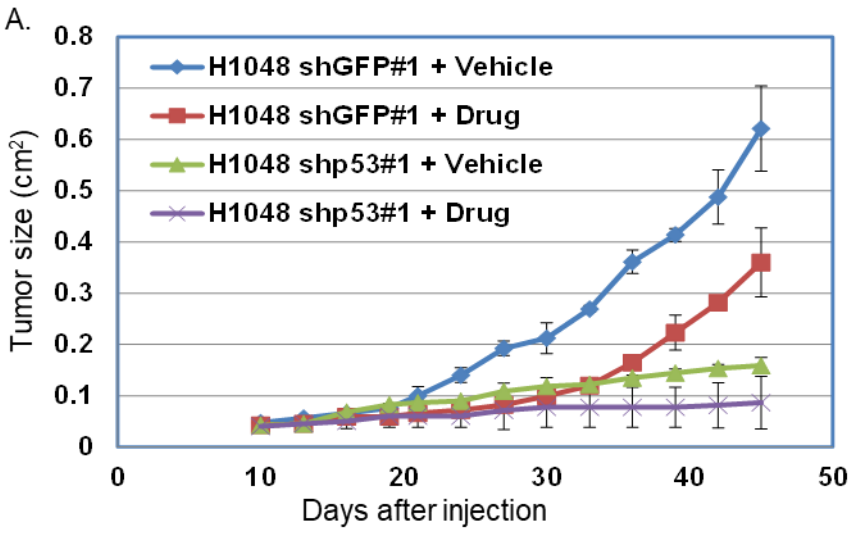

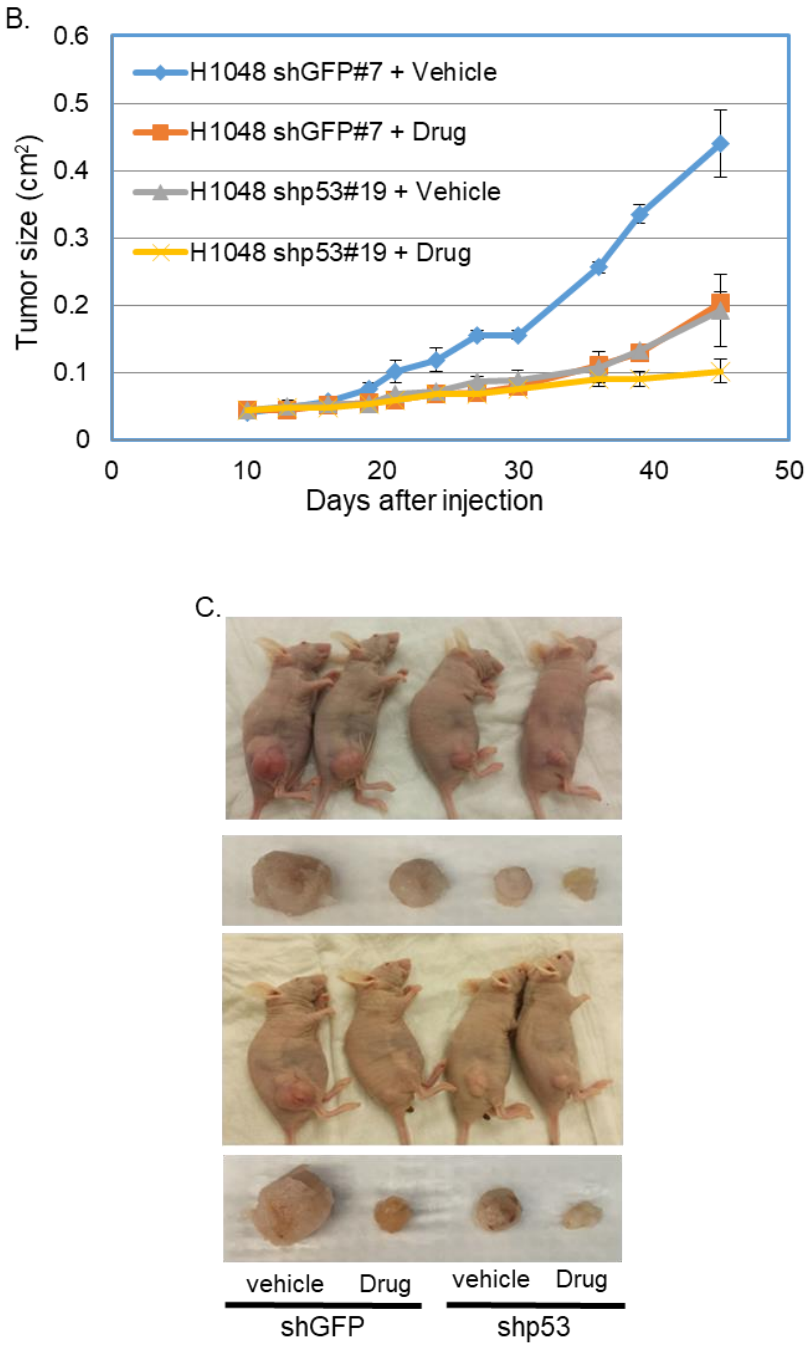

Figure 51. A small molecule inhibitor of Chk1 selectively reduces tumor size of lung cancer cells with p53 mutation. Rate of tumor growth (A, B) from H1048 cells expressing shGFP or shp53 treated with vehicle or PF00477736, 10mg per Kg (Drug). Data from two sets of clones (A, B) and a representative photograph (C) of tumors are shown.

Representative data from $n = 4$ mice in each experimental group is plotted as mean ± SEM. Assay was repeated in $n = 12$ mice per experimental group.

Discussion.

Targeting GOF p53 mutants to prevent tumor growth or to treat established tumors has recently become an area of active investigation established on reversing the apparent addiction of tumor cells to the GOF properties of mutant p53 (188, 191, 192). However, why or how growth of tumors or tumor cells becomes dependent on GOF p53 is not known.

The tumorigenic activity of GOF p53 and its ability to transcriptionally activate genes required for DNA replication (175, 189, 190, 193) drew the focus of this study on firing of DNA replication origins and progression of replication forks, the two crucial aspects of successful genome duplication. Consistently, the presented ChIP-seq and RNA-seq analysis (Figure 43) indicate that GOF p53 recognizes the promoter region of several genes involved in DNA replication, and up-regulates their expression suggesting that the oncoprotein creates an intracellular environment conducive to accelerated genome duplication. Here we present data to suggest a novel oncogenic pathway (Figure 53A, B), in which GOF p53-dependent growth advantage of cancer cells lies in its ability to localize on the upstream regulatory sequences of Cyclin A and Chk1 (Figure 44, 48), upregulating their expression (Figure 45, 46, 48). Since more origins are licensed than used [reviewed in (12, 194)], increase in Cyclin A expression leads to firing of more number of origins, (Figure 36), whereas increased Chk1 expression prevents their collapse (Figure 37), thus quickening genome duplication (Figure 38) and proliferation of cells with genetic abnormalities as evidenced by micronuclei formation (Figures 41, 42E). On the contrary, due to their inability to up-regulate Cyclin A

and Chk1 expression, p53-null cells or cell expressing GOF-deficient p53 mutants activate fewer origins than cells with GOF p53 (Figure 36), and face a vulnerability to collapse of replication forks (Figure 37), which is known to cause incomplete genome duplication, gross genome rearrangement and cell death (167, 168).

Cell cycle progression is deregulated in the absence of WT p53, which normally induces expression of the cyclin dependent kinase (cdk) inhibitor p21 (195). Consistently, data presented here show that lung cells from either p53-null or p53R172H-KI mice enters S phase at similar times with approximately 20% of the cells synthesizing DNA at early S phase, while approximately 5% of lung cells from mice with WT p53 enter S phase at similar time (Figure 35). Thus, the presence of GOF p53 does not hasten time of S phase entry any sooner than loss of p53 (Figure 35). However, expression analysis did reveal that at early S phase, GOF p53 up-regulates expression of Cyclin A, required for origin activation, and Chk1, required for stabilization of replication forks (Figure 45, 46, 48) and accordingly, increases the frequency of origin firing (Figure 36) and prevents collapse of progressing replication forks (Figure 37), accelerating genome duplication and cell growth (Figures 38, 42B).

Oncogene induced replication stress is thought to induce firing of dormant origins which facilitates completion of genome duplication (196). However, the observed increase in origin firing by GOF p53 is concomitant to S phase entry of cells and was dependent on the transactivation domain TADI of GOF p53, needed to up-regulate Cyclin A expression (Figure 42D). Since activation of cdk activates origins in replication factories (197, 198), GOF p53-induced Cyclin A expression at early S phase should activate origin firing in

replication factories. Increases in the levels of p-Chk1 in GOF p53 expressing cells (Figure 37A, B) may eventually fire dormant origins due to pausing of progressing replication forks at a later time point.

Our data also show that the increase in the frequency of origin firing by GOF p53 leads to micronuclei formation in lung cells expressing GOF p53 (Figure 41). It has been reported that oncogene induced increase in DNA replication induces fork reversal and generates unfinished replication intermediates (181). Although activation of Chk1 by GOF p53 prevents fork collapse, micronuclei formation in GOF p53 expressing cells may possibly be a consequence of mitotic processing of the intermediates generated by topological stress due to increase in origin firing as reported by Neelsen et al (29). In support of this notion, reduced micronuclei formation was observed in the presence of a cdk2 inhibitor that is known to inhibit origin firing but allow fork progression (Table 2).

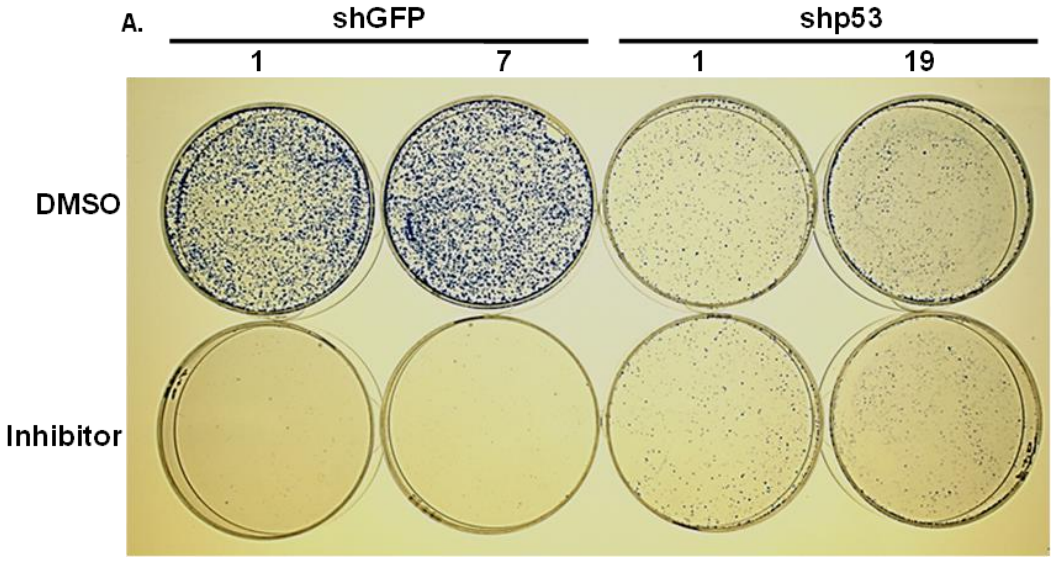

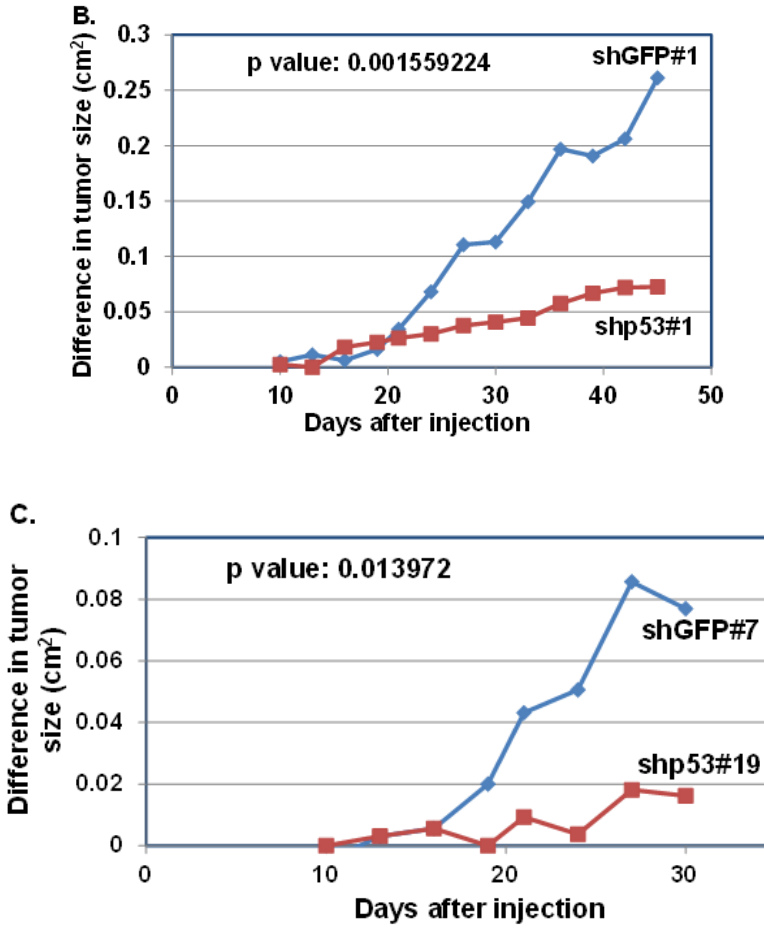

Figure. 52: A small molecule inhibitor of Chk1, PF0047736 (100nM), (Inhibitor), selectively inhibits proliferation of H1048 lung cancer cells expressing shGFP as opposed to H1048 cells expressing shp53 and reduces tumor size. A. Equal number (10,000) of cells were plated in each dish and treated with PF0047736 (100nM) 24 hours after plating cells. Cells were fixed with methanol and stained with methylene blue on 7th day. B, C. Extent of reduction in size of tumors generated by H1048 cells expressing shGFP (shGFP) or shp53 (shp53) after treatment with PF0047736 (10mg per Kg) with increase in time. Two different clone sets were injected. P values calculated using Student's *t* test are shown in the graphs.

Supporting the central role of GOF p53-mediated transactivation of Chk1 in preventing collapse of replication forks, it was observed that a Chk1 inhibitor (Figure 37G, H), or inhibition of Chk1 expression by transcriptional inactivation of GOF p53 leads to collapse

of replication forks (Figure 42G). It is known that the collapse of replication forks leads to either cell death or gross genomic rearrangement due to incomplete genome duplication (167, 168). GOF p53-mediated fork stabilization, therefore, should allow the cells to evade these events detrimental to cell growth, although the cells enter S phase as early as p53-null cells. Accordingly, a Chk1 inhibitor preferentially inhibited proliferation of cells and growth of tumors expressing GOF p53 (Figure 49, 52), while transactivation deficient GOF p53 with substitution at the amino acid residues 22 and 23 was incapable of increasing origin firing, micronuclei formation, replication fork stabilization and induction of cell proliferation and vulnerability to Chk1 inhibitor (Figure 49A, B) implicating GOF p53 transactivation in regulating all these functions. Consistently p53 mutants deficient in GOF property did not transactivate Cyclin A and Chk1 or increase origin firing and were not vulnerable to Chk1 inhibitor (Figure 48, 49B).

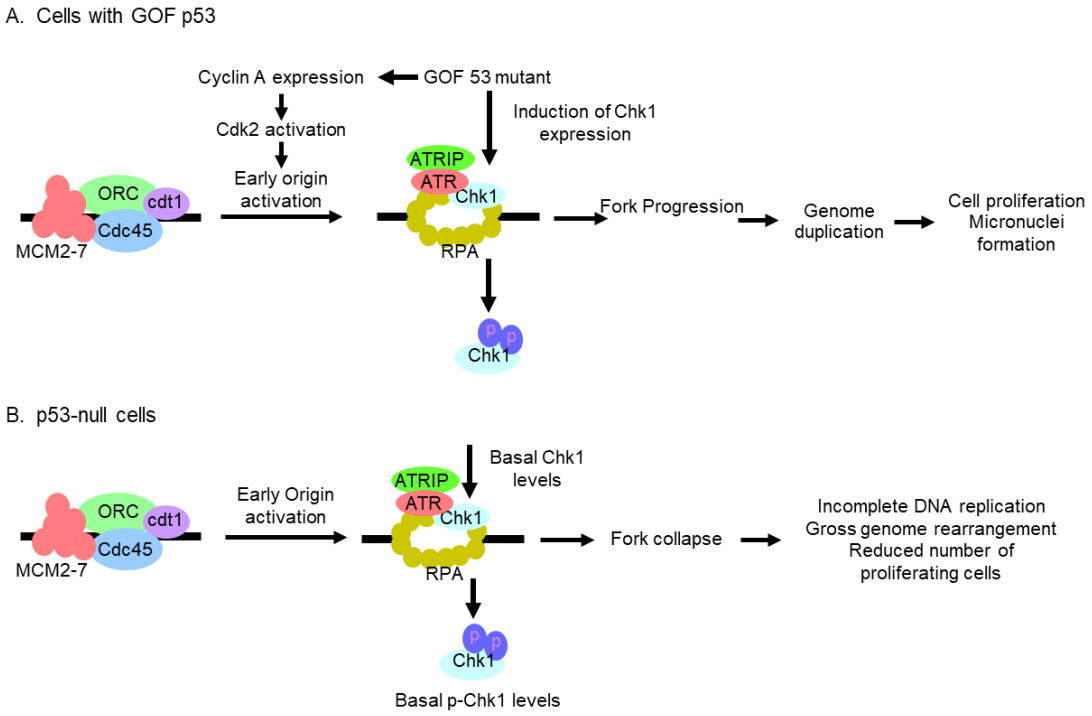

Figure 53. The downstream consequences of unscheduled origin firing (A) GOF p53-expressing and (B) p53-null lung cells are depicted.

Conclusion.

The results discussed above help explain the genetic instability and long latency period of tumorigenesis found in p53-null cells (59). Higher incidence of replication fork collapse and gross genome rearrangement in p53-null cells should lead to cell death, but also selection of genetically altered cells with survival advantage and tumorigenesis in the long run. GOF p53 driven increases in origin firing along with protection of replication forks should allow proliferation of cells with genetic abnormalities. These observations also explain dependence of tumor growth on GOF p53, lack of which would result in decreased origin firing and vulnerability to collapse of progressing replication forks, causing decelerated rates

of genome duplication and lethal genome rearrangement. Our model for the role of GOF p53 in stimulating replication and simultaneously protecting replication forks (Figure 53) provides solid mechanistic justification for developing cancer-cell selective therapeutics that target either GOF p53 transactivation function directly or target the protein products of GOF p53 transactivated genes. Such therapies, possibly in combination with other tumor type-specific targeted therapies, may lead to significant therapeutic gains in intractable cancers with high rates of GOF p53 mutation.

Literature Cited

1. Hanahan D, Weinberg RA. Hallmarks of cancer: the next generation. Cell. 2011;144(5):646-74. Epub 2011/03/08. doi: 10.1016/j.cell.2011.02.013. PubMed PMID: 21376230.
2. Macheret M, Halazonetis TD. DNA replication stress as a hallmark of cancer. Annual review of pathology. 2015;10:425-48. Epub 2015/01/27. doi: 10.1146/annurev-pathol-012414-040424. PubMed PMID: 25621662.
3. Negrini S, Gorgoulis VG, Halazonetis TD. Genomic instability--an evolving hallmark of cancer. Nature reviews Molecular cell biology. 2010;11(3):220-8. Epub 2010/02/24. doi: 10.1038/nrm2858. PubMed PMID: 20177397.
4. Bartkova J, Rezaei N, Liontos M, Karakaidos P, Kletsas D, Issaeva N, Vassiliou LV, Kolettas E, Niforou K, Zoumpourlis VC, Takaoka M, Nakagawa H, Tort F, Fugger K, Johansson F, Sehested M, Andersen CL, Dyrskjot L, Orntoft T, Lukas J, Kittas C, Helleday T, Halazonetis TD, Bartek J, Gorgoulis VG. Oncogene-induced senescence is part of the tumorigenesis barrier imposed by DNA damage checkpoints. Nature. 2006;444(7119):633-7. Epub 2006/12/01. doi: 10.1038/nature05268. PubMed PMID: 17136093.
5. Gorgoulis VG, Vassiliou LV, Karakaidos P, Zacharatos P, Kotsinas A, Liloglou T, Venere M, Ditullio RA, Jr., Kastrinakis NG, Levy B, Kletsas D, Yoneta A, Herlyn M, Kittas C, Halazonetis TD. Activation of the DNA damage checkpoint and genomic instability in human precancerous lesions. Nature. 2005;434(7035):907-13. Epub 2005/04/15. doi: 10.1038/nature03485. PubMed PMID: 15829965.
6. Beroukhim R, Mermel CH, Porter D, Wei G, Raychaudhuri S, Donovan J, Barretina J, Boehm JS, Dobson J, Urashima M, Mc Henry KT, Pinchback RM, Ligon AH, Cho YJ, Haery L, Greulich H, Reich M, Winckler W, Lawrence MS, Weir BA, Tanaka KE, Chiang DY, Bass AJ, Loo A, Hoffman C, Prensner J, Liefeld T, Gao Q, Yecies D, Signoretti S, Maher E, Kaye FJ, Sasaki H, Tepper JE, Fletcher JA, Tabernero J, Baselga J, Tsao MS, Demichelis F, Rubin MA, Janne PA, Daly MJ, Nucera C, Levine RL, Ebert BL, Gabriel S, Rustgi AK, Antonescu CR, Ladanyi M, Letai A, Garraway LA, Loda M, Beer DG, True LD, Okamoto A, Pomeroy SL, Singer S, Golub TR, Lander ES, Getz G, Sellers WR, Meyerson M. The landscape of somatic copy-number alteration across human cancers. Nature. 2010;463(7283):899-905. Epub 2010/02/19. doi: 10.1038/nature08822. PubMed PMID: 20164920; PMCID: PMC2826709.
7. Plug-DeMaggio AW, Sundsvold T, Wurscher MA, Koop JI, Klingelhutz AJ, McDougall JK. Telomere erosion and chromosomal instability in cells expressing the HPV oncogene 16E6. Oncogene. 2004;23(20):3561-71. Epub 2004/04/13. doi: 10.1038/sj.onc.1207388. PubMed PMID: 15077181.

8. Duensing S, Munger K. The human papillomavirus type 16 E6 and E7 oncoproteins independently induce numerical and structural chromosome instability. Cancer research. 2002;62(23):7075-82. Epub 2002/12/04. PubMed PMID: 12460929.
9. Bartkova J, Hamerlik P, Stockhausen MT, Ehrmann J, Hlobilkova A, Laursen H, Kalita O, Kolar Z, Poulsen HS, Broholm H, Lukas J, Bartek J. Replication stress and oxidative damage contribute to aberrant constitutive activation of DNA damage signalling in human gliomas. Oncogene. 2010;29(36):5095-102. Epub 2010/06/29. doi: 10.1038/onc.2010.249. PubMed PMID: 20581868.
10. Gaillard H, Garcia-Muse T, Aguilera A. Replication stress and cancer. Nature reviews Cancer. 2015;15(5):276-89. Epub 2015/04/25. doi: 10.1038/nrc3916. PubMed PMID: 25907220.
11. Bartkova J, Horejsi Z, Koed K, Kramer A, Tort F, Zieger K, Guldberg P, Sehested M, Nesland JM, Lukas C, Orntoft T, Lukas J, Bartek J. DNA damage response as a candidate anti-cancer barrier in early human tumorigenesis. Nature. 2005;434(7035):864-70. Epub 2005/04/15. doi: 10.1038/nature03482. PubMed PMID: 15829956.
12. Zeman MK, Cimprich KA. Causes and consequences of replication stress. Nature cell biology. 2014;16(1):2-9. Epub 2013/12/25. doi: 10.1038/ncb2897. PubMed PMID: 24366029; PMCID: PMC4354890.
13. Sarni D, Kerem B. Oncogene-Induced Replication Stress Drives Genome Instability and Tumorigenesis. International Journal of Molecular Sciences. 2017;18(7):1339. doi: 10.3390/ijms18071339. PubMed PMID: PMC5535832.
14. Cahilly-Snyder L, Yang-Feng T, Francke U, George DL. Molecular analysis and chromosomal mapping of amplified genes isolated from a transformed mouse 3T3 cell line. Somatic cell and molecular genetics. 1987;13(3):235-44. Epub 1987/05/01. PubMed PMID: 3474784.
15. Fakharzadeh SS, Trusko SP, George DL. Tumorigenic potential associated with enhanced expression of a gene that is amplified in a mouse tumor cell line. EMBO J. 1991;10(6):1565-9. PubMed PMID: 2026149.
16. Zhang Y, Lu H. Signaling to p53: ribosomal proteins find their way. Cancer cell. 2009;16(5):369-77. Epub 2009/11/03. doi: 10.1016/j.ccr.2009.09.024. PubMed PMID: 19878869; PMCID: PMC4369769.
17. Lindstrom MS, Jin A, Deisenroth C, White Wolf G, Zhang Y. Cancer-associated mutations in the MDM2 zinc finger domain disrupt ribosomal protein interaction and attenuate MDM2-induced p53 degradation. Molecular and cellular biology. 2007;27(3):1056-68. Epub 2006/11/23. doi: 10.1128/mcb.01307-06. PubMed PMID: 17116689; PMCID: PMC1800693.
18. Oliner JD, Kinzler KW, Meltzer PS, George DL, Vogelstein B. Amplification of a gene encoding a p53-associated protein in human sarcomas. Nature. 1992;358(6381):80-3. PubMed PMID: 1614537.
19. Momand J, Zambetti GP, Olson DC, George D, Levine AJ. The mdm-2 oncogene product forms a complex with the p53 protein and inhibits p53-mediated transactivation. Cell. 1992;69(7):1237-45. PubMed PMID: 1535557.

20. Brown DR, Deb S, Munoz RM, Subler MA, Deb SP. The tumor suppressor p53 and the oncoprotein simian virus 40 T antigen bind to overlapping domains on the MDM2 protein. Molecular and cellular biology. 1993;13(11):6849-57. PubMed PMID: 8413278.
21. Chen J, Marechal V, Levine AJ. Mapping of the p53 and mdm-2 interaction domains. Molecular and cellular biology. 1993;13(7):4107-14. PubMed PMID: 7686617.
22. Candeias MM, Malbert-Colas L, Powell DJ, Daskalogianni C, Maslon MM, Naski N, Bourougaa K, Calvo F, Fahraeus R. P53 mRNA controls p53 activity by managing Mdm2 functions. Nature cell biology. 2008;10(9):1098-105. Epub 2009/01/23. doi: 10.1038/ncb1770. PubMed PMID: 19160491.
23. Takagi M, Absalon MJ, McLure KG, Kastan MB. Regulation of p53 translation and induction after DNA damage by ribosomal protein L26 and nucleolin. Cell. 2005;123(1):49-63. Epub 2005/10/11. doi: 10.1016/j.cell.2005.07.034. PubMed PMID: 16213212.
24. Onel K, Cordon-Cardo C. MDM2 and prognosis. Mol Cancer Res. 2004;2(1):1-8. PubMed PMID: 14757840.
25. Ding L, Getz G, Wheeler DA, Mardis ER, McLellan MD, Cibulskis K, Sougnez C, Greulich H, Muzny DM, Morgan MB, Fulton L, Fulton RS, Zhang Q, Wendl MC, Lawrence MS, Larson DE, Chen K, Dooling DJ, Sabo A, Hawes AC, Shen H, Jhangiani SN, Lewis LR, Hall O, Zhu Y, Mathew T, Ren Y, Yao J, Scherer SE, Clerc K, Metcalf GA, Ng B, Milosavljevic A, Gonzalez-Garay ML, Osborne JR, Meyer R, Shi X, Tang Y, Koboldt DC, Lin L, Abbott R, Miner TL, Pohl C, Fewell G, Haipek C, Schmidt H, Dunford-Shore BH, Kraja A, Crosby SD, Sawyer CS, Vickery T, Sander S, Robinson J, Winckler W, Baldwin J, Chirieac LR, Dutt A, Fennell T, Hanna M, Johnson BE, Onofrio RC, Thomas RK, Tonon G, Weir BA, Zhao X, Ziaugra L, Zody MC, Giordano T, Orringer MB, Roth JA, Spitz MR, Wistuba, II, Ozenberger B, Good PJ, Chang AC, Beer DG, Watson MA, Ladanyi M, Broderick S, Yoshizawa A, Travis WD, Pao W, Province MA, Weinstock GM, Varmus HE, Gabriel SB, Lander ES, Gibbs RA, Meyerson M, Wilson RK. Somatic mutations affect key pathways in lung adenocarcinoma. Nature. 2008;455(7216):1069-75. Epub 2008/10/25. doi: 10.1038/nature07423. PubMed PMID: 18948947; PMCID: 2694412.
26. Berghmans T, Mascaux C, Haller A, Meert AP, Van Houtte P, Sculier JP. EGFR, TTF-1 and Mdm2 expression in stage III non-small cell lung cancer: a positive association. Lung Cancer. 2008;62(1):35-44. Epub 2008/03/22. doi: 10.1016/j.lungcan.2008.02.003. PubMed PMID: 18355939.
27. Iwakuma T, Lozano G. MDM2, an introduction. Mol Cancer Res. 2003;1(14):993-1000. PubMed PMID: 14707282.
28. Vaughan C, Mohanraj L, Singh S, Dumur CI, Ramamoorthy M, Garrett CT, Windle B, Yeudall WA, Deb S, Deb SP. Human Oncoprotein MDM2 Up-regulates Expression of NF-kappaB2 Precursor p100 Conferring a Survival Advantage to Lung Cells. Genes Cancer. 2011;2(10):943-55. Epub 2012/06/16. doi: 10.1177/1947601911436008. PubMed PMID: 22701761; PMCID: 3374626.

29. McDonnell TJ, Montes de Oca Luna R, Cho S, Amelse LL, Chavez-Reyes A, Lozano G. Loss of one but not two mdm2 null alleles alters the tumour spectrum in p53 null mice. The Journal of pathology. 1999;188(3):322-8. Epub 1999/07/27. doi: 10.1002/(sici)1096-9896(199907)188:3<322::aid-path372>3.0.co;2-f. PubMed PMID: 10419603.
30. Singh S, Ramamoorthy M, Vaughan C, Yeudall WA, Deb S, Palit Deb S. Human oncoprotein MDM2 activates the Akt signaling pathway through an interaction with the repressor element-1 silencing transcription factor conferring a survival advantage to cancer cells. Cell death and differentiation. 2013;20(4):558-66. Epub 2012/12/15. doi: 10.1038/cdd.2012.153. PubMed PMID: 23238568; PMCID: 3595481.
31. Frum RA, Singh S, Vaughan C, Mukhopadhyay ND, Grossman SR, Windle B, Deb S, Deb SP. The human oncoprotein MDM2 induces replication stress eliciting early intra-S-phase checkpoint response and inhibition of DNA replication origin firing. Nucleic Acids Res. 2014;42(2):926-40. Epub 2013/10/29. doi: 10.1093/nar/gkt944. PubMed PMID: 24163099; PMCID: 3902934.
32. Frum R, Ramamoorthy M, Mohanraj L, Deb S, Deb SP. MDM2 controls the timely expression of cyclin A to regulate the cell cycle. Mol Cancer Res. 2009;7(8):1253-67. PubMed PMID: 19671680.
33. Singh S, Ramamoorthy, M., Vaughan, C., Yeudall, W. A., Deb, S.and Deb, S. P. Human oncoprotein MDM2 activates the Akt signaling pathway through an interaction with the repressor element-1 silencing transcription factor (REST) conferring a survival advantage to cancer cells. Cell Death Differ. 2012:1-9.
34. Montes de Oca Luna R, Wagner DS, Lozano G. Rescue of early embryonic lethality in mdm2-deficient mice by deletion of p53. Nature. 1995;378(6553):203-6. PubMed PMID: 7477326.
35. Mendrysa SM, McElwee MK, Michalowski J, O'Leary KA, Young KM, Perry ME. mdm2 Is critical for inhibition of p53 during lymphopoiesis and the response to ionizing irradiation. Molecular and cellular biology. 2003;23(2):462-72. Epub 2003/01/02. PubMed PMID: 12509446; PMCID: PMC151546.
36. Liu G, Terzian T, Xiong S, Van Pelt CS, Audiffred A, Box NF, Lozano G. The p53-Mdm2 network in progenitor cell expansion during mouse postnatal development. The Journal of pathology. 2007;213(4):360-8. Epub 2007/09/26. doi: 10.1002/path.2238. PubMed PMID: 17893884.
37. Ringshausen I, O'Shea CC, Finch AJ, Swigart LB, Evan GI. Mdm2 is critically and continuously required to suppress lethal p53 activity in vivo. Cancer cell. 2006;10(6):501-14. Epub 2006/12/13. doi: 10.1016/j.ccr.2006.10.010. PubMed PMID: 17157790.
38. Lundgren K, Montes de Oca Luna R, McNeill YB, Emerick EP, Spencer B, Barfield CR, Lozano G, Rosenberg MP, Finlay CA. Targeted expression of MDM2 uncouples S phase from mitosis and inhibits mammary gland development independent of p53. Genes Dev. 1997;11(6):714-25. PubMed PMID: 9087426.
39. Bond GL, Hu W, Bond EE, Robins H, Lutzker SG, Arva NC, Bargonetti J, Bartel F, Taubert H, Wuerl P, Onel K, Yip L, Hwang SJ, Strong LC, Lozano G, Levine AJ. A

single nucleotide polymorphism in the MDM2 promoter attenuates the p53 tumor suppressor pathway and accelerates tumor formation in humans. Cell. 2004;119(5):591-602. Epub 2004/11/20. doi: 10.1016/j.cell.2004.11.022. PubMed PMID: 15550242.

40. Bond GL, Hu W, Levine A. A single nucleotide polymorphism in the MDM2 gene: from a molecular and cellular explanation to clinical effect. Cancer Res. 2005;65(13):5481-4. Epub 2005/07/05. doi: 10.1158/0008-5472.CAN-05-0825. PubMed PMID: 15994915.
41. Deben C, Deschoolmeester V, Lardon F, Rolfo C, Pauwels P. TP53 and MDM2 genetic alterations in non-small cell lung cancer: Evaluating their prognostic and predictive value. Critical reviews in oncology/hematology. 2016;99:63-73. Epub 2015/12/23. doi: 10.1016/j.critrevonc.2015.11.019. PubMed PMID: 26689115.
42. Ryan BM, Calhoun KM, Pine SR, Bowman ED, Robles AI, Ambs S, Harris CC. MDM2 SNP285 does not antagonize the effect of SNP309 in lung cancer. Int J Cancer. 2012;131(11):2710-6. Epub 2012/04/11. doi: 10.1002/ijc.27573. PubMed PMID: 22487911; PMCID: 3414691.
43. Liu G, Wheatley-Price P, Zhou W, Park S, Heist RS, Asomaning K, Wain JC, Lynch TJ, Su L, Christiani DC. Genetic polymorphisms of MDM2, cumulative cigarette smoking and nonsmall cell lung cancer risk. Int J Cancer. 2008;122(4):915-8. Epub 2007/10/25. doi: 10.1002/ijc.23178. PubMed PMID: 17957785.
44. Reinke V, Bortner DM, Amelse LL, Lundgren K, Rosenberg MP, Finlay CA, Lozano G. Overproduction of MDM2 in vivo disrupts S phase independent of E2F1. Cell growth & differentiation : the molecular biology journal of the American Association for Cancer Research. 1999;10(3):147-54. Epub 1999/04/01. PubMed PMID: 10099828.
45. Jones SN, Hancock AR, Vogel H, Donehower LA, Bradley A. Overexpression of Mdm2 in mice reveals a p53-independent role for Mdm2 in tumorigenesis. Proc Natl Acad Sci U S A. 1998;95(26):15608-12. PubMed PMID: 9861017.
46. Alkhalaf M, Ganguli G, Messaddeq N, Le Meur M, Wasylyk B. MDM2 overexpression generates a skin phenotype in both wild type and p53 null mice. Oncogene. 1999;18(7):1419-34. Epub 1999/03/02. doi: 10.1038/sj.onc.1202448. PubMed PMID: 10050879.
47. Ganguli G, Abecassis J, Wasylyk B. MDM2 induces hyperplasia and premalignant lesions when expressed in the basal layer of the epidermis. The EMBO journal. 2000;19(19):5135-47. Epub 2000/10/03. doi: 10.1093/emboj/19.19.5135. PubMed PMID: 11013216; PMCID: PMC302089.
48. Folberg-Blum A, Sapir A, Shilo BZ, Oren M. Overexpression of mouse Mdm2 induces developmental phenotypes in Drosophila. Oncogene. 2002;21(15):2413-7. Epub 2002/04/12. doi: 10.1038/sj.onc.1205305. PubMed PMID: 11948425.
49. Vogelstein B, Lane D, Levine AJ. Surfing the p53 network. Nature. 2000;408(6810):307-10. PubMed PMID: 11099028.

50. Levine AJ, Hu W, Feng Z. The P53 pathway: what questions remain to be explored? Cell death and differentiation. 2006;13(6):1027-36. Epub 2006/03/25. doi: 10.1038/sj.cdd.4401910. PubMed PMID: 16557269.
51. Vousden KH, Prives C. Blinded by the Light: The Growing Complexity of p53. Cell. 2009;137(3):413-31. Epub 2009/05/05. doi: 10.1016/j.cell.2009.04.037. PubMed PMID: 19410540.
52. Levine AJ, Oren M. The first 30 years of p53: growing ever more complex. Nature reviews Cancer. 2009;9(10):749-58. Epub 2009/09/25. doi: 10.1038/nrc2723. PubMed PMID: 19776744; PMCID: 2771725.
53. Lane DP. Cancer. p53, guardian of the genome. Nature. 1992;358(6381):15-6. Epub 1992/07/02. doi: 10.1038/358015a0. PubMed PMID: 1614522.
54. Levine AJ, Momand J, Finlay CA. The p53 tumour suppressor gene. Nature. 1991;351(6326):453-6. Epub 1991/06/06. doi: 10.1038/351453a0. PubMed PMID: 2046748.
55. Klusmann I, Rodewald S, Muller L, Friedrich M, Wienken M, Li Y, Schulz-Heddergott R, Dobbelstein M. p53 Activity Results in DNA Replication Fork Processivity. Cell reports. 2016;17(7):1845-57. Epub 2016/11/10. doi: 10.1016/j.celrep.2016.10.036. PubMed PMID: 27829155.
56. Bougeard G, Sesboue R, Baert-Desurmont S, Vasseur S, Martin C, Tinat J, Brugieres L, Chompret A, de Paillerets BB, Stoppa-Lyonnet D, Bonaiti-Pellie C, Frebourg T. Molecular basis of the Li-Fraumeni syndrome: an update from the French LFS families. Journal of medical genetics. 2008;45(8):535-8. Epub 2008/05/31. doi: 10.1136/jmg.2008.057570. PubMed PMID: 18511570.
57. Srivastava S, Zou ZQ, Pirollo K, Blattner W, Chang EH. Germ-line transmission of a mutated p53 gene in a cancer-prone family with Li-Fraumeni syndrome. Nature. 1990;348(6303):747-9. Epub 1990/12/20. doi: 10.1038/348747a0. PubMed PMID: 2259385.
58. Jacks T, Remington L, Williams BO, Schmitt EM, Halachmi S, Bronson RT, Weinberg RA. Tumor spectrum analysis in p53-mutant mice. Curr Biol. 1994;4(1):1-7. Epub 1994/01/01. PubMed PMID: 7922305.
59. Donehower LA, Harvey M, Slagle BL, McArthur MJ, Montgomery CA, Jr., Butel JS, Bradley A. Mice deficient for p53 are developmentally normal but susceptible to spontaneous tumours. Nature. 1992;356(6366):215-21. Epub 1992/03/29. doi: 10.1038/356215a0. PubMed PMID: 1552940.
60. Harris SL, Levine AJ. The p53 pathway: positive and negative feedback loops. Oncogene. 2005;24(17):2899-908. PubMed PMID: 15838523.
61. Wade M, Wahl GM. Targeting Mdm2 and Mdmx in cancer therapy: better living through medicinal chemistry? Mol Cancer Res. 2009;7(1):1-11. Epub 2009/01/17. doi: 10.1158/1541-7786.mcr-08-0423. PubMed PMID: 19147532; PMCID: PMC2629357.
62. Dornan D, Wertz I, Shimizu H, Arnott D, Frantz GD, Dowd P, O'Rourke K, Koeppen H, Dixit VM. The ubiquitin ligase COP1 is a critical negative regulator of p53. Nature. 2004;429(6987):86-92. Epub 2004/04/23. doi: 10.1038/nature02514. PubMed PMID: 15103385.

63. Leng RP, Lin Y, Ma W, Wu H, Lemmers B, Chung S, Parant JM, Lozano G, Hakem R, Benchimol S. Pirh2, a p53-induced ubiquitin-protein ligase, promotes p53 degradation. Cell. 2003;112(6):779-91. Epub 2003/03/26. PubMed PMID: 12654245.
64. Freed-Pastor WA, Prives C. Mutant p53: one name, many proteins. Genes Dev. 2012;26(12):1268-86. Epub 2012/06/21. doi: 10.1101/gad.190678.112. PubMed PMID: 22713868; PMCID: 3387655.
65. Muller PA, Vousden KH. p53 mutations in cancer. Nature cell biology. 2013;15(1):2-8. Epub 2012/12/25. doi: 10.1038/ncb2641. PubMed PMID: 23263379.
66. Brosh R, Rotter V. When mutants gain new powers: news from the mutant p53 field. Nature reviews Cancer. 2009;9(10):701-13. Epub 2009/08/21. doi: 10.1038/nrc2693. PubMed PMID: 19693097.
67. Soussi T, Kato S, Levy PP, Ishioka C. Reassessment of the TP53 mutation database in human disease by data mining with a library of TP53 missense mutations. Human mutation. 2005;25(1):6-17. Epub 2004/12/08. doi: 10.1002/humu.20114. PubMed PMID: 15580553.
68. Petitjean A, Achatz MI, Borresen-Dale AL, Hainaut P, Olivier M. TP53 mutations in human cancers: functional selection and impact on cancer prognosis and outcomes. Oncogene. 2007;26(15):2157-65. Epub 2007/04/03. doi: 10.1038/sj.onc.1210302. PubMed PMID: 17401424.
69. Mello SS, Attardi LD. Not all p53 gain-of-function mutants are created equal. Cell death and differentiation. 2013;20(7):855-7. Epub 2013/06/12. doi: 10.1038/cdd.2013.53. PubMed PMID: 23749181; PMCID: PMC3679467.
70. Zhang C, Liu J, Liang Y, Wu R, Zhao Y, Hong X, Lin M, Yu H, Liu L, Levine AJ, Hu W, Feng Z. Tumour-associated mutant p53 drives the Warburg effect. Nature communications. 2013;4:2935. Epub 2013/12/18. doi: 10.1038/ncomms3935. PubMed PMID: 24343302; PMCID: PMC3969270.
71. Vaughan CA, Singh S, Windle B, Sankala HM, Graves PR, Andrew Yeudall W, Deb SP, Deb S. p53 mutants induce transcription of NF-kappaB2 in H1299 cells through CBP and STAT binding on the NF-kappaB2 promoter and gain of function activity. Archives of biochemistry and biophysics. 2012;518(1):79-88. Epub 2011/12/27. doi: 10.1016/j.abb.2011.12.006. PubMed PMID: 22198284; PMCID: 3272778.
72. Vaughan CA, Singh S, Grossman SR, Windle B, Deb SP, Deb S. Gain-of-function p53 activates multiple signaling pathways to induce oncogenicity in lung cancer cells. Molecular oncology. 2017;11(6):696-711. doi: 10.1002/1878-0261.12068. PubMed PMID: 28423230; PMCID: PMC5467493.
73. Blandino G, Deppert W, Hainaut P, Levine A, Lozano G, Olivier M, Rotter V, Wiman K, Oren M. Mutant p53 protein, master regulator of human malignancies: a report on the Fifth Mutant p53 Workshop. Cell death and differentiation. 2012;19(1):180-3. Epub 2011/11/19. doi: 10.1038/cdd.2011.148. PubMed PMID: 22095277; PMCID: 3324325.
74. Dittmer D, Pati S, Zambetti G, Chu S, Teresky AK, Moore M, Finlay C, Levine AJ. Gain of function mutations in p53. Nature genetics. 1993;4(1):42-6. PubMed PMID: 8099841.

75. Muller PA, Trinidad AG, Caswell PT, Norman JC, Vousden KH. Mutant p53 regulates Dicer through p63-dependent and -independent mechanisms to promote an invasive phenotype. The Journal of biological chemistry. 2014;289(1):122-32. Epub 2013/11/14. doi: 10.1074/jbc.M113.502138. PubMed PMID: 24220032; PMCID: PMC3879536.
76. Stindt MH, Muller PA, Ludwig RL, Kehrloesser S, Dotsch V, Vousden KH. Functional interplay between MDM2, p63/p73 and mutant p53. Oncogene. 2015;34(33):4300-10. Epub 2014/11/25. doi: 10.1038/onc.2014.359. PubMed PMID: 25417702; PMCID: PMC4351904.
77. Gaiddon C, Lokshin M, Ahn J, Zhang T, Prives C. A subset of tumor-derived mutant forms of p53 down-regulate p63 and p73 through a direct interaction with the p53 core domain. Mol Cell Biol. 2001;21(5):1874-87. PubMed PMID: 11238924.
78. Li Y, Prives C. Are interactions with p63 and p73 involved in mutant p53 gain of oncogenic function? Oncogene. 2007;26(15):2220-5. PubMed PMID: 17401431.
79. Belyi VA, Ak P, Markert E, Wang H, Hu W, Puzio-Kuter A, Levine AJ. The origins and evolution of the p53 family of genes. Cold Spring Harbor perspectives in biology. 2010;2(6):a001198. Epub 2010/06/03. doi: 10.1101/cshperspect.a001198. PubMed PMID: 20516129; PMCID: 2869528.
80. Di Agostino S, Strano S, Emiliozzi V, Zerbini V, Mottolese M, Sacchi A, Blandino G, Piaggio G. Gain of function of mutant p53: the mutant p53/NF-Y protein complex reveals an aberrant transcriptional mechanism of cell cycle regulation. Cancer cell. 2006;10(3):191-202. Epub 2006/09/09. doi: 10.1016/j.ccr.2006.08.013. PubMed PMID: 16959611.
81. Sampath J, Sun D, Kidd VJ, Grenet J, Gandhi A, Shapiro LH, Wang Q, Zambetti GP, Schuetz JD. Mutant p53 cooperates with ETS and selectively up-regulates human MDR1 not MRP1. The Journal of biological chemistry. 2001;276(42):39359-67. PubMed PMID: 11483599.
82. Walerych D, Lisek K, Sommaggio R, Piazza S, Ciani Y, Dalla E, Rajkowska K, Gaweda-Walerych K, Ingallina E, Tonelli C, Morelli MJ, Amato A, Eterno V, Zambelli A, Rosato A, Amati B, Wisniewski JR, Del Sal G. Proteasome machinery is instrumental in a common gain-of-function program of the p53 missense mutants in cancer. Nature cell biology. 2016;18(8):897-909. Epub 2016/06/28. doi: 10.1038/ncb3380. PubMed PMID: 27347849.
83. Vaughan CA, Deb SP, Deb S, Windle B. Preferred binding of gain-of-function mutant p53 to bidirectional promoters with coordinated binding of ETS1 and GABPA to multiple binding sites. Oncotarget. 2014;5(2):417-27. Epub 2014/02/01. PubMed PMID: 24481480; PMCID: 3964217.
84. Pfister NT, Fomin V, Regunath K, Zhou JY, Zhou W, Silwal-Pandit L, Freed-Pastor WA, Laptenko O, Neo SP, Bargonetti J, Hoque M, Tian B, Gunaratne J, Engebraaten O, Manley JL, Borresen-Dale AL, Neilsen PM, Prives C. Mutant p53 cooperates with the SWI/SNF chromatin remodeling complex to regulate VEGFR2 in breast cancer cells. Genes & development. 2015;29(12):1298-315. Epub 2015/06/18. doi: 10.1101/gad.263202.115. PubMed PMID: 26080815; PMCID: PMC4495400.

85. Yue X, Zhao Y, Xu Y, Zheng M, Feng Z, Hu W. Mutant p53 in Cancer: Accumulation, Gain-of-Function, and Therapy. Journal of molecular biology. 2017;429(11):1595-606. Epub 2017/04/10. doi: 10.1016/j.jmb.2017.03.030. PubMed PMID: 28390900; PMCID: PMC5663274.
86. Vaughan CA, Singh S, Windle B, Sankala HM, Graves PR, Andrew Yeudall W, Deb SP, Deb S. p53 mutants induce transcription of NF-kappaB2 in H1299 cells through CBP and STAT binding on the NF-kappaB2 promoter and gain of function activity. Arch Biochem Biophys. 2011;518(1):79-88. PubMed PMID: 22198284.
87. Alexandrova EM, Yallowitz AR, Li D, Xu S, Schulz R, Proia DA, Lozano G, Dobbelstein M, Moll UM. Improving survival by exploiting tumour dependence on stabilized mutant p53 for treatment. Nature. 2015. Epub 2015/05/27. doi: 10.1038/nature14430. PubMed PMID: 26009011.
88. Brown DR, Thomas CA, Deb SP. The human oncoprotein MDM2 arrests the cell cycle: elimination of its cell-cycle-inhibitory function induces tumorigenesis. EMBO J. 1998;17(9):2513-25. PubMed PMID: 9564034.
89. Deb SP. Cell cycle regulatory functions of the human oncoprotein MDM2. Mol Cancer Res. 2003;1(14):1009-16. PubMed PMID: 14707284.
90. Manfredi JJ. The Mdm2-p53 relationship evolves: Mdm2 swings both ways as an oncogene and a tumor suppressor. Genes Dev. 2010;24(15):1580-9. PubMed PMID: 20679392.
91. Machida YJ, Hamlin JL, Dutta A. Right place, right time, and only once: replication initiation in metazoans. Cell. 2005;123(1):13-24. Epub 2005/10/11. doi: 10.1016/j.cell.2005.09.019. PubMed PMID: 16213209.
92. Grallert B, Boye E. The multiple facets of the intra-S checkpoint. Cell Cycle. 2008;7(15):2315-20. Epub 2008/08/05. PubMed PMID: 18677104.
93. Nakanishi M, Katsuno Y, Niida H, Murakami H, Shimada M. Chk1-cyclin A/Cdk1 axis regulates origin firing programs in mammals. Chromosome Res. 2010;18(1):103-13. Epub 2009/12/17. doi: 10.1007/s10577-009-9086-2. PubMed PMID: 20013152.
94. Sorensen CS, Syljuasen RG. Safeguarding genome integrity: the checkpoint kinases ATR, CHK1 and WEE1 restrain CDK activity during normal DNA replication. Nucleic Acids Res. 2012;40(2):477-86. Epub 2011/09/23. doi: 10.1093/nar/gkr697. PubMed PMID: 21937510; PMCID: 3258124.
95. Liu H, Takeda S, Kumar R, Westergard TD, Brown EJ, Pandita TK, Cheng EH, Hsieh JJ. Phosphorylation of MLL by ATR is required for execution of mammalian S-phase checkpoint. Nature. 2010;467(7313):343-6. Epub 2010/09/08. doi: 10.1038/nature09350. PubMed PMID: 20818375; PMCID: 2940944.
96. Errico A, Costanzo V. Mechanisms of replication fork protection: a safeguard for genome stability. Crit Rev Biochem Mol Biol. 2012;47(3):222-35. Epub 2012/02/14. doi: 10.3109/10409238.2012.655374. PubMed PMID: 22324461.
97. Branzei D, Foiani M. Maintaining genome stability at the replication fork. Nature reviews Molecular cell biology. 2010;11(3):208-19. Epub 2010/02/24. doi: 10.1038/nrm2852. PubMed PMID: 20177396.

98. Leng P, Brown DR, Shivakumar CV, Deb S, Deb SP. N-terminal 130 amino acids of MDM2 are sufficient to inhibit p53-mediated transcriptional activation. Oncogene. 1995;10(7):1275-82. PubMed PMID: 7731677.
99. Frum RA, Chastain PD, 2nd, Qu P, Cohen SM, Kaufman DG. DNA replication in early S phase pauses near newly activated origins. Cell Cycle. 2008;7(10):1440-8. PubMed PMID: 18418075.
100. Frum RA, Deb S, Deb SP. Use of the DNA fiber spreading technique to detect the effects of mutant p53 on DNA replication. Methods Mol Biol. 2013;962:147-55. Epub 2012/11/15. doi: 10.1007/978-1-62703-236-0_12. PubMed PMID: 23150444.
101. Jones RM, Mortusewicz O, Afzal I, Lorvellec M, Garcia P, Helleday T, Petermann E. Increased replication initiation and conflicts with transcription underlie Cyclin E-induced replication stress. Oncogene. 2012. Epub 2012/09/05. doi: 10.1038/onc.2012.387. PubMed PMID: 22945645.
102. Montagnoli A, Valsasina B, Croci V, Menichincheri M, Rainoldi S, Marchesi V, Tibolla M, Tenca P, Brotherton D, Albanese C, Patton V, Alzani R, Ciavolella A, Sola F, Molinari A, Volpi D, Avanzi N, Fiorentini F, Cattoni M, Healy S, Ballinari D, Pesenti E, Isacchi A, Moll J, Bensimon A, Vanotti E, Santocanale C. A Cdc7 kinase inhibitor restricts initiation of DNA replication and has antitumor activity. Nat Chem Biol. 2008;4(6):357-65. Epub 2008/05/13. doi: 10.1038/nchembio.90. PubMed PMID: 18469809.
103. Zhou R, Frum R, Deb S, Deb SP. The growth arrest function of the human oncoprotein mouse double minute-2 is disabled by downstream mutation in cancer cells. Cancer research. 2005;65(5):1839-48. PubMed PMID: 15753382.
104. Windle B, Parra, I., Silvas, E. Analysis of structure and function by high resolution visual mapping of extended DNA. M. Andreeff DP, editor1999.
105. Di Micco R, Fumagalli M, d'Adda di Fagagna F. Breaking news: high-speed race ends in arrest--how oncogenes induce senescence. Trends Cell Biol. 2007;17(11):529-36. PubMed PMID: 17980599.
106. Herold S, Herkert B, Eilers M. Facilitating replication under stress: an oncogenic function of MYC? Nat Rev Cancer. 2009;9(6):441-4. Epub 2009/05/23. doi: 10.1038/nrc2640. PubMed PMID: 19461668.
107. Luciani MG, Oehlmann M, Blow JJ. Characterization of a novel ATR-dependent, Chk1-independent, intra-S-phase checkpoint that suppresses initiation of replication in Xenopus. J Cell Sci. 2004;117(Pt 25):6019-30. Epub 2004/11/13. doi: 10.1242/jcs.01400. PubMed PMID: 15536124; PMCID: 2701543.
108. Sarkaria JN, Busby EC, Tibbetts RS, Roos P, Taya Y, Karnitz LM, Abraham RT. Inhibition of ATM and ATR kinase activities by the radiosensitizing agent, caffeine. Cancer research. 1999;59(17):4375-82. Epub 1999/09/15. PubMed PMID: 10485486.
109. Di Micco R, Fumagalli M, Cicalese A, Piccinin S, Gasparini P, Luise C, Schurra C, Garre M, Nuciforo PG, Bensimon A, Maestro R, Pelicci PG, d'Adda di Fagagna F. Oncogene-induced senescence is a DNA damage response triggered by DNA hyper-replication. Nature. 2006;444(7119):638-42. PubMed PMID: 17136094.

110. Zhu J, Woods D, McMahon M, Bishop JM. Senescence of human fibroblasts induced by oncogenic Raf. Genes Dev. 1998;12(19):2997-3007. Epub 1998/10/09. PubMed PMID: 9765202; PMCID: 317194.
111. Ben-Yehoyada M, Gautier J, Dupre A. The DNA damage response during an unperturbed S-phase. DNA Repair (Amst). 2007;6(7):914-22. Epub 2007/03/22. doi: 10.1016/j.dnarep.2007.02.005. PubMed PMID: 17374515.
112. Willis N, Rhind N. Regulation of DNA replication by the S-phase DNA damage checkpoint. Cell Div. 2009;4:13. PubMed PMID: 19575778.
113. de Boer J, Walf-Vorderwulbecke V, Williams O. In focus: MLL-rearranged leukemia. Leukemia. 2013. Epub 2013/03/22. doi: 10.1038/leu.2013.78. PubMed PMID: 23515098.
114. Liu H, Cheng EH, Hsieh JJ. Bimodal degradation of MLL by SCFSkp2 and APCCdc20 assures cell cycle execution: a critical regulatory circuit lost in leukemogenic MLL fusions. Genes Dev. 2007;21(19):2385-98. Epub 2007/10/03. doi: 10.1101/gad.1574507. PubMed PMID: 17908926; PMCID: 1993870.
115. Shew JY, Lin BT, Chen PL, Tseng BY, Yang-Feng TL, Lee WH. C-terminal truncation of the retinoblastoma gene product leads to functional inactivation. Proc Natl Acad Sci U S A. 1990;87(1):6-10. Epub 1990/01/01. PubMed PMID: 1688660; PMCID: 53188.
116. Masuda H, Miller C, Koeffler HP, Battifora H, Cline MJ. Rearrangement of the p53 gene in human osteogenic sarcomas. Proc Natl Acad Sci U S A. 1987;84(21):7716-9. Epub 1987/11/01. PubMed PMID: 2823272; PMCID: 299371.
117. Mullany LK, White P, Hanse EA, Nelsen CJ, Goggin MM, Mullany JE, Anttila CK, Greenbaum LE, Kaestner KH, Albrecht JH. Distinct proliferative and transcriptional effects of the D-type cyclins in vivo. Cell Cycle. 2008;7(14):2215-24. Epub 2008/07/19. PubMed PMID: 18635970.
118. Diao L, Chen YG. PTEN, a general negative regulator of cyclin D expression. Cell Res. 2007;17(4):291-2. Epub 2007/04/12. doi: 10.1038/cr.2007.24. PubMed PMID: 17426697.
119. Thelen M, Wymann MP, Langen H. Wortmannin binds specifically to 1-phosphatidylinositol 3-kinase while inhibiting guanine nucleotide-binding protein-coupled receptor signaling in neutrophil leukocytes. Proc Natl Acad Sci U S A. 1994;91(11):4960-4. PubMed PMID: 8197165.
120. Bell SP, Dutta A. DNA replication in eukaryotic cells. Annu Rev Biochem. 2002;71:333-74. Epub 2002/06/05. doi: 10.1146/annurev.biochem.71.110601.135425. PubMed PMID: 12045100.
121. Yaswen P, Campisi J. Oncogene-induced senescence pathways weave an intricate tapestry. Cell. 2007;128(2):233-4. Epub 2007/01/27. doi: 10.1016/j.cell.2007.01.005. PubMed PMID: 17254959.
122. Kozar K, Sicinski P. Cell cycle progression without cyclin D-CDK4 and cyclin D-CDK6 complexes. Cell Cycle. 2005;4(3):388-91. Epub 2005/03/02. PubMed PMID: 15738651.
123. Bermudez O, Hennen E, Koch I, Lindner M, Eickelberg O. Gli1 mediates lung cancer cell proliferation and Sonic Hedgehog-dependent mesenchymal cell activation. PLoS

One. 2013;8(5):e63226. Epub 2013/05/15. doi: 10.1371/journal.pone.0063226. PubMed PMID: 23667589; PMCID: 3646741.
124. Segurado M, Tercero JA. The S-phase checkpoint: targeting the replication fork. Biol Cell. 2009;101(11):617-27. Epub 2009/08/19. doi: 10.1042/BC20090053. PubMed PMID: 19686094.
125. Bueso-Ramos CE, Yang Y, deLeon E, McCown P, Stass SA, Albitar M. The human MDM-2 oncogene is overexpressed in leukemias. Blood. 1993;82(9):2617-23. Epub 1993/11/01. PubMed PMID: 8219216.
126. Karni-Schmidt O, Lokshin M, Prives C. The Roles of MDM2 and MDMX in Cancer. Annu Rev Pathol. 2016;11:617-44. doi: 10.1146/annurev-pathol-012414-040349. PubMed PMID: 27022975.
127. Moyer SM, Larsson CA, Lozano G. Mdm proteins: critical regulators of embry ogenesis and homeostasis. J Mol Cell Biol. 2017. doi: 10.1093/jmcb/mjx004. PubMed PMID: 28093454; PMCID: PMC5439424.
128. Jones SN, Roe AE, Donehower LA, Bradley A. Rescue of embryonic lethality in Mdm2-deficient mice by absence of p53. Nature. 1995;378(6553):206-8. PubMed PMID: 7477327.
129. Hilliard SA, Yao X, El-Dahr SS. Mdm2 is required for maintenance of the nephrogenic niche. Developmental biology. 2014;387(1):1-14. Epub 2014/01/21. doi: 10.1016/j.ydbio.2014.01.009. PubMed PMID: 24440154; PMCID: 3951515.
130. Mulay SR, Thomasova D, Ryu M, Anders HJ. MDM2 (murine double minute-2) links inflammation and tubular cell healing during acute kidney injury in mice. Kidney international. 2012;81(12):1199-211. Epub 2012/02/03. doi: 10.1038/ki.2011.482. PubMed PMID: 22297670.
131. Wienken M, Dickmanns A, Nemajerova A, Kramer D, Najafova Z, Weiss M, Karpiuk O, Kassem M, Zhang Y, Lozano G, Johnsen SA, Moll UM, Zhang X, Dobbelstein M. MDM2 Associates with Polycomb Repressor Complex 2 and Enhances Stemness-Promoting Chromatin Modifications Independent of p53. Molecular cell. 2016;61(1):68-83. Epub 2016/01/11. doi: 10.1016/j.molcel.2015.12.008. PubMed PMID: 26748827.
132. Tichelaar JW, Lu W, Whitsett JA. Conditional expression of fibroblast growth factor-7 in the developing and mature lung. J Biol Chem. 2000;275(16):11858-64. Epub 2000/04/15. PubMed PMID: 10766812.
133. Perl AK, Wert SE, Nagy A, Lobe CG, Whitsett JA. Early restriction of peripheral and proximal cell lineages during formation of the lung. Proceedings of the National Academy of Sciences of the United States of America. 2002;99(16):10482-7. Epub 2002/07/30. doi: 10.1073/pnas.152238499. PubMed PMID: 12145322; PMCID: 124949.
134. Olive KP, Tuveson DA, Ruhe ZC, Yin B, Willis NA, Bronson RT, Crowley D, Jacks T. Mutant p53 gain of function in two mouse models of Li-Fraumeni syndrome. Cell. 2004;119(6):847-60. Epub 2004/12/21. doi: 10.1016/j.cell.2004.11.004. PubMed PMID: 15607980.

135. Jackson IL, Xu PT, Nguyen G, Down JD, Johnson CS, Katz BP, Hadley CC, Vujaskovic Z. Characterization of the dose response relationship for lung injury following acute radiation exposure in three well-established murine strains: developing an interspecies bridge to link animal models with human lung. Health physics. 2014;106(1):48-55. Epub 2013/11/28. doi: 10.1097/HP.0b013e3182a32ccf. PubMed PMID: 24276549.
136. Burgess A, Vigneron S, Brioudes E, Labbe JC, Lorca T, Castro A. Loss of human Greatwall results in G2 arrest and multiple mitotic defects due to deregulation of the cyclin B-Cdc2/PP2A balance. Proceedings of the National Academy of Sciences of the United States of America. 2010;107(28):12564-9. Epub 2010/06/12. doi: 10.1073/pnas.0914191107. PubMed PMID: 20538976; PMCID: PMC2906566.
137. Singh S, Vaughan CA, Frum RA, Grossman SR, Deb S, Palit Deb S. Mutant p53 establishes targetable tumor dependency by promoting unscheduled replication. J Clin Invest. 2017;127(5):1839-55. Epub 2017/04/11. doi: 10.1172/JCI87724. PubMed PMID: 28394262; PMCID: 5409068.
138. Pardee AB. A restriction point for control of normal animal cell proliferation. Proc Natl Acad Sci U S A. 1974;71(4):1286-90. Epub 1974/04/01. PubMed PMID: 4524638; PMCID: 388211.
139. Banerjee T, Chakravarti D. A peek into the complex realm of histone phosphorylation. Mol Cell Biol. 2011;31(24):4858-73. Epub 2011/10/19. doi: 10.1128/MCB.05631-11. PubMed PMID: 22006017; PMCID: 3233023.
140. Kotton DN, Morrisey EE. Lung regeneration: mechanisms, applications and emerging stem cell populations. Nat Med. 2014;20(8):822-32. Epub 2014/08/08. doi: 10.1038/nm.3642. PubMed PMID: 25100528; PMCID: 4229034.
141. Liu X, Driskell RR, Engelhardt JF. Stem cells in the lung. Methods Enzymol. 2006;419:285-321. Epub 2006/12/05. doi: 10.1016/S0076-6879(06)19012-6. PubMed PMID: 17141060; PMCID: 1803078.
142. Reynolds SD, Malkinson AM. Clara cell: progenitor for the bronchiolar epithelium. The international journal of biochemistry & cell biology. 2010;42(1):1-4. Epub 2009/09/15. doi: 10.1016/j.biocel.2009.09.002. PubMed PMID: 19747565; PMCID: 2787899.
143. Hogan BL, Barkauskas CE, Chapman HA, Epstein JA, Jain R, Hsia CC, Niklason L, Calle E, Le A, Randell SH, Rock J, Snitow M, Krummel M, Stripp BR, Vu T, White ES, Whitsett JA, Morrisey EE. Repair and regeneration of the respiratory system: complexity, plasticity, and mechanisms of lung stem cell function. Cell Stem Cell. 2014;15(2):123-38. doi: 10.1016/j.stem.2014.07.012. PubMed PMID: 25105578; PMCID: PMC4212493.
144. Volckaert T, Dill E, Campbell A, Tiozzo C, Majka S, Bellusci S, De Langhe SP. Parabronchial smooth muscle constitutes an airway epithelial stem cell niche in the mouse lung after injury. The Journal of clinical investigation. 2011;121(11):4409-19. doi: 10.1172/JCI58097. PubMed PMID: 21985786; PMCID: PMC3204843.

145. Xing Y, Li A, Borok Z, Li C, Minoo P. NOTCH1 is required for regeneration of Clara cells during repair of airway injury. Stem Cells. 2012;30(5):946-55. doi: 10.1002/stem.1059. PubMed PMID: 22331706; PMCID: PMC4005608.
146. McCubrey JA, Rakus D, Gizak A, Steelman LS, Abrams SL, Lertpiriyapong K, Fitzgerald TL, Yang LV, Montalto G, Cervello M, Libra M, Nicoletti F, Scalisi A, Torino F, Fenga C, Neri LM, Marmiroli S, Cocco L, Martelli AM. Effects of mutations in Wnt/beta-catenin, hedgehog, Notch and PI3K pathways on GSK-3 activity-Diverse effects on cell growth, metabolism and cancer. Biochimica et biophysica acta. 2016;1863(12):2942-76. doi: 10.1016/j.bbamcr.2016.09.004. PubMed PMID: 27612668.
147. Coggle JE, Lambert BE, Moores SR. Radiation effects in the lung. Environ Health Perspect. 1986;70:261-91. PubMed PMID: 3549278; PMCID: PMC1474274.
148. Gorgoulis VG, Zacharatos P, Kotsinas A, Liloglou T, Kyroudi A, Veslemes M, Rassidakis A, Halazonetis TD, Field JK, Kittas C. Alterations of the p16-pRb pathway and the chromosome locus 9p21-22 in non-small-cell lung carcinomas: relationship with p53 and MDM2 protein expression. Am J Pathol. 1998;153(6):1749-65. doi: 10.1016/S0002-9440(10)65690-8. PubMed PMID: 9846966; PMCID: PMC2233978.
149. Gorgoulis VG, Zacharatos P, Kotsinas A, Mariatos G, Liloglou T, Vogiatzi T, Foukas P, Rassidakis G, Garinis G, Ioannides T, Zoumpourlis V, Bramis J, Michail PO, Asimacopoulos PJ, Field JK, Kittas C. Altered expression of the cell cycle regulatory molecules pRb, p53 and MDM2 exert a synergetic effect on tumor growth and chromosomal instability in non-small cell lung carcinomas (NSCLCs). Molecular medicine (Cambridge, Mass. 2000;6(3):208-37. PubMed PMID: 10965496; PMCID: PMC1949940.
150. Crosby LM, Waters CM. Epithelial repair mechanisms in the lung. American journal of physiology. 2010;298(6):L715-31. doi: 10.1152/ajplung.00361.2009. PubMed PMID: 20363851; PMCID: PMC2886606.
151. Araki S, Eitel JA, Batuello CN, Bijangi-Vishehsaraei K, Xie XJ, Danielpour D, Pollok KE, Boothman DA, Mayo LD. TGF-beta1-induced expression of human Mdm2 correlates with late-stage metastatic breast cancer. The Journal of clinical investigation. 2010;120(1):290-302. doi: 10.1172/JCI39194. PubMed PMID: 19955655; PMCID: PMC2798681.
152. Jung CR, Lim JH, Choi Y, Kim DG, Kang KJ, Noh SM, Im DS. Enigma negatively regulates p53 through MDM2 and promotes tumor cell survival in mice. The Journal of clinical investigation. 2010;120(12):4493-506. doi: 10.1172/JCI42674. PubMed PMID: 21060154; PMCID: PMC2993588.
153. Zhang K, Chu K, Wu X, Gao H, Wang J, Yuan YC, Loera S, Ho K, Wang Y, Chow W, Un F, Chu P, Yen Y. Amplification of FRS2 and activation of FGFR/FRS2 signaling pathway in high-grade liposarcoma. Cancer Res. 2013;73(4):1298-307. doi: 10.1158/0008-5472.CAN-12-2086. PubMed PMID: 23393200.
154. Senturk E, Manfredi JJ. Mdm2 and tumorigenesis: evolving theories and unsolved mysteries. Genes Cancer. 2012;3(3-4):192-8. Epub 2012/11/15. doi: 10.1177/1947601912457368. PubMed PMID: 23150752; PMCID: 3494366.

155. Senturk JC, Bohlman S, Manfredi JJ. Mdm2 selectively suppresses DNA damage arising from inhibition of topoisomerase II independent of p53. Oncogene. 2017;36(44):6085-96. doi: 10.1038/onc.2017.229. PubMed PMID: 28692049.
156. Arena G, Cisse MY, Pyrdziak S, Chatre L, Riscal R, Fuentes M, Arnold JJ, Kastner M, Gayte L, Bertrand-Gaday C, Nay K, Angebault-Prouteau C, Murray K, Chabi B, Koechlin-Ramonatxo C, Orsetti B, Vincent C, Casas F, Marine JC, Etienne-Manneville S, Bernex F, Lombes A, Cameron CE, Dubouchaud H, Ricchetti M, Linares LK, Le Cam L. Mitochondrial MDM2 Regulates Respiratory Complex I Activity Independently of p53. Molecular cell. 2018;69(4):594-609 e8. doi: 10.1016/j.molcel.2018.01.023. PubMed PMID: 29452639.
157. Shaikh MF, Morano WF, Lee J, Gleeson E, Babcock BD, Michl J, Sarafraz-Yazdi E, Pincus MR, Bowne WB. Emerging Role of MDM2 as Target for Anti-Cancer Therapy: A Review. Ann Clin Lab Sci. 2016;46(6):627-34. PubMed PMID: 27993876.
158. Gannon HS, Donehower LA, Lyle S, Jones SN. Mdm2-p53 signaling regulates epidermal stem cell senescence and premature aging phenotypes in mouse skin. Developmental biology. 2011;353(1):1-9. doi: 10.1016/j.ydbio.2011.02.007. PubMed PMID: 21334322; PMCID: PMC3075331.
159. Abbas HA, Maccio DR, Coskun S, Jackson JG, Hazen AL, Sills TM, You MJ, Hirschi KK, Lozano G. Mdm2 is required for survival of hematopoietic stem cells/progenitors via dampening of ROS-induced p53 activity. Cell Stem Cell. 2010;7(5):606-17. doi: 10.1016/j.stem.2010.09.013. PubMed PMID: 21040902; PMCID: PMC3026610.
160. Soussi T, Wiman KG. TP53: an oncogene in disguise. Cell death and differentiation. 2015. Epub 2015/05/30. doi: 10.1038/cdd.2015.53. PubMed PMID: 26024390.
161. Chibazakura T, Kamachi K, Ohara M, Tane S, Yoshikawa H, Roberts JM. Cyclin A promotes S-phase entry via interaction with the replication licensing factor Mcm7. Molecular and cellular biology. 2011;31(2):248-55. Epub 2010/11/17. doi: 10.1128/MCB.00630-10. PubMed PMID: 21078875; PMCID: 3019979.
162. Coverley D, Laman H, Laskey RA. Distinct roles for cyclins E and A during DNA replication complex assembly and activation. Nature cell biology. 2002;4(7):523-8. Epub 2002/06/25. doi: 10.1038/ncb813. PubMed PMID: 12080347.
163. Girard F, Strausfeld U, Fernandez A, Lamb NJ. Cyclin A is required for the onset of DNA replication in mammalian fibroblasts. Cell. 1991;67(6):1169-79. PubMed PMID: 1836977.
164. Lecona E, Fernandez-Capetillo O. Replication stress and cancer: It takes two to tango. Exp Cell Res. 2014;329(1):26-34. Epub 2014/09/27. doi: 10.1016/j.yexcr.2014.09.019. PubMed PMID: 25257608.
165. Lopes M, Cotta-Ramusino C, Pellicioli A, Liberi G, Plevani P, Muzi-Falconi M, Newlon CS, Foiani M. The DNA replication checkpoint response stabilizes stalled replication forks. Nature. 2001;412(6846):557-61. Epub 2001/08/03. doi: 10.1038/35087613. PubMed PMID: 11484058.
166. Magdalou I, Lopez BS, Pasero P, Lambert SA. The causes of replication stress and their consequences on genome stability and cell fate. Semin Cell Dev Biol.

2014;30:154-64. Epub 2014/05/14. doi: 10.1016/j.semcdb.2014.04.035. PubMed PMID: 24818779.

167. Carr AM, Paek AL, Weinert T. DNA replication: failures and inverted fusions. Semin Cell Dev Biol. 2011;22(8):866-74. Epub 2011/10/25. doi: 10.1016/j.semcdb.2011.10.008. PubMed PMID: 22020070.
168. Cortez D. Preventing replication fork collapse to maintain genome integrity. DNA Repair (Amst). 2015. Epub 2015/05/11. doi: 10.1016/j.dnarep.2015.04.026. PubMed PMID: 25957489.
169. Yamamoto M, Yoshida M, Ono K, Fujita T, Ohtani-Fujita N, Sakai T, Nikaido T. Effect of tumor suppressors on cell cycle-regulatory genes: RB suppresses p34cdc2 expression and normal p53 suppresses cyclin A expression. Exp Cell Res. 1994;210(1):94-101. PubMed PMID: 8270002.
170. Terzian T, Suh YA, Iwakuma T, Post SM, Neumann M, Lang GA, Van Pelt CS, Lozano G. The inherent instability of mutant p53 is alleviated by Mdm2 or p16INK4a loss. Genes Dev. 2008;22(10):1337-44. PubMed PMID: 18483220.
171. Sarmento LM, Povoa V, Nascimento R, Real G, Antunes I, Martins LR, Moita C, Alves PM, Abecasis M, Moita LF, Parkhouse RM, Meijerink JP, Barata JT. CHK1 overexpression in T-cell acute lymphoblastic leukemia is essential for proliferation and survival by preventing excessive replication stress. Oncogene. 2014;0. doi: 10.1038/onc.2014.248. PubMed PMID: 25132270.
172. Frum R, Deb SP. Flow cytometric analysis of MDM2-mediated growth arrest. Methods Mol Biol. 2003;234:257-67. PubMed PMID: 12824538.
173. Dorn ES, Chastain PD, 2nd, Hall JR, Cook JG. Analysis of re-replication from deregulated origin licensing by DNA fiber spreading. Nucleic Acids Res. 2009;37(1):60-9. Epub 2008/11/18. doi: 10.1093/nar/gkn912. PubMed PMID: 19010964; PMCID: 2615611.
174. Robertson G, Hirst M, Bainbridge M, Bilenky M, Zhao Y, Zeng T, Euskirchen G, Bernier B, Varhol R, Delaney A, Thiessen N, Griffith OL, He A, Marra M, Snyder M, Jones S. Genome-wide profiles of STAT1 DNA association using chromatin immunoprecipitation and massively parallel sequencing. Nat Methods. 2007;4(8):651-7. Epub 2007/06/15. doi: 10.1038/nmeth1068. PubMed PMID: 17558387.
175. Scian MJ, Stagliano KE, Deb D, Ellis MA, Carchman EH, Das A, Valerie K, Deb SP, Deb S. Tumor-derived p53 mutants induce oncogenesis by transactivating growth-promoting genes. Oncogene. 2004;23(25):4430-43. PubMed PMID: 15077194.
176. Sarmento LM, Povoa V, Nascimento R, Real G, Antunes I, Martins LR, Moita C, Alves PM, Abecasis M, Moita LF, Parkhouse RM, Meijerink JP, Barata JT. CHK1 overexpression in T-cell acute lymphoblastic leukemia is essential for proliferation and survival by preventing excessive replication stress. Oncogene. 2015;34(23):2978-90. Epub 2014/08/19. doi: 10.1038/onc.2014.248. PubMed PMID: 25132270.
177. Vaughan CA, Frum R, Pearsall I, Singh S, Windle B, Yeudall A, Deb SP, Deb S. Allele specific gain-of-function activity of p53 mutants in lung cancer cells. Biochem Biophys Res Commun. 2012;428(1):6-10. Epub 2012/09/20. doi: 10.1016/j.bbrc.2012.09.029. PubMed PMID: 22989750.

178. Gagou ME, Zuazua-Villar P, Meuth M. Enhanced H2AX phosphorylation, DNA replication fork arrest, and cell death in the absence of Chk1. Mol Biol Cell. 2010;21(5):739-52. Epub 2010/01/08. doi: 10.1091/mbc.E09-07-0618. PubMed PMID: 20053681; PMCID: 2828961.
179. Zuazua-Villar P, Rodriguez R, Gagou ME, Eyers PA, Meuth M. DNA replication stress in CHK1-depleted tumour cells triggers premature (S-phase) mitosis through inappropriate activation of Aurora kinase B. Cell Death Dis. 2014;5:e1253. Epub 2014/05/24. doi: 10.1038/cddis.2014.231. PubMed PMID: 24853431; PMCID: 4047883.
180. Blow JJ, Gillespie PJ. Replication licensing and cancer--a fatal entanglement? Nat Rev Cancer. 2008;8(10):799-806. Epub 2008/08/30. doi: 10.1038/nrc2500. PubMed PMID: 18756287; PMCID: 2577763.
181. Neelsen KJ, Zanini IM, Herrador R, Lopes M. Oncogenes induce genotoxic stress by mitotic processing of unusual replication intermediates. J Cell Biol. 2013;200(6):699-708. Epub 2013/03/13. doi: 10.1083/jcb.201212058. PubMed PMID: 23479741; PMCID: 3601361.
182. Neelsen KJ, Zanini IM, Mijic S, Herrador R, Zellweger R, Ray Chaudhuri A, Creavin KD, Blow JJ, Lopes M. Deregulated origin licensing leads to chromosomal breaks by rereplication of a gapped DNA template. Genes Dev. 2013;27(23):2537-42. Epub 2013/12/04. doi: 10.1101/gad.226373.113. PubMed PMID: 24298053; PMCID: 3861667.
183. Battershill JM, Burnett K, Bull S. Factors affecting the incidence of genotoxicity biomarkers in peripheral blood lymphocytes: impact on design of biomonitoring studies. Mutagenesis. 2008;23(6):423-37. Epub 2008/08/06. doi: 10.1093/mutage/gen040. PubMed PMID: 18678752.
184. Kirsch-Volders M, Plas G, Elhajouji A, Lukamowicz M, Gonzalez L, Vande Loock K, Decordier I. The in vitro MN assay in 2011: origin and fate, biological significance, protocols, high throughput methodologies and toxicological relevance. Arch Toxicol. 2011;85(8):873-99. Epub 2011/05/04. doi: 10.1007/s00204-011-0691-4. PubMed PMID: 21537955.
185. Luzhna L, Kathiria P, Kovalchuk O. Micronuclei in genotoxicity assessment: from genetics to epigenetics and beyond. Front Genet. 2013;4:131. Epub 2013/07/23. doi: 10.3389/fgene.2013.00131. PubMed PMID: 23874352; PMCID: 3708156.
186. Beckerman R, Prives C. Transcriptional regulation by p53. Cold Spring Harb Perspect Biol. 2010;2(8):a000935. Epub 2010/08/04. doi: 10.1101/cshperspect.a000935. PubMed PMID: 20679336; PMCID: 2908772.
187. Oren M, Rotter V. Mutant p53 gain-of-function in cancer. Cold Spring Harb Perspect Biol. 2010;2(2):a001107. Epub 2010/02/26. doi: 10.1101/cshperspect.a001107. PubMed PMID: 20182618; PMCID: 2828285.
188. Vaughan C, Pearsall I, Yeudall A, Deb SP, Deb S. p53: Its Mutations and Their Impact on Transcription. Subcell Biochem. 2014;85:71-90. Epub 2014/09/10. doi: 10.1007/978-94-017-9211-0_4. PubMed PMID: 25201189.

189. Lanyi A, Deb D, Seymour RC, Ludes-Meyers JH, Subler MA, Deb S. 'Gain of function' phenotype of tumor-derived mutant p53 requires the oligomerization/nonsequence-specific nucleic acid-binding domain. Oncogene. 1998;16(24):3169-76. Epub 1998/07/22. doi: 10.1038/sj.onc.1201857. PubMed PMID: 9671396.
190. Lin J, Teresky AK, Levine AJ. Two critical hydrophobic amino acids in the N-terminal domain of the p53 protein are required for the gain of function phenotypes of human p53 mutants. Oncogene. 1995;10(12):2387-90. Epub 1995/06/15. PubMed PMID: 7784087.
191. Pagliarini R, Shao W, Sellers WR. Oncogene addiction: pathways of therapeutic response, resistance, and road maps toward a cure. EMBO Rep. 2015;16(3):280-96. Epub 2015/02/15. doi: 10.15252/embr.201439949. PubMed PMID: 25680965; PMCID: 4364868.
192. Alexandrova EM, Yallowitz AR, Li D, Xu S, Schulz R, Proia DA, Lozano G, Dobbelstein M, Moll UM. Improving survival by exploiting tumour dependence on stabilized mutant p53 for treatment. Nature. 2015;523(7560):352-6. Epub 2015/05/27. doi: 10.1038/nature14430. PubMed PMID: 26009011; PMCID: 4506213.
193. Scian MJ, Stagliano KE, Ellis MA, Hassan S, Bowman M, Miles MF, Deb SP, Deb S. Modulation of gene expression by tumor-derived p53 mutants. Cancer research. 2004;64(20):7447-54. Epub 2004/10/20. doi: 10.1158/0008-5472.CAN-04-1568. PubMed PMID: 15492269.
194. Hills SA, Diffley JF. DNA replication and oncogene-induced replicative stress. Curr Biol. 2014;24(10):R435-44. Epub 2014/05/23. doi: 10.1016/j.cub.2014.04.012. PubMed PMID: 24845676.
195. Warfel NA, El-Deiry WS. p21WAF1 and tumourigenesis: 20 years after. Curr Opin Oncol. 2013;25(1):52-8. Epub 2012/11/20. doi: 10.1097/CCO.0b013e32835b639e. PubMed PMID: 23159848.
196. Alver RC, Chadha GS, Blow JJ. The contribution of dormant origins to genome stability: from cell biology to human genetics. DNA Repair (Amst). 2014;19:182-9. Epub 2014/04/29. doi: 10.1016/j.dnarep.2014.03.012. PubMed PMID: 24767947; PMCID: 4065331.
197. Thomson AM, Gillespie PJ, Blow JJ. Replication factory activation can be decoupled from the replication timing program by modulating Cdk levels. J Cell Biol. 2010;188(2):209-21. Epub 2010/01/20. doi: 10.1083/jcb.200911037. PubMed PMID: 20083602; PMCID: 2812520.
198. Ge XQ, Blow JJ. Chk1 inhibits replication factory activation but allows dormant origin firing in existing factories. J Cell Biol. 2010;191(7):1285-97. Epub 2010/12/22. doi: 10.1083/jcb.201007074. PubMed PMID: 21173116; PMCID: 3010067.

APPENDIX A

List of primers.

cDNA primers

GAPDH	5’-GTC AAC GGA TTT GGT CGT ATT-3’
	5’- GAT CTC GCT CCT GGA AGA TGG-3’
musGAPDH	5’-CCA GCC TCG TCC CGT AGA CA-3’
	5'- GCC TCA CCC CAT TTG ATG TTA GTG -3'
musP53	5’-CAC GTG CTC ACC CTG GCT AA-3’
	5’-CTC AAC ATC CTG GGG CAG CA-3’
p53	5’-AAG GAA ATT TGC GTG TGG AGT-3’
	5’-AAA GCT GTT CCG TCC CAG TA-3’
CHEK 1	5’-GAA AGG GGC AAA AAG G-3’
	5’-ATG TAT GAG GGG CTG GTA-3’
mus CHEK1	5’-GGT TCA GGG CAT CAG TTT-3’
	5’-GGT CTC TTT CAG GCA TTG-3’
CCNA2	5’-GAC GGC GCT CCA AGA GG-3’
	5’-AAT GGT GAA CGC AGG CTG TT-3’
musCCNA2	5’-CCC CAG AAG TAG CAG AGT TT-3’
	5’-GGT ACG GGT CAG CAT CTA TC-3’

CCNE 1	5’-CAG TAT CCC CAG CAA ATC T-3’
	5’-AGT TCT CTA TGT CGC ACC AC-3’
CDC25A	5’-GGC AGG GGA GAA GAG CAA-3’
	5’-CAG GGA CAG AAG AGG CGT AG-3’
MDM2	5’-TGG CGT GCC AAG CTT CTC TGT- 3’
	5’-ACC TGA GTC CGA TGA TTC CTG CT- 3’
musMDM2	5’ AGG GGA AAG ATA AAG TGG AA -3’
	5’- ATA AAC AAT GCT GCT GGA AG -3’
Cyclin D2	5’- TGG GGA AGT TGA AGT GGA AC -3’
	5’- ATC CAC GTC TGT GTT GGT GA -3’
musCyclin D2	5’- AAA TGG GGG CAG ATG GAG A -3’
	5’- GGC AAA GGA GGA AGG CGT AT -3’
SHH	5’-TCT GCT GCT AGT CCT CGT CT-3’
	5’-TGT CGG GGT TGT AAT TGG GG-3’
musCCSP	5’- ACA TCA CCC CAC ATC TAC AGA CAC CAA -3’
	5’- TGA GGA GGG CCT CAA GGA CTT GAA -3’
musHes1	5'- TGA AGG ATT CCA AAA ATA AAA TTC TCT GG -3'
	5'- CGC CTC TTC TCC ATG ATA GGC TTT GAT GA -3'

Cloning primers

CHEK1 promoter	5’- GCTCTCCCCGCCTGTTCTTTG-3’
	5’-GCAGAAAACGCCTGCGGCAGCG- 3’

ChIP primers

CCNA2	5’-CCT TTG GTT TAC CCT TCA CTC G -3’
	5’- CCA AAG AAT AGT CGT AGC CG-3’
CHEK 1	5’- GTA CCA GGA GGT TCC CGT TG-3’
	5’-GGG TCT GGG GAA GAG AGG AA -3’

Genotyping primers

TightMDM2	5'- CTG TGA GTG AGA ACA GGT GTC AC -3'
	5'- GGC TAT AAT CTT CTG AGT CGA GAG -3'
CCSP-rtTA	5’-GGC AGG GGA GAA GAG CAA-3’
	5’-CAG GGA CAG AAG AGG CGT AG-3’
SPC-rtTA	5’-TGG CGT GCC AAG CTT CTC TGT- 3’
	5’-ACC TGA GTC CGA TGA TTC CTG CT- 3’
Tet-O-Cre	5’ AGG GGA AAG ATA AAG TGG AA -3’

	5’- ATA AAC AAT GCT GCT GGA AG -3’
p53LSL-R172H	5’- TGG GGA AGT TGA AGT GGA AC -3’
	5’- ATC CAC GTC TGT GTT GGT GA -3’
p53+/-	5'- AGC GTG GTG GTA CCT TAT GAG C-3'
	5'- GGA TGG TGG TAT ACT CAG AGC C-3'
	5'- GCT ATC AGG ACA TAG CGT TGG C-3'
MDM2+/-	5'- TGT GGC TGG AGC ATG GGT ATT G-3'
	5'- ATC TGA GAG CTC GTG CCC TTC G-3'
	5'- GGC GGA AAG AAC CAG CTG GGG C-3'

VITA

Shilpa Singh was born May 20th, 1987 in India. She graduated from Kendriya Vidyalaya School in 2004. She graduated with distinction in Bachelor of Pharmacy, Mumbai University,2008. She completed her Master's in Pharmaceutical Sciences with a concentration in Medicinal Chemistry from Virginia Commonwealth University, 2012. She started working part time in Dr. Swati Palit's lab in 2011 as a lab technician while completing her M.S. degree and later joined the lab after being accepted into Integrative Life Sciences PhD program in 2012.